



INSTITUTO DE
TECNOLOGÍA
QUÍMICA

EXCELENCIA
SEVERO
OCHOA

CONSEJO SUPERIOR DE INVESTIGACIONES CIENTÍFICAS
CSIC

UNIVERSITAT
POLITÈCNICA
DE VALÈNCIA

UNIVERSITAT POLITÈCNICA DE VALÈNCIA
DEPARTAMENTO DE QUÍMICA
INSTITUTO UNIVERSITARIO MIXTO DE TECNOLOGÍA
QUÍMICA (UPV – CSIC)

Doctoral Thesis

*Mechanistic Studies on the Photochemical Formation
and Cleavage of Oxetanes Derived from Pyrimidine
Bases*

Alejandro Blasco Brusola

Directors:

Prof. Miguel A. Miranda Alonso

Dr. Ignacio Vayá Pérez

Valencia, December 2020

D. Miguel Ángel Miranda Alonso, catedrático de universidad en la Universitat Politècnica de València, y D. Ignacio Vayá Pérez, investigador Ramón y Cajal en la Universitat Politècnica de València,

CERTIFICAN: Que la presente tesis doctoral, titulada: **“Mechanistic Studies on the Photochemical Formation and Cleavage of Oxetanes Derived from Pyrimidine Bases”**, ha sido desarrollada por ALEJANDRO BLASCO BRUSOLA, bajo su dirección, en el Departamento de Química-Instituto de Tecnología Química (UPV/CSIC) de la Universitat Politècnica de València.

D. Miguel A. Miranda Alonso

D. Ignacio Vayá Pérez

*La razón por la que las personas fracasan
realmente no es porque pusieron sus metas muy
altas y no llegaron, sino porque las pusieron
muy bajas y las alcanzaron*

-Jordan Belfort

Acknowledgments

Most of my predecessors like to describe their time as a PhD student as an “adventure”, I prefer to refer it as a rollercoaster: In the beginning you are overwhelmed with a strong urge to scream in terror and you just wish it to be over as soon as possible...until the adrenaline starts to kick in, and you begin to actually enjoy the ride. Suddenly the twists and turns become more predictable, giving you a sensation of being in greater control of the situation, hence boosting self-confidence, and even making you look forward for the next loop. You feel alive. And like most rollercoasters, you rarely ride it alone.

This thesis, that so much hard work has taken, is dedicated to all the people who were, in one way or another, next to me, and who have helped me make this 3-year ride more bearable.

First and foremost are my parents, who were able to guide me both personally and professionally to become the best doctor I could aspire to be.

Professionally I will always be grateful to both of my directors: Prof. Miguel Angel Miranda Alonso and Dr. Ignacio Váya Pérez. They were one of the few who, since the very beginning, had treated me like an adult, a professional in the making, as opposed to a teenager that needed to be disciplined. Thank you for your guidance, respect and encouragement, and your constructive criticism. I would never have gotten this far without you.

My gratitude I also give to the technicians who have made my work possible in the short time in which it was required:

Estrella Mateos Otero, our lovely NMR specialist who has been almost as a second mother to me within the ITQ building, and always knew how to cheer me up.

Manuel Adelantado Mateu, lab superior technician in the Department of Chemistry of UPV. Without his competent skills to ever so rapidly repair all the stubborn equipment that the Department owns, including high pressure liquid chromatography (HPLC) and the UV absorption equipment. I have no doubt that I would have accomplished less than half of what I did in those years were he not a part of our team.

Thank you, of course, to “*la Generalitat Valenciana*” for the financial support through the Santiago Grisolia grant.

And last, but not least, I have to give special thanks to my closest friends, to whom I have dedicated this thesis: Alex Escamilla Dominguez, an old childhood friend who has been at my side through thick and thin, and with whom I have spent so many great moments and shared many laughs. Tú molas, tio!

But most especially, this is dedicated to my best friends in the world, my Vietnamese princesses: **Phùng Thị Hoa** and **Phạm Ái Linh**. I would have fallen into despair long ago without your emotional support and cheerful nature, I am very fortunate to have met you and hope to forever have you as my closest of friends! *Tôi yêu cả hai bạn!*

CONTENTS

CHAPTER 1: Introduction	1
1. Photochemistry	4
1.1. General overview	4
1.2. Photochemistry of carbonyl compounds	9
1.3. Photochemistry of aromatic compounds	13
1.4. The best of both worlds: Benzophenone	16
2. Oxetanes	18
2.1. General overview	18
2.2. Oxetanes in nature	20
2.3. The relation between oxetanes and DNA damage.....	21
2.3.1. Mutagenesis.....	21
2.3.2. Photochemical perspective	23
2.4. Oxetane synthesis.....	28
2.4.1. Chemical pathway.....	28
2.4.2. Photochemical pathway (Paternò-Büchi)	32
2.5. Oxetane breaking	37
2.5.1. Chemical breakdown.....	37
2.5.2. Enzymatic breakdown	39
2.5.3. Photo-induced carbonyl-olefin metathesis	42
3. Transient absorption spectroscopy	44
3.1. Laser flash photolysis.....	44
3.2. Femtosecond transient absorption spectroscopy.....	47
4. Relevant predecessors	50
5. References	53
CHAPTER 2: Objectives	73

CHAPTER 3: Influence of the Linking Bridge on the Photoreactivity of Benzophenone-Thymine Conjugates..... 77

1. Introduction.....	79
2. Results and discussion.....	82
3. Conclusions.....	92
4. Experimental section.....	93
5. Supplementary material.....	102
6. References.....	116

CHAPTER 4: Regiochemical memory in the adiabatic photolysis of thymine-derived oxetanes. A combined ultrafast spectroscopic and CASSCF/CASPT2 computational study 123

1. Introduction.....	125
2. Results and discussion.....	127
3. Conclusions.....	141
4. Experimental section.....	142
5. Supplementary material.....	147
6. References.....	158

CHAPTER 5: Regioselectivity in the adiabatic photocleavage of DNA-based oxetanes 167

1. Introduction.....	169
2. Results and discussion.....	173
3. Conclusions.....	181
4. Experimental section.....	182
5. Supplementary material.....	187
6. References.....	203

Conclusions	209
Abstracts	215
Abstract	217
Resumen	221
Resum	225
Annex: Publications and Conferences	229

ABBREVIATIONS AND SYMBOLS

(6-4)PP	Pyrimidine-Pyrimidone (6-4) Photoproduct
A	Acceptor
A*	Acceptor in its excited state
ANO	Atomic Natural Orbital
Ar	Aryl
BP	Benzophenone
BPN	4-Benzoylbenzylamine
BSSE	Basis Set Superposition Error
CAS	Choice of the Active Space
CASPT2	Complete-Active-Space Second-Order Perturbation Theory
CASSCF	Complete-Active-Space Self-Consistent Field
CI	Conical Intersection
CP	Counterpoise
CPD	Cyclobutane Pyrimidine Dimer
CSF	Configuration State Functions
D	Donor
D*	Donor in its excited state
DCM	Dichloromethane

DDR	DNA Damage Response
DET	Dexter Electron Transfer
DFT	Density Functional Theory
DIBAL	Diisobutylaluminium hydride
DIR	Diradical
DMF	Dimethylformamide
DMT	1,3-Dimethylthymine
D_{6h}	A geometrical plane of benzophenone
E	Energy
EDC	1-Ethyl-3-(3-dimethylaminopropyl)carbodiimide
ESI	Electrospray Ionization
ET	Energy Transfer
FADH	Flavin cofactor
FRET	Förster Resonance Energy Transfer
HCl	Hydrochloric acid
HH	Head-to-Head
HOBt	1-Hydroxybenzotriazole
HOMO	Highest Occupied Molecular Orbital
HRMS	High-Resolution Mass Spectrometry
HT	Head-to-Tail
IC	Internal Conversion

IPEA	Ionization-Potential Electron-Affinity Parameter
ISC	Intersystem Crossing
k_Q	Intramolecular quenching rate constants
KOH	Potassium hydroxide
KP	Ketoprofen
LA	Lewis Acid
LDA	Lithium diisopropylamide
LFP	Laser Flash Photolysis
LIIC	Linear Interpolation of Internal Coordinates
LUMO	Lowest Unoccupied Molecular Orbital
MeCN	Acetonitrile
MeOH	Methanol
MgSO ₄	Magnesium sulphate
MS	Multistate
NaOH	Sodium hydroxide
NER	Nucleotide Excision Repair
NO [•]	Nitric Oxide radical
NO ₃	Peroxynitrite
NSAIDs	Non-Steroidal Anti-Inflammatory Drugs
Nu	Nucleophile
O ₂ ^{•-}	Superoxide anion radical

$^1\text{O}_2$	Singlet oxygen
$\cdot\text{OH}$	Hydroxyl radical
OXE	Oxetane
P	Product
PB	Paternò-Büchi
PCM	Polarizable Continuum Model
PET	Photoinduced Electron Transfer
Ph	Phenyl
PP	Photoproduct
PS	Photosensitizer
Q	Quencher
R	Reactant
R^*	Reactant in its excited state
RedAl	Bis(2-methoxyethoxy)aluminum dihydride
ROS	Reactive Oxygen Species
S_0	Ground State
S_1	Singlet Excited State, first energy level
S_n	Singlet Excited State, n^{th} energy level
SA	State Averaged
SOC	Spin-Orbit Coupling
SS	State-Specific

STC	Singlet-Triplet Crossing
S-VDZP	S-Type Valence Double- ζ Plus Polarization
T ₁	Triplet Excited State, first energy level
T _n	Triplet Excited State, n^{th} energy level
THF	Tetrahydrofuran
Thy	Thymine
TS	Transition State
TTET	Triplet-Triplet Energy Transfer
UPLC	Ultra Performance Liquid Chromatography
Ura	Uracil
UV	Ultraviolet
VR	Vibrational Relaxation

CHAPTER 1:

Introduction

Introduction

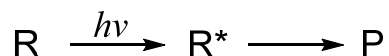
Imagine to be able to capture the magic of plants' photosynthesis in a bottle, where our test-tubes are the leaves and our labs are the forest. Imagine to be able to 'heat up' a specific molecule in a solution without *directly* affecting the others. Let's take it one step further, and imagine that we could use this "magic" to slow down time, take snapshots of entities that so far were only theoretical, and bring them to the light (pun unintended). Now imagine it has already been done, and perfected, for over 100 years...*That* is what photochemistry is all about, and in this particular thesis it is utilised for the synthesis (and breaking) of a particularly useful four-membered ring that is very present in medicinal chemistry as a building block for many natural products; this ring is, of course, an oxetane. In this thesis we shall discuss the importance of photochemistry in the world of science, the role of oxetanes in the solar-mediated damage of DNA and in synthetic organic chemistry (specially carbonyl-olefin metathesis); as well as the most advanced pieces of equipment used for the research of excited oxetane transients that have so far eluded the eyes of all of our predecessors: laser flash photolysis and ultrafast transient absorption spectroscopy on the femtosecond scale.

1. Photochemistry

1.1. General overview

Every atom in the universe that possesses at least one electron has the ability to absorb light, the wavelength (or “colour”) of the light waves that it can absorb is the only variable. “Photochemistry” is a term used to describe the field of chemical reactions in which a net chemical change is induced by the interaction of a molecule with light. “Photophysics”, similarly, is the interaction in which a net physical change is induced by the interactivity of a molecule with light, whether or not a chemical change ultimately takes place. These fields cover a wide range of disciplinary specialities, ranging from chemical physics to molecular spectroscopy and computational science.

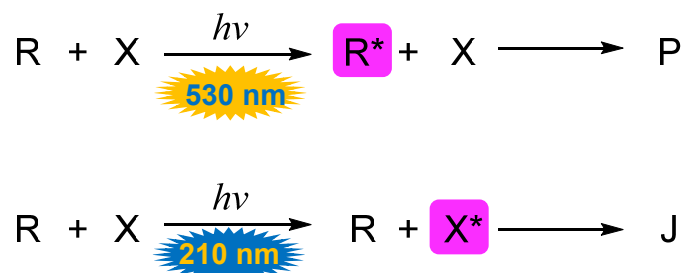
As shown in Scheme 1.1, a standard photochemical reaction includes the light irradiation of a specific reactant (R), which would absorb a photon, thus raising the energy level of the reactant from ground state to excited state (R*), and eventually lead to a photoproduct (P).



Scheme 1.1. Schematic representation of a standard photochemical process. R: Reactant; R*: Reactant in its excited state; P: Photoproduct; $h\nu$: Photon.

This photoproduct (P) can be produced in a single step, or in several steps via excited unstable intermediates; and its photo-synthesis can require a single reactant (R) or several. The reason photochemistry has gained increasing popularity is due to its chemospecificity, since different molecules may have different absorption wavelengths. For example, let’s imagine we have two molecules in solution: R and X. R may absorb visible

light at $\lambda = 530$ nm exclusively and form P, while X might only absorb UV light at $\lambda = 210$ nm and form J; therefore, by choosing the appropriate wavelength one can control the reaction pathway (Scheme 1.2). Note that photoproducts P and J may be the result of reactants R and X bonding with each other to form a new molecule, or the excited species may just act as a photosensitiser, transferring its absorbed energy to the other molecule without itself being consumed in the reaction.



Scheme 1.2. Schematic representation of photochemical reactions arising from the absorption of light at different energies.

The way this photo-mechanism works is by the initial absorption of a photon by a molecule, an electron would rise in a few femtoseconds (to put it into perspective, 1 femtosecond corresponds to 10^{-15} seconds) to a higher energy level without changing its spin, reaching the **singlet excited state** (S_n). After a few femto- to picoseconds, vibrational relaxation will follow, and subsequently, the molecule would lose part of the excess energy and fall down to the lowest singlet energy level (S_1); from this point on, the molecule could either deescalate to the ground state and release energy in the form of heat and/or fluorescence, or, it could change its spin to one that is parallel to its electron pair and drop to an intermediate energy level via intersystem crossing (ISC), and reach the **triplet excited state** (generally T_1), in the case that S_1 and T_1 energetically overlap. From T_1 , the molecule would eventually lose the excess of its energy in the form

of heat and/or phosphorescence and return to its ground state. The whole process is represented in the standard Jablonski diagram illustrated in Figure 1.1. Normally, T_1 display lifetimes in the μs time-scale, while S_1 in general last mere ns.

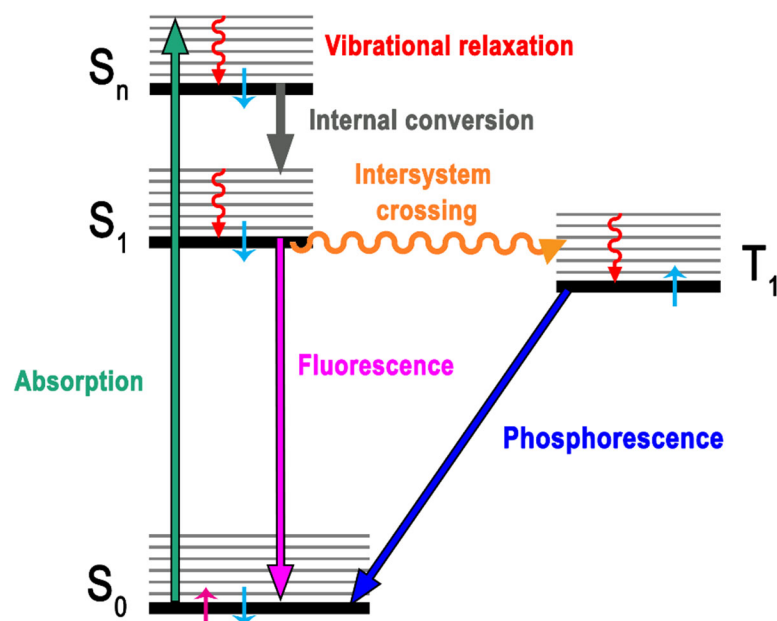
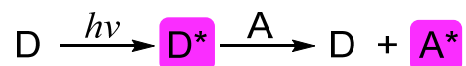


Figure 1.1. Standard Jablonski diagram showing the main photophysical processes that might take place once a molecule absorbs light. Electrons and their spins are represented by a small light blue and magenta arrows.

Sometimes it is unfeasible, or too risky, to directly excite a molecule, or perhaps the wavelength necessary for direct irradiation would also be absorbed by other molecules in solution, giving rise to unwanted side reactions. For this reason, an energy “donor” (D) is used for excitation, which acts by donating the energy it absorbed from a photon (at a wavelength only D can absorb) to the target molecule. When D^* in its excited state transfers its energy to an acceptor, A, rising the excited state

of the latter and reducing D to its ground state, it is called a **photoinduced energy transfer** (ET) process (Scheme 1.3), and it occurs non-radiatively (i.e. without the absorption or emission of a photon).



Scheme 1.3. Photoinduced energy transfer from donor, D, to acceptor, A.

If the energy for D* is higher than for A* and the lifetime of the former is long enough, then one of two ET reactions can take place: Förster resonance energy transfer (FRET) and Dexter energy transfer (DET). FRET is a dynamic quenching mechanism in which, via a dipole-dipole interaction, energy is transferred from donor to acceptor, without any transfer of mass. It can take place across relatively large distances, of up to 100 Å. By contrast, DET is a quenching mechanism that requires a wavefunction overlap between a donor and acceptor, therefore it can only occur at relatively short distances of ~10 Å or lower. In this process, an excited electron is transferred from donor to acceptor, and an electron is transferred from the acceptor to the donor, with no net charge change but effectively exciting the acceptor. The processes are represented in Figure 1.2.

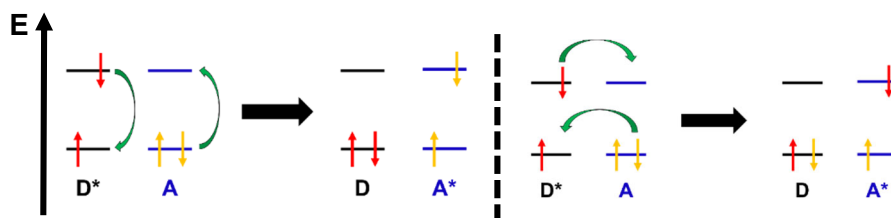


Figure 1.2. Left: Förster resonance energy transfer. Right: Dexter energy transfer. D: Donor; A: Acceptor; E: Energy.

There are some reactions in which the excited chromophore might donate an electron to the acceptor without receiving another one back, therefore producing two charged ions in essentially a redox reaction; this reaction is called **photoinduced electron transfer (PET)**, as shown in Figure 1.3.

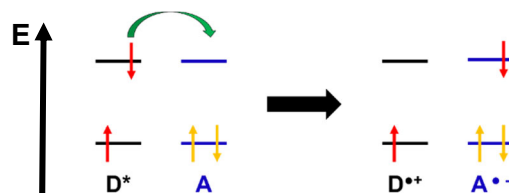
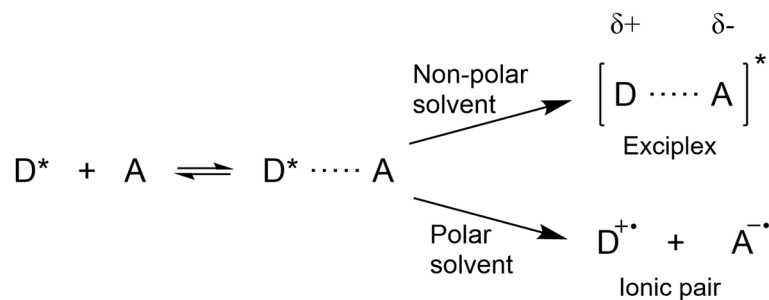


Figure 1.3. Photoinduced electron transfer from an excited donor, D^* , to acceptor, A.

When a charge-transfer complex between the excited donor and the acceptor is formed, that is called an **exciplex**. It possesses a mixture of the photochemical and photophysical properties of both molecules and a relatively large dipole moment (see Scheme 1.4), and in general exciplexes are stabilized in non-polar solvents. Exciplexes can be detected using different techniques such as fluorescence and transient absorption spectroscopies, as stated in section 3.



Scheme 1.4. Electron transfer mechanisms for the formation of ionic pairs (favoured in polar solvents) and exciplexes (favoured in non-polar solvents).

1.2. Photochemistry of carbonyl compounds

The ways in which carbonyl compounds behave after the absorption of photons is well documented.¹ Commonly used as starting materials for a wide range of reactions, carbonyl-containing organic molecules got increasing attention for their efficiency as photosensitisers and photocatalysts.²⁻³ Their absorption power lies on their double-bond, formed by the fusion of the two half-full 2p orbitals of the C and the O (see Figure 1.4, with formaldehyde as an example), and also on one of the sp^2 hybridized orbitals of both atoms.

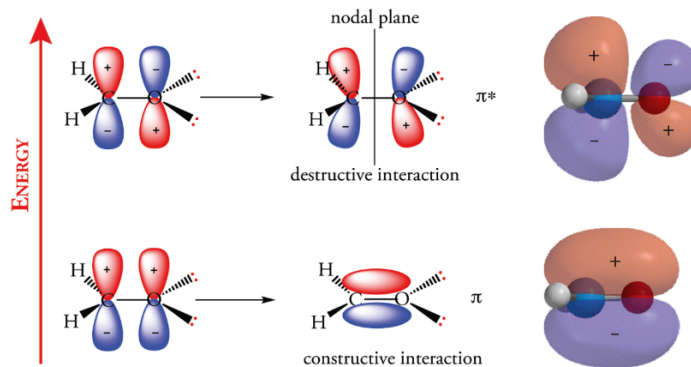


Figure 1.4. Representation of the bonding (below) and antibonding (top) orbitals of formaldehyde. Taken from “Organic Chemistry: Structure, Mechanism, Synthesis” by Robert J. Ouellette and J. David Rawn (2019).⁴

When a carbonyl compound absorbs a photon, it is believed that an electron from one of the O non-bonding (n) orbitals can be ejected to the higher π^* orbital, since the n electrons are on a higher energy level than π -orbital electrons, so the energy gap towards the π^* is lower. As a result, two transitions are made possible, $n \rightarrow \pi^*$ and $\pi \rightarrow \pi^*$. The existence of an unpaired electron in a n orbital gives the molecule the diradical appearance, which rapidly undergoes ISC to its triplet excited state, and to any subsequent reactions thereafter (Figure 1.5). The molar absorption coefficient for $n \rightarrow \pi^*$ is relatively low ($40 \text{ M}^{-1} \text{ cm}^{-1}$), which is why it is usually obscured by the stronger $\pi \rightarrow \pi^*$ absorption.¹

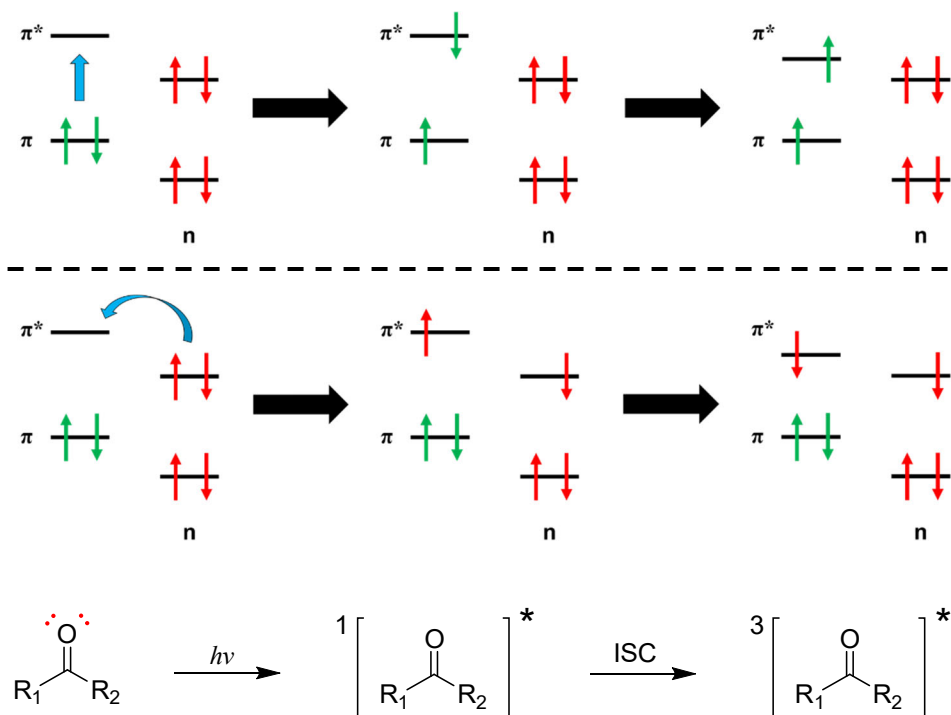


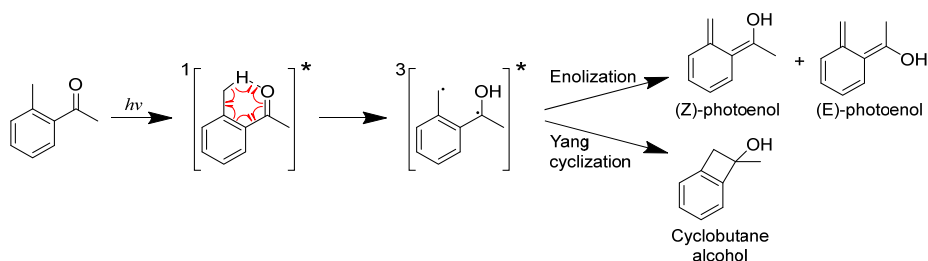
Figure 1.5. The two possible electronic transitions after photo-excitation of a carbonyl compound to its triplet excited state.

The easily-accessible triplet excited state helps to explain the high photoreactivity of carbonyl compounds. If R_1 and/or R_2 (Figure 1.5) are aromatic, depending on their substituents, they could affect the energy levels of the triplets, and consequently the one of lower energy.

An important number of photo-induced reactions of carbonyl compounds can be initiated through the formation of the $n\pi^*$ excited state of the molecule due to its high reactivity. However, the $\pi\pi^*$ excited state can be the lowest lying one depending on the substituents it has attached, R_1 and R_2 (Scheme 1.5). The excited state can undergo several chemical reactions, including but not limited to, a hydrogen abstraction to form an alcohol, cyclisation with an alkene to form an oxetane (as we will see in

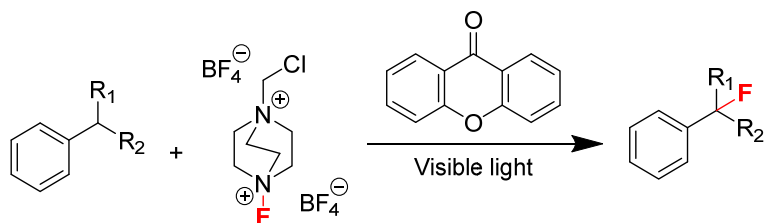
section 2.4.2) and even a release of $R_1\cdot$ and $R_2\cdot$, which would undergo further radical reactions (i.e. Norrish type I reaction).⁵

Carbonyl compounds are used, among other things, to synthesise a wide variety of natural products and bioactive compounds, through a Diels-Alder strategy; an example of which would be the catalytic enantioselective photoenolization of 2-alkylphenyl ketones,⁶ in which the formation of the diradical (Norrish type II reaction)⁷ allows for free rotation of the carbon α to the $O\cdot$, allowing for *E* and *Z* isomers to form, and even undergo Yang cyclisation⁸ to form a cyclobutane (Scheme 1.5).



Scheme 1.5. Photoenolization and Yang cyclisation of a 2-alkylphenyl ketone.

Ketones and quinones can also be used as photosensitisers in metal-free strategies for the synthesis of natural products. For example, Chen *et al.* (2013) synthesised fluorinated benzylic derivatives under visible light, with the use of xanthone as a photosensitiser with relatively high yields (Scheme 1.6).⁹



Scheme 1.6. Fluorination of a benzylic derivative with Selectfluor, using xanthone as a catalyst under visible light.

More research is being done to further improve these reactions to give rise to more economical metal-free processes, which will allow to reduce manufacture costs while providing more environmentally friendly approaches.

1.3. Photochemistry of aromatic compounds

Aromaticity in organic chemistry, contrary to what one might expect, is not a reference to its scent (although it is somewhat related), but to the property of having a planar cyclic structure with delocalized π bonds in resonance, result of having several double-bond-single-bonds in sequence to increase stability. For a compound to be aromatic it requires a number of delocalized π -electrons that follow Hückel's rule of $4n + 2$, where n is a whole number, with the first four sets of total values being 6, 10, 14 and 18 π -electrons.¹⁰

The smallest and simplest aromatic compound (i.e. where $n = 1$) is benzene. In benzene each carbon has sp^2 hybridized molecular orbitals and they each contribute an electron to a π -bond, which are all equally dispersed and spread out throughout the ring, making the molecule perfectly symmetrical since all C-C bonds are the same length. Figure 1.6

shows the geometry of the bonding and antibonding orbitals for the D_{6h} undistorted structures of benzene in its ground state. For the lowest orbital, π_1 , it is evenly spread across all the molecular framework, all bonding.¹¹ When reaching the next energy level (HOMO), we find not one but two iso-energetic orbitals, π_{2a} and π_{2b} , a set of degenerate pairs both containing a single node but overall bonding. Next up (LUMO), there are two anti-bonding orbitals of the same energy, π^*_{3a} and π^*_{3b} , each possessing two nodes. And finally, the highest energy level is occupied by an anti-bonding orbital, π^*_4 , with three nodes.

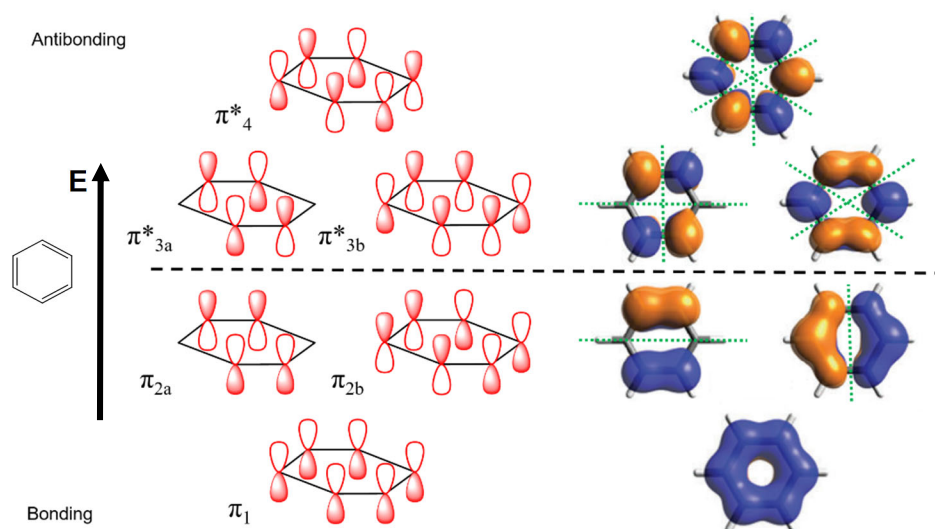


Figure 1.6. Energy diagram of the π molecular orbitals for D_{6h} structures of benzene. Nodal planes are represented by green dotted lines. 3D orbital images were taken from Casanova *et al.* (2010).¹¹

In the previous section, it was mentioned that for carbonyl compounds there were two types of photo-induced electronic transitions when absorbing photons ($n \rightarrow \pi^*$ and $\pi \rightarrow \pi^*$); for aromatic compounds, only $\pi\pi^*$ transitions are possible (Figure 1.7).¹²⁻¹³

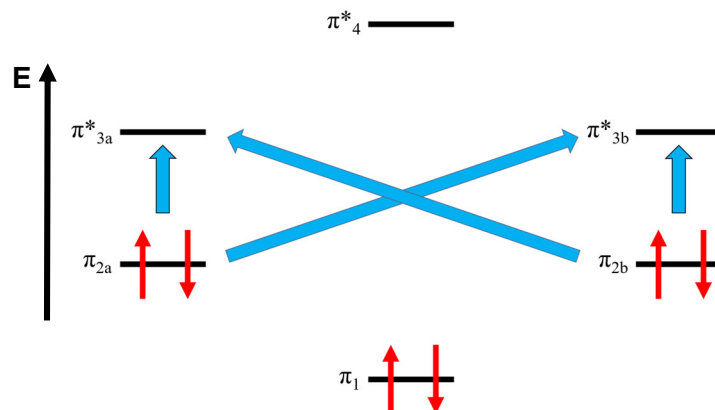
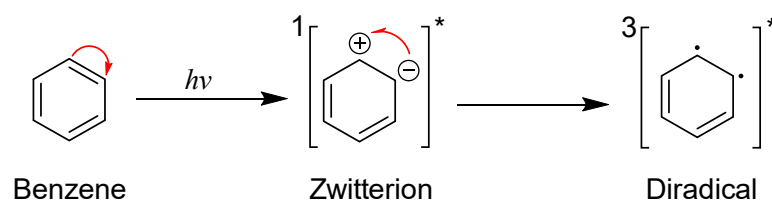
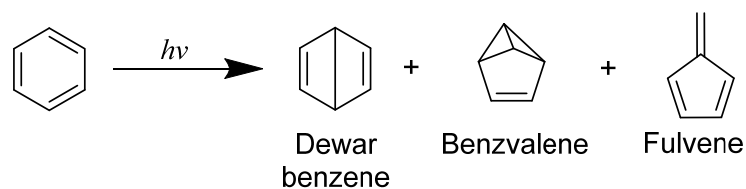


Figure 1.7. Potential photo-induced electronic transitions in benzene.¹²

Due to this nature, it is expected for diradicals and/or ion pairs to appear as transient intermediates from $T_1(\pi, \pi^*)$, and the ISC rate is relatively low compared to olefins (Scheme 1.7). The primary photochemical processes for aromatic compounds include: Electron transfer, α - and β -cleavage, addition to olefins, pericyclic reactions, substitution reactions and photosensitization (see Scheme 1.8 for some examples).¹²



Scheme 1.7. Photo-excitation of benzene and potential electron transitions.



Scheme 1.8. Photo-induced isomerization reactions of benzene ($\lambda < 200$ nm).

1.4. *The best of both worlds: Benzophenone*

Benzophenone (BP) is a molecule that contains both a carbonyl and an aromatic ring, and it is one of the most well-known compounds in photochemistry and photophysics,^{12, 14-21} as well as medicine,²² having been studied since Ciamician and Silber published its sun-induced photoreduction in 1900.²³ There have been many transient absorption and phosphorescence emission studies made to analyse its photoreactivity in both rigid matrix (77 K) and in fluid deaerated solution. Benzophenone has a small energy gap between the S_1 and T_2 excited states, and they have a strong spin-orbit coupling interaction; because of this, ISC is an efficient competitor to IC and fluorescence emission. Since the rate of ISC is much greater than that of radiative emission (10^{11} s⁻¹ vs. 10^6 s⁻¹, respectively), the T_1 is formed with near complete yield ($\phi \sim 1$; see Figure 1.8).²⁴

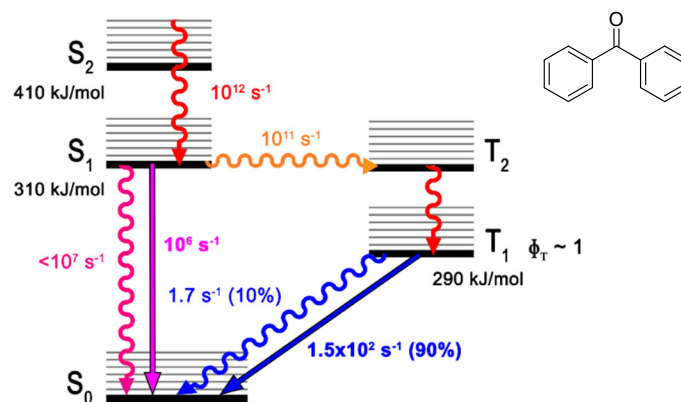


Figure 1.8. State diagram for excited benzophenone at 77 K. Straight lines: Radiative emission. Curly lines: Non-radiative emission.

Benzophenone has a $T_1 \rightarrow T_n$ absorption maximum at $\lambda \approx 520 \text{ nm}$ and an average decay lifetime of several μs (Figure 1.9).

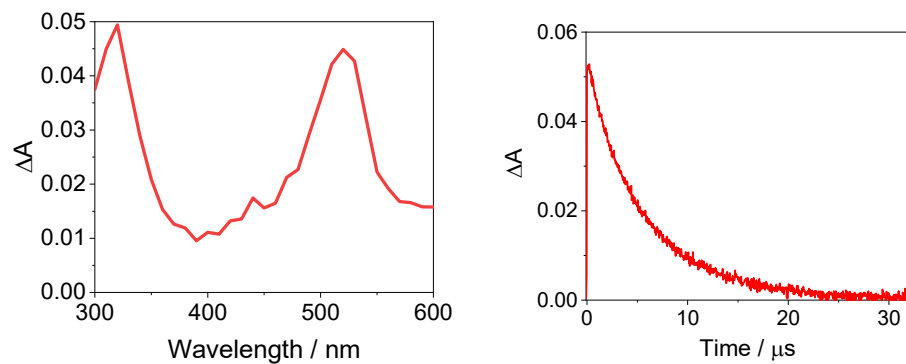


Figure 1.9. (Left) Absorption spectrum for benzophenone in its T_1 excited state 100 ns after excitation at 266 nm. (Right) Transient absorption decay monitored at 520 nm.

2. Oxetanes

Oxetanes are outstandingly useful pendant motifs in chemistry and medicine. They can be found in a wide variety of natural drugs and are ideal intermediates for the synthesis of stereochemically pure species that are otherwise nigh impossible to make. They are also partly responsible for the production of some species that cause damage to DNA and eventually skin cancer. In this chapter we shall explore their nature, natural occurrence, their relation with DNA damage, how can they be synthesised, and most importantly, how can they be broken down.

2.1. General Overview

Oxetanes are four-membered rings composed of three carbon atoms and an oxygen one, where “ox” stands for the O atom itself, and “ane” for being a fully saturated molecule. These strained cyclic ethers are highly polar and relatively small in size (see Figure 1.10), which makes them particularly useful when incorporated in pharmaceutical drugs, since they tend to improve aqueous solubility and reduce lipophilicity, in turn increasing metabolic stability.²⁵

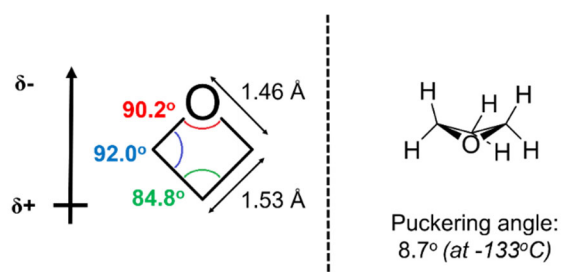


Figure 1.10. Structural configuration and properties of an oxetane ring.

They have a planar configuration and a relatively elevated ring strain (106 kJ/mol), which is slightly lower than that of epoxides (112 kJ/mol), making their structure more stable. Additionally, their heteroatom-induced puckering angle reduces gauche interactions compared to cyclobutane; however, certain substituents in the ring can increase such interactions, therefore further puckering the conformation.²⁶ The lone pairs of electrons in the O atom are especially exposed due to the strain of the ring, in an angle in which it is highly susceptible to Lewis acids, making them efficient hydrogen-bond acceptors.

These properties have encouraged the pharmaceutical industry to use oxetanes as intermediates for the synthesis of valuable enantioenriched building blocks for drugs, as well as labelling tools to promote selective reactions (e.g. with protein side chains), and to increase bioactivity for therapeutic purposes.

2.2. Oxetanes in nature

The occurrence of oxetane rings in nature is scarce, but biologically important. Particularly famous is Paclitaxel or Taxol (Figure 1.11), a cancer therapy reagent extracted from western yew stem bark (*Taxus brevifolia*);²⁷⁻²⁸ its mechanism of action induces stabilization of dysfunctional microtubules during mitosis. In Taxol, the oxetane makes the structure more rigid and acts as a hydrogen-bond acceptor.

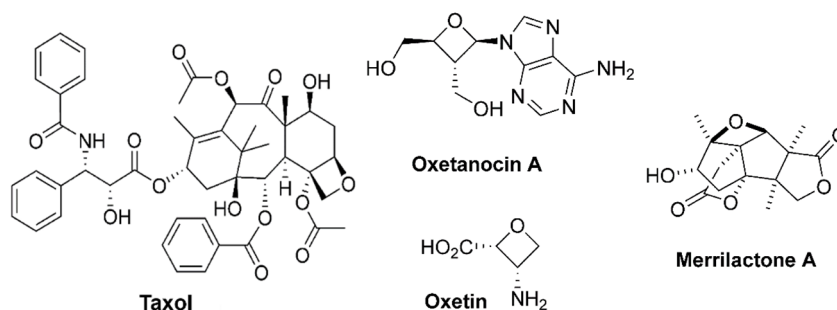


Figure 1.11. Chemical structure of several natural molecules containing an oxetane ring. Adapted from Bull and *et al.* (2016).²⁵

Oxetanocin A can be found in soil bacteria *Bacillus megaterium*, it inhibits replication of HIV virus.²⁹ Oxetin is an antibacterial herbicide extracted from *Streptomyces* sp. OM-2317, inhibiting bacteria such as *Bacillus subtilis* and *Piricularia oryzae*, as well as enzyme glutamine synthase from spinach.³⁰ Merrilactone A is a rat hormone growth-stimulant, and it is present in the pericarps of *Illicium merrillianum* plants.³¹

2.3. *The relation between oxetanes and DNA damage*

2.3.1. Mutagenesis

Mutagenesis, or the processes in which the genetic information of a living organism suffers a change or mutation, plays a most important role in evolution from a Darwinian perspective; it is also the cause of melanomas, photoaging and skin cancer among other diseases.³²⁻³⁵ These are caused by prolonged damage to the DNA in the cells and an insufficient response from the cellular “DNA damage response” (DDR) pathways to repair it.³⁶⁻³⁹

The indirect harm received by the DNA from UV light can take place through endogenous or exogenous agents, such as drugs, that may act as photosensitisers (PS). In this context, absorption of light by a PS may cause, for example, the chain to react with molecules in its immediate surroundings, creating reactive oxygen species (ROS) and performing hydrolytic reactions with water.⁴⁰⁻⁴⁸ Additionally, the double helix could suffer damage indirectly through energy transferred by photosensitisers,^{15, 49-50} i.e. drugs acting as energy donors after absorbing photons (see section 1.1), interacting with DNA to form certain bulky organic photoproducts which will be mentioned in section 2.3.2., which are an important focus of this thesis.

Excessive exposure to sunlight is the main cause of skin cancer in humans, as well as other illnesses, including but not limited to: Cutaneous malignant melanoma and squamous cell carcinoma (see Figure 1.12).⁵¹⁻⁵² Skin lesions and carcinogenesis is also believed to be a direct consequence of sunlight photo-damage of DNA. As a matter of fact, UV radiation has been widely accepted as a class I carcinogen since at least 2009,⁵³ and any human with significant deficiencies in their cells’ natural

abilities to deal with this kind of damage in the DNA will likely suffer from at least one of the following syndromes: Cockayne syndrome, Xeroderma Pigmentosum, Cerebro-oculo-facio-skeletal syndrome and UV-sensitive syndrome.⁵⁴ In addition, such lesions could also cause immunodepressive and inflammatory reactions in the epithelial cells and accelerate tumour development;⁵⁵ this can be especially serious if the genes affected are those that are in control of the genomic integrity of the cell.⁵⁶ Finally, in more extreme cases, over-exposure to UV light can lead to necrosis,⁵⁷ growth retardation,⁵⁴ telangiectasia,⁵⁸ xerosis cutis,⁵⁹ premature aging⁶⁰⁻⁶¹ and cellular senescence.⁶²

The chemical explanations for the aforementioned DNA photo-damage shall be explained in the following section.



Figure 1.12. (Left) Melanoma on a patient's skin. Image taken from public domain - National Cancer Institute. (Right) Cutaneous squamous cell carcinoma. Image extracted from Schmults *et al.* (2018).⁶³

2.3.2. Photochemical perspective

The DNA double helix significantly favours the absorption of UVC light (200-280 nm), as shown in Figure 1.13,³³ but this is completely blocked by the Earth's ozone layer, as well as 90% of UVB radiation (280-315 nm). By contrast, UVA light (315-400 nm), although it is only marginally absorbed by the DNA itself,³⁹ it can still cause harm via certain cellular non-DNA chromophores (e.g. porphyrins or flavins),⁶⁴ which do have higher molar absorption coefficient values for it, causing the formation of ROS that react with the DNA bases.⁶⁵ This is one of the reasons why UVA's photoproducts are considered more mutagenic than those produced by UVB radiation.

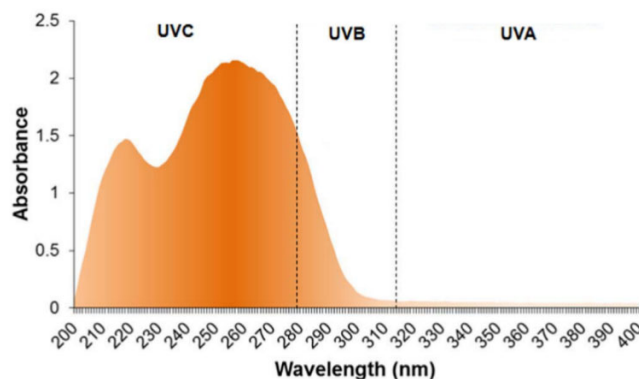


Figure 1.13. Absorption spectrum of DNA. Adapted from A. P. Schuch *et al.* (2017).³³

Common examples of ROS are the superoxide anion radical ($O_2^{\cdot-}$) and hydroxyl radical ($\cdot OH$),⁶⁶ formed by a Type I mechanism, which involves electron transfer between a chromophore, or photosensitiser, and its target (e.g. a DNA base), where the chromophore is reduced into an anion radical which in turn can react with an oxygen molecule, giving rise to the aforementioned $O_2^{\cdot-}$, or with H_2O_2 leading to the formation of $\cdot OH$.

However, a second mechanism can also be observed, Type II, which involves a direct transfer of energy from the photosensitiser in its triplet excited state to an oxygen molecule, forming singlet oxygen ($^1\text{O}_2$),⁶⁷ whose highly destructive oxidation power over DNA is the main cause of natural aging.⁶⁸ Lipid peroxidation, which causes the destabilization of cell membranes, is another cause of mutagenesis, since the unsaturated aldehydes that they form undergo alkylation reactions with DNA bases, causing cross-links in the double helix or hindering the ability of a protein to perform basic metabolic functions such as replication and transcription.⁶⁹ ROS have a higher affinity towards guanine due to its higher oxidation potential, inducing hydrolysis reactions.⁷⁰⁻⁷² Additionally, ROS can also destroy collagen and actin, disturbing the integrity of dermis and epidermis.⁷³

Within the context of DNA damage, of greatest interest for this work is the light-induced formation of two bulky photo-products such as cyclobutane pyrimidine dimers (CPDs) and, to a lesser degree, pyrimidine-pyrimidone (6-4) photoproducts ((6-4)PPs).^{50, 74-76} These photoproducts are normally formed in higher yields for Thy units; their structures are shown in Figure 1.14. These two dimers are the ones that appear in the largest amounts, their ratios vary depending on the light wavelength and intensity that the DNA receives, although the yield for the CPDs is commonly higher than that of (6-4)PPs.

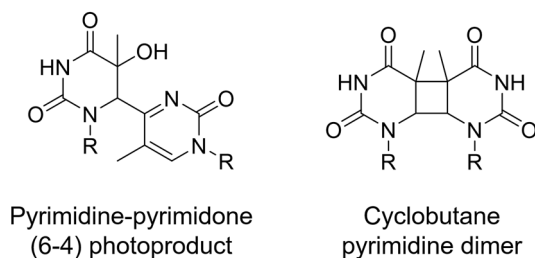
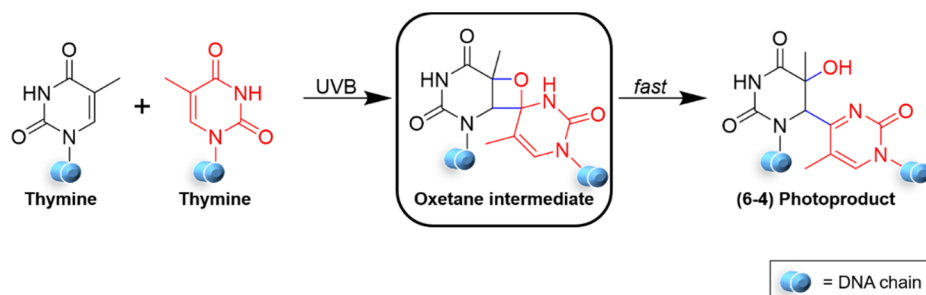


Figure 1.14. Chemical structures of the most common photo-induced DNA lesions: CPDs and (6-4)PPs. R: DNA chain.

Generally, CPDs are the result of [2+2] cycloaddition of the double-bonds from the C5 and C6 carbons of two adjacent thymine units through Frenkel excitons, giving rise to a four-membered carbon ring (i.e. a cyclobutane).⁷⁷⁻⁸¹ On the other hand, (6-4)PPs are believed to be the result of a Paternò-Büchi reaction between the C5=C6 double-bond of a DNA base and the carbonylic C4 of an adjacent base, creating a highly unstable **oxetane intermediate**^{32, 82-88} (the implications of this will be discussed in a further chapter). It can quickly degrade into a dimer containing an alcohol in the C5 of the first DNA base and a single covalent bond that links its C6 with the previously carbonylic C4 of the second base (hence the name “(6-4)PP”) (see Scheme 1.9).



Scheme 1.9. Formation of (6-4)PP between two Thy units via a highly unstable oxetane intermediate.

CPDs are formed in both hetero- and euchromatin regions of the cell, which are DNA-protein complexes present in eukaryotic cells that package the double helix into dense and compact structures to save space inside the cell; however, (6-4)PPs are exclusively found in the euchromatin region, which is more lightly packed than heterochromatin and contains larger amounts of genes. Since (6-4)PPs have a significantly higher molar absorption coefficient for UVA light than their DNA base counterpart, they can still further react, forming Dewar valence isomers,^{33, 89} which is the result of a pericyclic reaction inside C4 molecule in which an intramolecular 4π electrocyclization of the pyrimidone ring took place after it absorbed the UVA photon. Studies using microorganisms have shown that about 20% of (6-4)PPs are converted into Dewar isomers,⁹⁰ which are considered to be more mutagenic than CPDs.⁹¹ The formation of these two bulky dimers causes distortions in the DNA chains, forming DNA cross-links made of strong C-C covalent bonds between DNA bases, both within a same helix (preventing transcription, blocking polymerases and hindering other metabolic processes) and between bases of two separate strands (effectively fusing the DNA strands together and largely hindering self-replication as well as other essential biofunctions), as represented in Figure 1.15.⁹² These lesions are highly cytotoxic and can give rise to tumorigenic transformation of keratinocytes and chromosomal aberrations.⁹³

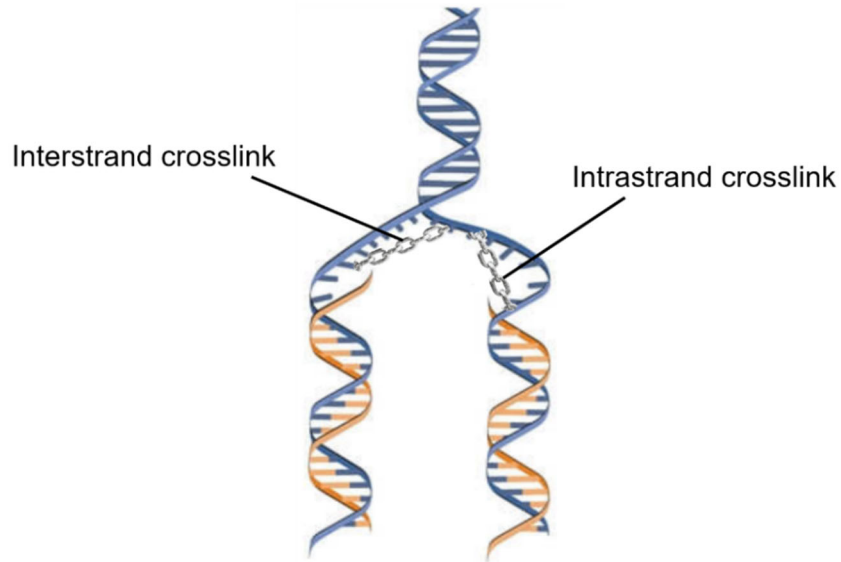


Figure 1.15. Visual representation of DNA cross-linkage.

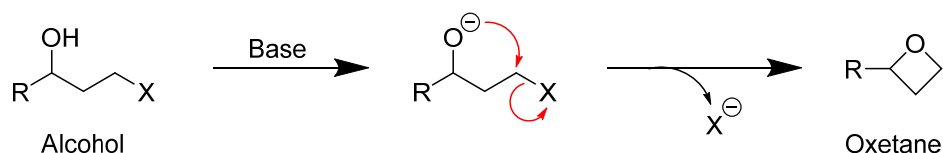
Degradation of melanin may also occur when excessive formation of peroxynitrite (NO_3^-) takes place, formed from the reaction between UVA-induced $\text{O}_2^{\cdot-}$ and nitric oxide radical (NO^{\cdot}), which excites melanin to its triplet excited state, giving it the energy of a UV photon and transferring it to DNA, allowing for CPD creation even after 3 hours in the dark.⁹⁴

2.4. Oxetane synthesis

2.4.1. Chemical pathway

The chemical synthesis of 4-membered ring ethers is relatively difficult compared to 3-, 5- and 6-membered rings due to the ring strain inherent to oxetanes.⁹⁵ So, in order to improve the rate of reaction and have pragmatically useful yields, the use of anions and efficient leaving groups becomes a necessity.

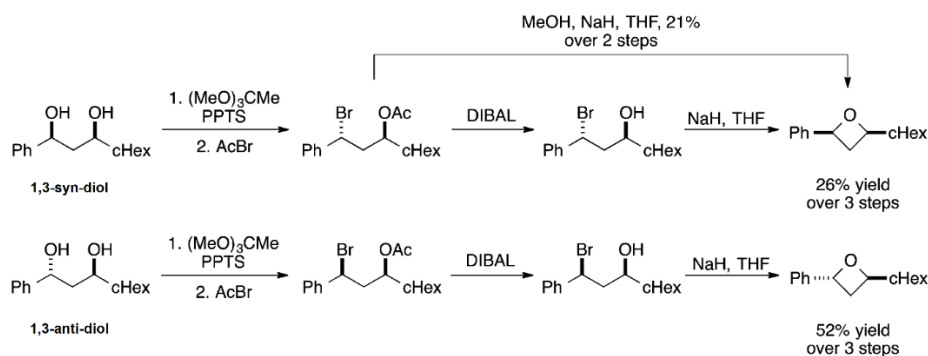
Usually, the C-O bond formation is the first step in intramolecular Williamson etherification reactions; it is a nucleophilic substitution (usually with a halogen) in a basic environment between an aliphatic carbon and a hydroxyl group on a β - position (Scheme 1.10).⁹⁶



Scheme 1.10. Intramolecular Williamson etherification reaction. R: Organic substituent; X: Leaving group.

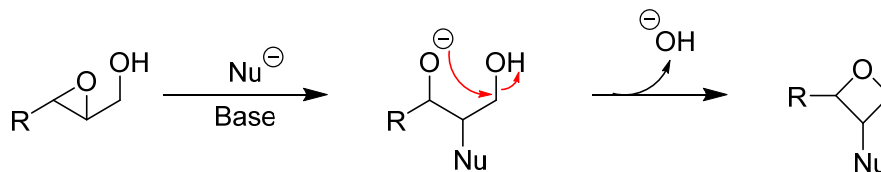
This method, although the most common since 1878,⁹⁷ is relatively inefficient due to the high number of side reactions, such as Grob fragmentation of the haloalkoxide into an alkene and an aldehyde.⁹⁸ An example of a stereocontrolled synthesis following such a method would be one by Nelson *et al.* (Scheme 1.11),⁹⁹ who synthesised *syn*- and *anti*-1,3-diols from a common precursor, and subsequently formed two acetoxybromides with inverse stereochemistry. This was done by conversion to the ortho esters, followed by the addition of acetyl bromide. Diisobutylaluminium hydride (DIBAL) was used to cleave the acetyl group,

and an internal cyclisation was achieved via the use of sodium hydride in tetrahydrofuran (THF). The result was a highly stereoselective process with poor to moderate yields. A one-pot procedure was also developed, in which, instead of DIBAL, one equivalent of methanol was used with an excess of base.



Scheme 1.11. Stereoselective oxetane synthesis with a 1,3-diol. The image was extracted from Bull *et al's* review (2016).²⁵

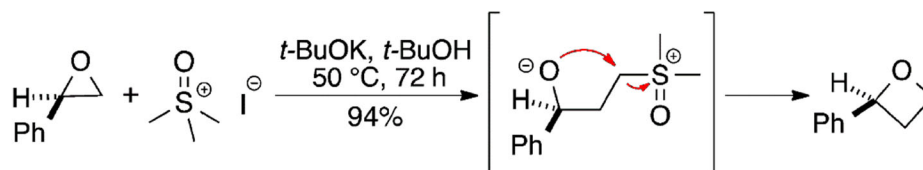
Another method to obtain oxetanes would be the ring-opening of epoxides and subsequent Williamson etherification; usually via the use of epoxy alcohols and nucleophiles (Nu^-) (Scheme 1.12).¹⁰⁰



Scheme 1.12. Synthesis of oxetane from a 2,3-epoxy alcohol.

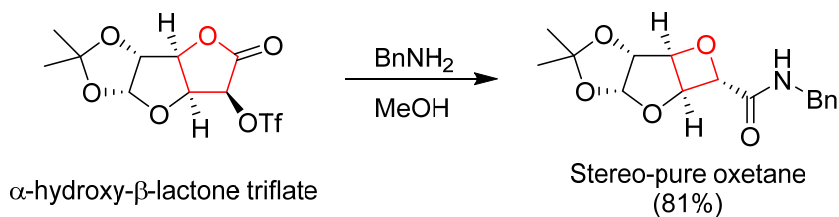
The ring opening can be generated via the addition of sodium bis(2-methoxyethoxy)aluminum dihydride (RedAl) or dimethyl cuprate, followed by $\text{KO}t\text{Bu}$ in THF to induce monotosylation and cyclisation in high yield

and in a one-pot reaction. Ring opening of epoxides can also be induced without the need of an alcohol group by using trimethyloxosulfonium ylide that is generated in situ from its corresponding iodide, which does a nucleophilic attack on the epoxide ring to form an open intermediate, which leads to a cyclisation reaction and the release of dimethyl sulfoxide (Scheme 1.13).¹⁰¹



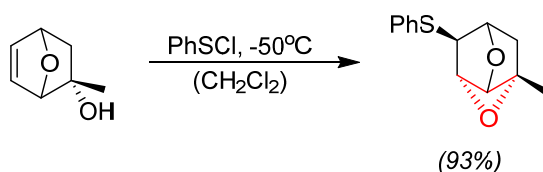
Scheme 1.13. Synthesis of oxetane from epoxide with trimethyloxosulfonium ylide. The image was extracted from Bull *et al.*'s review (2016).²⁵

A relative opposite to the epoxide's ring-opening would be the ring-contraction of a tetrahydrofuran.¹⁰² This procedure is commonly used with saccharides as starting materials for oxetane synthesis, since they commonly possess a 1,3-functionality and can give rise to highly diastereomerically pure four-membered rings.¹⁰³ As an example, Fleet *et al.* (2011)¹⁰⁴ synthesised an oxetane with 100% enantiomeric excess and 81% yield using α -hydroxy- γ -lactone triflate, which itself was prepared from other sugars in methanol (Scheme 1.14). Benzylamine (BnNH₂) performs a nucleophilic attack on the carbonyl of the γ -lactone, causing the ring to open, and finally displacing the triflate and forming the oxetane.



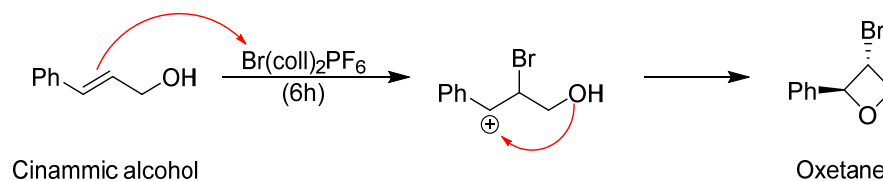
Scheme 1.14. Oxetane synthesis by ring contraction of α -hydroxy- γ -lactone triflate.

In some cases, oxetanes can be synthesised by using electrophiles, as opposed to nucleophiles, intramolecularly if it contains a double-bond in a 1,3-position to a hydroxy group. Arjona *et al.* (1989)¹⁰⁵ used a range of electrophiles containing S and Se on a 7-oxanorbornenic substrate, the most effective being PhSCl in dichloromethane at -50°C , with 93% yield and no by-products (Scheme 1.15).



Scheme 1.15. Electrophilic cyclisation of a 7-oxanorbornenic alcohol to produce an enantiopure oxetane.

As a final note, the author feels pertinent to mention an unusual, yet potentially interesting synthetic method for oxetanes: A 4-endo-trig cyclisation, not much used because of the inherent strain of the transition state. Homsí and Rousseau (1999)¹⁰⁶ achieved this reaction with high stereoselectivity and with 36% yield by using bis(collidine)bromine(I) hexafluorophosphate. The same oxetane was observed for both *E*- and *Z*-alkenes (Scheme 1.16) due to the coupling constant of 6 Hz.



Scheme 1.16. 4-endo-trig cyclisation of a cinammic alcohol. Coll: Collidine.

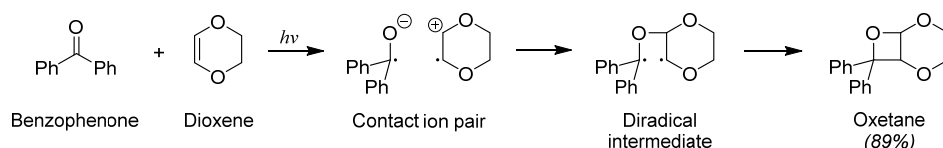
2.4.2. Photochemical pathway (Paternò-Büchi)

Light-induced cyclisation to form oxetanes from excited ketones and olefins was discovered by Emanuele Paternò and George Büchi as far back as 1909,¹⁰⁷ and has increased in popularity ever since.^{17, 108-109}

Although the chemical pathways discussed in the previous section can give rise to high yields and stereoselectivity, the reactions are usually costly, requiring a wide range of toxic organometallic reagents and taking place in many steps. Synthesising oxetanes via a light-induced process might occasionally have relative low yields, but the processes are cheap, single-stepped and chemospecific.

The photo-induced synthesis of oxetanes, i.e. the Paternò-Büchi reaction, is achieved by exposing a solution of a carbonyl compound and an alkene to light, leading to a formal [2+2] cycloaddition reaction. It can take place from the singlet excited state of the carbonyl directly (concerted), or it can undergo ISC to form a triplet, followed by an attack on the alkene to form a 1,4-diradical intermediate,¹¹⁰ and subsequently the oxetane (Scheme 1.17).

Usually, the reaction starts with the excitation of the carbonyl compound to its singlet excited state, followed by ISC to the T_1 excited state. It has been often suggested in literature that the Paternò-Büchi reaction initiates with the formation of the C-O bond, where the single n -electron of the carbonylic O is attracted to the π orbital of the alkene, followed by an unstable diradical intermediate between the two remaining carbons before the cycle is closed.¹¹¹⁻¹¹⁴ The first to show some proof of the existence of this C-C diradical were Peters *et al.* (1981),¹¹⁵ using benzophenone as a chromophore and dioxene to form an oxetane with 89% yield (Scheme 1.19).



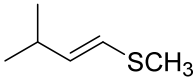
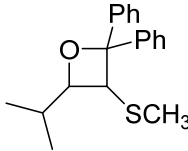
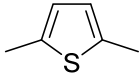
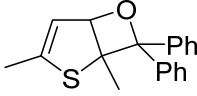
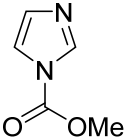
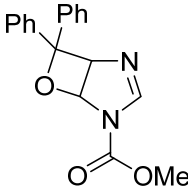
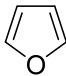
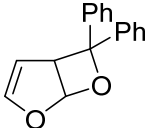
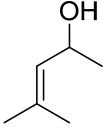
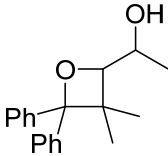
Scheme 1.19. Paternò-Büchi reaction with benzophenone and dioxene via a contact ion pair and a diradical intermediate between oxetane carbon atoms.

They associated the appearance of a new peak in the excited absorption spectrum of the solution at $\lambda_{\text{max}} = 535$ nm after 600 ps to the formation of the diradical intermediate, which showed a shift from the benzophenone λ_{max} of ca. 525 nm. They also suggested a contact ion pair as a precursor to the diradical intermediate.

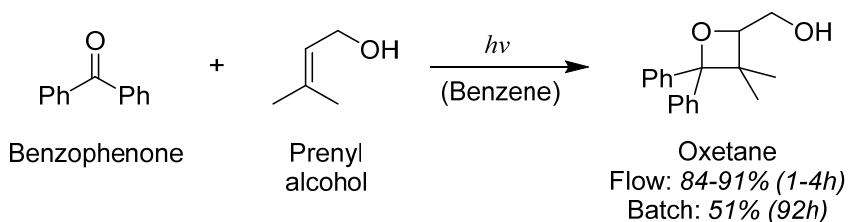
Benzophenone, as mentioned in section 1.4, is a commonly used chromophore for photoinduced oxetane synthesis or as photosensitiser due to its high commercial availability, its well-known photochemical and photophysical properties, and the fact that it possesses both aromatic and carbonylic properties. In medicinal chemistry, BP is often found in natural products with anti-cancer and anti-viral properties.²² Under the appropriate irradiation conditions, BP can react with a wide range of

molecules containing C=C double bonds to form oxetanes by simply putting both reactants in solution; some examples are shown in Table 1.1.¹¹⁶

Table 1.1. Examples of alkenes undergoing the Paternò-Büchi reaction with BP, and their resulting oxetanes.

Alkene	Oxetane
 <p>Alkenyl sulphide</p>	
 <p>2,5-dimethylthiophene</p>	
 <p>N-acetylimidazole</p>	
 <p>Furan</p>	
 <p>Allylic alcohol</p>	

Although photochemical reactions are relatively cheap, highly selective and easy to set-up (they mostly require but a light source and a stirrer), they often give rise to poor yields due to unwanted side-reactions, especially after long irradiation periods. Continuous flow strategies have been used to encourage a more uniform distribution of photons within a solution, which could potentially increase the yield a significant amount, but requires a large quantity of dissolved reactant(s). Ryu *et al.* (2011)¹¹⁷ utilised a microflow photoreaction system to prove this idea, with both a 15 W black light and a 300 W mercury lamp, as well as a batch process, to form an oxetane with benzophenone and prenyl alcohol, getting twice as much yield with the flow compared to the batch process in a fraction of the time (Scheme 1.20).

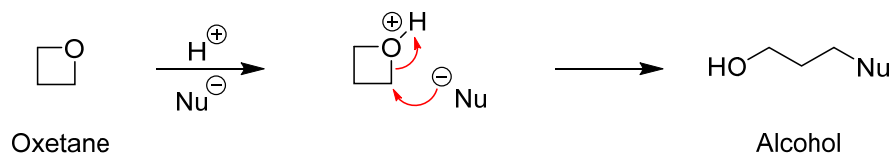


Scheme 1.20. Comparison of the Paternò-Büchi reaction for BP and prenyl alcohol between continuous flow and batch process, showing irradiation times and yields.

2.5. Oxetane breaking

2.5.1. Chemical breakdown

Although the relative chemical stability of the oxetane ring is key in medicinal chemistry, it is still under a high degree of strain (106 kJ/mol, as mentioned in section 2.1) and therefore it is susceptible to further chemical reactions, making oxetanes optimal synthetic intermediates. Simple ring-opening reactions are achieved using nucleophiles under acidic conditions. The O would be protonated, further increasing the strain on the ring, making the C at position 2 (*ortho* to the O) susceptible to nucleophilic attack. Nucleophilic addition would ensue, leading to an alcohol at position 1 and the nucleophile at position 3 (illustrated in Scheme 1.21). If water acted as a nucleophile (Nu⁻), a 1,3-diol would be formed.¹¹⁸

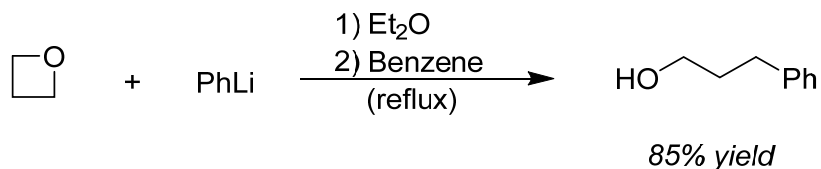


Scheme 1.21. Simple ring-opening of oxetane via nucleophilic attack at position 2 under acidic conditions, forming an alcohol or diol if water is used as a nucleophile.

A wide variety of nucleophiles have been utilised in literature for this purpose, including but not limited to: Amines,¹¹⁹ tetramethylsilane cyanide (TMSCN),¹²⁰ LiAlH₄,¹²¹ azaenolates¹²² and Grignard reagents.¹²³

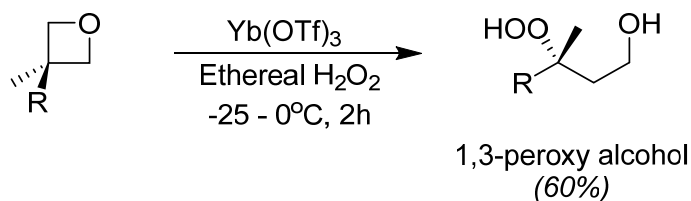
Searles (1951)¹²⁴ tested the reaction of oxetanes with a variety of organometallic reagents, including PhMgBr and *n*-BuLi, in benzene under reflux for 4h, with yields of up to 85% with PhLi (Scheme 1.22). However, if this reaction was carried out with an epoxide instead of an oxetane it

would probably only lead to a deprotonation of a ring H. The reaction at room temperature has also been reported by using CuI (10 mol %) as a catalyst, with yields up to 75%.¹²⁵



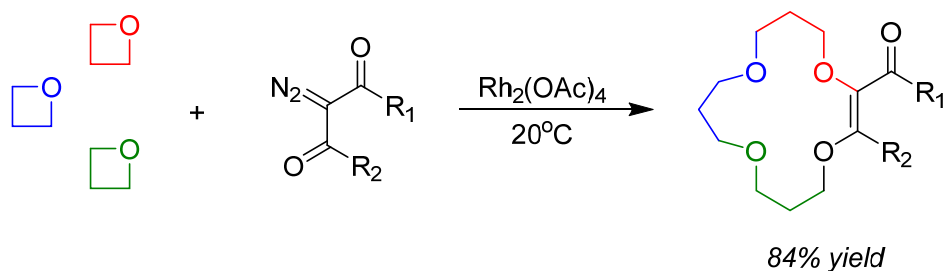
Scheme 1.22. Oxetane ring-opening with phenyl lithium. Adapted from Searles (1951).¹²⁴

The work by Dussault *et al.* (2002)¹⁰⁰ proved that the ring-opening process can be regioselective, by the use of organometallic catalysts, acting as Lewis acids to form 1,3-peroxy alcohols. The oxetanes were placed with ethereal H₂O₂ and a range of organometallic catalysts, with yields of up to 60% with a 0.1 equivalent Yb(OTf)₃ (Scheme 1.23).



Scheme 1.23. Ring-opening of enantioenriched oxetane with the presence of ethereal H₂O₂ and Yb(OTf)₃ as a Lewis acid. R: C₆H₁₃.

Lacour *et al.* (2011)¹²⁶ synthesised a range of 15-membered macrocycles from three oxetane units, using organometallic catalyst Rh₂(OAc)₂ in a 1 mol % quantity to induce a condensation reaction with an α -diazo- β -ketoester, and under mild conditions (20°C), using the oxetanes themselves as a solvent. The resulting yield was up to 84% (see Scheme 1.24).



Scheme 1.24. Macrocyclization reaction of three oxetanes with an α -diazo- β -ketoester.

2.5.2. Enzymatic breakdown

Considering the potentially high photochemical power of sunlight, understanding the mechanistic cycloreversion processes that lead to the photoreactivation of the DNA has gained interest in recent research, since it opens the possibility of creating more efficient artificial attempts to repair the damage in DNA caused by sunlight in the future. Human cells have a wide variety of natural methods to repair the DNA photo-induced damage caused by UV light, or at least make the damage tolerable and not hinder the normal metabolic functions of the cell; in extreme cases, where the damage is irreparable, the cell can be programmed to self-destruct via apoptosis. Human cells possess 5 DNA repair pathways present at different stages of a cell cycle: Base excision repair, mismatch repair, homologous recombination, non-homologous end joining and nucleotide excision repair (NER).^{49, 127} The latter, is the one responsible for the repair of CPDs and (6-4)PPs in humans, as well as other bulky lesions such as benzo[a]-pyrene adducts, or damage caused by chemotherapeutic agents, although (6-4)PPs are repaired at a higher rate than CPDs.

It is nonetheless noteworthy the superior efficiency of the light-induced photorepair mechanisms found in bacteria, plant life, yeasts and insects via the use of DNA photolyases.¹²⁸⁻¹³⁶ Photolyases are activated by UV and blue light after binding to a Flavin cofactor, reducing it to FADH⁻ and subsequently transferring an electron to the photoproduct, which forms a radical anion species that breaks the covalent bond(s) that were bonding the pyrimidine bases together. These enzymes do not give rise to as many mutagenic side reactions due to the reacting electron returning to the Flavin cofactor and hence reactivating the cycle again. While the ring-opening for the CPDs is currently well understood,^{39, 136-139} the same cannot be said for the (6-4)PPs, its break-up mechanism is highly debatable.

The most commonly accepted mechanism for the formation of the (6-4)PPs, as mentioned in section 2.3.2, is via the formation of a highly unstable **oxetane intermediate**, although this has never been experimentally proven due its short lifetime. Similarly, it has been suggested that in the reverse reaction an oxetane might be formed too, following an electron-transfer mechanism from FADH⁻ cofactor.¹⁴⁰ Alternatively, after FADH⁻ absorbs a photon, it can induce a forward electron transfer towards the (6-4)PP, forming an anion radical (6-4)PP^{•-}, followed by a proton donation from histidine 364 (a protein residue from photolyase), resulting in the formation of a neutral radical intermediate (see Figure 1.16) in which the OH “floats” between C5 of the left thymine and the C4 of the right aromatic ring. The C5-O bond is then broken, the histidine recuperates the proton from the alcohol and the C4-C6 undergoes a homolytic fission to give rise to the two separate thymine units and FADH⁻.

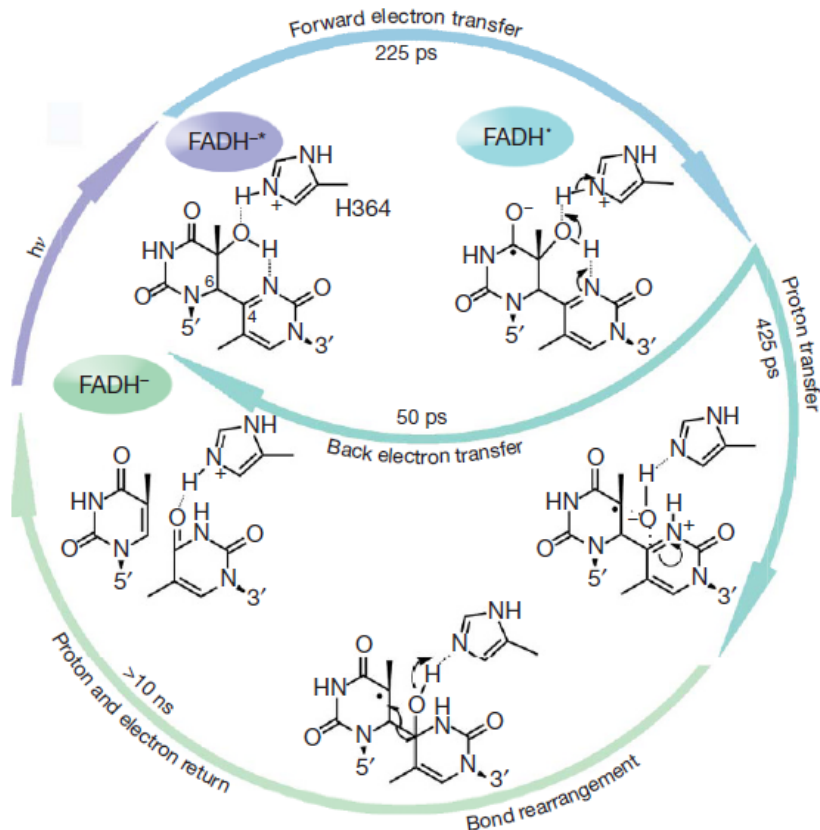
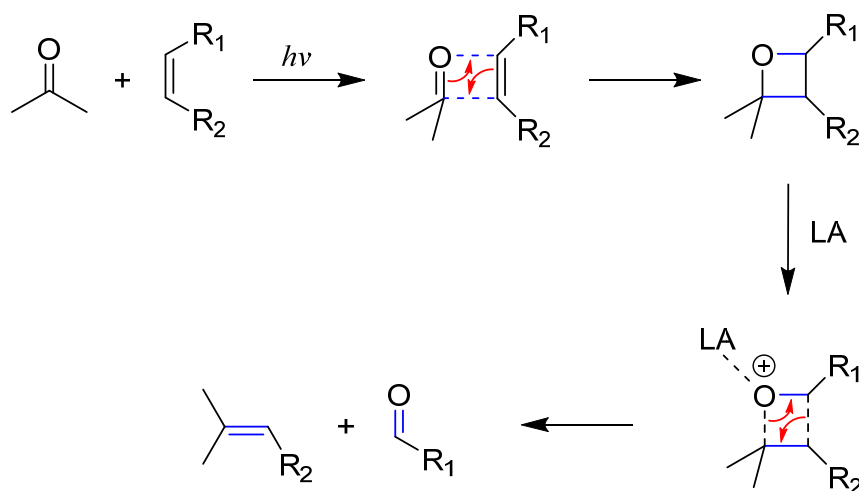


Figure 1.16. Photorepair cycle of (6-4)PP by its corresponding photolyase enzyme. FADH^{•-} acts as a catalytic cofactor and histidine 364 as proton donor. Adapted from Zhong *et al.* (2010).¹⁴⁰

While this process is photophysically inefficient, with a quantum yield of ~ 0.1 due to back electron transfer side reactions, it does enforce a cycloreversion via an oxetane-like transition state, though the exact mechanism for this is currently just speculation, which makes it a subject of interest for the understanding of DNA repair.

2.5.3. Photo-induced carbonyl-olefin metathesis

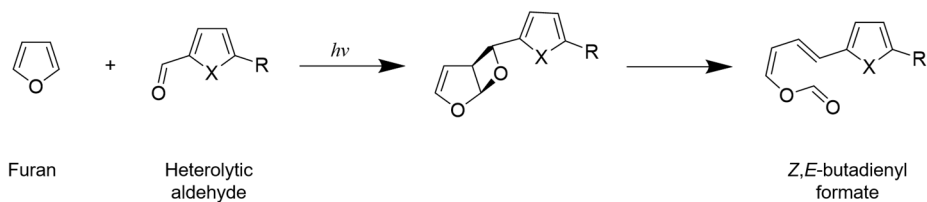
While we have seen the many uses for oxetanes in the fine fields of medicine, the question remains, what's in it for us humble organic chemists? The answer lies in the process of photo-induced carbonyl-olefin metathesis. This is a process that can lead to the formation of a new C=C double-bond via an oxetane intermediate (Paternò-Büchi reaction) and subsequent re-opening (for instance, with the aid of a Lewis acid) in a different fashion, forming two new products (Scheme 1.25).¹⁴¹⁻¹⁴²



Scheme 1.25. Carbonyl-olefin metathesis of a ketone and an alkene, forming a different alkene and an aldehyde. LA: Lewis acid.

Carbon-carbon bond formation is one of the most important stepping stones in synthetic organic chemistry, since they form the back-bone of organic molecules, which is why this process is in high use by modern industry for the synthesis of polymers, pharmaceuticals and agrochemicals, among others. This process opens the possibility for the formation of highly substituted alkenes that are difficult to obtain

otherwise, an example of which would be D'Auria *et al.*'s (2010)¹⁴³ synthesis of *Z,E*-butadienyl formate derivatives from furan and a 2-substituted heterocyclic aldehyde (Scheme 1.26).



Scheme 1.26. A highly enantioselective photo-induced synthesis of a *Z,E*-butadienyl formate derivative from furan and a 2-substituted heterocyclic aldehyde. R: H, Ph or thiophene; X: O or S. Adapted from D'Auria *et al.* (2010).¹⁴³

Although it is still scarcely used in modern organic chemistry, it has great potential due to the fact that it can be carried out in a metal-free mode and can be done at room temperature, and more methods are continuously being researched to make the process more sustainable, selective and cheap.

3. Transient absorption spectroscopy

Since microscopes are out of the question for the analysis of substances that are both too small and too unstable to even observe, highly specialized techniques have been developed for this purpose. Gradually improving in efficiency and accuracy for decades, transient absorption spectroscopy techniques are key for the understanding of most photochemical and photophysical processes, and in the following chapter we shall discuss two of the most important ones in the field: Laser flash photolysis and femtosecond transient absorption spectroscopy.

3.1. *Laser flash photolysis.*

Laser flash photolysis (LFP) is a time-resolved technique designed to create and detect the absorption (or emission) of transient species generated upon excitation with short pulses (of ca. 10 ns).¹⁴⁴ This technique can be used to detect species in their triplet excited state, as well as certain radical species, among others. The laser initially shoots a monochromatic pump beam (previously polarised by the use of specific mirrors and lenses) within the UV or visible spectral range (typically 266, 308, 355 and 532 nm) generating an excited molecule. This species gives rise to a range of several possible transient intermediates that are analysed using a xenon probe beam and subsequently coded into a graph. In general, the observed transients show half-lives in the range of nanoseconds or microseconds, and concentrations of mere μM can be used. The process of how the LFP measurements are taken is illustrated in Figure 1.17.

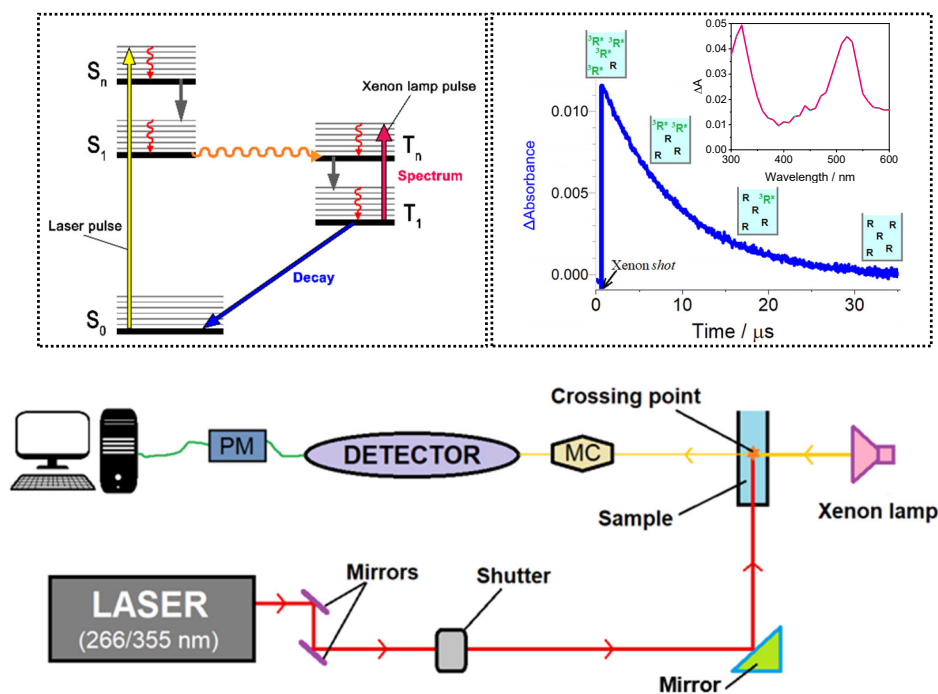


Figure 1.17. (Top left) Jablonski diagram of a molecule being excited using the LFP technique. (Top right) A standard first-order decay transient absorption trace with illustrations of the excited transient species remaining in solution. The y axis represents the molar absorptivity difference between the molecule in the ground state and the transient species formed. (Top right inset) Transient absorption spectrum of BP. (Bottom) A schematic illustration of the Laser Flash Photolysis equipment set-up. Red line: Laser beam; yellow line: Xenon lamp beam; MC: Monochromator; PM: Photomultiplier.

Step 1: The solution at the appropriate absorbance (normally, ca. 0.2-0.5) at the exciting wavelength is placed in a quartz cuvette and properly situated within the LFP equipment.

Step 2: A laser pulse is shot (~ 10 ns) to the sample; therefore, some molecules are excited to their S_n excited state.

Step 3: The laser beam is cut off by the shutter to prevent damage due to excessive irradiation.

Step 4: Intersystem-crossing can occur, so most of the molecules are now in their T_1 excited state.

Step 5: Spectroscopic analysis, which starts before the laser pulse is shot, is connected with the Xe lamp monitoring, before, during and after laser pulse excitation. In this step, it is key that the Xe lamp is perfectly aligned with the excitation beam; the cross-interaction of both beams within the sample would induce the $T_1 \rightarrow T_n$ absorption of the excited molecules. As stated above, other species, such as radicals, etc., can also be formed. Xenon excitation can be monochromatic or polychromatic.

Step 6: Measurements for the transient absorption intensity are begun and the results are coded by the LFP software into a graph. As the T_n excited molecules lose their energy and return to their ground state, the signal becomes less intense over time until it flattens completely.

The graph obtained represents a visual adaptation done by the LFP software to represent the difference in absorption (ΔA) between the molar absorption coefficients of the molecules in their ground state (ϵ_0) and their transient excited species (ϵ_T), which is directly proportional to the concentration of excited molecules in solution, as shown in the equation below at time t (eq. 1).

$$\Delta A_{t=t} = (\epsilon_T - \epsilon_0) \times l \times C_T \quad (\text{eq. 1})$$

Where l is the length of the cuvette.

3.2. Femtosecond transient absorption spectroscopy

LFP is a useful spectroscopic technique, but it has the significant disadvantage of only being able to detect transient species that can live for longer than a few tens of nanoseconds, so what happens if the species we wish to detect is shorter lived than that? How do we identify, let alone analyse, a species that disappears in one quadrillionth of the blink of an eye?

For this purpose, ultrafast time-resolved absorption spectroscopy was invented, capable to efficiently detect excited species at a femtosecond time-scale (10^{-15} of a second). The results that are obtained are similar to those of LFP, but with much shorter time-scales (fs - ps as opposed to ns - μ s).¹⁴⁵⁻¹⁴⁶

Initially, an optical pulse and probe pump are simultaneously shot by an amplified femtosecond laser. The pump beam would go on a more direct path to excite the molecules in solution, while the probe beam would go through a different path, reflecting on some specific mirrors into a delay line, within an adjustable distance from the mirrors. The longer the distance that the probe beam has to travel before reaching the pump beam and the sample, the larger the optical delay, and hence, the longer the time-scale that is monitored by the detection system (Figure 1.18). The equipment software makes a transient absorption spectrum at different delay-times (from hundreds of fs to ps and ns), which is like a “snapshot” of the current solution.

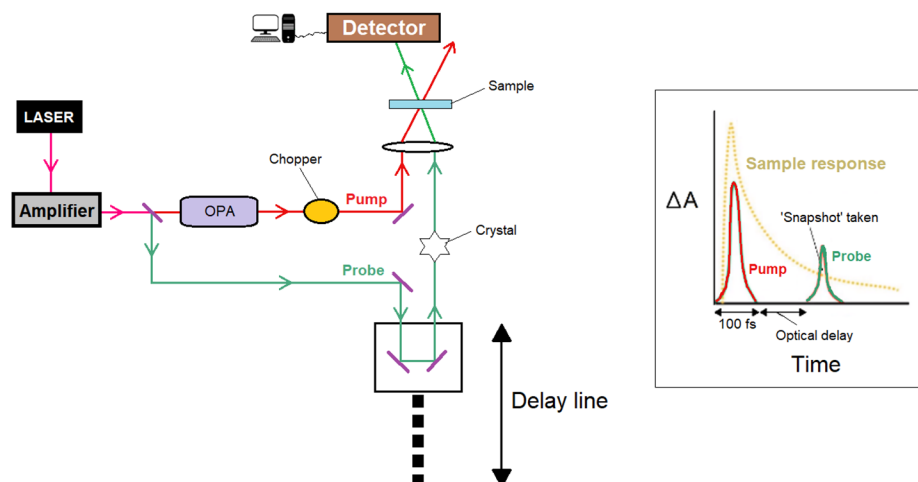


Figure 1.18. Inner workings of the femtosecond laser equipment. OPA: Optical parametric amplifier.

The probe pulse shot is of sufficiently low intensity so as to avoid multiphoton processes to take place while probing, and it is done so with a delay time towards the pump pulse (in the case of our particular set-up, from *ca.* 100 fs up to 8 ns). The difference in absorption between the excited molecule and the ground state is measured (ΔA), and the spectrum contains the contributions from a range of processes:

Ground state bleach: A negative signal in the ground state absorption region, since after excitation the concentration of ground state molecules in solution decreases.

Stimulated emission: When the excited state is populated, stimulated emission will occur when the probe beam reaches the excited molecules, and only for optically allowed transitions. The spectral profile would be similar to the fluorescence spectrum of the excited state.

Excited-state absorption: A positive signal is observed in the wavelength region in which the excited molecules absorb the probe photons.

Product absorption: A positive signal can be observed corresponding to a product formed after irradiation that isn't the excited state substance itself.

4. Relevant predecessors

As the reader might have intuitively deduced, none of this thesis's work comes from a vacuum, but it is standing on the shoulders of those who came before. In the world of scientists, the life of a student is never over, one must continue to study, learn and progress, to build up from the foundations of previous works and improve them, refine them, perfect them. And this thesis is no exception, the main objective being the understanding of the formation and reverse Paternò-Büchi reaction of pyrimidine base-benzophenone oxetanes. To achieve this, it is necessary to study in detail the photo-induced formation and ring-opening of the theoretical oxetane intermediates that are supposed to arise during the (6-4)PP repair reactions. Therefore, we have found in previous works the synthesis of more stable analogous oxetanes that show similar photochemical properties to this (6-4)PP precursor when irradiated with UV light; the most common analogue is that which includes a pyrimidine-derived base (thymine, uracil or cytosine) and a benzophenone-like substance as a chromophore (Figure 1.19).¹⁴⁷⁻¹⁵⁴

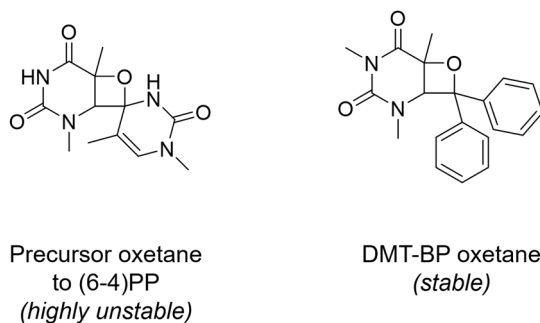


Figure 1.19. (Left) Highly unstable oxetane which is supposed to be the precursor of the (6-4)PP. (Right) More stable analogue oxetane composed of 1,3-dimethyl thymine (DMT) and benzophenone (BP).

The synthesis of the analogue is relatively simple, merely requiring a mixed solution of 0.1 M of the methylated pyrimidine base and 0.2 M of benzophenone in nitrogen-purged acetonitrile, followed by 6-8 h of vigorous stirring under UV irradiation. Two pure oxetane isomers will be formed (Figure 1.20), and can be purified via simple silica gel chromatography.

Song *et al.* (2006)¹⁴⁹⁻¹⁵⁰ and Vendrell-Criado *et al.* (2016)¹⁵⁵ synthesised a range of pyrimidine base-benzophenone oxetane analogues with different substituents for their own projects, irradiating with a 125 W high pressure Hg-lamp (>290 nm) or a multi-lamp photoreactor ($\lambda_{\text{max}} = 350$ nm), respectively. For this thesis, some of these analogues, in addition to others that have been designed, were adopted in this thesis for LFP and ultrafast transient absorption spectroscopy analysis.

Belmadoui *et al.* (2006)¹⁵⁶ designed a dyad of thymidine and (S)- α -ketoprofen to study the nucleic acid-excited drug interaction, linking the chromophore and the DNA base via a saccharide link 7 atoms long, and after irradiation, four oxetanes were formed via a highly stereospecific Paternò-Büchi cyclisation reaction. Belmadoui reported that the photochemical cycloreversion of said oxetanes was an **adiabatic process**, meaning it gave rise to triplet excited state ketoprofen with a high quantum yield and little energy being lost in unwanted fashions. This fact was further explored for this thesis, as will be seen in chapter 2.

Falvey *et al.* (2001)¹⁴⁷ were one of the first to test the photolysis of the DMT-BP oxetane analogue (Figure 1.19) using LFP techniques, and the first to show it was a clean adiabatic reaction that produced DMT and excited BP with no side-products.

Philips *et al.* (2008)¹⁵⁷ used ultrafast transient absorption spectroscopy purposed to further study the photo-induced ring-opening mechanism of the aforementioned oxetane. He used this resource to suggest that a C-C diradical intermediate in its singlet excited state had been formed. It would later break into DMT in its ground state, and BP in its singlet excited state ($^1\text{BP}^*$), followed by ISC to its triplet excited state ($^3\text{BP}^*$), which is the species detected by transient absorption spectroscopy.

It is worth mentioning that previous studies of the photolysis of the DMT-BP oxetane have focused simply on one of the regioisomers, the “head-to-head” (HH-1) one but not the “head-to-tail” (HT-1) (Figure 1.20), and that the ultrafast spectroscopic studies are rather limited. In this thesis, we worked on expanding these studies and reporting our findings.

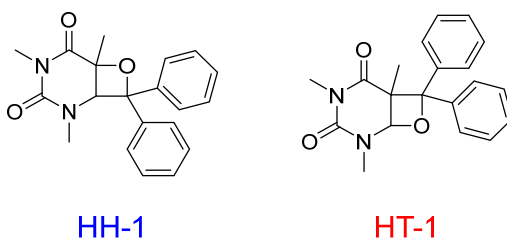


Figure 1.20. Chemical structure of the head-to-head (HH) and head-to-tail (HT) DMT-BP oxetanes.

5. References

1. Dantas, J. A.; Correia, J. T. M.; Paixão, M. W.; Corrêa, A. G., Photochemistry of carbonyl compounds: Application in metal-free reactions. *ChemPhotoChem* **2019**, *3*, 506-520.
2. Sideri, I. K.; Voutyritsa, E.; Kokotos, C. G., Photoorganocatalysis, small organic molecules and light in the service of organic synthesis: The awakening of a sleeping giant. *Org. Biomol. Chem.* **2018**, *16*, 4596-4614.
3. Liu, Y. Y.; Liu, J.; Lu, L. Q.; Xiao, W. J., Organocatalysis combined with photocatalysis. *Top. Curr. Chem.* **2019**, *377*, 37-52.
4. Ouellette, R. J.; Rawn, J. D., Aldehydes and ketones. In *Org. Chem.* **2018**; pp 561-594.
5. Sivaguru, P.; Wang, Z.; Zanoni, G.; Bi, X., Cleavage of carbon-carbon bonds by radical reactions. *Chem. Soc. Rev.* **2019**, *48*, 2615-2656.
6. Wagner, P. J.; Chen, C. P., Rotation-controlled excited-state reaction - photoenolization of ortho-alkyl phenyl ketones. *J. Am. Chem. Soc.* **1976**, *98*, 239-241.
7. Oelgemoller, M.; Hoffmann, N., Studies in organic and physical photochemistry - an interdisciplinary approach. *Org. Biomol. Chem.* **2016**, *14*, 7392-7442.
8. Chen, C., The past, present, and future of the Yang reaction. *Org. Biomol. Chem.* **2016**, *14*, 8641-8647.
9. Xia, J. B.; Zhu, C.; Chen, C., Visible light-promoted metal-free C-H activation: Diarylketone-catalyzed selective benzylic mono- and difluorination. *J. Am. Chem. Soc.* **2013**, *135*, 17494-17500.

10. Watson, M. D.; Fechtenkötter, A.; Müllen, K., Big is beautiful-“aromaticity” revisited from the viewpoint of macromolecular and supramolecular benzene chemistry. *Chem. Rev.* **2001**, *101*, 1267-1300.
11. Casanova, D.; Alemany, P., Quantifying the symmetry content of the electronic structure of molecules: Molecular orbitals and the wave function. *Phys. Chem. Chem. Phys.* **2010**, *12*, 15523-15529.
12. Turro, N. J.; Ramamurthy, V.; Scaiano, J. C., *Modern molecular photochemistry of organic molecules*. First India Edition; Viva books private limited: India, **2017**; p 1084.
13. Liu, W.; Li, J.; Huang, C. Y.; Li, C. J., Aromatic chemistry in the excited state: Facilitating metal-free substitutions and cross-couplings. *Angew. Chem. Int. Ed.* **2020**, *59*, 1786-1796.
14. Marazzi, M.; Mai, S.; Roca-Sanjuan, D.; Delcey, M. G.; Lindh, R.; Gonzalez, L.; Monari, A., Benzophenone ultrafast triplet population: Revisiting the kinetic model by surface-hopping dynamics. *J. Phys. Chem. Lett.* **2016**, *7*, 622-626.
15. Dumont, E.; Wibowo, M.; Roca-Sanjuan, D.; Garavelli, M.; Assfeld, X.; Monari, A., Resolving the benzophenone DNA-photosensitization mechanism at QM/MM level. *J. Phys. Chem. Lett.* **2015**, *6*, 576-580.
16. Sergentu, D. C.; Maurice, R.; Havenith, R. W.; Broer, R.; Roca-Sanjuan, D., Computational determination of the dominant triplet population mechanism in photoexcited benzophenone. *Phys. Chem. Chem. Phys.* **2014**, *16*, 25393-25403.
17. Liu, X. L.; Wang, J. B.; Tong, Y.; Song, Q. H., Regioselectivity and competition of the Paterno-Buchi reaction and triplet-triplet energy

transfer between triplet benzophenones and pyrimidines: Control by triplet energy levels. *Chem. Eur. J.* **2013**, *19*, 13216-13223.

18. Nguyen, T. X.; Kattnig, D.; Mansha, A.; Grampp, G.; Yurkovskaya, A. V.; Lukzen, N., Kinetics of photoinduced electron transfer between DNA bases and triplet 3,3',4,4'-benzophenone tetracarboxylic acid in aqueous solution of different pH's: Proton-coupled electron transfer? *J. Phys. Chem. A* **2012**, *116*, 10668-10675.

19. Bonancía, P.; Jiménez, M. C.; Miranda, M. A., Transient absorption spectroscopy detection of sensitized delayed fluorescence in chiral benzophenone/naphthalene systems. *Chem. Phys. Lett.* **2011**, *515*, 194-196.

20. Perez-Ruiz, R.; Groeneveld, M.; van Stokkum, I. H. M.; Tormos, R.; Williams, R. M.; Miranda, M. A., Fast transient absorption spectroscopy of the early events in photoexcited chiral benzophenone–naphthalene dyads. *Chem. Phys. Lett.* **2006**, *429*, 276-281.

21. Castro, G. T.; Blanco, S. E.; Giordano, O. S., UV Spectral properties of benzophenone. Influence of solvents and substituents. *Molecules* **2000**, *5*, 424-425.

22. Surana, K.; Chaudhary, B.; Diwaker, M.; Sharma, S., Benzophenone: A ubiquitous scaffold in medicinal chemistry. *Med. Chem. Commun.* **2018**, *9*, 1803-1817.

23. Ciamician, G.; Silber, P., Vorläufige benachrichtigung. *Chem. Ber.* **1900**, *33*, 2911-2913.

24. Favaro, G.; Ortica, F.; Romani, A., Role of heteroaromatic cycles in the inter- and intra-molecular dynamics of excited aryl ketones. *J. Photochem. Photobiol. C* **2013**, *16*, 22-45.

25. Bull, J. A.; Croft, R. A.; Davis, O. A.; Doran, R.; Morgan, K. F., Oxetanes: Recent advances in synthesis, reactivity, and medicinal chemistry. *Chem. Rev.* **2016**, *116*, 12150-12233.
26. Luger, P.; Buschmann, J., Oxetane: The first X-ray analysis of a nonsubstituted four-membered ring. *J. Am. Chem. Soc.* **1984**, *106*, 7118-7121.
27. Friedman, M. D.; Lacouture, M.; Dang, C., Dermatologic adverse events associated with use of adjuvant lapatinib in combination with paclitaxel and trastuzumab for HER2-positive breast cancer: A case series analysis. *Clin. Breast Cancer* **2016**, *16*, 69-74.
28. Wani, M. C.; Taylor, H. L.; Wall, M. E.; Coggon, P.; McPhail, A. T., Plant antitumor agents. VI. Isolation and structure of taxol, a novel antileukemic and antitumor agent from *Taxus brevifolia*. *J. Am. Chem. Soc.* **1971**, *93*, 2325-2327.
29. Shimada, N.; Hasegawa, S.; Harada, T.; Tomisawa, T.; Fujii, A.; Takita, T., Oxetanocin, a novel nucleoside from bacteria. *J. Antibiot.* **1986**, *39*, 1623-1625.
30. Omura, S.; Murata, M.; Imamura, N.; Iwai, Y.; Tanaka, H., Oxetin, a new antimetabolite from an actinomycete - fermentation, isolation, structure and biological-activity *J. Antibiot.* **1984**, *37*, 1324-1332.
31. Huang, J. M.; Yokoyama, R.; Yang, C. S.; Fukuyama, Y., Merrilactone A, a novel neurotrophic sesquiterpene dilactone from *Illicium merrillianum*. *Tetrahedron Lett.* **2000**, *41*, 6111-6114.
32. Taylor, J. S., Unraveling the molecular pathway from sunlight to skin cancer. *Acc. Chem. Res.* **1994**, *27*, 76-82.

33. Schuch, A. P.; Moreno, N. C.; Schuch, N. J.; Menck, C. F. M.; Garcia, C. C. M., Sunlight damage to cellular DNA: Focus on oxidatively generated lesions. *Free Radic. Biol. Med.* **2017**, *107*, 110-124.
34. Bosch, R.; Philips, N.; Suarez-Perez, J. A.; Juarranz, A.; Devmurari, A.; Chalensouk-Khaosaat, J.; Gonzalez, S., Mechanisms of photoaging and cutaneous photocarcinogenesis, and photoprotective strategies with phytochemicals. *Antioxidants (Basel)* **2015**, *4*, 248-268.
35. Cadet, J.; Sage, E.; Douki, T., Ultraviolet radiation-mediated damage to cellular DNA. *Mutat. Res.* **2005**, *571*, 3-17.
36. Batista, L. F.; Kaina, B.; Meneghini, R.; Menck, C. F., How DNA lesions are turned into powerful killing structures: Insights from UV-induced apoptosis. *Mutat. Res.* **2009**, *681*, 197-208.
37. Shindo, Y.; Hashimoto, T., Ultraviolet B-induced cell death in four cutaneous cell lines exhibiting different enzymatic antioxidant defences: Involvement of apoptosis. *J. Derm. Sci.* **1998**, *17*, 140-150.
38. Gimenez, E.; Manzano-Agugliaro, F., DNA damage repair system in plants: A worldwide research update. *Genes (Basel)* **2017**, *8*, 299-316.
39. Chatterjee, N.; Walker, G. C., Mechanisms of DNA damage, repair, and mutagenesis. *Environ. Mol. Mutagen.* **2017**, *58*, 235-263.
40. Yu, S. L.; Lee, S. K., Ultraviolet radiation: DNA damage, repair, and human disorders. *Mol. Cell. Toxicol.* **2017**, *13*, 21-28.
41. Markovitsi, D., UV-induced DNA damage: The role of electronic excited states. *Photochem. Photobiol.* **2016**, *92*, 45-51.
42. Markovitsi, D.; Sage, E.; Lewis, F. D.; Davies, J., Interaction of UV radiation with DNA. *Photochem. Photobiol. Sci.* **2013**, *12*, 1256-1258.

43. De La Harpe, K.; Kohler, B., Observation of long-lived excited states in DNA oligonucleotides with significant base sequence disorder. *J. Phys. Chem. Lett.* **2011**, *2*, 133-138.
44. Rastogi, R. P.; Richa; Kumar, A.; Tyagi, M. B.; Sinha, R. P., Molecular mechanisms of ultraviolet radiation-induced DNA damage and repair. *J. Nucleic Acids* **2010**, *2010*, 1-32.
45. Markovitsi, D.; Gustavsson, T.; Banyasz, A., Absorption of UV radiation by DNA: Spatial and temporal features. *Mutat. Res.* **2010**, *704*, 21-28.
46. Kohler, B., Nonradiative decay mechanisms in DNA model systems. *J. Phys. Chem. Lett.* **2010**, *1*, 2047-2053.
47. Mendez-Hurtado, J.; Lopez, R.; Suarez, D.; Menendez, M. I., Theoretical study of the oxidation of histidine by singlet oxygen. *Chem. Eur. J.* **2012**, *18*, 8437-8447.
48. Cadet, J.; Douki, T.; Ravanat, J. L., Oxidatively generated damage to cellular DNA by UVB and UVA radiation. *Photochem. Photobiol.* **2015**, *91*, 140-155.
49. Karran, P.; Brem, R., Protein oxidation, UVA and human DNA repair. *DNA Repair* **2016**, *44*, 178-185.
50. Cadet, J.; Mouret, S.; Ravanat, J. L.; Douki, T., Photoinduced damage to cellular DNA: Direct and photosensitized reactions. *Photochem. Photobiol.* **2012**, *88*, 1048-1065.
51. Lucas, R. M.; Norval, M.; Neale, R. E.; Young, A. R.; De Gruijl, F. R.; Takizawa, Y.; van der Leun, J. C., The consequences for human

health of stratospheric ozone depletion in association with other environmental factors. *Photochem. Photobiol. Sci.* **2015**, *14*, 53-87.

52. Leiter, U.; Keim, U.; Eigentler, T.; Katalinic, A.; Holleczek, B.; Martus, P.; Garbe, C., Incidence, mortality, and trends of nonmelanoma skin cancer in Germany. *J. Invest. Dermatol.* **2017**, *137*, 1860-1867.

53. El Ghissassi, F.; Baan, R.; Straif, K.; Grosse, Y.; Secretan, B.; Bouvard, V.; Benbrahim-Tallaa, L.; Guha, N.; Freeman, C.; Galichet, L.; Coglianò, V., Special report: Policy. A review of human carcinogens-part D: Radiation. *Lancet Oncol.* **2009**, *10*, 751-752.

54. Knoch, J.; Kamenisch, Y.; Kubisch, C.; Berneburg, M., Rare hereditary diseases with defects in DNA-repair. *Eur. J. Dermatol.* **2012**, *22*, 443-455.

55. Fujiki, H., Gist of Dr. Katsusaburo Yamagiwa's papers entitled "Experimental study on the pathogenesis of epithelial tumors" (I to VI reports). *Cancer Sci.* **2014**, *105*, 143-149.

56. Menck, C. F. M.; Munford, V., DNA repair diseases: What do they tell us about cancer and aging? *Genet. Mol. Biol.* **2014**, *37*, 220-233.

57. Tringali, G.; Sampaolese, B.; Clementi, M. E., Expression of early and late cellular damage markers by ARPE-19 cells following prolonged treatment with UV-A radiation. *Mol. Med. Rep.* **2016**, *14*, 3485-3489.

58. Hickson, I.; Zhao, Y.; Richardson, C. J.; Green, S. J.; Martin, N. M. B.; Orr, A. I.; Reaper, P. M.; Jackson, S. P.; Curtin, N. J.; Smith, G. C. M., Identification and characterization of a novel and specific inhibitor of the ataxia-telangiectasia mutated kinase ATM. *Cancer Res.* **2004**, *64*, 9152-9159.

59. Dalziel, K. L., Aspects of cutaneous ageing. *Clin. Exp. Derm.* **1991**, *16*, 315-323.
60. Black, J. O., Xeroderma Pigmentosum. *Head Neck Pathol.* **2016**, *10*, 139-144.
61. Martelijn, J. A.; Lans, H.; Vermeulen, W.; Hoeijmakers, J. H., Understanding nucleotide excision repair and its roles in cancer and ageing. *Nat. Rev. Mol. Cell Biol.* **2014**, *15*, 465-481.
62. Debacq-Chainiaux, F.; Borlon, C.; Pascal, T.; Royer, V.; Eliaers, F.; Ninane, N.; Carrard, G.; Friguet, B.; de Longueville, F.; Boffe, S.; Remacle, J.; Toussaint, O., Repeated exposure of human skin fibroblasts to UVB at subcytotoxic level triggers premature senescence through the TGF-beta1 signaling pathway. *J. Cell Sci.* **2005**, *118*, 743-758.
63. Que, S. K. T.; Zwald, F. O.; Schmults, C. D., Cutaneous squamous cell carcinoma: Incidence, risk factors, diagnosis, and staging. *J. Am. Acad. Dermatol.* **2018**, *78*, 237-247.
64. Barona-Castano, J. C.; Carmona-Vargas, C. C.; Brocksom, T. J.; de Oliveira, K. T., Porphyrins as catalysts in scalable organic reactions. *Molecules* **2016**, *21*, 310-337.
65. Kvam, E.; Tyrrell, R. M., Artificial background and induced levels of oxidative base damage in DNA from human cells. *Carcinogenesis* **1997**, *18*, 2281-2283.
66. Hoebeke, M.; Schuitmaker, H. J.; Jannink, L. E.; Dubbelman, T. M. A. R.; Jakobs, A.; Van de Vorst, A., Electron spin resonance evidence of the generation of superoxide anion, hydroxyl radical and singlet oxygen during the photohemolysis of human erythrocytes with bacteriochlorin a. *Photochem. Photobiol.* **1997**, *66*, 502-508.

67. Foote, C. S., Definition of type-I and type-II photosensitized oxidation. *Photochem. Photobiol.* **1991**, *54*, 659-659.
68. Terao, J.; Minami, Y.; Bando, N., Singlet molecular oxygen-quenching activity of carotenoids: Relevance to protection of the skin from photoaging. *J. Clin. Biochem. Nutr.* **2011**, *48*, 57-62.
69. Blair, I. A., DNA adducts with lipid peroxidation products. *J. Biol. Chem.* **2008**, *283*, 15545-15549.
70. Shukla, P. K.; Mishra, P. C., H₂O₃ as a reactive oxygen species: Formation of 8-oxoguanine from its reaction with guanine. *J. Phys. Chem. B.* **2007**, *111*, 4603-4615.
71. Evans, M. D.; Dizdaroglu, M.; Cooke, M. S., Oxidative DNA damage and disease: Induction, repair and significance. *Mutat. Res.* **2004**, *567*, 1-61.
72. Cadet, J.; Douki, T.; Ravanat, J. L., Oxidatively generated damage to the guanine moiety of DNA: Mechanistic aspects and formation in cells. *Acc. Chem. Res.* **2008**, *41*, 1075-1083.
73. Yamaba, H.; Haba, M.; Kunita, M.; Sakaida, T.; Tanaka, H.; Yashiro, Y.; Nakata, S., Morphological change of skin fibroblasts induced by UV Irradiation is involved in photoaging. *Exp. Dermatol.* **2016**, *25*, 45-51.
74. Mouret, S.; Baudouin, C.; Charveron, M.; Favier, A.; Cadet, J.; Douki, T., Cyclobutane pyrimidine dimers are predominant DNA lesions in whole human skin exposed to UVA radiation. *Proc. Natl. Acad. Sci. USA* **2006**, *103*, 13765-13770.

75. Fraga-Timiraos, A. B.; Lhiaubet-Vallet, V.; Miranda, M. A., Repair of a dimeric azetidine related to the thymine-cytosine (6-4) photoproduct by electron transfer photoreduction. *Angew. Chem. Int. Ed.* **2016**, *55*, 6037-6040.
76. Cadet, J.; Douki, T.; Pouget, J. P.; Ravanat, J. L., UVB and UVA induced formation of photoproducts within cellular DNA. In *From DNA photolesions to mutations, skin cancer and cell death*, Sage, E.; Drouin, R.; Rouabhia, M., Eds. Royal Society of Chemistry: **2007**; pp 1-14.
77. Cadet, J.; Grand, A.; Douki, T., Solar UV radiation-induced DNA bipyrimidine photoproducts: Formation and mechanistic insights. *Top. Curr. Chem.* **2015**, *356*, 249-275.
78. Pilles, B. M.; Bucher, D. B.; Liu, L.; Clivio, P.; Gilch, P.; Zinth, W.; Schreier, W. J., Mechanism of the decay of thymine triplets in DNA single strands. *J. Phys. Chem. Lett.* **2014**, *5*, 1616-1622.
79. Cuquerella, M. C.; Lhiaubet-Vallet, V.; Bosca, F.; Miranda, M. A., Photosensitized pyrimidine dimerisation in DNA. *Chem. Sci.* **2011**, *2*, 1219-1232.
80. Climent, T.; González-Ramírez, I.; González-Luque, R.; Merchán, M.; Serrano-Andrés, L., Cyclobutane pyrimidine photodimerization of DNA/RNA nucleobases in the triplet state. *J. Phys. Chem. Lett.* **2010**, *1*, 2072-2076.
81. Schreier, W. J.; Kubon, J.; Regner, N.; Haiser, K.; Schrader, T. E.; Zinth, W.; Clivio, P.; Gilch, P., Thymine dimerization in DNA model systems: Cyclobutane photolesion is predominantly formed via the singlet channel. *J. Am. Chem. Soc.* **2009**, *131*, 5038-5039.

82. Asgatay, S.; Petermann, C.; Harakat, D.; Guillaume, D.; Taylor, J. S.; Clivio, P., Evidence that the (6-4) photolyase mechanism can proceed through an oxetane intermediate. *J. Am. Chem. Soc.* **2008**, *130*, 12618-12619.
83. Hitomi, K.; Nakamura, H.; Kim, S. T.; Mizukoshi, T.; Ishikawa, T.; Iwai, S.; Todo, T., Role of two histidines in the (6-4) photolyase reaction. *J. Biol. Chem.* **2001**, *276*, 10103-10109.
84. Varghese, A. J.; Wang, S. Y., Thymine-thymine adduct as a photoproduct of thymine. *Science* **1968**, *160*, 186-187.
85. Joseph, A.; Prakash, G.; Falvey, D. E., Model studies of the (6-4) photoproduct photolyase enzyme: Laser flash photolysis experiments confirm radical ion intermediates in the sensitized repair of thymine oxetane adducts. *J. Am. Chem. Soc.* **2000**, *122*, 11219-11225.
86. Rahn, R. O.; Hosszu, J. L., Photochemical studies of thymine in ice. *Photochem. Photobiol.* **1969**, *10*, 131-137.
87. Clivio, P.; Fourrey, J. L.; Gasche, J.; Favre, A., DNA photodamage mechanistic studies: Characterization of a thietane intermediate in a model reaction relevant to "6-4 lesions". *J. Am. Chem. Soc.* **1991**, *113*, 5481-5483.
88. Wang, Y.; Gaspar, P. P.; Taylor, J. S., Quantum chemical study of the electron-transfer-catalyzed splitting of oxetane and azetidene intermediates proposed in the photoenzymatic repair of (6-4) photoproducts of DNA. *J. Am. Chem. Soc.* **2000**, *122*, 5510-5519.
89. Liu, J.; Taylor, J. S., Remarkable photoreversal of a thio analog of the Dewar valence isomer of the (6-4) photoproduct of DNA to the parent nucleotides. *J. Am. Chem. Soc.* **1996**, *118*, 3287-3288.

90. Meador, J. A.; Baldwin, A. J.; Pakulski, J. D.; Jeffrey, W. H.; Mitchell, D. L.; Douki, T., The significance of the Dewar valence photoisomer as a UV radiation-induced DNA photoproduct in marine microbial communities. *Environ. Microbiol.* **2014**, *16*, 1808-1820.
91. Douki, T.; Sage, E., Dewar valence isomers, the third type of environmentally relevant DNA photoproducts induced by solar radiation. *Photochem. Photobiol. Sci.* **2016**, *15*, 24-30.
92. Cadet, J.; Anselmino, C.; Douki, T.; Voituriez, L., Photochemistry of nucleic acids in cells. *J. Photochem. Photobiol. B* **1992**, *15*, 277-298.
93. Wischermann, K.; Popp, S.; Moshir, S.; Scharfetter-Kochanek, K.; Wlaschek, M.; de Gruijl, F.; Hartschuh, W.; Greinert, R.; Volkmer, B.; Faust, A.; Rapp, A.; Schmezer, P.; Boukamp, P., UVA radiation causes DNA strand breaks, chromosomal aberrations and tumorigenic transformation in HaCaT skin keratinocytes. *Oncogene* **2008**, *27*, 4269-4280.
94. Premi, S.; Wallisch, S.; Mano, C. M.; Weiner, A. B.; Bacchiocchi, A.; Wakamatsu, K.; Bechara, E. J.; Halaban, R.; Douki, T.; Brash, D. E., Chemiexcitation of melanin derivatives induces DNA photoproducts long after UV exposure. *Science* **2015**, *347*, 842-847.
95. Di Martino, A.; Galli, C.; Gargano, P.; Mandolini, L., Ring-closure reactions. Part 23. Kinetics of formation of three- to seven-membered-ring N-tosylazacycloalkanes. The role of ring strain in small- and common-sized-ring formation. *J. Chem. Soc. Perkin Trans.* **1985**, 1345-1349.
96. Searles, S.; Nickerson, R. G.; Witsiepe, W. K., Oxetanes. IX. Structural and solvent effects in the reaction of γ -bromoalcohols with base. *J. Org. Chem.* **1959**, *24*, 1839-1844.

97. Reboul, M., Oxede de Propylene Normal et Poluoxypropylenes. *Ann. Chim. (Paris)* **1878**, *14*, 495-497.
98. Prantz, K.; Mulzer, J., Synthetic applications of the carbonyl generating grob fragmentation. *Chem. Rev.* **2010**, *110*, 3741–3766.
99. Aftab, T.; Carter, C.; Hart, J.; A., N., A method for the stereospecific conversion of 1,3-diols into oxetanes. *Tetrahedron Lett.* **1999**, *40*, 8679-8683.
100. Dussault, P. H.; Trullinger, T. K.; Noor-e-Ain, F., Opening of substituted oxetanes with H₂O₂ and alkyl hydroperoxides: Stereoselective approach to 3-peroxyalcohols and 1,2,4-trioxepanes. *Org. Lett.* **2002**, *4*, 4591-4593.
101. Okuma, K.; Tanaka, Y.; Kaji, S.; Ohta, H., Reaction of dimethyloxosulfonium methylide with epoxides. Preparation of oxetanes. *J. Org. Chem.* **1983**, *48*, 5133-5134.
102. Austin, G. N.; Fleet, G. W. J.; Peach, J. M.; Prout, K.; Son, J. C., Chiral oxetanes from sugar lactones - synthesis of derivatives of 3,5-anhydro-1,2-O-isopropylidene-alpha-D-glucuronic acid and of 3,5-anhydro-1,2-O-isopropylidene-beta-L-iduronic acid. *Tetrahedron Lett.* **1987**, *28*, 4741-4744.
103. Hintzer, K.; Koppenhoefer, B.; Schurig, V., Access to (S)-2-methyloxetane and the precursor (S)-1,3-butanediol of high enantiomeric purity. *J. Org. Chem.* **1982**, *47*, 3850-3854.
104. Jenkinson, S. F.; Fleet, G. W., Oxetanes from the ring contraction of alpha-triflates of gamma-lactones: Oxetane nucleosides and oxetane amino acids. *Chimia (Aarau)* **2011**, *65*, 71-75.

105. Arjona, O.; Fernandez de la Pradilla, R.; Plumet, J.; Viso, A., Regioselective electrophilic additions to 2-oxygenated-7-oxabicyclo[2.2.1]hept-5-enes - a simple entry into the 4,7-dioxatricyclo[3.2.1.0^{3,6}]octane skeleton. *Tetrahedron* **1989**, *45*, 4565-4578.
106. Homsí, F.; Rousseau, G., 4-Endo-trig cyclisation processes using bis(collidine)bromine(I) hexafluorophosphate as reagent: Preparation of 2-oxetanones, 2-azetidiones, and oxetanes. *J. Org. Chem.* **1999**, *64*, 81-85.
107. Paternò, E.; Chieffi, G., Sintesi in chimica organica per mezzo della luce. Nota II. Composti degli idrocarburi non saturi con aldeidi e chetoni. *Gazz. Chim. Ital.* **1909**, *39*, 341-361.
108. D'Auria, M.; Racioppi, R., Oxetane synthesis through the Paterno-Buchi reaction. *Molecules* **2013**, *18*, 11384-11428.
109. Hoffmann, N., Photochemical reactions as key steps in organic synthesis. *Chem. Rev.* **2008**, *108*, 1052-1103.
110. Abe, M., Diradicals. *Chem. Rev.* **2013**, *113*, 7011-7088.
111. Griesbeck, A. G.; Abe, M.; Bondock, S., Selectivity control in electron spin inversion processes: Regio- and stereochemistry of Paternò-Büchi photocyclo-additions as a powerful tool for mapping intersystem crossing processes. *Acc. Chem. Res.* **2004**, *37*, 919-928.
112. Palmer, I. J.; Ragazos, I. N.; Bernardi, F.; Olivucci, M.; Robb, M. A., An MC-SCF study of the (photochemical) Paterno-Buchi reaction. *J. Am. Chem. Soc.* **1994**, *116*, 2121-2132.

113. Wang, L.; Huang, Y. C.; Liu, Y.; Fun, H. K.; Zhang, Y.; Xu, J. H., Photoinduced [4 + 4], [4 + 2], and [2 + 2] cycloadditions of *o*-quinones with oxazoles: Chemo-, regio-, and diastereoselectivity. *J. Org. Chem.* **2010**, *75*, 7757-7768.
114. Bach, T.; Jödicke, K., Diastereomerically pure 3-(Silyloxy)oxetanes by a selective Paternò-Büchi reaction. *Chem. Ber.* **1993**, *126*, 2457-2466.
115. Freilich, S. C.; Peters, K. S., Observation of the 1,4-biradical in the Paterno-Buchi reaction. *J. Am. Chem. Soc.* **1981**, *103*, 6257-6259.
116. Griesbeck, A. G.; Sokolova, T., *Product Class 3: Oxetanes and Oxetan-3-ones*, in Science of Synthesis. Compounds with one saturated carbon heteroatom bond **2008**, *37*, pp 433-471.
117. Fukuyama, T.; Kajihara, Y.; Hino, Y.; Ryu, I., Continuous microflow [2 + 2] photocycloaddition reactions using energy-saving compact light sources. *J. Flow Chem.* **2011**, *1*, 40-45.
118. Xianming, H.; Kellogg, R. M., Acid catalyzed ring-opening reactions of optically pure 2-aryl-3,3-dimethyloxetanes. *Tetrahedron Asymmetry* **1995**, *6*, 1399-1408.
119. Papini, A.; Ricci, A.; Taddei, M.; Seconi, G.; P., D., Regiospecific conversion of oxiranes, oxetanes, and lactones into difunctional nitrogen compounds via aminosilanes and aminostannanes. *J. Chem. Soc. Perkin Trans. I* **1984**, 2261-2265.
120. Mullis, J. C.; Weber, W. P., Regiospecificity of reactions of epoxides and oxetanes with trimethylsilyl cyanide. *J. Org. Chem.* **1982**, *47*, 2873-2875.

121. Searles Jr., S.; Pollart, K. A.; Lutz, E. F., Oxetanes. VI. Reductive cleavage and substituent effects. *J. Am. Chem. Soc.* **1957**, *79*, 948-951.
122. Hudrlik, P. F.; Wan, C. N., Reactions of oxetane with imine salts derived from cyclohexanone. *J. Org. Chem.* **1975**, *40*, 2963-2965.
123. Hadzic, P.; Popsavin, M., From D-xylose to terminal polyols: A simple synthetic route. *Carbohydr. Res.* **2010**, *345*, 543-546.
124. Searles, S., The Reaction of trimethylene oxide with Grignard reagents and organolithium compounds. *J. Am. Chem. Soc.* **1951**, *73*, 124-125.
125. Huynh, C.; Derguini-Boumechal, F.; Linstrumelle, G., Copper-catalysed reactions of Grignard reagents with epoxides and oxetane. *Tetrahedron Lett.* **1979**, *20*, 1503-1506.
126. Rix, D.; Ballesteros-Garrido, R.; Zeghida, W.; Besnard, C.; Lacour, J., Macrocyclisation of oxetane building blocks with diazocarbonyl derivatives under rhodium(II) catalysis. *Angew. Chem. Int. Ed.* **2011**, *50*, 7308-7311.
127. Sancar, A.; Tan, M. S., Nucleotide excision repair. *Photochem. Photobiol.* **1993**, *57*, 905-921.
128. Yamamoto, J.; Hitomi, K.; Hayashi, R.; Getzoff, E. D.; Iwai, S., Role of the carbonyl group of the (6-4) photoproduct in the (6-4) photolyase reaction. *Biochemistry* **2009**, *48*, 9306-9312.
129. Essen, L. O.; Klar, T., Light-driven DNA repair by photolyases. *Cell. Mol. Life Sci.* **2006**, *63*, 1266-1277.

130. Borg, O. A.; Eriksson, L. A.; Durbeej, B., Electron-transfer induced repair of 6-4 photoproducts in DNA: A computational study. *J. Phys. Chem. A* **2007**, *111*, 2351-2361.
131. Zhang, M.; Wang, L.; Zhong, D., Photolyase: Dynamics and mechanisms of repair of sun-induced DNA damage. *Photochem. Photobiol.* **2017**, *93*, 78-92.
132. Benjdia, A., DNA photolyases and SP lyase: Structure and mechanism of light-dependent and independent DNA lyases. *Curr. Opin. Struct. Biol.* **2012**, *22*, 711-720.
133. Ozturk, N., Phylogenetic and functional classification of the photolyase/cryptochrome family. *Photochem. Photobiol.* **2017**, *93*, 104-111.
134. Cohrs, K. C.; Schumacher, J., The two cryptochrome/photolyase family proteins fulfill distinct roles in DNA photorepair and regulation of conidiation in the gray mold fungus *botrytis cinerea*. *Appl. Environ. Microbiol.* **2017**, *83*, 1-18.
135. Faraji, S.; Dreuw, A., Proton-transfer-steered mechanism of photolesion repair by (6-4)-photolyases. *J. Phys. Chem. Lett.* **2012**, *3*, 227-230.
136. Liu, Z.; Guo, X.; Tan, C.; Li, J.; Kao, Y. T.; Wang, L.; Sancar, A.; Zhong, D., Electron tunneling pathways and role of adenine in repair of cyclobutane pyrimidine dimer by DNA photolyase. *J. Am. Chem. Soc.* **2012**, *134*, 8104-8414.
137. Improta, R.; Santoro, F.; Blancafort, L., Quantum mechanical studies on the photophysics and the photochemistry of nucleic acids and nucleobases. *Chem. Rev.* **2016**, *116*, 3540-3593.
-

138. Manova, V.; Georgieva, R.; Borisov, B.; Stoilov, L., Efficient removal of cyclobutane pyrimidine dimers in barley: Differential contribution of light-dependent and dark DNA repair pathways. *Physiol. Plant.* **2016**, *158*, 236-253.
139. Alzueta, O. R.; Cuquerella, M. C.; Miranda, M. A., Triplet energy transfer versus excited state cyclisation as the controlling step in photosensitized bipyrimidine dimerization. *J. Org. Chem.* **2019**, *84*, 13329-13335.
140. Li, J.; Liu, Z.; Tan, C.; Guo, X.; Wang, L.; Sancar, A.; Zhong, D., Dynamics and mechanism of repair of ultraviolet-induced (6-4) photoproduct by photolyase. *Nature* **2010**, *466*, 887-890.
141. Ravindar, L.; Lekkala, R.; Rakesh, K. P.; Asiri, A. M.; Marwani, H. M.; Qin, H. L., Carbonyl-olefin metathesis: A key review. *Org. Chem. Front.* **2018**, *5*, 1381-1391.
142. Becker, M. R.; Watson, R. B.; Schindler, C. S., Beyond olefins: New metathesis directions for synthesis. *Chem. Soc. Rev.* **2018**, *47*, 7867-7881.
143. D'Auria, M.; Racioppi, R.; Viggiani, L., Paternò-Büchi reaction between furan and heterocyclic aldehydes: Oxetane formation vs. metathesis. *Photochem. Photobiol. Sci.* **2010**, *9*, 1134-1138.
144. Cosa, G.; Scaiano, J. C., Laser techniques in the study of drug photochemistry. *Photochem. Photobiol.* **2004**, *80*, 159-174.
145. Foggi, P.; Bussotti, L.; Neuwahl, F. V. R., Photophysical and photochemical applications of femtosecond time-resolved transient absorption spectroscopy. *Int. J. Photoenergy* **2001**, *3*, 103-109.

146. Berera, R.; van Grondelle, R.; Kennis, J. T., Ultrafast transient absorption spectroscopy: Principles and application to photosynthetic systems. *Photosynth. Res.* **2009**, *101*, 105-118.
147. Joseph, A.; Falvey, D. E., Photolysis of thymine oxetanes produces triplet excited carbonyl compounds with high efficiency. *J. Am. Chem. Soc.* **2001**, *123*, 3145-3146.
148. Hei, X. M.; Song, Q. H.; Li, X. B.; Tang, W. J.; Wang, H. B.; Guo, Q. X., Origin of a large temperature dependence of regioselectivity observed for [2 + 2] photocycloaddition (Paternò-Büchi reaction) of 1,3-dimethylthymine with benzophenone and its derivatives: Conformational property of the intermediary triplet 1,4-diradicals. *J. Org. Chem.* **2005**, *70*, 2522-2527.
149. Song, Q. H.; Zhai, B. C.; Hei, X. M.; Guo, Q. X., The Paternò-Büchi reaction of 1,3-dimethyluracil and 1,3-dimethylthymine with 4,4'-disubstituted benzophenones. *Eur. J. Org. Chem.* **2006**, *2006*, 1790-1800.
150. Song, Q. H.; Wang, H. B.; Li, X. B.; Hei, X. M.; Guo, Q. X.; Yu, S. Q., Notable substituent and temperature effects on the regioselectivity and the efficiency in Paternò-Büchi reaction of 4,4'-disubstituted benzophenones with 1,3-dimethyluracil and 1,3-dimethylthymine. *J. Photochem. Photobiol. A* **2006**, *183*, 198-204.
151. Kong, F. F.; Zhai, B. C.; Song, Q. H., Substituent effects on the regioselectivity of the Paterno-Buchi reaction of 5- or/and 6-methyl substituted uracils with 4,4'-disubstituted benzophenones. *Photochem. Photobiol. Sci.* **2008**, *7*, 1332-1336.

152. Kong, F. F.; Wang, J. B.; Song, Q. H., Heavy atom effects in the Paterno-Buchi reaction of pyrimidine derivatives with 4,4'-disubstituted benzophenones. *Beilstein J. Org. Chem.* **2011**, *7*, 113-118.
153. Joseph, A.; Falvey, D. E., Photoinduced electron transfer cleavage of oxetane adducts of uracil and cytosine. *Photochem. Photobiol. Sci.* **2002**, *1*, 632-635.
154. Encinas, S.; Belmadoui, N.; Climent, M. J.; Gil, S.; Miranda, M. A., Photosensitization of thymine nucleobase by benzophenone derivatives as models for photoinduced DNA damage: Paternò-Büchi vs energy and electron transfer processes. *Chem. Res. Toxicol.* **2004**, *17*, 857-862.
155. Vendrell-Criado, V.; Lhiaubet-Vallet, V.; Yamaji, M.; Cuquerella, M. C.; Miranda, M. A., Blocking cyclobutane pyrimidine dimer formation by steric hindrance. *Org. Biomol. Chem.* **2016**, *14*, 4110-4115.
156. Belmadoui, N.; Encinas, S.; Climent, M. J.; Gil, S.; Miranda, M. A., Intramolecular interactions in the triplet excited states of benzophenone-thymine dyads. *Chem. Eur. J.* **2006**, *12*, 553-561.
157. Kwok, W. M.; Guan, X.; Chu, L. M.; Tang, W.; Phillips, D. L., Observation of singlet cycloreversion of thymine oxetanes by direct photolysis. *J. Phys. Chem. B* **2008**, *112*, 11794-11797.

CHAPTER 2:

Objectives

UVA light from the sun can penetrate the ozone layer and easily get into human cells, inducing damage to DNA via certain endogenous or exogenous photosensitizers (such as drugs). An example of a chromophore that can induce photosensitized damage to DNA would be benzophenone, a recurrent motif found in a range of bioactive molecules. This kind of harm can give rise to bulky dimers such as cyclobutane pyrimidine dimers (CPDs) and pyrimidine-pyrimidone (6-4) photoproducts ((6-4)PPs), which in most cases covalently fuse thymine (Thy) nucleosides; this process prevents DNA replication as well as other essential metabolic reactions of the cell, potentially leading to melanomas and cell death. Some organisms have efficient DNA repair mechanisms involving an electron transfer process to break-down the (6-4)PPs back into the Thy monomers, via what some believe to be a reverse Paternò-Büchi (PB) reaction through oxetane-like transient intermediates.

Little is truly known about the mechanism of the reverse PB reaction that is linked to the photorepair of (6-4)PPs, and therefore an effort to better understand this process has been made in this thesis. Since the theoretical Thy-Thy oxetane (Thy^oThy) intermediate is too unstable to be isolated (let alone analysed), artificial oxetanes have to be used that are stable at room temperature and mimic the structure of Thy^oThy.

In this regard, the main goal of this thesis has been to investigate the photoreactivity of a series of oxetanes following the PB reaction under a variety of chemical conditions, with special emphasis on the photoinduced cycloreversion of the same oxetanes under the appropriate irradiation. Therefore, a variety of oxetanes arising from the intermolecular interaction between Thy or uracil (Ura) derivatives and BP have been synthesized; besides, other derivatives where both Thy and BP moieties are covalently linked by a spacer of variable length and different nature were also

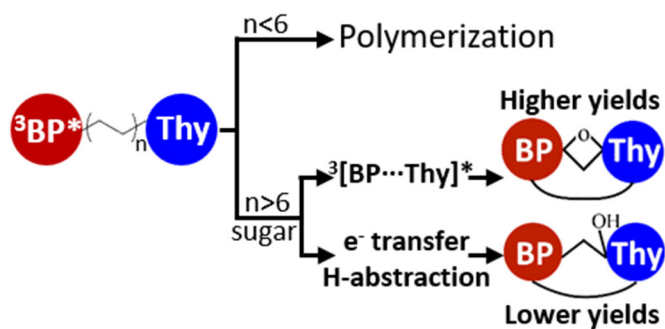
designed. The photochemical and photophysical reactivity of all these systems have been investigated by means of transient absorption spectroscopy (from the femtosecond to the microsecond time scale), in addition to detailed computational analysis including multiconfigurational quantum-chemistry calculations.

Concerning the intramolecular interactions between Thy and BP linked by a covalent bridge, four dyads using spacers of different length and nature (sugar vs. linear spacers) were prepared in order to check how the photoreactivity between both units can be affected as a function of the interchromophoric distance. In this context, the photochemical reactivity and the photophysical properties of the different derivatives were studied by means of spectroscopic techniques; besides, the main photoproducts arising from steady-state irradiation were also isolated and characterized.

Additionally, we have further investigated the chemical mechanism of the photolysis of a variety of oxetanes arising from the intermolecular interaction between Thy or Ura derivatives with BP. In this context, some derivatives were synthesized by varying the substituents at different positions of the nucleobases. The photoreactivity of the synthesized oxetanes, including as well the head-to-head and head-to-tail regioisomers, were investigated by means of transient absorption spectroscopy.

CHAPTER 3:

Influence of the Linking Bridge on the Photoreactivity of Benzophenone-Thymine Conjugates



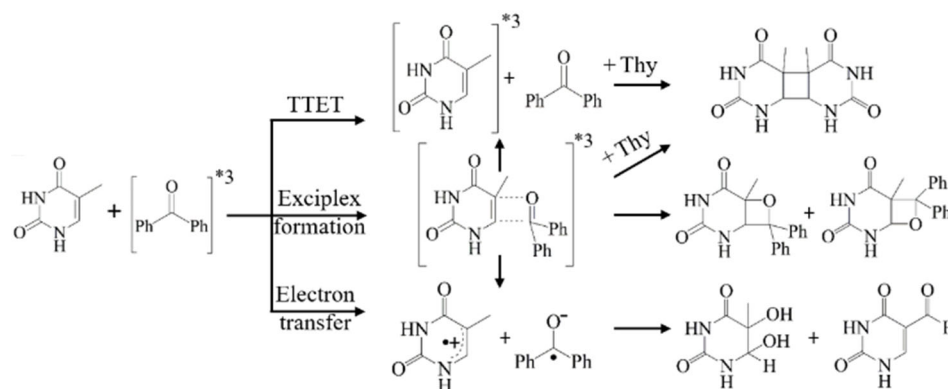
1. Introduction

The interaction of solar UV light with DNA can give rise to chemical modifications in its structure that may result in cell death and eventually in the appearance of cancer.¹⁻² Direct photoinduced damage is mainly associated with the formation of cyclobutane pyrimidine dimers (CPDs) and to a lesser extent pyrimidine (6-4) pyrimidone photoproducts ((6-4)PPs), which are highly mutagenic;³⁻⁷ in addition, oxidative DNA lesions can also be formed in lower yields.⁸ Formally, CPDs are generated through a [2+2] cycloaddition between two adjacent nucleobases while the (6-4)PPs arise from a Paternò-Büchi (PB) photochemical reaction to form an oxetane intermediate, which rapidly evolves through ring-opening and isomerization to afford the (6-4)PPs as photoproducts.⁹⁻¹⁰ Both lesions, CPDs and (6-4)PPs, can be efficiently repaired by two mechanisms: in humans, the nucleotide excision repair predominates, while in other organisms (i.e. bacteria and plants) the photolyase-mediated mechanism reverses the damage through a photoinduced electron transfer process.¹¹⁻¹⁵

Photoinduced damage to DNA can occur not only upon direct absorption of UVB light but also through photosensitization.^{3, 16} In this case, excitation of an exogenous or endogenous photosensitizer (PS) at comparatively longer wavelengths leads, after intersystem crossing, to reactive long-lived triplet excited states. In this context, some non-steroidal anti-inflammatory drugs (NSAIDs) photosensitize DNA damage upon absorption of UVA light.¹⁷ A typical example is ketoprofen (KP),¹⁸⁻²³ whose photobehaviour can be attributed to its benzophenone (BP) substructure, as the BP chromophore itself is known to elicit DNA damage by photosensitization.²⁴⁻²⁵ Interestingly, this scaffold is present in a variety of

drugs, which exhibit a broad range of biological activities such as anticancer, anti-inflammatory, antimicrobial and antiviral.²⁶

One of the most relevant interactions in the DNA photosensitization by BP derivatives occurs between the BP chromophore and the thymine (Thy) nucleobase. A simplified mechanism explaining these interactions is shown in Scheme 3.1. Absorption of UVA-light by BP rapidly generates its excited triplet state ($^3\text{BP}^*$), which can mediate formation of $^3\text{Thy}^*$ by triplet-triplet energy transfer (TTET), either directly or through a triplet exciplex $^3[\text{BP}\cdots\text{Thy}]^*$. Subsequently, $^3\text{Thy}^*$ or $^3[\text{BP}\cdots\text{Thy}]^*$ may react with another thymine moiety leading ultimately to CPDs as formal [2+2] cycloadducts.²⁷ Alternatively, $^3[\text{BP}\cdots\text{Thy}]^*$ can also evolve to oxetane derivatives. Exciplexes of this type have recently been detected in BP-Thy conjugates.²⁸ Finally, an electron transfer process may also occur, albeit to a lesser extent, producing oxidative damage.²⁹



Scheme 3.1. Simplified mechanism showing the excited state interactions between BP and Thy, which may finally result in the formation of some photoproducts inducing damage to DNA.

Bichromophoric systems composed of a nucleobase (or nucleoside) covalently linked to a photosensitizer (or a photoactive drug) have been previously used as models to investigate the excited-state interactions underlying photosensitized DNA damage.³⁰⁻³² In particular, the photoreactivity of two dyads containing KP covalently linked to thymidine at positions 5' or 3' of the sugar moiety has been previously investigated.³³ The behaviour of both regioisomers was found to be strongly influenced by the relative spatial arrangement (*cisoid* or *transoid*, for positions 5' and 3', respectively) of the KP and Thy units. Photolysis of the *cisoid* isomer gave rise to four oxetanes plus two additional photoproducts arising from a formal intramolecular hydrogen abstraction; on the contrary, irradiation of the *transoid* isomer resulted only in slow polymerization. Accordingly, the ³KP* triplet excited state was markedly shorter-lived in the *cisoid* isomer, in line with its higher reactivity. In this context, recent theoretical calculations on ligand/DNA interactions have found that photosensitized DNA damage depends on the relative orientation of the chromophore interacting with Thy.³⁴

In view of the rich photoreactivity observed for the dyads containing KP covalently linked to thymidine at position 5' of the sugar, which leads to complex photoproduct mixtures, it appeared interesting to investigate whether appropriate changes in the nature of the spacer could modulate the intramolecular BP/Thy photoreactivity, resulting in an enhanced chemo- regio- and/or stereoselectivity. Therefore, with the general goal of getting a better understanding of ligand/DNA interactions, a series of photosensitizer-nucleobase dyads have been designed in the present work (Figure 3.1) and submitted to a systematic study of their photochemical and photophysical properties, including careful identification of the photoproducts obtained by steady-state photolysis

and transient spectroscopic characterization of the reactive triplet excited states in the nanosecond and femtosecond timescales. In dyads **D4**, **D6** and **D10** both chromophores are separated by a linear chain composed of four, six or ten linking atoms. In the *cisoid* dyad **D7**, which we have reinvestigated for comparison, the BP and Thy units are separated by the sugar moiety, where the *cisoid* arrangement of BP and Thy can increase the number of reactive conformations with respect to the linear linkers.

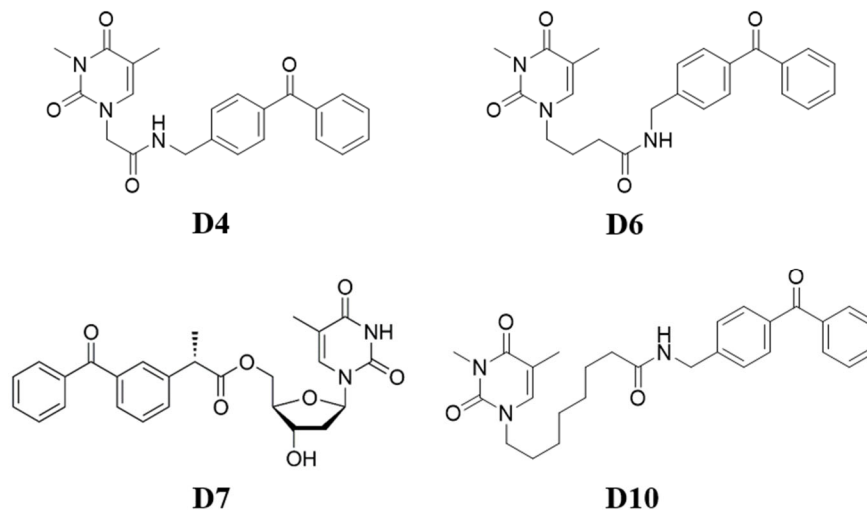
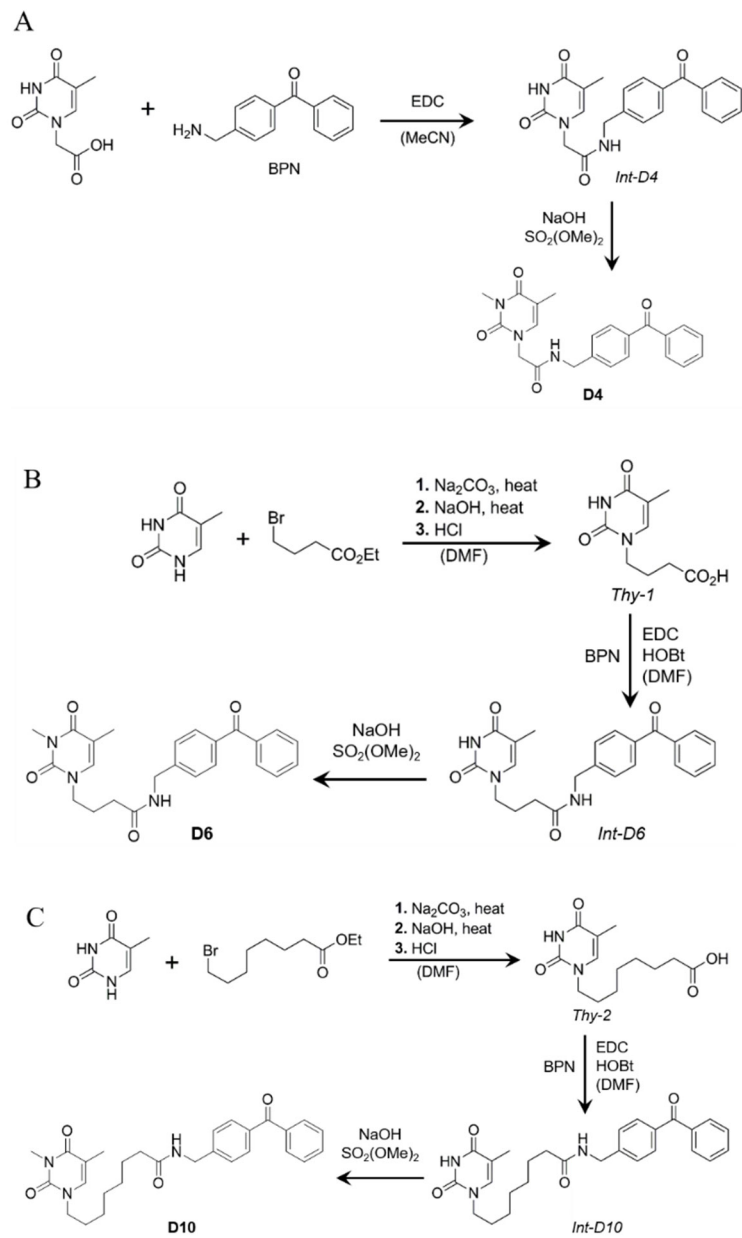


Figure 3.1. Chemical structure of the investigated dyads.

2. Results and discussion

The synthesis of the selected dyads is described in detail in the Supplementary material. For **D7**, the reported synthesis³³ involves covalent KP linking to the 5' position of the sugar through an ester bond; by contrast, for the linear dyads **D4**, **D6** and **D10** (see Scheme 3.2), a Thy-derived alkanolic acid of variable length is conjugated with the BP derivative 4-benzoylbenzylamine (BPN) through an amide bond.



Scheme 3.2. Schematic representation of the synthesis of **D4**, **D6** and **D10**.

The photoreactivity of the obtained dyads was first investigated by means of steady-state photolysis and transient absorption spectroscopy. Thus, isoabsorptive solutions ($A_{350} = 0.05$, concentration ca. 20 μM) of the three new compounds were irradiated in deaerated acetonitrile in a multilamp photoreactor emitting at $\lambda_{\text{max}} = 350$ nm. The course of the reaction was followed by monitoring the decrease of the UV absorption at 254 nm (Figure 3.2), which is mainly associated with the diaryl ketone (see Figure S3.1 in the supplementary material).

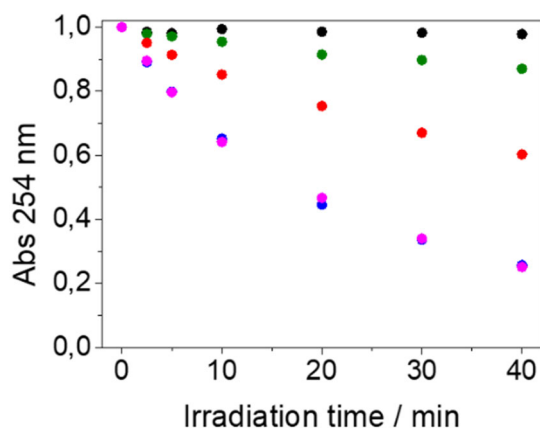
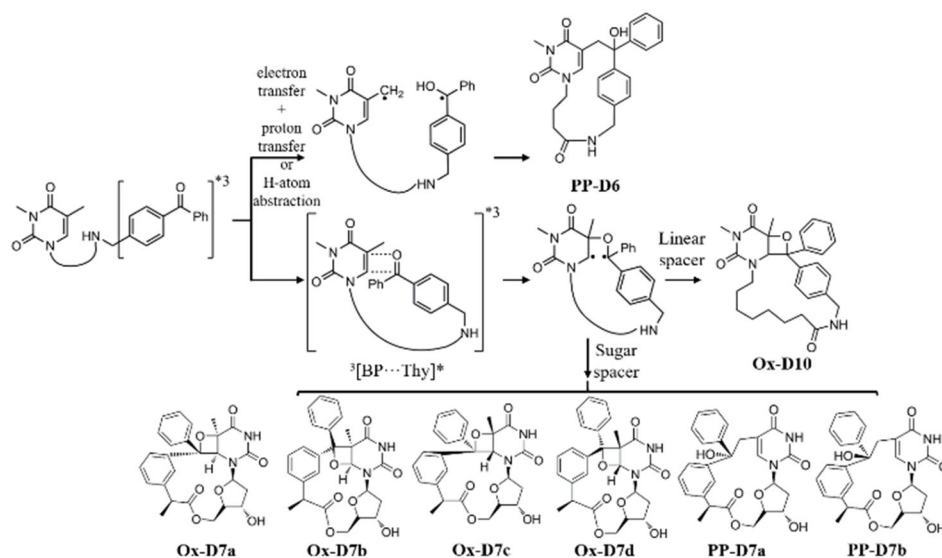


Figure 3.2. Photochemical reactivity of BPN (black), **D4** (green), **D6** (red), **D7** (blue) and **D10** (magenta) followed by the decrease in the absorbance of the carbonyl band at 254 nm against the irradiation time. Irradiations were performed in deaerated acetonitrile (~ 20 μM) using a multilamp photoreactor ($\lambda_{\text{max}} = 350$ nm) through quartz cells.

A progressive disappearance of the absorption at ca. 254 nm was observed for the dyads, whereas the reference compound BPN was nearly unreactive under the same conditions (see also Figure S3.11 in the supplementary material). The photochemical reactivity followed the order **D4** < **D6** < **D10** \approx **D7**. For product studies, higher concentrations of the dyads (2.6 mM) were used. Irradiation of **D4** gave only rise to unidentified

polymeric material. By contrast, **D6** and **D10** led to the formation of well-defined photoproducts that were separated and purified by semipreparative HPLC, and characterized by ¹H- and ¹³C-NMR, as well as HRMS (see supplementary material). Thus, photolysis of **D6** resulted not only in polymerization, but also in the formation of photoproduct **PP-D6** (see Scheme 3.3) in very low yields (~3%) after HPLC purification, which may arise from a direct H-atom abstraction or through an electron transfer process followed by proton transfer, to afford formal hydrogen abstraction chemistry. The intermediate radical pair contains a Thy-derived radical at the C5-methyl group, which under aerobic conditions would be trapped by oxygen, to give a 5-formyluracil. Thus, this chemistry would be connected with the oxidative damage to DNA.³⁵ However, it should be noted that oxidation of Thy in the biomolecule is less favored than that of the guanine nucleobase, which has the lowest oxidation potential and would be a better electron donor than Thy towards the excited BP moiety.²¹ Conversely, the main photoproduct resulting from irradiation of **D10** was an oxetane (**Ox-D10**), ca. 20% yield after HPLC purification, which clearly arises from a Paternò-Büchi reaction between the excited carbonyl of BP and the C5=C6 double bond of Thy. The regio- and stereochemistry of **Ox-D10** were unambiguously established by X-ray crystallography (see Figure 3.3). The photoproducts arising from irradiation of **D7**, namely **Ox-D7a**, **Ox-D7b**, **Ox-D7c**, **Ox-D7d**, **PP-D7a** and **PP-D7b** have been previously characterized;³³ higher yields were observed for the oxetane formation, while photoproducts **PP-D7a** and **PP-D7b** were obtained in lower yields.



Scheme 3.3. Simplified mechanism for the photoproduct formation upon steady-state photolysis of **D6**, **D7** and **D10**.

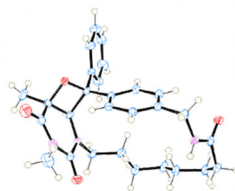


Figure 3.3. Structure of **Ox-D10** in the crystalline state: C blue, H white, O red and N violet. Thermal ellipsoids are drawn at the 50% probability level.

In order to characterize the excited states involved in the photochemical reactivity of each dyad and to elucidate the mechanistic pathways leading to the isolated photoproducts, transient absorption experiments were performed on **D4**, **D6** and **D10**, using BPN as a reference compound. Measurements in the femtosecond time scale were conducted upon excitation at 280 nm in MeCN; control experiments demonstrated that, under the employed conditions, the degree of photodecomposition of the four compounds was lower than 5%.

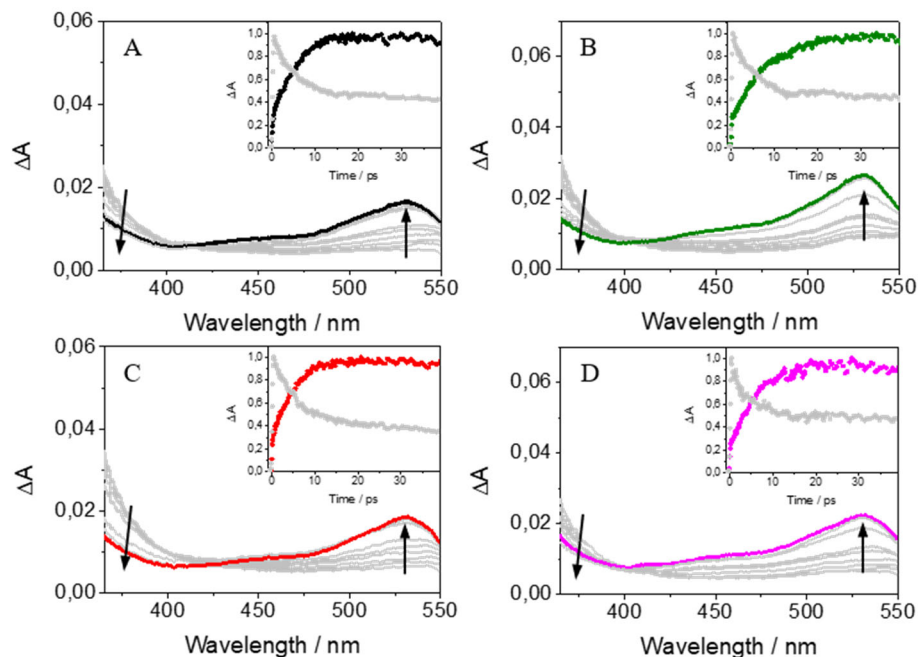


Figure 3.4. Femtosecond transient absorption spectra from 0.5 to 40 ps for BPN (A), **D4** (B), **D6** (C) and **D10** (D) upon excitation at 280 nm in MeCN. The insets show the kinetic traces at 340 nm (gray) and 530 nm: BPN (black), **D4** (green), **D6** (red) and **D10** (magenta).

As expected, the photobehaviour of BPN at the really early times after excitation was very similar to that displayed by BP,^{28, 36} but with different kinetics. Hence, the triplet excited state of BPN displayed a maximum at *ca.* 530 nm; it was formed within *ca.* 5.5 ps through intersystem crossing (ISC) concomitantly with the disappearance of the band centered at 340 nm, associated with the singlet-singlet absorption. Interestingly, a similar trend with analogous kinetics was detected for **D4**, **D6** and **D10** (see Figure 3.4). This suggests that the photoreactivity of all dyads occurs once the triplet excited state of the benzophenone chromophore has been completely formed. Therefore, nanosecond laser flash photolysis (LFP)

experiments were performed upon excitation at 355 nm with the aim of investigating the transient species at longer times. Thus, photolysis of BPN gave rise to its triplet-triplet absorption band with maxima centered at ca. 320 and 530 nm. A similar trend was observed for the dyads (see Figure S3.12 in the supplementary material).

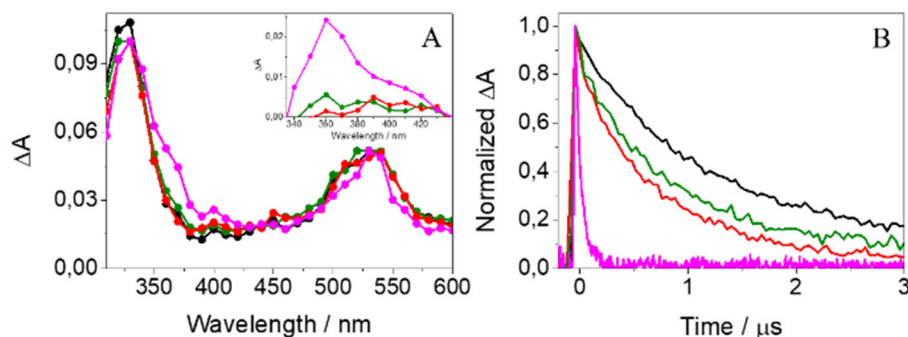


Figure 3.5. LFP spectra recorded at the very beginning after the laser pulse (A) and decay traces at 530 nm (B) for BPN (black), **D4** (green), **D6** (red) and **D10** (magenta). The inset in (A) shows the transient absorption spectra obtained by subtraction of the $^3\text{BPN}^*$ spectrum from that of the corresponding dyad. All measurements were performed in deaerated MeCN at $\lambda_{\text{exc}} = 355$ nm.

A more detailed analysis of the LFP spectra revealed marginal absorption between 350 and 420 nm, only for **D10**. This band is difficult to visualize due to overlap with that of 320 nm; however, it can be clearly observed by subtracting the $^3\text{BPN}^*$ spectrum from that of the corresponding dyad (inset in Figure 3.5A). The weak absorption band found for **D10** displays a maximum at ~ 360 nm, analogous to that of $^3\text{Thy}^*$.³⁷ Indeed, a very similar band was previously detected for related Thy-benzophenone conjugates, and it was associated with the formation of $^3\text{Thy}^*$ by triplet-triplet energy transfer (TTET) from $^3\text{BP}^*$.³⁸ Moreover, the involvement of triplet exciplexes arising from the photocleavage of oxetanes composed of BP

and dimethylthymine (DMT) has been recently proposed. The signature of these exciplexes ($^3[\text{BP}\cdots\text{DMT}]^*$) is the appearance of an absorption band at *ca.* 400 nm, whose formation depends on the oxetane regiochemistry.²⁸ Therefore, by analogy, the weak absorption detected for **D10** could also be associated with a triplet exciplex between the benzophenone and thymine units.

Interestingly, **D10** is the only linear dyad that generates an oxetane upon absorption of UVA light. This must be related with the length of the spacer compared to **D4** and **D6**, which may allow reaching the appropriate conformational arrangement between the two chromophores enabling closer interaction between the carbonyl group of BP and the C5=C6 double bond of Thy, thus favoring the formation of a triplet exciplex ($^3[\text{BP}\cdots\text{Thy}]^*$). This species would later evolve towards the formation of the oxetane (see Scheme 3.3). In this context, the shorter interchromophoric distance in **D4** and **D6** might be associated with a higher strain to reach the proper conformational arrangement to form $^3[\text{BP}\cdots\text{Thy}]^*$. Indeed, a significant degree of polymerization was observed for both dyads, although in the case of **D6** the (sterically less demanding) hydrogen abstraction product **PP-D6** was obtained in low yields.

Analysis of the triplet decay traces at 530 nm evidenced a clear intramolecular quenching for all dyads (see Figure 3.5B). This quenching was not associated to triplet-triplet annihilation since the results obtained at different laser intensities were very similar. The decays followed in all cases a first-order exponential law; the reference compound BPN showed a triplet lifetime of 1.5 μs , which was markedly shortened in **D10** ($\sim 0,05$ μs) in line with its highest photochemical reactivity. By contrast, **D4** was the dyad with the longest lifetime, *ca.* 1.0 μs , which agrees well with its lowest reactivity. Accordingly, **D6** exhibited an intermediate triplet lifetime

(~0,8 μs), shorter than **D4** but longer than **D10**, in line with its photoreactivity. Thus, a good correlation was found between the results obtained in the steady-state photolysis and the laser flash photolysis experiments.

The triplet lifetimes obtained by LFP for all dyads and for the reference compounds BPN and KP are summarized in Table 3.1, together with the intramolecular quenching rate constants (k_Q), calculated by subtraction of the reciprocal lifetimes. Thus, the k_Q values for the dyads were in the order of 10^5 - 10^7 s^{-1} , whereas the reported intermolecular photoreaction rate constant between ${}^3\text{BP}^*$ and DMT is 3.5×10^8 $\text{M}^{-1}\text{s}^{-1}$.³⁹ Considering that the concentration of dyads employed in the product studies was in the order of 2.6 mM, the intermolecular reaction rates would be 9.1×10^5 s^{-1} . Accordingly, polymerization competes with the intramolecular reaction for **D4** and to a lesser extent for **D6**; conversely, the intramolecular process is much faster and prevails in the case of **D10**.

Table 3.1. Photophysical data (triplet lifetimes and intramolecular quenching rate constants) obtained for the investigated dyads and their reference compounds.

	τ (${}^3\text{BP}^*$) / μs	k_Q / s^{-1}
BPN	1.5	-
D4 ^a	1.0	3.3×10^5
D6 ^a	0.8	5.8×10^5
D10 ^a	0.05	1.9×10^7
KP	1.3	-
D7 ^b	0.03	3.3×10^7
^a determined as $(1/\tau_{\text{dyad}} - 1/\tau_{\text{BPN}})$; ^b determined as $(1/\tau_{\text{D7}} - 1/\tau_{\text{KP}})$		

Having established that the photobehaviour of the linear dyads is highly influenced by the distance between the BP and Thy moieties, the photophysical properties of **D7** were reinvestigated. It has been reported that steady-state irradiation of **D7** gives mainly rise to the formation of oxetanes, along with minor amounts of photoproducts arising from a formal intramolecular hydrogen abstraction process.³³ Accordingly, a fast deactivation of the triplet excited state of KP was evidenced for **D7**, which was attributed to its high reactivity due to the strong intramolecular interaction between the KP and Thy units. In order to get a deeper insight into the photophysical properties of **D7**, femtosecond transient absorption measurements ($\lambda_{\text{exc}} = 280 \text{ nm}$) were performed using KP as a reference. As expected, the triplet excited state of KP, with $\lambda_{\text{max}} = 530 \text{ nm}$,⁴⁰⁻⁴¹ was formed within ca. 9.5 ps. The same was true for **D7** (see Figure S3.13 in the supplementary material), suggesting that its photoreactions occur once ${}^3\text{KP}^*$ is completely formed. Consequently, the photophysical properties of **D7** were reinvestigated in longer timescales by means of LFP.

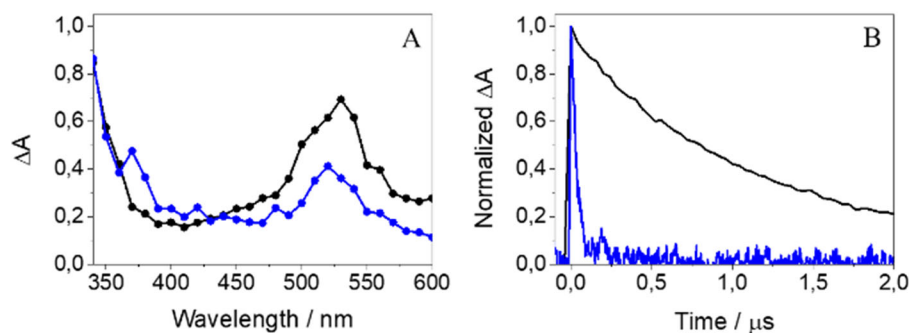


Figure 3.6. LFP spectra recorded at the very beginning after the laser pulse (A) and decay traces at 530 nm (B) for KP (black) and **D7** (blue) after excitation at 355 nm in deaerated MeCN.

Excitation of **D7** at 355 nm resulted in the formation of $^3\text{KP}^*$ with maximum at 530 nm (see Figure 3.6). In agreement with a previous report,³³ the triplet lifetime of KP in the dyad was strongly quenched (~ 30 ns) compared to the isolated chromophore (1.3 μs), in line with its high photochemical reactivity. Interestingly, the transient absorption spectrum of **D7** clearly showed a band with maximum *ca.* 370 nm, very similar to that observed for **D10**. Again, this band could be associated with a triplet exciplex between KP and Thy, which would evolve towards the formation of the oxetanes.

Overall, the photoreactivity of the investigated dyads has evidenced remarkable differences due to the interchromophoric distance between BP and Thy, and also to the conformational arrangement provided by the spacer.

3. Conclusions

The photobehaviour of a series of dyads composed of benzophenone and thymine separated by spacers of different length has been investigated in the present work by means of steady-state photolysis and transient absorption spectroscopy. In general, the photoreactivity of the dyads can be satisfactorily correlated with their photophysical properties. Ultrafast spectroscopy reveals that, in all cases, the photochemical reactions occur once the triplet excited state of the BP chromophore has been fully populated after a few picoseconds. In this context, nanosecond laser flash photolysis demonstrates that **D10** and **D7** have the shortest triplet lifetimes, due to a faster intramolecular quenching, in line with their higher photoreactivity. Interestingly, a transient absorption band with maximum centered at *ca.* 370 nm is detected for both **D10** and **D7** upon laser flash

photolysis, which can be attributed to the formation of a triplet exciplex that might finally evolve towards the formation of oxetanes. In conclusion, the obtained results suggest that not only the interchromophoric distance between benzophenone and thymine plays a significant role in the photobehaviour of the investigated dyads, but also the conformational arrangement enhanced by the degree of flexibility of the spacer.

4. Experimental section

Chemicals and reagents. Thymine (Thy) and 4-benzoylbenzylamine (BPN) hydrochloride were purchased from Achemblock. Ethyl 8-bromooctanoate was purchased from Fluorochem. Thymine-1-acetic acid, 1-ethyl-3-(3-dimethylaminopropyl)carbodiimide (EDC), ethyl 4-bromobutyrate, 1-hydroxybenzotriazole (HOBt), dimethyl sulphate, sodium carbonate and potassium carbonate were purchased from Sigma-Aldrich. Sodium hydroxide (NaOH), hydrochloric acid solution (HCl), acetonitrile (MeCN) spectroscopic grade, dimethylformamide (DMF), dichloromethane (DCM), methanol (MeOH), ethyl acetate and magnesium sulphate anhydrous were purchased from Scharlab.

Synthesis of the dyads

Synthesis of *N*-(4-benzoylbenzyl)-2-(5-methyl-2,4-dioxo-3,4-dihydropyrimidin-1(2*H*)-yl)acetamide (*Int-D4*): to a solution of 74.5 mg of thymine-1-acetic acid (0.4 mmol) in MeCN, 100 mg (0.4 mmol) of 4-benzoylbenzylamine hydrochloride (BPN) and 180 mg of EDC (0.94 mmol) were added. The mixture was stirred at room temperature overnight. The organic solvent was removed under reduced pressure and the crude was purified by column chromatography (SiO₂, CH₂Cl₂/MeOH,

95:5). The intermediate *Int-D4* was obtained as a colorless solid (105 mg, 70% yield).

^1H NMR (400 MHz, CD_3OD) δ 7.78-7.47 (m, 9H), 7.41 (s, 1H), 4.52 (s, 2H), 4.48 (s, 2H), 1.89 (s, 3H); $^{13}\text{C}\{^1\text{H}\}$ NMR (100 MHz, CD_3OD) δ 196.9, 168.5, 165.6, 151.8, 143.5, 142.3, 137.5, 136.1, 133.1, 130.0, 129.5, 128.2, 127.1, 109.9, 49.9, 42.7, 10.9; HRMS (ESI): m/z calcd. for (MH^+) $\text{C}_{21}\text{H}_{20}\text{N}_3\text{O}_4$: 378.1457, found: 378.1454.

Synthesis of *N*-(4-benzoylbenzyl)-2-(3,5-dimethyl-2,4-dioxo-3,4-dihydropyrimidin-1(2*H*)-yl)acetamide (dyad **D4**): to a solution of *Int-D4* (22.8 mg, 0.06 mmol) in 4 mL of NaOH (2.5 M) in pure water, 30 μL of dimethyl sulphate (0.2 mmol) were added dropwise. The mixture was stirred at room temperature overnight. The crude product was extracted with ethyl acetate, dried with anhydrous MgSO_4 , filtered and concentrated under reduced pressure. The final product **D4** was obtained as a colorless solid (20 mg, 83% yield).

^1H NMR (400 MHz, CD_3OD) δ 7.76-7.47 (m, 9H), 7.43 (s, 1H), 4.52 (s, 2H), 4.48 (s, 2H), 2.16 (s, 3H), 1.92 (s, 3H); $^{13}\text{C}\{^1\text{H}\}$ NMR (100 MHz, CD_3OD) δ 196.9, 168.4, 164.7, 151.9, 143.5, 140.4, 137.5, 136.3, 132.4, 130.0, 129.5, 128.1, 127.0, 108.9, 50.9, 42.5, 26.9, 11.5; HRMS (ESI): m/z calcd. for (MH^+) $\text{C}_{22}\text{H}_{22}\text{N}_3\text{O}_4$: 392.1610, found: 392.1613.

The synthesis of the intermediate *Thy-1* has been explained elsewhere.⁴² Briefly, to a solution of 6.35 g (50 mmol) of thymine in 100 mL of dimethyl formamide (DMF), 15.5 g of Na_2CO_3 were added. Then, 8.6 mL (70 mmol) of ethyl 4-bromobutyrate were added and left stirring at 125°C using a reaction block for 6h. After this time, the crude was cooled down to room temperature and left stirring for 2 days. DMF was removed under reduced pressure and, after addition of 50 mL of water, the unreacted thymine

precipitated, which was removed by filtration. The dissolved product was extracted with dichloromethane, washed with brine ($\times 2$) and dried with MgSO_4 . The solvent was removed under reduced pressure and the residue was subsequently dissolved in 100 mL of NaOH 2M and stirred under reflux for 2 hours. Then, the solution was acidified with HCl 4 M to pH 1 and the final product was purified by recrystallization. The intermediate *Thy-1* was obtained as a white solid (4.8 g, 45% yield).

Synthesis of *N*-(4-benzoylbenzyl)-4-(5-methyl-2,4-dioxo-3,4-dihydropyrimidin-1(2*H*)-yl)butanamide (*Int-D6*): to a solution containing 1.7 g of thymine-1-butanoic acid (8.0 mmol), 2.1 g of EDC (11.0 mmol) and 1.18 g hydroxy benzotriazole (HOBT, 8.7 mmol) in anhydrous DMF, a solution of 1.8 g of BPN (7.3 mmol) in DMF was added dropwise. The mixture was stirred for 2 hours at 0 °C using an ice bath. The DMF was removed under reduced pressure, and the crude was dissolved in dichloromethane and washed with NaHCO_3 1 M ($\times 3$), HCl 1 M ($\times 3$) and brine ($\times 3$). The final product *Int-D6* was purified by recrystallization with methanol as a white solid (1.86 g, 60% yield).

^1H NMR (400 MHz, CD_3OD) δ 7.78-7.45 (m, 9H), 7.41 (s, 1H), 4.46 (s, 2H), 3.78 (t, $J = 7.2$ Hz, 2H), 2.33 (t, $J = 7.2$ Hz, 2H), 2.05 (m, 2H), 1.87 (s, 3H); $^{13}\text{C}\{^1\text{H}\}$ NMR (100 MHz, DMSO-d_6) δ 195.4, 171.4, 164.3, 150.9, 144.7, 141.4, 137.1, 135.5, 132.6, 129.8, 129.5, 128.5, 127.1, 108.4, 46.8, 41.8, 32.1, 24.6, 11.9; HRMS (ESI): m/z calcd. for (MH^+) $\text{C}_{23}\text{H}_{24}\text{N}_3\text{O}_4$: 406.1760, found: 406.1764.

Synthesis of *N*-(4-benzoylbenzyl)-4-(3,5-dimethyl-2,4-dioxo-3,4-dihydropyrimidin-1(2*H*)-yl)butanamide (dyad **D6**): to a solution of 135 mg of *Int-D6* (0.3 mmol) in 4 mL of NaOH (2.5 M), 100 μ L of SO₂(OMe)₂ (1 mmol) were added dropwise. The mixture was stirred overnight at room temperature. The crude product was extracted with ethyl acetate (\times 3), washed with 1M NaHCO₃ and dried with anhydrous MgSO₄, filtered and concentrated under reduced pressure. The final product was purified by precipitation in dichloromethane/hexane to get **D6** as a white solid (118 mg, 85% yield).

¹H NMR (400 MHz, CD₃OD) δ 7.75-7.44 (m, 9H), 7.42 (s, 1H), 4.45 (s, 2H), 3.81 (t, *J* = 7.2 Hz, 2H), 3.29 (s, 3H), 2.32 (t, *J* = 7.2 Hz, 2H), 2.02 (m, 2H), 1.89 (s, 3H); ¹³C{¹H} NMR (100 MHz, CD₃OD) δ 196.8, 173.4, 164.6, 151.8, 143.9, 139.8, 137.5, 136.3, 132.4, 130.0, 129.5, 128.1, 127.1, 108.9, 48.5, 42.4, 32.1, 26.9, 24.6, 11.5; Yield: 85%. HRMS (ESI): *m/z* calcd. for (MH⁺) C₂₄H₂₆N₃O₄: 420.1923, found: 420.1927.

Synthesis of 8-(5-methyl-2,4-dioxo-3,4-dihydropyrimidin-1(2*H*)-yl)octanoic acid (*Thy-2*): to a solution of 6.35 g of thymine (50 mmol) in DMF (100 mL), 7.5 g of Na₂CO₃ (50 mmol) and 14.8 mL of ethyl 8-bromooctanoate (70 mmol) were added. The temperature was risen using a reaction block until the solution was clear, and the mixture was stirred for 6 h. Then, it was cooled down and left stirring for 2 days at room temperature. The DMF was removed under reduced pressure, and the crude was dissolved in water (50 mL). The product was extracted with dichloromethane, washed with brine (\times 3) and dried with anhydrous MgSO₄. The solvent was removed under reduced pressure and subsequently dissolved in 50 mL of NaOH (2.5 M) and stirred under reflux, using a reaction block, for 2 hours. Then, the mixture was cooled down to room temperature. The solution was acidified with HCl (4 M) to pH 1, and

the precipitate was purified by silica gel chromatography using a mixture of ethyl acetate/methanol/acetic acid (8:2:0.1). The intermediate *Thy-2* was obtained as a white solid (10 g, 75% yield).

^1H NMR (400 MHz, CD_3OD) δ 7.44 (s, 1H), 3.71 (t, $J = 7.6$ Hz, 2H), 2.22 (t, $J = 7.6$ Hz, 2H), 1.87 (s, 3H), 1.67-1.60 (m, 4H), 1.36 (m, 6H); $^{13}\text{C}\{^1\text{H}\}$ NMR (100 MHz, CD_3OD) δ 176.1, 166.6, 151.6, 141.9, 109.7, 48.0, 34.7, 28.8, 28.5, 25.9, 25.0, 20.7, 10.8; HRMS (ESI): m/z calcd. for (MH^+) $\text{C}_{13}\text{H}_{21}\text{N}_2\text{O}_4$: 269.1512, found: 269.1501.

Synthesis of *N*-(4-benzoylbenzyl)-8-(5-methyl-2,4-dioxo-3,4-dihydropyrimidin-1(2*H*)-yl)octanamide (*Int-D10*): to a solution of *Thy-2* (0.73 g, 2.7 mmol) in DMF, 0.78 g of EDC (4.1 mmol) and 0.44 g of HOBt (3.3 mmol) were added; the mixture was kept at 0 °C using an ice bath for 15 min. Then, a solution of BPN (0.74 g, 3.0 mmol) in DMF was added dropwise. The mixture was stirred at 0 °C for 2 hours. Then, DMF was removed under reduced pressure and the crude was dissolved in ethyl acetate and washed with 1M NaHCO_3 , HCl 1M and brine. The final product *Int-D10* was purified by recrystallization and obtained as a white solid (563 mg, 45% yield).

^1H NMR (400 MHz, CD_3OD) δ 7.76-7.43 (m, 9H), 7.41 (s, 1H), 4.46 (s, 2H), 3.69 (t, $J = 7.2$ Hz, 2H), 2.27 (t, $J = 7.2$ Hz, 2H), 1.86 (s, 3H), 1.65 (m, 4H), 1.36 (m, 6H); $^{13}\text{C}\{^1\text{H}\}$ NMR (100 MHz, CD_3OD) δ 196.9, 174.9, 165.5, 151.5, 144.2, 141.8, 137.5, 136.2, 132.4, 130.0, 129.6, 128.1, 127.1, 109.7, 47.9, 42.3, 35.6, 28.7, 28.5, 28.5, 25.9, 25.4, 10.8; HRMS (ESI): m/z calcd. for (MH^+) $\text{C}_{27}\text{H}_{32}\text{N}_3\text{O}_4$: 462.2393, found: 462.2398.

Synthesis of *N*-(4-benzoylbenzyl)-8-(3,5-dimethyl-2,4-dioxo-3,4-dihydropyrimidin-1(2*H*)-yl)octanamide (dyad **D10**): to a solution of *Int-D10* (260 mg, 0.56 mmol) in 3 mL of NaOH (2.5 M), 250 μ L of SO₂(OMe)₂ (2.5 mmol) were added dropwise. The mixture was stirred overnight at room temperature. The crude product was extracted with ethyl acetate (\times 3), washed with 1M NaHCO₃ and dried with anhydrous MgSO₄, filtered and concentrated under reduced pressure. The final product was purified by precipitation in dichloromethane/hexane to get **D10** as a white solid (236 mg, 89% yield).

¹H NMR (400 MHz, CDCl₃) δ 7.75-7.44 (m, 9H), 6.96 (s, 1H), 4.52 (s, 2H), 3.69 (t, *J* = 7.2 Hz, 2H), 3.34 (s, 3H), 2.25 (t, *J* = 7.2 Hz, 2H), 1.93 (s, 3H), 1.68 (m, 4H), 1.35 (m, 6H); ¹³C{¹H} NMR (100 MHz, CD₃OD) δ 196.8, 174.9, 164.6, 151.7, 144.1, 139.9, 137.5, 136.2, 132.4, 130.0, 129.6, 128.1, 127.1, 112.2, 49.1, 42.4, 35.6, 28.6, 28.5, 28.4, 26.9, 25.9, 25.4, 11.5; Yield: 89%. HRMS (ESI): *m/z* calcd. for (MH⁺) C₂₈H₃₄N₃O₄: 476.2549, found: 476.2546.

(*Z*)-3-hydroxy-1³-methyl-3-phenyl-1¹,1²,1³,1⁴-tetrahydro-6-aza-1(5,1)-pyrimidina-4(1,4)-benzenacyclodecaphane-1²,1⁴,7-trione (**PP-D6**). ¹H NMR (400 MHz, CD₃OD) δ 7.64-7.26 (m, 9H), 6.91 (m, 1H), 5.43 (s, 1H), 4.32 (d, *J* = 13.6 Hz, 1H), 4.03 (d, *J* = 13.6 Hz, 1H), 3.70 (m, 1H), 3.55 (d, *J* = 13.6 Hz, 1H), 3.27 (s, 3H), 3.14 (m, 1H), 3.03 (d, *J* = 13.6 Hz, 1H), 2.23 (m, 1H), 1.84 (m, 1H), 1.70 (m, 1H), 1.15 (m, 1H); ¹³C{¹H} NMR (100 MHz, CD₃OD) δ 174.7, 165.5, 151.2, 147.1, 145.0, 142.4, 138.5, 128.9, 127.8, 127.3, 126.9, 126.9, 126.5, 126.4, 108.1, 78.5, 48.7, 43.1, 38.0, 32.5, 27.0, 25.9; HRMS (ESI): *m/z* calcd. for (MH⁺) C₂₄H₂₆N₃O₄: 420.1923, found: 420.1927.

1⁴,1⁶-dimethyl-1⁸-phenyl-1⁷-oxa-1²,1⁴,4-triaza-1(8,2)-bicyclo[4.2.0]octana-2(1,4)-benzenacyclododecaphane-1³,1⁵,5-trione (**Ox-D10**). ¹H NMR (400 MHz, CDCl₃) δ 7.50-7.08 (m, 9H), 5.91 (m, 1H), 4.90 (dd, *J*₁ = 8.8 Hz, *J*₂ = 14 Hz, 1H), 4.52 (s, 1H), 3.80 (dd, *J*₁ = 4 Hz, *J*₂ = 14 Hz, 1H), 3.57 (m, 1H), 3.34 (s, 3H), 2.49 (m, 1H), 2.24 (m, 1H), 2.00 (m, 1H), 1.62 (s, 3H), 1.8-0.2 (m, 10H); ¹³C{¹H} NMR (100 MHz, CDCl₃) δ 172.9, 168.6, 151.7, 143.7, 140.5, 138.6, 128.7, 128.5, 128.4, 128.0, 126.0, 90.7, 75.1, 69.0, 51.7, 42.7, 36.4, 28.6, 27.9, 27.3, 26.7, 26.6, 26.3, 24.4; HRMS (ESI): *m/z* calcd. for (MH⁺) C₂₈H₃₄N₃O₄: 476.2549, found: 476.2545. CCDC 2022525.

Steady-state photolysis. Irradiations were performed in a multilamp Luzchem photoreactor emitting at λ_{max} = 350 nm (14 × 8 W lamps). Isoabsorptive solutions at 350 nm (*A* = 0.05, concentration ~20 μM) of the different bichromophoric systems were irradiated at different times in acetonitrile under N₂ through quartz cells. For photoproduct studies, higher concentrations of the dyads (2.6 mM) were used; irradiations were performed through Pyrex for 3h.

Analytical instrumentation. A semipreparative JASCO HPLC system (PU-2080 Plus pump, DG-2080-54 line degasser and LG-2080-04 gradient unit) connected to a JASCO (UV-1575) detector was used to separate and purify the different photoproducts, using an isocratic flux (2 mL/min) of MeCN as an eluent, and a SEA18 Teknokroma column, 5 μm (25 cm × 1 cm).

Spectroscopic Techniques. The ¹H and ¹³C NMR spectra were recorded at 400 and 100 MHz, respectively, using a Bruker AVANCE III instrument; chemical shifts are reported in ppm.

High-resolution mass spectrometry (HRMS) was performed in an Ultra Performance Liquid Chromatography (UPLC) ACQUITY system (Waters Corp.) with a conditioned autosampler at 4 °C. The separation was accomplished on an ACQUITY UPLC BEH C18 column (50 mm × 2.1 mm i.d., 1.7 μm), which was maintained at 40 °C. The analysis was performed using acetonitrile and water (60:40 v/v containing 0.01% formic acid) as the mobile phase with a flow rate of 0.5 mL/min, and injection volume was 5 μL. The Waters ACQUITY™ XevoQToF Spectrometer (Waters Corp.) was connected to the UPLC system *via* an electrospray ionization (ESI) interface. This source was operated in positive ionization mode with the capillary voltage at 1.5 kV at 100 °C and the temperature of the desolvation was 300 °C. The cone and desolvation gas flows were 40 L h⁻¹ and 800 L h⁻¹, respectively. The collision gas flow and collision energy applied were 0.2 mL/min and 12 V, respectively. All data collected in Centroid mode were acquired using Masslynx™ software (Waters Corp.). Leucine-enkephalin was used at a concentration of 500 pg/μL as the lock mass generating an [M+H]⁺ ion (*m/z* 556.2771) and fragment at *m/z* 120.0813 and flow rate of 50 μL/min to ensure accuracy during the MS analysis.

Steady-state absorption spectra were recorded in a JASCO V-760 spectrophotometer. Laser Flash Photolysis (LFP) measurements were performed using a pulsed Nd:YAG L52137 V LOTIS TII at the excitation wavelength of 355 nm. The single pulses were *ca.* 10 ns duration, and the energy was ~12 mJ/pulse. The laser flash photolysis system consisted of the pulsed laser, a 77250 Oriel monochromator and an oscilloscope DP04054 Tektronix. The output signal from the oscilloscope was transferred to a personal computer. Absorbances of all solutions were adjusted at ~0.20 at 355 nm in MeCN. All UV and LFP measurements

were done using $10 \times 10 \text{ mm}^2$ quartz cuvettes at room temperature in deaerated conditions (25 min N_2 bubbling), using 30 mL of fresh solution in order to avoid data acquisition from photodegraded products.

Femtosecond transient absorption experiments were performed using a pump-probe system. The femtosecond pulses were generated with a mode-locked Ti-Sapphire laser of a compact Libra HE (4 W power at 4 kHz) regenerative amplifier delivering 100 fs pulses at 800 nm (1 mJ/pulse). The output of the laser was split into two parts to generate the pump and the probe beams. Thus, tunable femtosecond pump pulses were obtained by directing the 800 nm light into an optical parametric amplifier. In the present case, the pump was set at 280 nm and passed through a chopper prior to focus onto a rotating cell (1 mm optical path) containing the samples in organic solution. The white light used as probe was produced after part of the 800 nm light from the amplifier travelled through a computer controlled 8 ns variable optical delay line and impinge on a CaF_2 rotating crystal. This white light was in turn split in two identical portions to generate reference and probe beams that then are focused on the rotating cell containing the sample. The pump and the probe beams were made to coincide to interrogate the sample. The power of the pump beam was set to 180 μW . A computer-controlled imaging spectrometer was placed after this path to measure the probe and the reference pulses to obtain the transient absorption decays/spectra. The experimental data were treated and compensated by the chirp using the ExciPro program.

5. Supplementary material

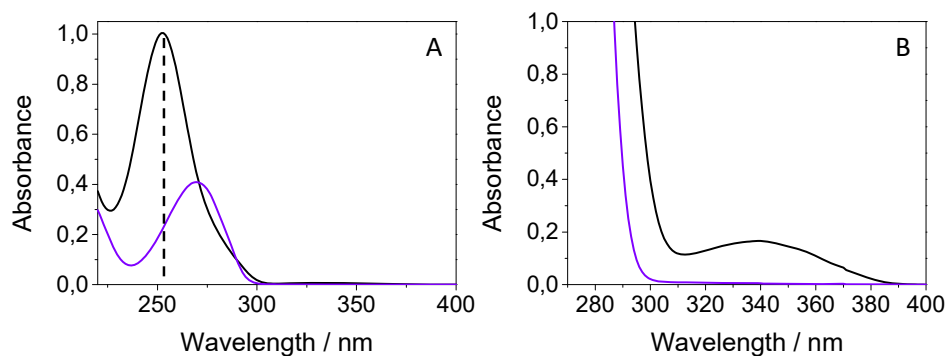


Figure S3.1. UV absorption spectra for BPN (black) and DMT (violet) in MeCN at 5×10^{-5} M (A) and 1 mM (B). The dashed line indicates the absorption at 254 nm, which was used for monitoring the course of the reaction.

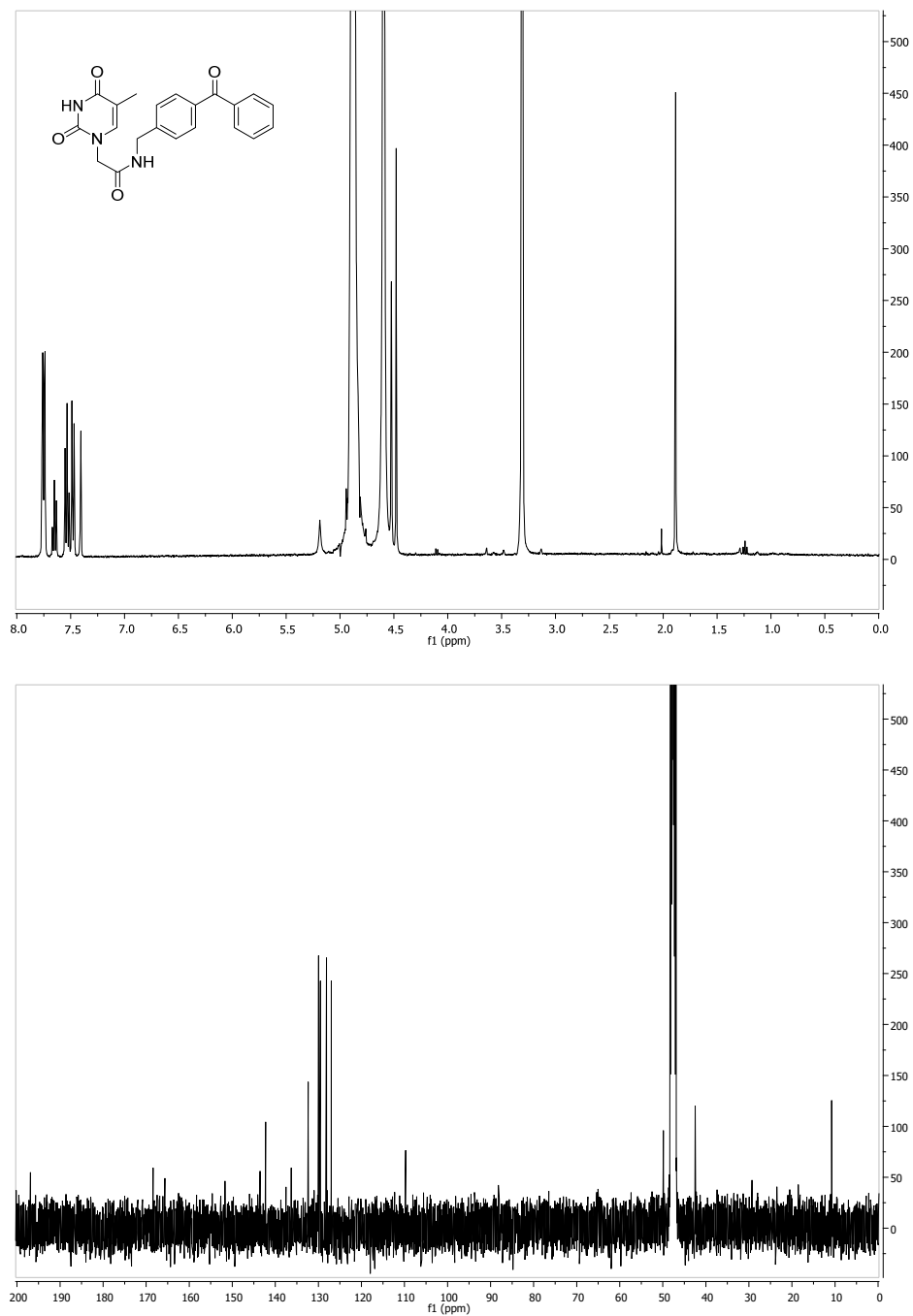


Figure S3.2. 1H - and ^{13}C -NMR for *int-D4* in CD_3OD .

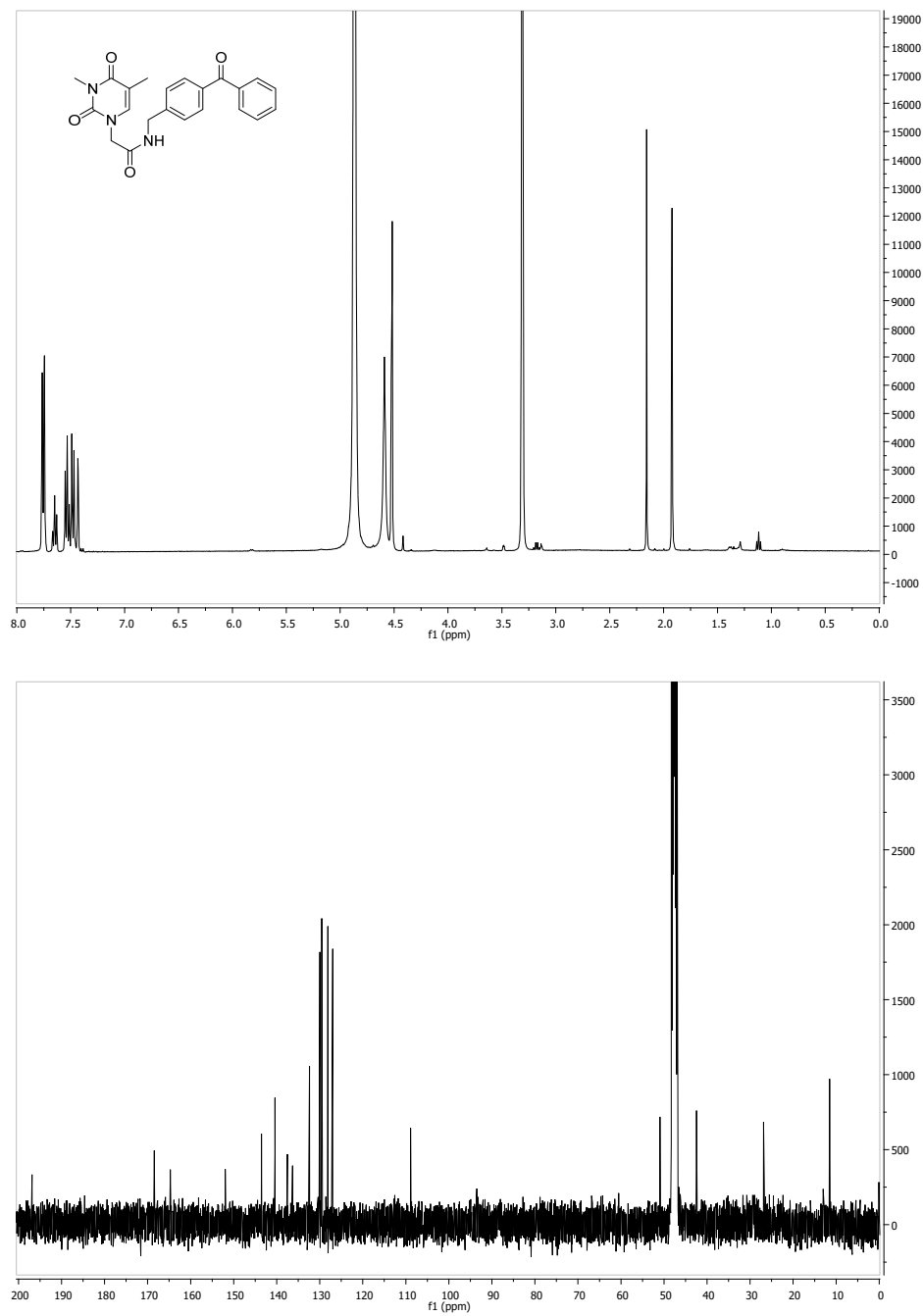


Figure S3.3. 1H - and ^{13}C -NMR for **D4** in CD_3OD .

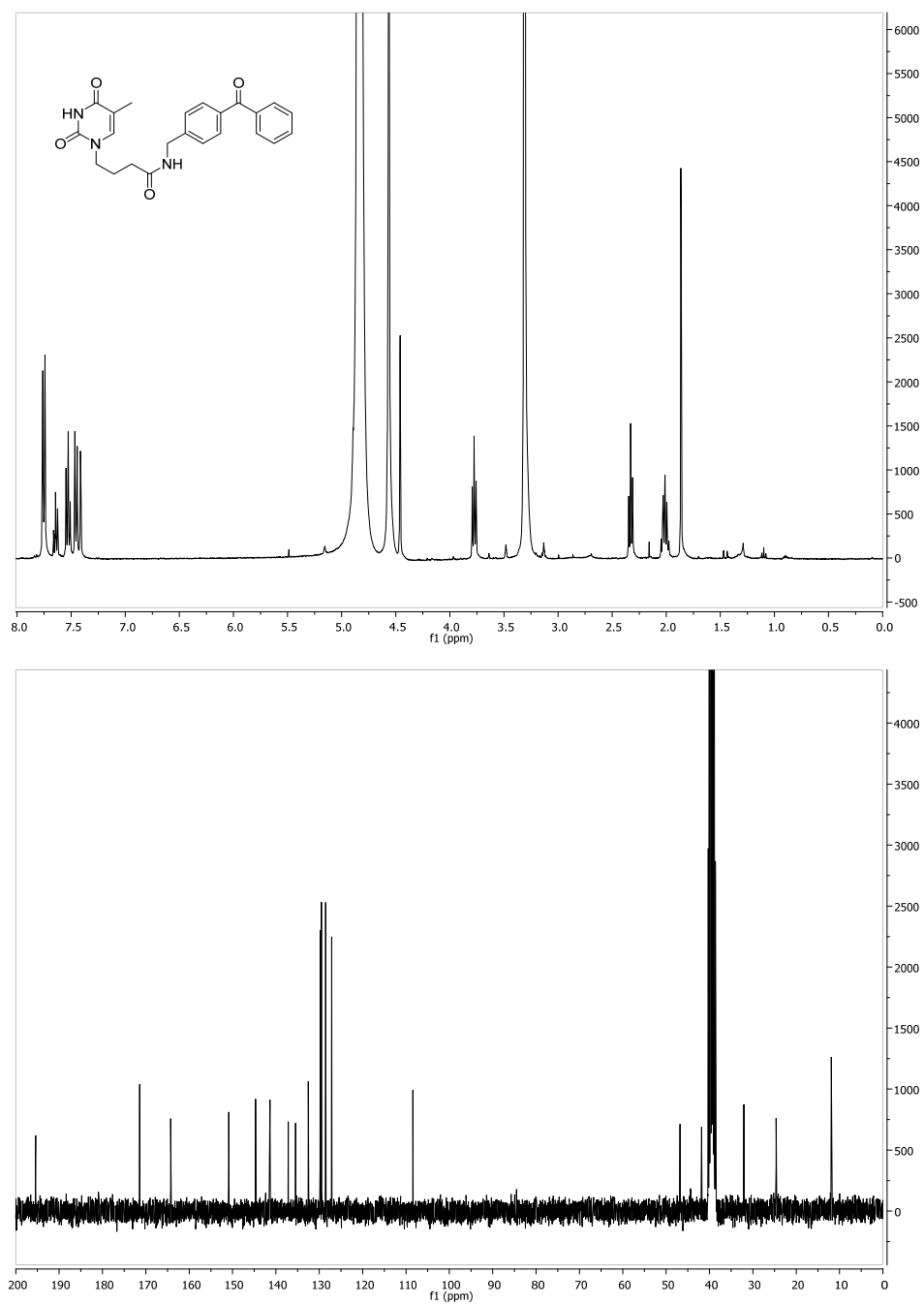


Figure S3.4. ¹H-NMR in CD₃OD and ¹³C-NMR for *int-D6* in DMSO-d₆.

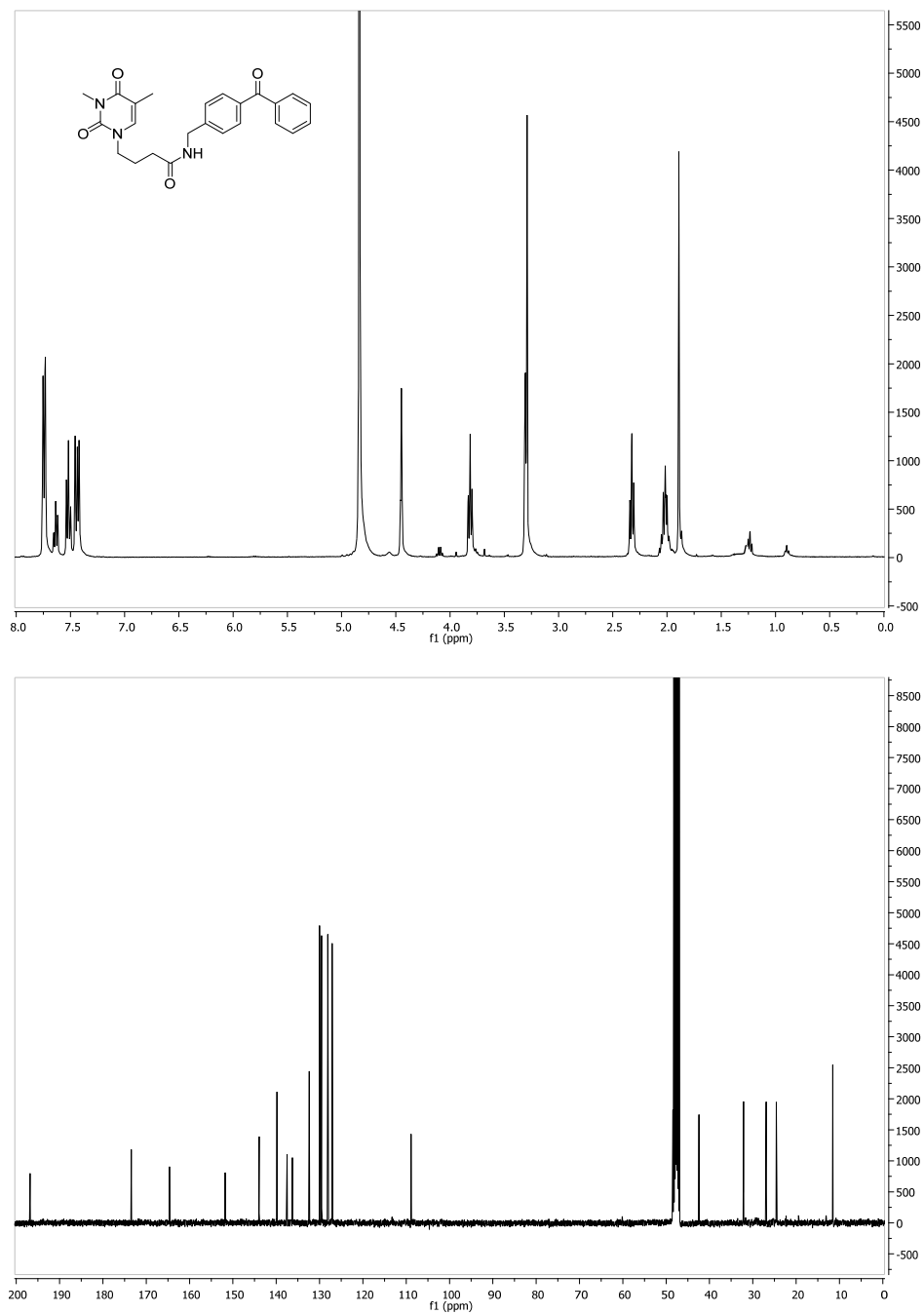


Figure S3.5. ¹H- and ¹³C-NMR for D6 in CD₃OD.

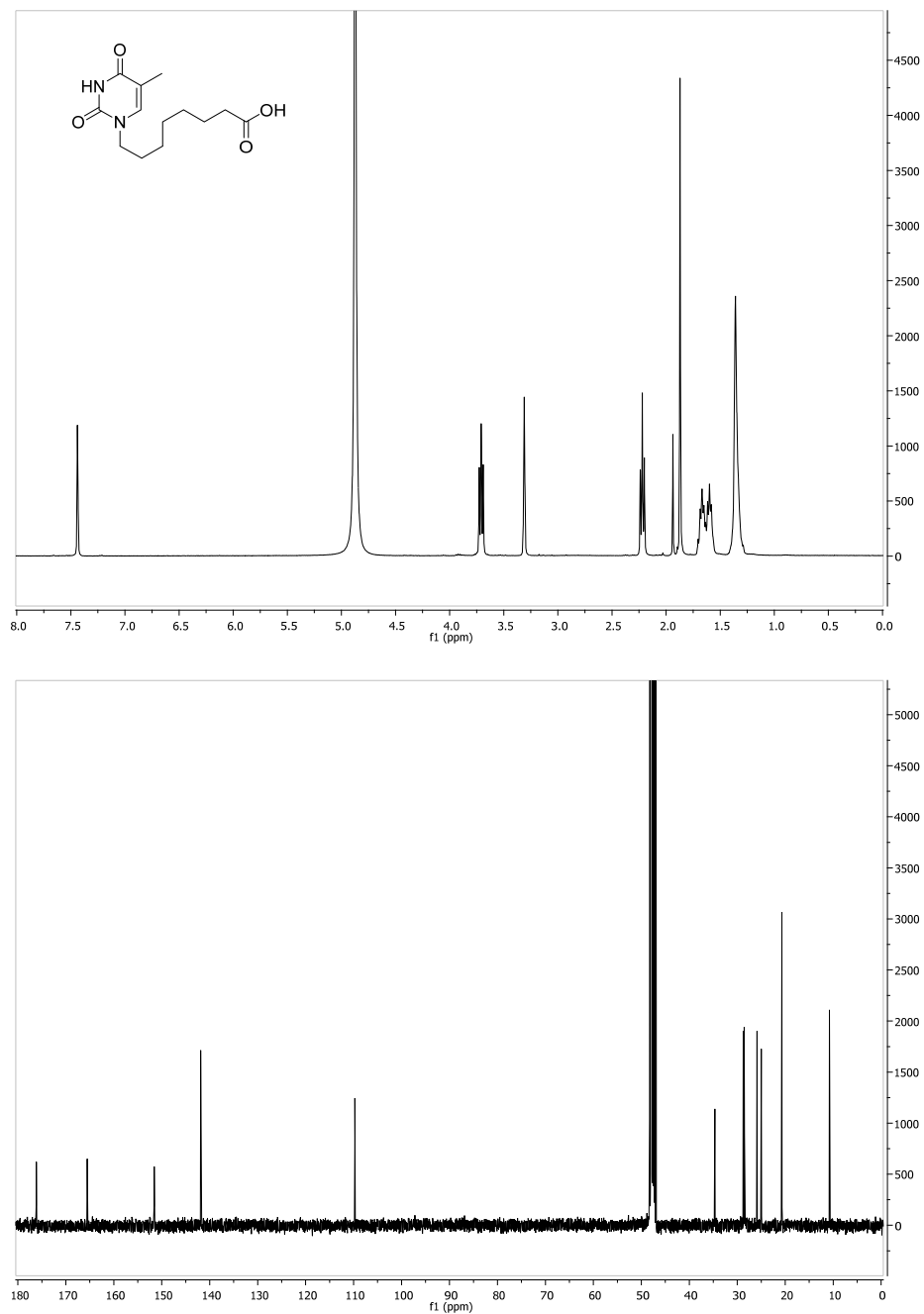


Figure S3.6. ¹H- and ¹³C-NMR for Thy-2 in CD₃OD.

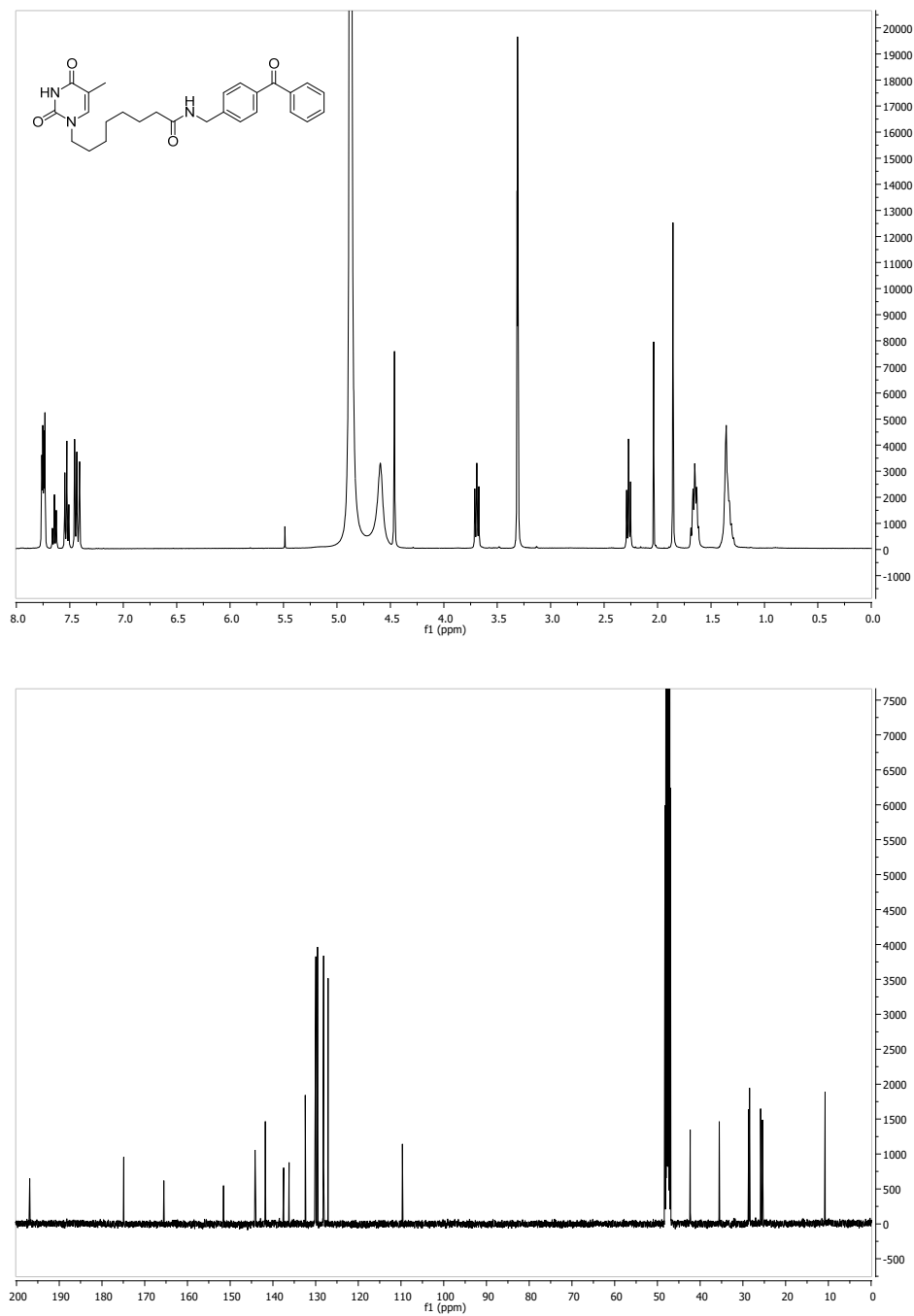


Figure S3.7. 1H - and ^{13}C -NMR for *int-D10* in CD_3OD .

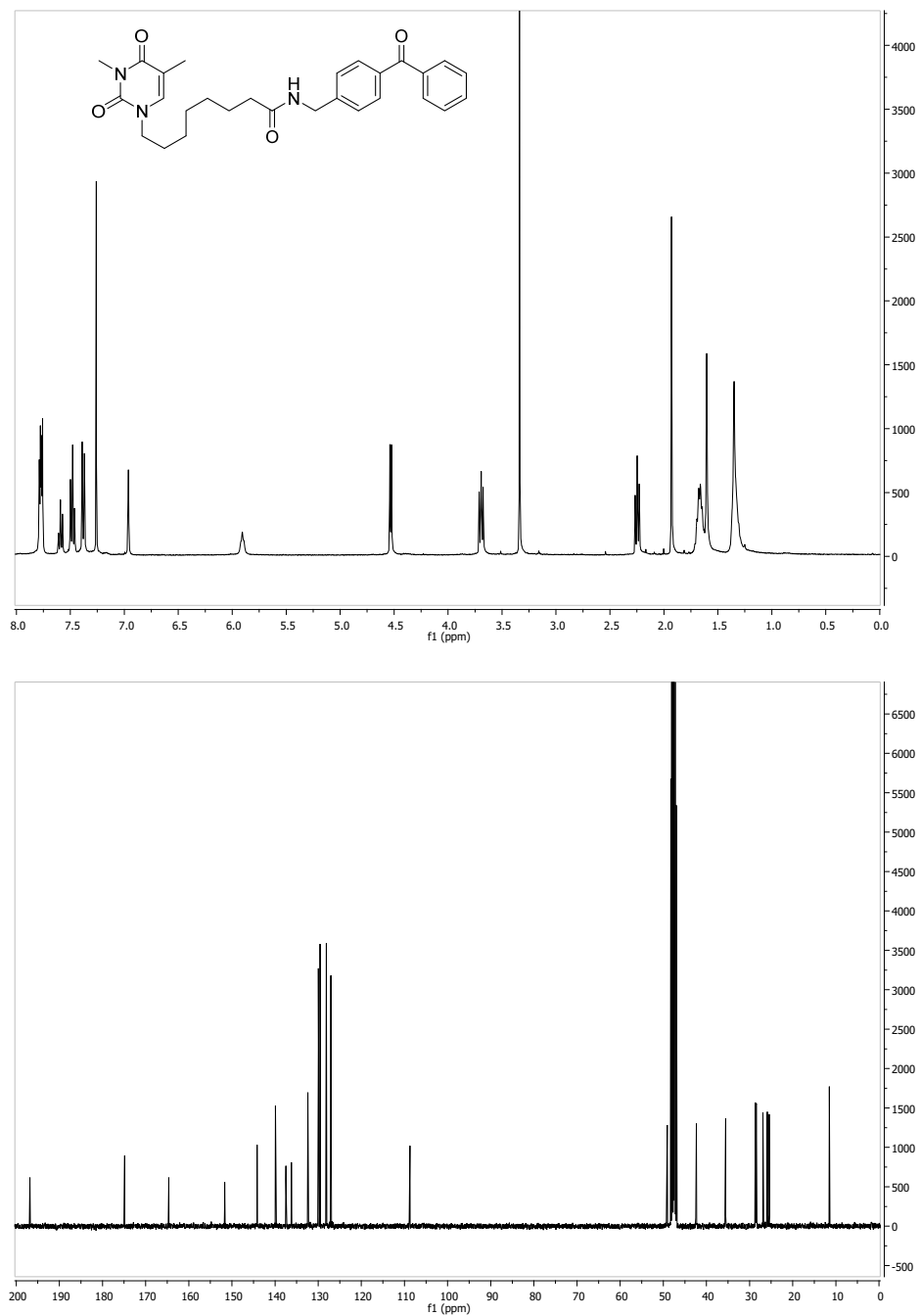


Figure S3.8. $^1\text{H-NMR}$ in CDCl_3 and $^{13}\text{C-NMR}$ for **D10** in CD_3OD .

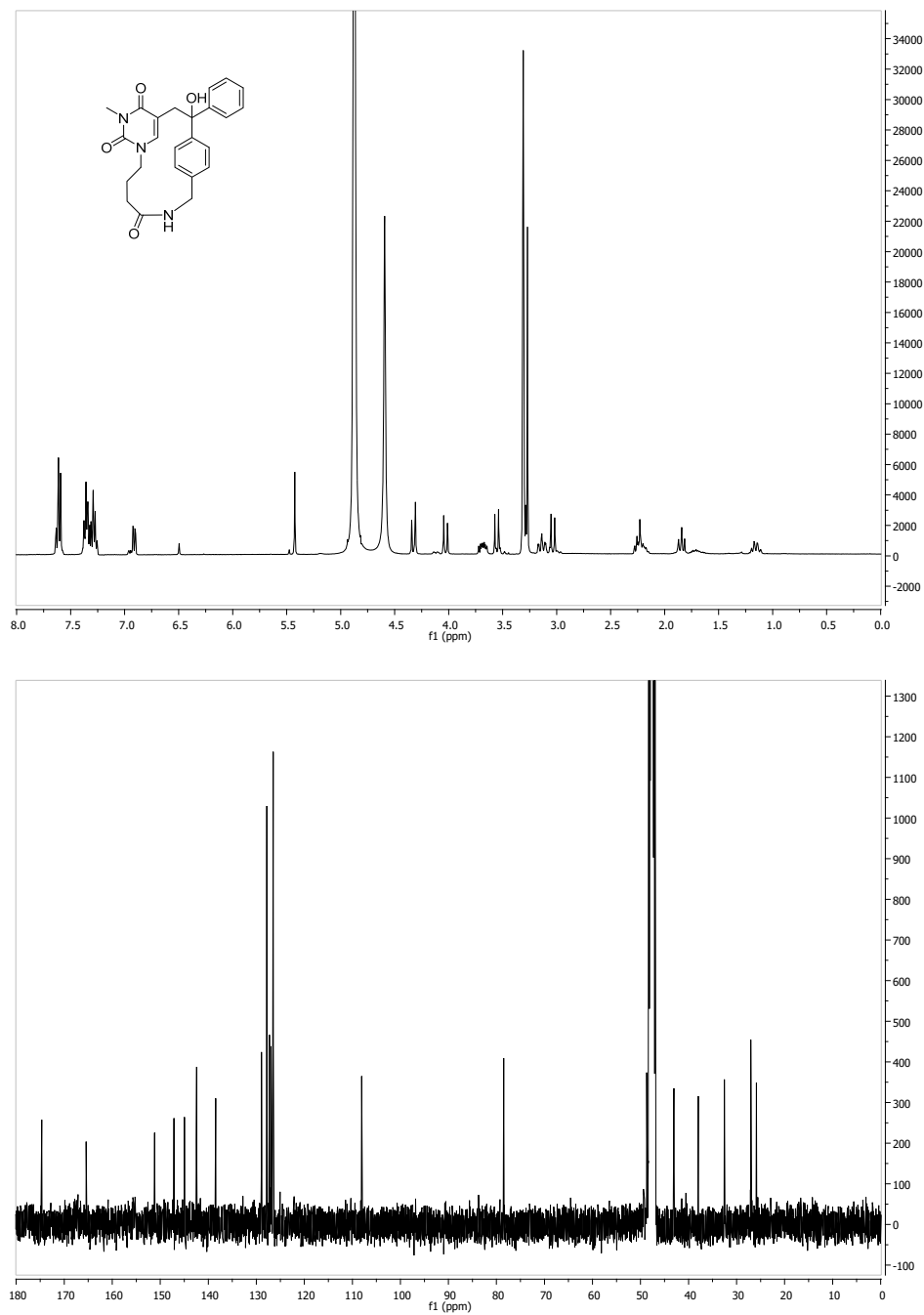


Figure S3.9. ¹H- and ¹³C-NMR for PP-D6 in CD₃OD.

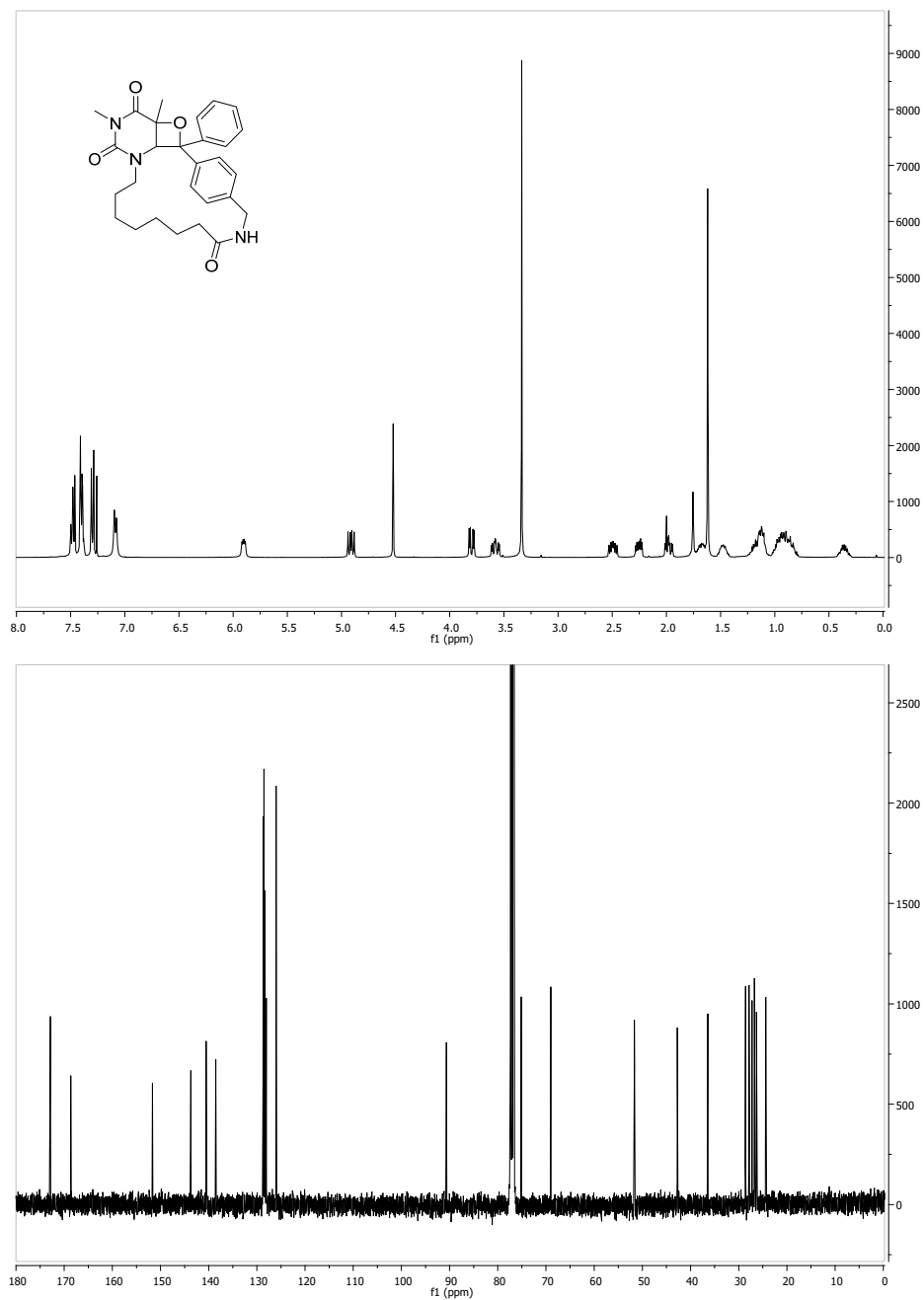


Figure S3.10. ¹H- and ¹³C-NMR for Ox-D10 in CDCl₃.

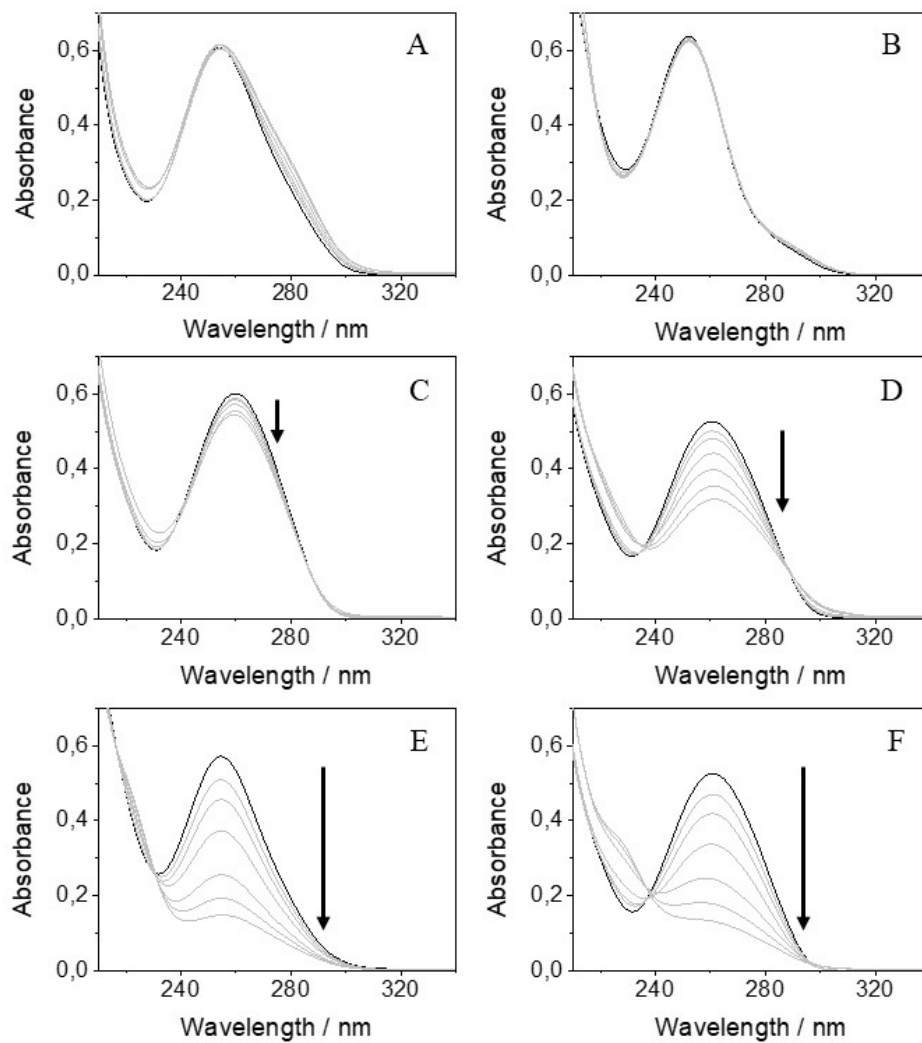


Figure S3.11. UV absorption spectra for BPN (A), KP (B), D4 (C), D6 (D), D7 (E) and D10 (F) upon irradiation at different times (0, 2.5, 5, 10, 20, 30 and 40 min) in deaerated MeCN within a photoreactor emitting at $\lambda_{\max} = 350$ nm.

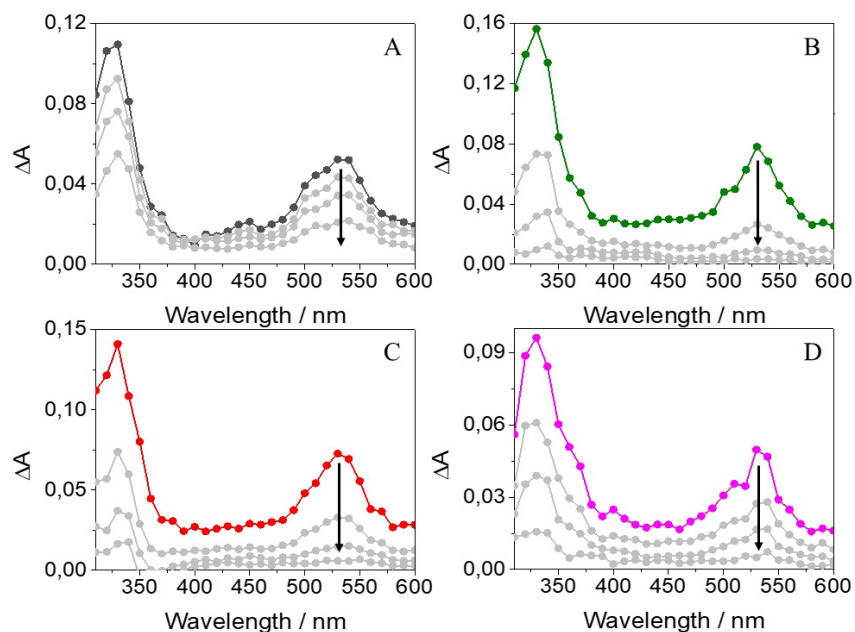


Figure S3.12. Laser flash photolysis spectra for BPN (A), **D4** (B), **D6** (C) and **D10** (D) upon excitation at 355 nm in deaerated MeCN. The spectra were recorded at 0.1, 0.5, 1.0 and 2.0 μs after the laser pulse except for **D10**, that were obtained after 0.02, 0.04, 0.08 and 0.14 μs .

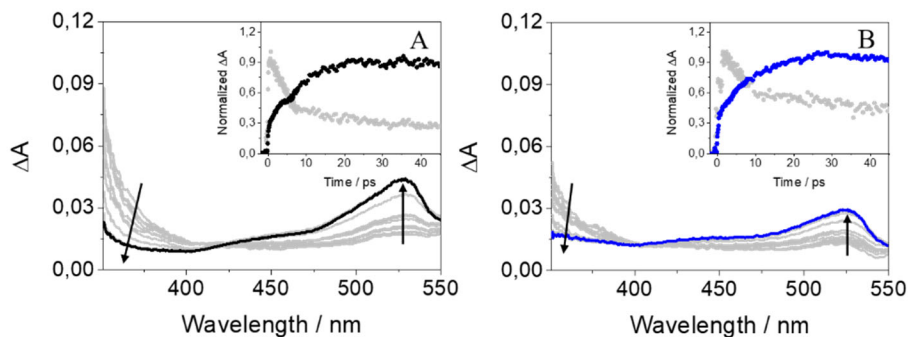


Figure S3.13. Femtosecond transient absorption spectra from 0.5 to 40 ps for KP (A) and **D7** (B). The insets show the kinetic traces at 340 (gray) and 530 nm (black for KP and blue for **D7**) upon excitation at 280 nm in acetonitrile.

X-ray Crystallography data for Ox-D10. Computing details and crystal data.

Colorless crystals of **Ox-D10** (CCDC 2022525) were obtained from slow evaporation of its saturated dichloromethane solution.

Data collection: APPEX3v2018.7-2 (BRUKER AXS, 2005); cell refinement: APPEX3v2018.7-2 (BRUKER AXS, 2005); data reduction: APPEX3v2018.7-2 (BRUKER AXS, 2005); program(s) used to solve structure: SHELXT2018/2 (Sheldrick, 2015); program(s) used to refine structure: SHELXL2018/3 (Sheldrick, 2018); molecular graphics: ORTEP for Windows (Farrugia, 2012); software used to prepare material for publication: WinGX publication routines (Farrugia, 2012).

$C_{28}H_{33}N_3O_4 \cdot CH_2Cl_2$	$F(000) = 1184$
Mr = 560.5	$D_x = 1.326 \text{ Mg m}^{-3}$
Orthorhombic, Pna2 ₁	Cu $K\alpha$ radiation, $\lambda = 1.54178 \text{ \AA}$
Hall symbol: P 2c -2n	Cell parameters from 8103 reflections
a = 9.4467 (2) \AA	$\Theta = 3.1\text{-}74.5^\circ$
b = 28.7768 (6) \AA	$\mu = 2.40 \text{ mm}^{-1}$
c = 10.3242 (2) \AA	T = 100 K
V = 2806.59 (10) \AA^3	Plate, colorless
Z = 4	0.27 × 0.12 × 0.04 mm

Data collection

Bruker D8 VENTURE PHOTON III-14	$T_{\min} = 0.799$, $T_{\max} = 0.929$
Diffractionmeter	32650 measured reflections
Radiation source: INCOATEC	
microfocus sealed tube,	5676 independent reflections
Incoatec $I\mu S$ 3.0	4896 reflections with $I > 2\sigma(I)$
Incoatec multilayer mirror monochromator	$R_{\text{int}} = 0.082$
Detector resolution: 7.3910 pixels mm^{-1}	$\Theta_{\max} = 74.4^\circ$, $\Theta_{\min} = 3.1^\circ$
ω and phi scans	$h = -11 \rightarrow 10$

Absorption correction: multi-scan	$k = -31 \rightarrow 35$
BRUKER SADABS2016/2	$l = -12 \rightarrow 12$
<i>Refinement</i>	
Refinement on F^2	Hydrogen site location: inferred from neighboring sites
Least-squares matrix: full	H-atom parameters constrained
$R[F^2 > 2\sigma(F^2)] = 0.049$	$w = 1/[\sigma^2(Fo^2) + (0.0763P)^2 + 1.0782P]$
$wR(F^2) = 0.133$	where $P = (Fo^2 + 2Fc^2)/3$
$S = 1.03$	$(\Delta/\sigma)_{\max} < 0.001$
5676 reflections	$\Delta\rho_{\max} = 0.37 \text{ e } \text{\AA}^{-3}$
349 parameters	$\Delta\rho_{\min} = -0.66 \text{ e } \text{\AA}^{-3}$
2 restraints	Absolute structure: Flack x determined using 1921
0 constraints	quotients $[(+)-(-)]/[(+)+(-)]$ (Parsons, Flack and Wagner, Acta Cryst. B69 (2013) 249-259).
Primary atom site location: dual	
Secondary atom site location: dual	Absolute structure parameter: 0.009 (10)

Special details

Geometry. All e.s.d.'s (except the e.s.d. in the dihedral angle between two l.s. planes) are estimated using the full covariance matrix. The cell e.s.d.'s are taken into account individually in the estimation of e.s.d.'s in distances, angles and torsion angles; correlations between e.s.d.'s in cell parameters are only used when they are defined by crystal symmetry. An approximate (isotropic) treatment of cell e.s.d.'s is used for estimating e.s.d.'s involving l.s. planes.

6. References

1. Friedel, M. G.; Cichon, M. K.; Carell, T., *DNA damage and repair: photochemistry*. 2nd ed.; CRC Handbook of Organic Photochemistry and Photobiology CRC Press LLC: Boca Raton, 2004.
2. Kraemer, K. H., Sunlight and skin cancer: Another link revealed. *Proc. Natl. Acad. Sci. USA* **1997**, *94*, 11-14.
3. Cadet, J.; Mouret, S.; Ravanat, J. L.; Douki, T., Photoinduced damage to cellular DNA: Direct and photosensitized reactions. *Photochem. Photobiol.* **2012**, *88*, 1048-1065.
4. Rastogi, R. P.; Richa; Kumar, A.; Tyagi, M. B.; Sinha, R. P., Molecular mechanisms of ultraviolet radiation-induced DNA damage and repair. *J. Nucleic Acids* **2010**, *2010*, 592980.
5. Sinha, R. P.; Hader, D. P., UV-induced DNA damage and repair: A review. *Photochem. Photobiol. Sci.* **2002**, *1*, 225-236.
6. Chatterjee, N.; Walker, G. C., Mechanisms of DNA damage, repair, and mutagenesis. *Environ. Mol. Mutagen.* **2017**, *58*, 235-263.
7. Brash, D. E.; Haseltine, W. A., UV-induced mutation hotspots occur at DNA damage hotspots. *Nature* **1982**, *298*, 189-192.
8. Cadet, J.; Berger, M.; Douki, T.; Ravanat, J. L., Oxidative damage to DNA: Formation, measurement, and biological significance. In *Physiology biochemistry and pharmacology*, Giessen, E. H., Ed. Springer: **1997**; Vol. 131, 1-87.

9. Taylor, J. S.; Cohrs, M. P., DNA, light and Dewar pyrimidones: The structure and biological significance of TpT3. *J. Am. Chem. Soc.* **1987**, *109*, 2834-2835.
10. Taylor, J. S.; Garrett, D. S.; Cohrs, M. P., Solution-state structure of the Dewar pyrimidone photoproduct of thymidylyl-(3'-5')-thymidine. *Biochemistry* **1988**, *27*, 7206-7215.
11. Kim, S. T.; Malhotra, K.; Smith, C. A.; Taylor, J. S.; Sancar, A., Characterization of (6-4) Photoproduct DNA Photolyase. *J. Biol. Chem.* **1994**, *269*, 8535-8540.
12. Li, J.; Liu, Z.; Tan, C.; Guo, X.; Wang, L.; Sancar, A.; Zhong, D., Dynamics and mechanism of repair of ultraviolet-induced (6-4) photoproduct by photolyase. *Nature* **2010**, *466*, 887-890.
13. Todo, T.; Ryo, H.; Yamamoto, K.; Toh, H.; Inui, T.; Ayaki, H.; Nomura, T.; Ikenaga, M., similarity among the drosophila (6-4)photolyase, a human photolyase homolog, and the DNA photolyase-blue-light photoreceptor family. *Science* **1996**, *272*, 109-112.
14. Todo, T.; Takemori, H.; Ryo, H.; Ihara, M.; Matsunaga, T.; Nikaido, O.; Sato, K.; Nomura, T., A new photoreactivating enzyme that specifically repairs ultraviolet light-induced (6-4)photoproducts. *Nature* **1993**, *361*, 371-374.
15. Todo, T.; Tsuji, H.; Otsoshi, E.; Hitomi, K.; Kim, S. T.; Ikenaga, M., Characterization of a human homolog of 6-4 photolyase. *Mutat. Res.* **1997**, *384*, 195-204.
16. Epe, B.; Pflaum, M.; Boiteux, S., DNA damage induced by photosensitizers in cellular and cell-free systems. *Mutat. Res.* **1993**, *299*, 135-145.

17. Michaud, S.; Hajj, V.; Latapie, L.; Noiro, A.; Sartor, V.; Fabre, P. L.; Chouini-Lalanne, N., Correlations between electrochemical behaviours and DNA photooxidative properties of non-steroidal anti-inflammatory drugs and their photoproducts. *J. Photochem. Photobiol. B* **2012**, *110*, 34-42.
18. Maguery, M. C.; Chouini-Lalanne, N.; Ader, J. C.; Paillous, N., Comparison of the DNA damage photoinduced by fenofibrate and ketoprofen, two phototoxic drugs of parent structure. *Photochem. Photobiol.* **1998**, *68*, 679-684.
19. Vinette, A. L.; McNamee, J. P.; Bellier, P. V.; McLean, J. R. N.; Scaiano, J. C., Prompt and delayed nonsteroidal anti-inflammatory drug-photoinduced DNA damage in peripheral blood mononuclear cells measured with the comet assay. *Photochem. Photobiol.* **2003**, *77*, 390-396.
20. Lhiaubet, V.; Gutierrez, F.; Penaud-Berruyer, F.; Amouyal, E.; Daudey, J. P.; Poteau, R.; Chouini-Lalanne, N.; Paillous, N., Spectroscopic and theoretical studies of the excited states of fenofibric acid and ketoprofen in relation with their photosensitizing properties. *New J. Chem.* **2000**, *24*, 403-410.
21. Lhiaubet, V.; Paillous, N.; Chouini-Lalanne, N., Comparison of DNA damage photoinduced by ketoprofen, fenofibric acid and benzophenone via electron and energy transfer. *Photochem. Photobiol.* **2001**, *74*, 670-678.
22. Cuquerella, M. C.; Lhiaubet-Vallet, V.; Cadet, J.; Miranda, M. A., Benzophenone photosensitized DNA damage. *Acc. Chem. Res.* **2012**, *45*, 1558-1570.

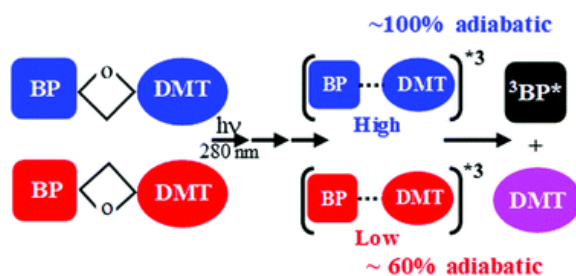
23. Bignon, E.; Marazzi, M.; Besancenot, V.; Gattuso, H.; Drouot, G.; Morell, C.; Eriksson, L. A.; Grandemange, S.; Dumont, E.; Monari, A., Ibuprofen and ketoprofen potentiate UVA-induced cell death by a photosensitization process. *Sci. Rep.* **2017**, *7*, 8885.
24. Bosca, F.; Miranda, M. A., Photosensitizing drugs containing the benzophenone chromophore. *J. Photochem. Photobiol. B* **1998**, *43*, 1-26.
25. Rogers, J. E.; Kelly, L. A., Nucleic acid oxidation mediated by naphthalene and benzophenone imide and diimide derivatives: Consequences for DNA redox chemistry. *J. Am. Chem. Soc.* **1999**, *121*, 3854-3861.
26. Surana, K.; Chaudhary, B.; Diwaker, M.; Sharma, S., Benzophenone: A ubiquitous scaffold in medicinal chemistry. *Med. Chem. Commun.* **2018**, *9*, 1803-1817.
27. Cuquerella, M. C.; Lhiaubet-Vallet, V.; Bosca, F.; Miranda, M. A., Photosensitized pyrimidine dimerization in DNA. *Chem. Sci.* **2011**, *2*, 1219-1232.
28. Blasco-Brusola, A.; Navarrete-Miguel, M.; Giussani, A.; Roca-Sanjuán, D.; Vayá, I.; Miranda, M. A., Regiochemical memory in the adiabatic photolysis of thymine-derived oxetanes. A combined ultrafast spectroscopic and CASSCF/CASPT2 computational study. *Phys. Chem. Chem. Phys.* **2020**, *22*, 20037-20042.
29. Burrows, C. J.; Muller, J. C., Oxidative nucleobase modifications leading to strand scission. *Chem. Rev.* **1998**, *98*, 1109-1151.
30. Belmadoui, N.; Climent, M. J.; Miranda, M. A., Photochemistry of a naphthalene-thymine dyad in the presence of acetone. *Tetrahedron* **2006**, *62*, 1372-1377.

31. Bonancia, P.; Vayá, I.; Climent, M. J.; Gustavsson, T.; Markovitsi, D.; Jimenez, M. C.; Miranda, M. A., Excited-state interactions in diastereomeric flurbiprofen-thymine dyads. *J. Phys. Chem. A* **2012**, *116*, 8807-8814.
32. Encinas, S.; Climent, M. J.; Gil, S.; Abrahamsson, U. O.; Davidsson, J.; Miranda, M. A., Singlet excited-state interactions in naphthalene-thymine dyads. *ChemPhysChem* **2004**, *5*, 1704-1709.
33. Belmadoui, N.; Encinas, S.; Climent, M. J.; Gil, S.; Miranda, M. A., Intramolecular interactions in the triplet excited states of benzophenone-thymine dyads. *Chem. Eur. J.* **2006**, *12*, 553-561.
34. Dumont, E.; Wibowo, M.; Roca-Sanjuan, D.; Garavelli, M.; Assfeld, X.; Monari, A., Resolving the benzophenone DNA-photosensitization mechanism at QM/MM level. *J. Phys. Chem. Lett.* **2015**, *6*, 576-580.
35. Delatour, T.; Douki, T.; D'Ham, C.; Cadet, J., Photosensitization of thymine nucleobase by benzophenone through energy transfer, hydrogen abstraction and one-electron oxidation. *J. Photochem. Photobiol. B* **1998**, *44*, 191-198.
36. Tamai, N.; Asahi, T.; Masuhara, H., Intersystem crossing of benzophenone by femtosecond transient grating spectroscopy. *Chem. Phys. Lett.* **1992**, *198*, 413-418.
37. Gut, I. G.; Wood, P. D.; Redmond, R. W., Interaction of triplet photosensitizers with nucleotides and DNA in aqueous solution at room temperature. *J. Am. Chem. Soc.* **1996**, *118*, 2366-2373.
38. Miró, P.; Gómez-Mendoza, M.; Sastre, G.; Cuquerella, M. C.; Miranda, M. A.; Marín, M. L., Generation of the thymine triplet state by through-bond energy transfer. *Chem. Eur. J.* **2019**, *25*, 7004-7011.

39. Joseph, A.; Prakash, G.; Falvey, D. E., Model studies of the (6-4) photoproduct photolyase enzyme: Laser flash photolysis experiments confirm radical ion intermediates in the sensitized repair of thymine oxetane adducts. *J. Am. Chem. Soc.* **2000**, *122*, 11219-11225.
40. Martinez, L. J.; Scaiano, J. C., Transient intermediates in the laser flash photolysis of ketoprofen in aqueous solution: Unusual photochemistry of the benzophenone chromophore. *J. Am. Chem. Soc.* **1997**, *119*, 11066-11070.
41. Pérez-Ruiz, R.; Groeneveld, M.; van Stokkum, I. H. M.; Tormos, R.; Williams, R. M.; Miranda, M. A., Fast transient absorption spectroscopy of the early events in photoexcited chiral benzophenone-naphthalene dyads. *Chem. Phys. Lett.* **2006**, *429*, 276-281.
42. Martens, J.; Maison, W.; Schlemminger, I.; Westerhoff, O.; Groger, H. **2000**. "Preparation of precursors for PNA monomers". WO 2000002864.

CHAPTER 4:

Regiochemical memory in the adiabatic photolysis of thymine-derived oxetanes. A combined ultrafast spectroscopic and CASSCF/CASPT2 computational study



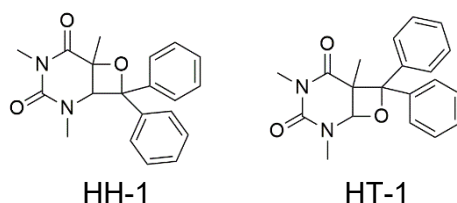
1. Introduction

Solar ultraviolet light is known to induce cellular DNA damage through a number of processes including the dimerization of neighbouring pyrimidines.¹⁻⁴ Cyclobutane pyrimidine dimers (CPDs) and to a lesser extent pyrimidine (6-4) pyrimidone photoproducts ((6-4)PPs) are the most abundant UV-induced lesions in DNA;⁴⁻⁶ their formation may result in the appearance of mutations, cell death and cancer.⁷⁻⁹ In humans, these lesions are normally repaired through a process known as nucleotide excision repair; however, other organisms (i.e. bacteria, plants, etc.) have developed efficient photorepair mechanisms¹⁰⁻¹³ that involve binding of a specific enzyme to the DNA lesion and reactivation through a photoinduced electron transfer process.¹⁴⁻²¹

Previously, the photoinduced cycloreversion of oxetanes generated from 1,3-dimethylthymine (DMT) and carbonyl compounds has been investigated as a model for the photoenzymatic repair of DNA (6-4)PPs.²²⁻³⁰ Direct photolysis of some oxetane derivatives was observed to result in a rare adiabatic cleavage leading to the triplet excited state of the corresponding carbonyl species, along with ground state DMT.^{24, 30} A more recent work has proposed that cycloreversion takes place in a stepwise manner from the singlet excited state, with population of the triplet excited carbonyl at a later stage.²⁸ All these studies have been performed on the chemically stable head-to-head (HH) oxetane obtained from the Paternò-Büchi reaction between DMT and the photoactive carbonyl derivative (this is also the regioisomer structurally closer to the purported intermediate formed between two adjacent thymines that ultimately leads to the (6-4)PP); however, the photobehaviour of its

chemically less stable head-to-tail (HT) regioisomer, which is also obtained in the reaction,³¹⁻³² has not yet been addressed.

With this background, in order to gain deeper insight into the mechanism of the photoinduced cycloreversion of thymine-derived oxetanes, the photobehaviour of the head-to-head and head-to-tail regioisomers obtained from benzophenone (BP) and DMT (HH-1 and HT-1, respectively; see Scheme 4.1) has been investigated by means of a combined experimental and theoretical approach. This involves transient absorption spectroscopy from the femtosecond to the microsecond time scales, in addition to a detailed computational analysis including multiconfigurational quantum-chemistry calculations (complete-active-space self-consistent field/complete-active-space second-order perturbation theory, CASSCF/CASPT2). Thus, ultrafast spectroscopy in tandem with high-level computational analysis have allowed us to settle the primary processes preceding the photolytic reactions with the aim of delineating the complex excited state relaxation processes that are involved.



Scheme 4.1. Chemical structures of head-to-head (HH-1) and head-to-tail (HT-1) DMT-BP oxetane regioisomers.

2. Results and discussion

The synthesis of HH-1 and HT-1 has been described earlier.³¹ Briefly, a solution containing DMT (100 mM) and BP (200 mM) in acetonitrile (MeCN) was placed into Pyrex tubes and irradiated *ca.* 8h under nitrogen in a multilamp Luzchem photoreactor emitting at $\lambda_{\text{max}} = 350$ nm (12×8 W lamps). The crude was purified by column chromatography (SiO_2 , hexane/ethyl acetate, 80/20, v/v) followed by recrystallization of the separated fractions; the purity of both compounds was checked by ^1H -NMR (see Figure S4.1 in the supplementary material). Direct steady-state UVC-photolysis of HH-1 and HT-1 gave rise to BP and DMT as the only photoproducts.

Laser flash photolysis (LFP) measurements were conducted in deaerated MeCN ($\lambda_{\text{exc}} = 266$ nm) on isoabsorptive solutions at the excitation wavelength for HH-1, HT-1 and BP, as a reference compound. Since oxetanes can in principle be partially degraded during the measurements, fresh solutions were employed after each light pulse, in order to rule out possible artefacts due to secondary excitation of photodegradation products.

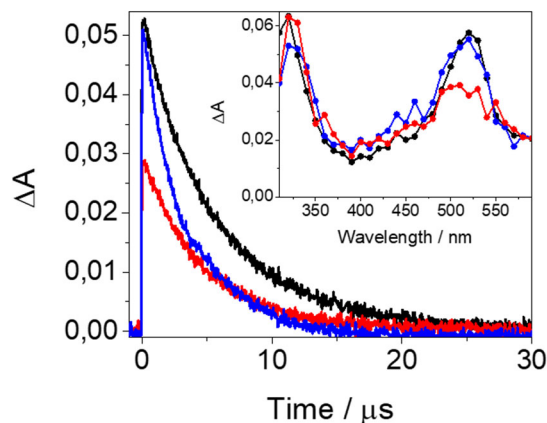


Figure 4.1. LFP decay traces for BP (black), HH-1 (blue) and HT-1 (red) at 530 nm upon excitation at 266 nm in deaerated MeCN. The inset shows the transient absorption spectra 150 ns after the laser pulse.

The profile of the transient absorption spectra for HH-1 and HT-1 was very similar to that of ${}^3\text{BP}^*$ (inset in Figure 4.1).³³ However, a weak absorption in the 350-400 nm region was noticed for both regioisomers. The most interesting finding was the observation of a transient absorption at 530 nm (where ${}^3\text{BP}^*$ displays its maximum)³⁴ immediately after the laser pulse. Our results indicate that, within the duration of the shot, a practically quantitative adiabatic population of the triplet excited state of benzophenone is indeed accomplished for HH-1.²⁴ By contrast, photolysis of HT-1 also induced population of ${}^3\text{BP}^*$ albeit to a much lesser extent (*ca.* 60%). Thus, a clear regiodifferentiation has been observed in the adiabatic photochemical reaction, which was much more effective for HH-1. The decay traces followed a one order law with lifetimes of about 5 μs for BP and HT-1 and slightly shorter for HH-1 ($\sim 3.5 \mu\text{s}$).

The weak absorption in the 350-400 nm region detected for both oxetanes could be associated with a transient species with some ${}^3\text{DMT}^*$ character,

as the maximum of the triplet-triplet absorption of thymine (Thy) is centred at 370 nm.³⁵⁻³⁶ In this context, LFP measurements ($\lambda_{\text{exc}} = 355$ nm) were conducted in deaerated MeCN on mixtures containing BP and increasing amounts of DMT; under these conditions, the only absorbing species is BP. As shown in Figure 4.2A, a clear quenching of $^3\text{BP}^*$ was evidenced upon addition of DMT, with a rate constant of ca. $1.2 \times 10^9 \text{ M}^{-1} \text{ s}^{-1}$, which is in the order of the previously reported value.²³

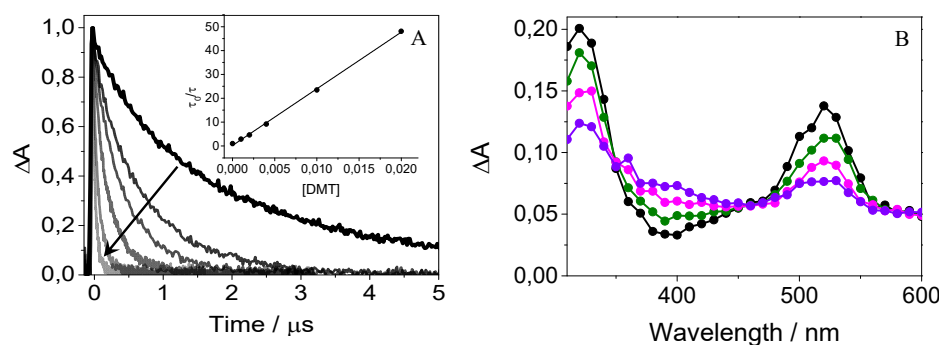


Figure 4.2. (A) Normalized LFP decay traces for BP/DMT mixtures (from 1:0 to 1:10) at 530 nm. The inset shows the Stern-Volmer analysis for $^3\text{BP}^*$ quenching. (B) LFP absorption spectra for BP (black) and BP/DMT mixtures at 1:1 (green), 1:5 (magenta) and 1:10 (violet) molar ratios recorded 30 ns after the laser pulse. Measurements were performed upon excitation at 355 nm in deaerated MeCN.

The nature of $^3\text{BP}^*$ quenching upon interaction with thymine derivatives has been discussed previously, and attributed mainly to the Paternò-Büchi reaction.^{23, 26, 37} Oxetane formation has been proposed to proceed through 1,4-diradical intermediates of triplet nature,²³ and recently the involvement of triplet exciplex precursors $^3[\text{BP} \cdots \text{Thy}]^*$ has also been inferred.³⁷ This is in fact not surprising in view of the number of examples dealing with oxetane formation through complex-type intermediates such as exciplexes.³⁸ In fact, the transient absorption spectra of Figure 4.2B

clearly show the appearance of a new absorption around 400 nm that increases with DMT concentration. A similar transient has been detected in related products and assigned to $^3\text{Thy}^*$;³⁷ however, a triplet exciplex-like state between BP and DMT ($^3[\text{BP}\cdots\text{DMT}]^*$) cannot be discarded. Indeed, this species would be expected to contain the signatures of both BP and DMT triplet excited states, as it is actually the case for the detected transient.

In order to investigate the possible participation of the triplet exciplex $^3[\text{BP}\cdots\text{DMT}]^*$ in the cycloreversion processes, a computational analysis based on multiconfigurational quantum-chemistry and the CASSCF/CASPT2 method efficiently combined with density functional theory (DFT) has been performed for HH-1 and HT-1. Computational details as well as analyses to benchmark the methodology can be found in the supplementary material. This high-level analysis allowed us to achieve an interpretation of the experimental observations, and to obtain clear evidence supporting the chemical mechanism involved in the photoinduced oxetane cleavage (see Figure 4.3).

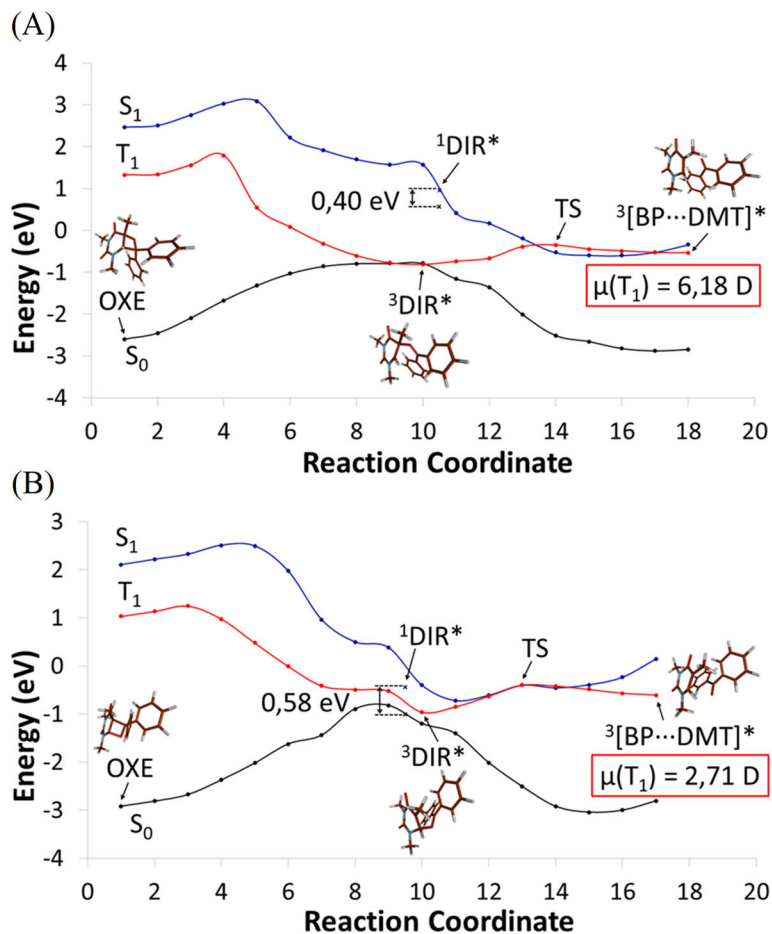


Figure 4.3. Chemical mechanism of the photoinduced cycloreversion process for HH-1 (A) and HT-1 (B). Double-headed arrows indicate the energy gap between S_0 and S_1 at the S_1 equilibrium structure in the diradical region (${}^1\text{DIR}^*$). The reference energy is the sum of the separated triplet BP and ground state DMT molecules. The reaction coordinate, according to the optimized structures, is mostly associated with the breaking of the CC and CO bonds between DMT and BP. See Tables S4.1 - S4.5 in the supplementary material for further details on the electronic-structure and methodological aspects and Tables S4.6-S4.7 in the supplementary material for benchmarking analyses in the supplementary material.

Five key equilibrium structures characterize the photoinduced cycloreversion process: the ground state (S_0) oxetane (OXE), the singlet (S_1) and triplet (T_1) diradicals ($^1\text{DIR}^*$ and $^3\text{DIR}^*$, respectively) with the C-C bond broken, the triplet exciplex ($^3[\text{BP}\cdots\text{DMT}]^*$) and the transition state (TS) between $^3\text{DIR}^*$ and $^3[\text{BP}\cdots\text{DMT}]^*$ related to the C-O bond cleavage. Irradiation of the oxetanes induces population of the excited singlet electronic state. As can be seen from left to right in Figure 4.3, the energy of S_1 decreases significantly along the C-C bond breaking step towards the region of the diradical (DIR^* ; point 10 in Figure 4.3). At this region, an important difference between the two regioisomers can be observed. The energy gap S_1 - S_0 for HT-1 (0.80 eV) is much lower than that for HH-1 (2.35 eV) applying the same methodological procedure for determining the properties of the diradical structure. Such trend is maintained by comparing the state-specific (SS) and multistate (MS) approaches of the CASPT2 (Table S4.7 in the supplementary material), which according to previous studies,³⁹ points to a solid conclusion. The distinct behaviour can be attributed to the different nature of S_1 at this region, as it can be observed in the electron-density difference between S_0 and S_1 for each regioisomer (see Figure 4.4). Thus, S_1 in HT-1 develops a charge transfer character from DMT to BP (see also the large dipole moment in Table S4.1 in the supplementary material), typical of the oxetane ring electronic structure; similar features were previously detected for the thymine-thymine dimer formation.⁴⁰ Meanwhile, S_1 in HH-1 displays a high multiconfigurational character with contributions from electronic configurations corresponding to excitations delocalized over BP and the diradical configuration localized at the broken bond (see Table S4.2 in the supplementary material). This coupling between electronic configurations increases the energy splitting between S_0 and S_1 .

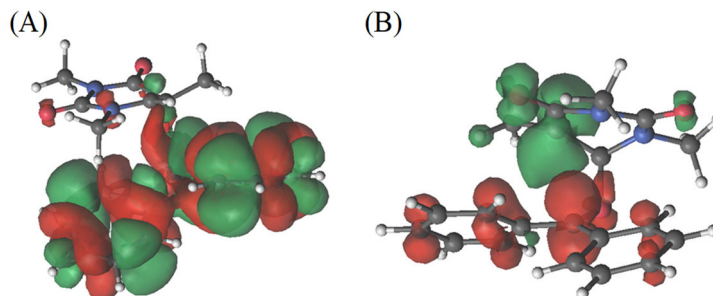


Figure 4.4. S_1 - S_0 electron-density difference at the ${}^3\text{DIR}^*$ geometry for (A) HH-1 and (B) HT-1, computed from the CASSCF wavefunctions of each electronic state. Green and red colours indicate departure and arrival regions, respectively, of electron-density in the S_0 to S_1 excitation. See the nature of the orbitals contributing to the electron densities in Figures S4.3 and S4.8 in the supplementary material.

Computational searches of the S_1 minimum (${}^1\text{DIR}^*$) at the diradical region (with only the C-C bond broken) decrease the energy gap between S_0 and S_1 down to 0.58 and 0.40 eV for HT-1 and HH-1, respectively. From this point, the system can access a nearby conical intersection (CI) (not computed here but estimated in the surroundings) to decay non-radiatively to the ground state or to continue the S_1 surface towards the dissociation of the C-O bond of the oxetane ring. The latter process is favourable considering the downhill energy profile towards the singlet-triplet crossing (STC) with the T_1 surface. This STC involving the energy profiles of S_1 and T_1 is responsible of the so-called “adiabatic” generation of ${}^3\text{BP}^*$ upon excitation of HH-1 or HT-1, which occurs via a triplet exciplex. Non-negligible spin-orbit coupling (SOC) values have been determined for both regioisomers ($\sim 4 \text{ cm}^{-1}$) at the points where S_1 and T_1 become near-degenerate, which allows population of the triplet state. However, significant differences appear for HH-1 and HT-1 regarding the probability of this “adiabatic” $S_1 \rightarrow T_1$ path. Thus, for HH-1, S_1 crosses T_1 at the TS region related to the C-O bond breaking on the triplet T_1 manifold

(see Figure 4.3A), while for HT-1 this crossing occurs before the TS and becomes trapped at the diradical region due to the energy barrier to the transition state (Figure 4.3B). This is a consequence of the large S_0 - S_1 gap at the diradical and the fact that $^1\text{DIR}^*$ is much more energetic for HH-1 than for HT-1. In the latter, $^1\text{DIR}^*$ almost coincides energetically with the equilibrium geometry of the triplet diradical ($^3\text{DIR}^*$).

At the $^3\text{DIR}^*$ diradical, the ground state S_0 and the lowest-lying triplet excited state T_1 show a small energy gap for both HH-1 and HT-1, and therefore this point corresponds to a singlet-triplet crossing. According to the wavefunctions (see Tables S4.1 and S4.2 in the supplementary material), both S_0 and T_1 states have a diradical nature (with the unpaired electrons at the C atoms of the broken bond and non-parallel and parallel spins for S_0 and T_1 , respectively). This STC point, if reached, shall allow non-radiative decay via intersystem crossing (ISC), even though the SOC, lower than 0.5 cm^{-1} in both systems, points to a slow process.

Therefore, the fact that HH-1 has a high $^1\text{DIR}^*$ energy, clearly above the energy of $^3[\text{BP}\cdots\text{DMT}]^*$, in addition to the S_1/T_1 STC occurring at the TS, points to a favourable production of the triplet exciplex. On the contrary, for HT-1, the lower $^1\text{DIR}^*$ energy and the earlier S_1/T_1 STC nearby the S_0/T_1 STC in addition to the energy barrier to reach TS, makes the evolution towards $^3[\text{BP}\cdots\text{DMT}]^*$ less competitive as compared to the non-radiative decays to the ground state. These findings agree with the lower intensity of the transient absorption band at 530 nm detected by LFP for HT-1.

In order to obtain further key mechanistic information on the early stages of oxetane cycloreversion, and in an attempt to provide additional experimental evidence supporting the formation of triplet-like excimer

states, the photobehaviour of both regioisomers was investigated by means of femtosecond transient absorption spectroscopy and further computational analysis on $^3[\text{BP}\cdots\text{DMT}]^*$. Previous reports have shown that excitation of BP at 360 nm induces formation of a broad transient band from 500 to 600 nm with maximum at 575 nm, assigned to its singlet-singlet absorption band. The intersystem crossing to the triplet excited state, with maximum centred at 525 nm, has been found to proceed within *ca.* 9.6 ps.⁴¹ This is in good agreement with a later work performed at $\lambda_{\text{exc}} = 267$ nm, where deactivation of the benzophenone singlet excited state at 340 nm, leading to the triplet through ISC, has been found to occur in about 10.6 ps.²⁸ Herein, isoabsorptive solutions of HH-1, HT-1 and BP in MeCN were subjected to femtosecond laser excitation at 280 nm, making sure that the degree of photodegradation was lower than 5 % at the end of each experiment. The transient absorption spectra from 0.1 to 40 ps are shown in Figure S4.14 in the supplementary material. In the case of BP, an absorption band with maximum at 530 nm was formed within *ca.* 10.4 ps, along with the deactivation of the band at 340 nm, associated to $^1\text{BP}^*$ (Figures 4.5A and D); this value for the ISC is very similar to those previously reported.^{28, 41}

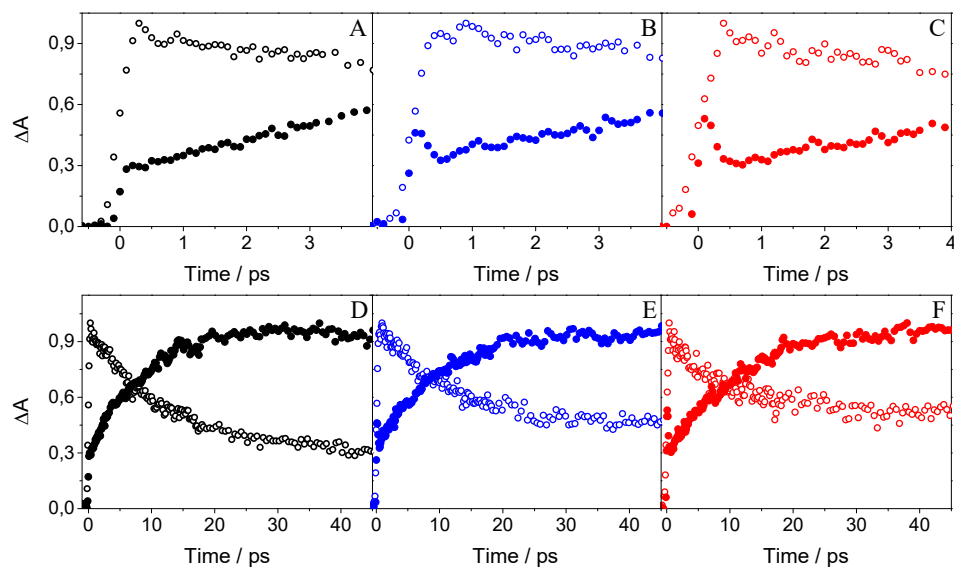


Figure 4.5. Femtosecond kinetic traces at 340 nm (open circles) and 530 nm (solid circles) at different time windows for: (A) and (D) BP; (B) and (E) HH-1 and (C) and (F) HT-1 after excitation at 280 nm in MeCN.

Analysis of the kinetics at 530 nm, where the singlet excited state also exhibits some absorption very early after excitation,⁴¹ revealed an ultrafast decay of ~ 270 fs for both HH-1 and HT-1 (Figures 4.5B and C), not detected for BP. This time constant, which is in the order of that reported by Kwok et al.,²⁸ was attributed to the C-C bond scission from the singlet state to generate a diradical intermediate. After the initial ultrafast decay, the trace at 530 nm started to grow, in accordance with the triplet excited state formation, with a lifetime of ~ 10.7 ps, which is very similar to that detected for BP.

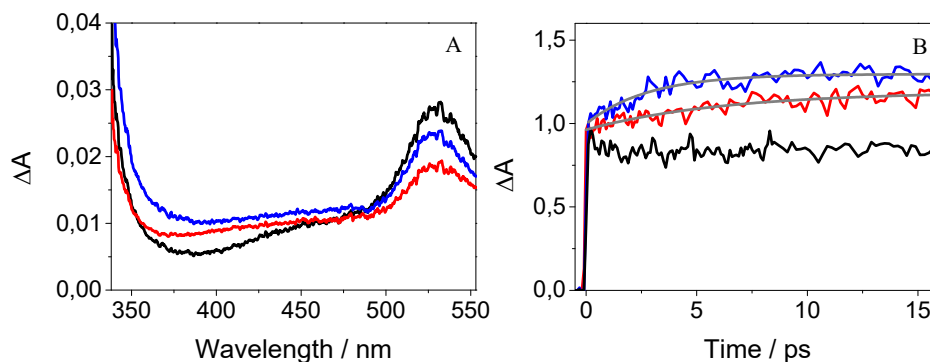


Figure 4.6. (A) Femtosecond transient absorption spectra recorded 20 ps after the laser pulse, and (B) normalized kinetic traces at 400 nm for BP (black), HH-1 (blue) and HT-1 (red) upon excitation at 280 nm in MeCN. The best exponential fit for the data is shown in gray.

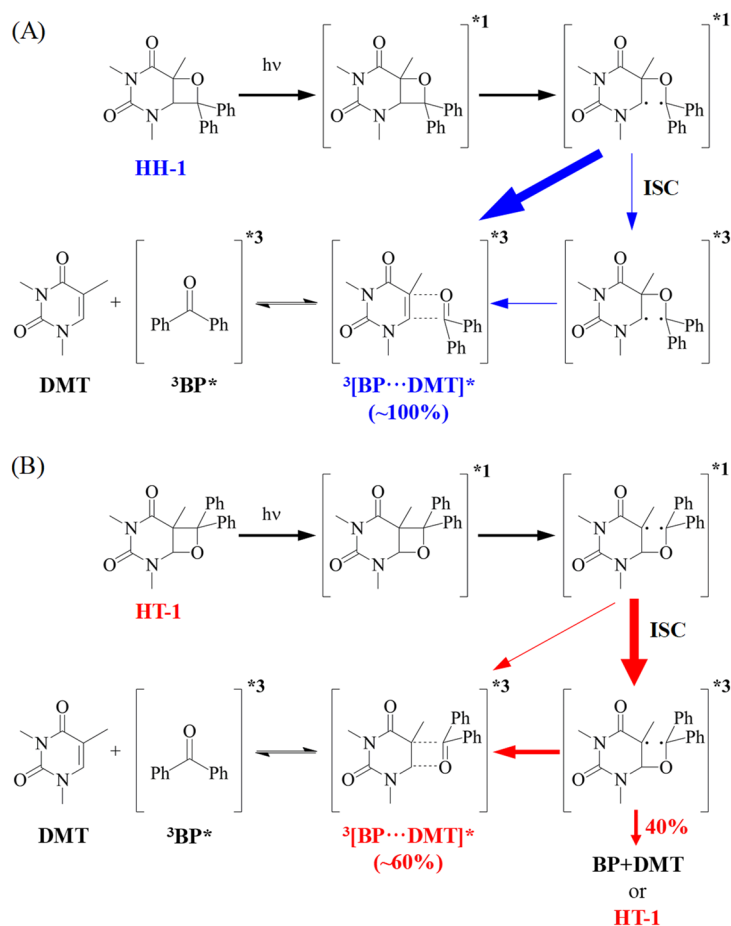
It is worth to highlight the transient absorption detected around 400 nm for both regioisomers (Figure 4.6A), which is absent in BP and lower for HT-1 than for HH-1; as stated above, this band can be taken as a signature of the triplet exciplex state $^3[\text{BP}\cdots\text{DMT}]^*$, which is supported by computational analysis. Thus, significant binding energies were obtained for $^3[\text{BP}\cdots\text{DMT}]^*$ of around 10-12 kcal/mol for both regioisomers (see Table S4.3 in the supplementary material), which points to relatively stable triplet excited state structures. Such binding interactions are due to the delocalization of the excitation among both BP and DMT that characterizes the wavefunction of $^3[\text{BP}\cdots\text{DMT}]^*$ (see Tables S4.1 and S4.2 in the supplementary material). Note that the exciplex maintains the $\pi\pi^*$ nature of the BP moiety upon increasing the accuracy of the CASPT2 methodology (Table S4.7 in the supplementary material).

The triplet exciplex displayed a slightly higher binding energy (~ 2 kcal/mol) for HH-1 than for HT-1 (see Table S4.3 in the supplementary material), which is related to the higher dipole moment found for HH-1

(see Figure 4.3). Experiments using solvents with lower dielectric constant than MeCN were attempted to verify whether the exciplex signature at *ca.* 400 nm changes the relative intensity between HH-1 and HT-1 since computations predict an inversion of stability in non-polar solvents (see Table S4.3 in the supplementary material). However, hydrogen transfer from the benzophenone triplet leading to the ketyl radical was detected, which prevented reproducing the same types of measurements and analyses as in MeCN.

An additional piece of evidence supporting the formation of triplet exciplexes was provided by the computed transient absorption spectra for the more stable HH-1 exciplex (Tables S4.4 and S4.5 in the supplementary material). Herein, it was identified a strong transition ($T_1 \rightarrow T_7$) occurring at 378 nm, which can be directly related to the absorption detected experimentally at *ca.* 400 nm. As we computed in previous studies,⁴² $T_1 \rightarrow T_n$ and $T_2 \rightarrow T_n$ transitions characteristic of isolated ${}^3\text{BP}^*$ occur at energies out of the 400 nm region, and therefore ${}^3\text{BP}^*$ cannot be responsible for the absorption observed at this wavelength.

Further analysis of the kinetics at 400 nm (Figure 4.6B) evidenced a flat profile for BP; by contrast, both oxetane regioisomers (specially HH-1) displayed a clear growth, in agreement with ${}^3[\text{BP}\cdots\text{DMT}]^*$ formation, which was faster for HH-1 (~2.8 ps) than for HT-1 (~6.3 ps). These results are in full agreement with those obtained from computational analysis. Thus, the faster and more efficient formation of the transient at ~400 nm for HH-1 (compared to HT-1) is directly related to its lower energy barrier to reach the triplet exciplex. This is also in line with the higher degree of adiabatic cycloreversion observed for HH-1, as in this case it is much less likely to reach the CI where radiationless deactivation leads back to the starting oxetane or to the dissociated BP and DMT in the ground state.



Scheme 4.2. Proposed mechanism for the photoinduced cycloreversion process for HH-1 (A) and HT-1 (B). The width of the coloured arrows represents the efficiency of a process.

In view of the photophysical and theoretical results, a detailed mechanism for the oxetane cycloreversion is proposed (Scheme 4.2). Note that this mechanism is different from the enzymatic repair, which is triggered by electron transfer. Direct photolysis of HH-1 or HT-1 ($\lambda_{\text{exc}} = 280 \text{ nm}$) instantaneously generates its excited singlet state. Then, diradical singlet intermediates are formed after $\sim 270 \text{ fs}$ through C-C bond scission. For HT-1, the singlet diradicals cross efficiently to triplet diradical states,

whose spectroscopic detection is difficult due to their low absorption around 530 nm and their spectral overlap with the benzophenone triplets.⁴³⁻⁴⁵ Then, around 40% are deactivated to the ground state by ISC while the other 60% evolve to exciplex-like states $^3[\text{BP}\cdots\text{DMT}]^*$ in ca. 6.3 ps. On the contrary, a highly-efficient (~100%) and faster (~2.8 ps) evolution from the singlet diradical to $^3[\text{BP}\cdots\text{DMT}]^*$ occurs for HH-1. The exciplexes present a spectral fingerprint characterized by an absorption at ~400 nm and are in equilibrium with the dissociated $^3\text{BP}^*$ (~10.7 ps) and DMT.

3. Conclusions

The photoinduced cycloreversion of oxetanes derived from DMT and BP has been investigated by means of ultrafast spectroscopy and high-level computational analysis (CASSCF/CASPT2). When the photobehaviour of both HH-1 and HT-1 is compared, an interesting regiochemical memory is observed, revealed by significant differences related to the intermediates generated during oxetane cleavage. Ultrafast spectroscopy shows the regioselective formation of a triplet exciplex $^3[\text{BP}\cdots\text{DMT}]^*$ from diradical intermediates, which occurs to a much higher extent for HH-1. These species (diradicals and exciplexes) have been identified by theoretical analysis, whose results agree with the experimental data. The differences observed in the adiabatic cycloreversion reaction between both regioisomers can be satisfactorily explained on the bases of both the theoretical and experimental results, and a mechanistic proposal is summarized in Scheme 4.2.

4. Experimental section

Chemicals and Reagents

Benzophenone and thymine were purchased from Sigma-Aldrich. Spectrophotometric HPLC solvents were obtained from Scharlab and used without further purification.

Spectroscopic Techniques

The ^1H -NMR spectra were recorded in CDCl_3 at 400 MHz using a Bruker AVANCE III instrument; chemical shifts are reported in ppm.

Laser Flash Photolysis (LFP) measurements were performed using a pulsed Nd: YAG L52137 V LOTIS TII at the excitation wavelength of 266 nm or 355 nm. The single pulses were *ca.* 10 ns duration, and the energy was ~ 12 mJ/pulse. The laser flash photolysis system consisted of the pulsed laser, a 77250 Oriel monochromator and an oscilloscope DP04054 Tektronix. The output signal from the oscilloscope was transferred to a personal computer. Absorbances of HH-1, HT-1 and BP in MeCN were adjusted at ~ 0.20 at 266 nm. Quenching of the triplet excited state of benzophenone (2 mM) after addition of increasing amounts of DMT were performed at $\lambda_{\text{exc}} = 355$ nm. All measurements were done using 10×10 mm² quartz cuvettes at room temperature in deaerated conditions (25 min N_2 bubbling), using 30 mL of fresh solution in order to avoid data acquisition from photodegraded products.

Femtosecond transient absorption experiments were performed using a typical pump-probe system. The femtosecond pulses were generated with a mode-locked Ti-Sapphire laser of a compact Libra HE (4 W power at 4 kHz) regenerative amplifier delivering 100 fs pulses at 800 nm (1 mJ/pulse). The output of the laser was split into two parts to generate the

pump and the probe beams. Thus, tuneable femtosecond pump pulses were obtained by directing the 800 nm light into an optical parametric amplifier. In the present case, the pump was set at 280 nm and passed through a chopper prior to focus onto a rotating cell (1 mm optical path) containing the samples in organic solution. The white light used as probe was produced after part of the 800 nm light from the amplifier travelled through a computer controlled 8 ns variable optical delay line and impinge on a CaF₂ rotating crystal. This white light was in turn split in two identical portions to generate reference and probe beams that then are focused on the rotating cell containing the sample. The pump and the probe beams were made to coincide to interrogate the sample. The power of the pump beam was set to 180 μ W. A computer-controlled imaging spectrometer was placed after this path to measure the probe and the reference pulses to obtain the transient absorption decays/spectra. The experimental data were treated and compensated by the chirp using the ExciPro program.

Computational Details

Density functional theory (DFT) and multiconfigurational quantum chemistry (CASSCF and CASPT2) was used for the computations of this work by using the GAUSSIAN 09, revision D.01,⁴⁶ and MOLCAS 8⁴⁷ software packages, respectively.

Geometry optimizations. The structures of the singlet ground state of the oxetane (OXE), the triplet state of the diradical (³DIR*), the triplet state of the exciplex (³[BP \cdots DMT]*), the triplet transition state (TS) between the diradical and the exciplex and the isolated BP and DMT molecules were optimized using the DFT method with the M06-2X functional, without any symmetry restriction and the standard 6-31++G** basis set. The equilibrium structure of the S₁ state of the diradical (¹DIR*) was

determined with the CASSCF method, with an active space of 6 electrons distributed in 6 orbitals, and the atomic natural orbital (ANO) S-type valence double- ζ plus polarization (ANO-S-VDZP) basis set.

On the one hand, a series of intermediate geometries were obtained by means of the linear interpolation of internal coordinates (LIIC) technique between OXE, $^3\text{DIR}^*$, TS and $^3[\text{BP}\cdots\text{DMT}]^*$ of HH-1. This strategy provides connected but non-optimized paths; therefore, the energy barriers must be considered as upper bounds. For HT-1, LIIC procedure was also used to obtain geometries between $^3\text{DIR}^*$, TS and $^3[\text{BP}\cdots\text{DMT}]^*$. Meanwhile, between OXE and $^3\text{DIR}^*$, due to invalid interpolated structures obtained in the LIIC procedure, ground-state (S_0) constrained geometries were determined using the C-C bond length as scanning coordinate and with the M06-2X/6-31++G** level of theory.

Excited-state single-point calculations. The ground- and excited-state energies on top of the optimized and LIIC (or scanned) geometries were calculated using the state specific (SS)-CASPT2 method, which includes the dynamic correlation, with the state averaged (SA)-CASSCF wave functions with an active space of 12 electrons distributed in 12 orbitals, demanding three singlet and three triplet states in the SA-CASSCF procedure and with the ANO-S-VDZP basis set. The ionization-potential electron-affinity parameter (IPEA) was set to 0.0 au as originally established in MOLCAS, and an imaginary level shift of 0.2 au⁴⁸ was used to minimize the presence of weakly intruder states. Oscillator strengths (f) at the exciplex were calculated according to the formula $f = \frac{2}{3} E_{VA} TDM^2$, where E_{VA} stands for the CASPT2 vertical absorption energy, and TDM refers to the transition dipole moment between the initial φ_1 and final φ_2

SA-CASSCF wave functions, according to the formula $TDM = \langle \varphi_1 | \vec{d} | \varphi_2 \rangle$, where \vec{d} is the dipole moment operator.

Binding energies of the triplet exciplex. They were determined by the formula ${}^3BP^* + {}^1DMT^* - {}^3[BP \cdots DMT]^*$, where the terms stand for the triplet lowest-energy state of the optimized isolated BP, the singlet ground-state energy of the optimized isolated DMT and the triplet lowest-energy state of the optimized exciplex, respectively. Distinct levels of theory were used: (i) DFT/M06-2X/6-31++G** level of theory, (ii) level (i) with the Grimme's dispersion with the original D3 damping function,⁴⁹⁻⁵⁰ (iii) level (i) with the polarizable continuum model (PCM) with the default parameters of GAUSSIAN 09, revision D.01, for the MeCN solvent, (iv) CASPT2/ANO-S-VDZP energies on top of DFT geometries obtained at the level (i) and (v) CASPT2/ANO-S-VDZP energies on top of DFT geometries with PCM obtained at the level (iii). For (v) the solvent correction computed at the DFT level in (iii) was used. Basis set superposition error (BSSE) does not affect significantly DFT energies but it does contribute to the CASPT2 energies and therefore it must be corrected. Therefore, for (iv) and (v), the counterpoise (CP) correction⁵¹ was computed as originally described elsewhere.⁵²

Benchmarking of methodology and additional theoretical analyses

Choice of the active space for the CASSCF/CASPT2 computations.

The choice of the active space (CAS(12,12)) was made based on our previous knowledge of studies of the monomers thymine and BP and dimers of nucleobases.⁵²⁻⁵⁴ For nucleobases, 6 π and π^* orbitals per molecule is an acceptable choice in dimer computations.⁵² For BP, the same size is also reasonable for $\pi\pi^*$ states. For $n\pi^*$ states, the oxygen lone pair (n) can be added.⁵³ To keep an efficient CAS and with the same

size for all the structures and both systems in our study, we used CAS(12,12). The $n\pi^*$ state of BP only appears at the $^3[\text{BP}\cdots\text{DMT}]^*$ geometry for the S_1 . As shown in our previous study in BP,⁵³ while T_1 has mainly $\pi\pi^*$ nature, S_1 is $n\pi^*$. CAS(14,13) test computations at the $^3[\text{BP}\cdots\text{DMT}]^*$ structure for HH-1 show that indeed T_1 keeps the same energy and, as expected, S_1 deviates more, increasing its relative energy (Table S4.6 in the supplementary material). This state in this region does not affect, however, the general conclusions of the work. Regarding the active orbitals in the singlet and triplet computations of this point ($^3[\text{BP}\cdots\text{DMT}]^*$) for HH-1 and HT-1 (Figures S4.5, S4.6, S4.10 and S4.11 in the supplementary material), note also that for the singlets of HH-1, the inclusion of this lone pair converged to a solution in which the π and π^* orbitals are present. Attempts made to remove those orbitals from the active space were made, but in this way the lone pair was not included and the solution without the lone pair ($\pi\pi^*$ state) was higher in energy, as was expected since the lowest excited state is $n\pi^*$. This was not happening for HT-1 despite starting from the same guess orbitals and reflects intrinsic differences in the electronic structure of both systems.

State-specific (SS) and multistate (MS) CASPT2. The energy splitting at the $^3\text{DIR}^*$ was compared at both levels of theory to further analyse the accuracy of the SS-CASPT2 for this region; S_0S_1 gap here is crucial in the comparison between HH-1 and HT-1. As shown in Table S4.7 in the supplementary material, MS slightly increases this gap but the with a similar value for HH-1 and HT-1 therefore maintaining the trends and the comparative behaviour between both systems. Note that, as pointed out in previous studies, the real solution within the CASPT2 framework can be expected in between the gaps provided at the SS and MS levels.⁵⁵

5. Supplementary material

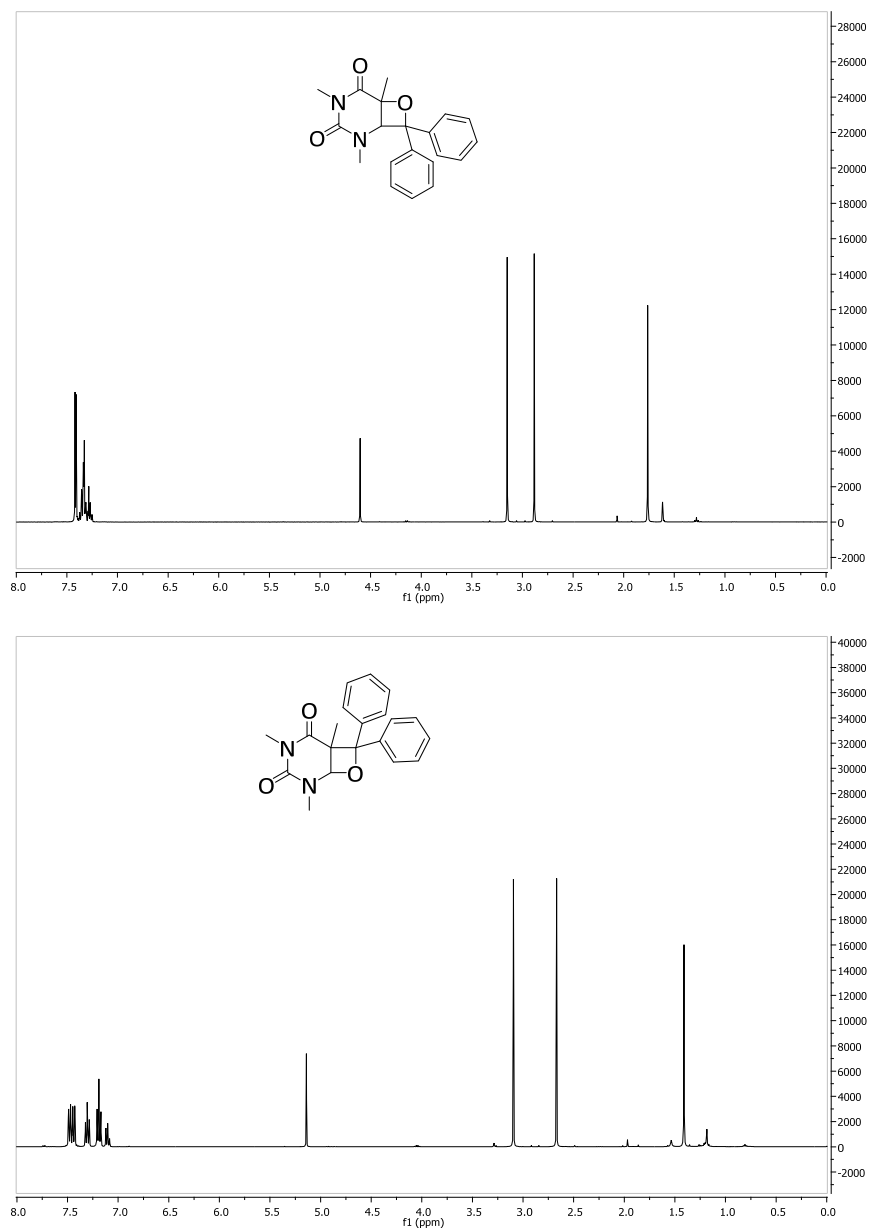


Figure S4.1. ¹H-NMR spectra of HH-1 (top) and HT-1 (bottom) in CDCl₃.

Table S4.1. Nature of the states in each relevant geometry for HT-1: energies (E; in eV), weight of the main configuration state functions in the CASSCF wavefunction and dipole moment (μ ; in Debye). The reference energy is the sum of the separated triplet BP and ground state DMT molecules. See shape of the natural orbitals in Figures S4.2-S4.13.

Geometry	State	Nature	E	Weight	μ
OXE	S ₀	cs (HF) ^a	-2.91	0.831	1.93
	S ₁	$\pi_{BP1} \rightarrow \pi_{BP2}^*$	2.11	0.372	1.87
		$\pi_{BP2} \rightarrow \pi_{BP1}^*$		0.314	
³ DIR*	S ₀	$\pi_{C,DMT} \rightarrow \pi_{C,BP}^*$	-1.19	0.736	2.85
	S ₁	cs (HF) ^a	-0.4	0.730	9.94
	T ₁	$\sigma_{CC,BP-DMT} \rightarrow \sigma_{CC,BP-DMT}^*$	-0.96	0.798	2.66
³ [BP...DMT]*	S ₀	cs (HF) ^a	-2.80	0.770	2.58
	S ₁	$n_{O,BP} \rightarrow \pi_{BP(DMT)}^*$	0.15	0.333	3.44
		$n_{O,BP} \rightarrow \pi_{DMT(BP)}^*$		0.207	
	T ₁	$\pi_{DMT} \rightarrow \pi_{DMT(BP)}^*$	-0.60	0.551	2.71
$\pi_{DMT} \rightarrow \pi_{DMT,BP}^*$		0.280			
¹ DIR*	S ₀	cs (HF) ^a	-1.02	0.925	11.60
	S ₁	$\pi_{C,DMT} \rightarrow \pi_{C,BP}^*$	-0.43	0.916	4.35

^a Closed-shell Hartree-Fock configuration state function.

Table S4.2. Nature of the states in each relevant geometry for HH-1: energies (E; in eV), weight of the main configuration state functions in the CASSCF wavefunction and dipole moment (μ ; in Debye). The reference energy is the sum of the separated triplet BP and ground state DMT molecules. See shape of the natural orbitals in Figures S4.2-S4.13.

Geometry	State	Nature	E	Weight	μ
OXE	S ₀	cs (HF) ^a	-2.59	0.860	4.14
	S ₁	$\pi_{BP3} \rightarrow \pi_{BP1}^*$	2.47	0.391	4.00
		$\pi_{BP1} \rightarrow \pi_{BP3}^*$		0.333	
	³ DIR*	S ₀	cs (HF) ^a 2 ($\sigma_{CC} \rightarrow \sigma_{CC}^*$)	-0.79	0.418 0.356
S ₁		$2\sigma_{CC} \rightarrow \pi_{BP1}^*\sigma_{CC}^*$	1.57	0.212	
		$\pi_{BP1} \rightarrow \pi_{BP1}^*$		0.187	4.01
		$\sigma_{CC} \rightarrow \pi_{BP1}^*$		0.124	
T ₁		$\pi_{BP1}\sigma_{CC} \rightarrow \pi_{BP1}^*\sigma_{CC}^*$	-0.81	0.102	4.13
³ [BP...DMT]*		S ₀	cs (HF) ^a	-2.84	0.768
	S ₁	$n_{O,BP} \rightarrow \pi_{C,BP}^*$	-0.34	0.844	4.22
	T ₁	$\pi_{DMT} \rightarrow \pi_{(BP)DMT}^*$	-0.53	0.619	6.18
¹ DIR*	S ₀	cs (HF) ^a	0.56	0.139	3.68
		$\pi_{DMT} \rightarrow \pi_{(BP)DMT}^*$		0.371	
		$\pi_{DMT} \rightarrow \pi_{BP1}^*$		0.118	
		2 ($\pi_{DMT} \rightarrow \pi_{(BP)DMT}^*$)		0.126	
		$\pi_{BP1}\pi_{DMT} \rightarrow \pi_{BP1}^*\pi_{(BP)DMT}^*$		0.122	
	S ₁	cs (HF) ^a	0.96	0.195	3.63
		$\pi_{DMT} \rightarrow \pi_{BP-DMT}^*$		0.230	
		$\pi_{BP(DMT)} \rightarrow \pi_{BP-DMT}^*$		0.114	
2 ($\pi_{DMT} \rightarrow \pi_{BP-DMT}^*$)		0.176			
	$2\pi_{DMT} \rightarrow \pi_{BP-DMT}^*\pi_{BP(DMT)}^*$		0.122		

^a Closed-shell Hartree-Fock configuration state function.

Table S4.3. Binding energies calculated with different levels of theory (see Computational Details) for both triplet exciplexes ($^3[\text{BP}\cdots\text{DMT}]^*$) of HH-1 and HT-1.

	HH-1 (eV)	HT-1 (eV)	HH-1 (kcal/mol)	HT-1 (kcal/mol)
DFT GD3	0.50	0.60	11.5	13.8
DFT	0.43	0.49	9.9	11.3
DFT PCM	0.40	0.33	9.2	7.6
CASPT2	0.53	0.60	12.2	13.8
CASPT2 PCM	0.50	0.44	11.5	10.1

Table S4.4. Oscillator strengths and energies of the lowest-energy transitions at the triplet exciplex ($^3[\text{BP}\cdots\text{DMT}]^*$) for HH-1.

	HH-1 (eV)	HT-1 (eV)	HH-1 (kcal/mol)	HT-1 (kcal/mol)
DFT GD3	0.50	0.60	11.5	13.8
DFT	0.43	0.49	9.9	11.3
DFT PCM	0.40	0.33	9.2	7.6
CASPT2	0.53	0.60	12.2	13.8
CASPT2 PCM	0.50	0.44	11.5	10.1

Table S4.5. Nature of the triplet T_1 and T_7 states at the triplet exciplex ($^3[\text{BP}\cdots\text{DMT}]^*$) for HH-1 and weight of the main configuration state functions (CSFs). Single-occupied natural orbitals in each CSF are shown. See shape of the natural orbitals in Figure S4.6.

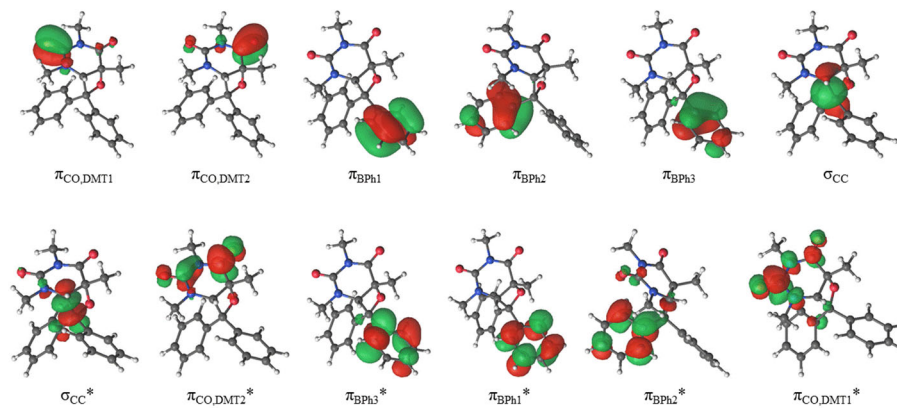
Geometry	State	Nature	Weight
$^3[\text{BP}\cdots\text{DMT}]^*$	T_1	$\pi_{\text{DMT}}\pi_{\text{DMT}(\text{BP})}^*$	0.625
		$\pi_{\text{BP}2}\pi_{\text{DMT}(\text{BP})}^*$	0.201
	T_7	$\pi_{\text{BP}2}\pi_{\text{DMT}(\text{BP})}^*\pi_{\text{DMT}}\pi_{\text{BP}(\text{DMT})}^*$	0.189
		$\pi_{\text{BP}2}\pi_{\text{DMT}(\text{BP})}^*\pi_{\text{DMT}}\pi_{\text{BP}(\text{DMT})}^*$	0.161

Table S4.6. CASPT2 energy gaps (in eV) at the $^3[\text{BP}\cdots\text{DMT}]^*$ of the HH-1 system calculated with the active spaces CAS(12,12) and CAS (14,13).

	CAS(12,12)	CAS(14,13)
S₁S₀	2.503	3.473
T₁S₀	2.307	2.382
T₂S₀	3.705	3.810
T₃S₀	3.773	3.832

Table S4.7. SS and MS-CASPT2 energy gaps (in eV) between states at the $^3\text{DIR}^*$ for HH-1 and HT-1.

	HH-1		HT-1	
	ΔE (SS-CASPT2)	ΔE (MS-CASPT2)	ΔE (SS-CASPT2)	ΔE (MS-CASPT2)
S₁S₀	2.357	2.758	0.796	1.204
T₁S₀	-0.027	-0.009	0.232	0.294
T₂T₁	2.442	2.838	2.441	2.836
T₃T₂	0.691	0.735	0.687	0.775

**Figure S4.2.** Natural orbitals of the CASSCF active space of the singlet states at the oxetane structure (OXE) for HH-1.

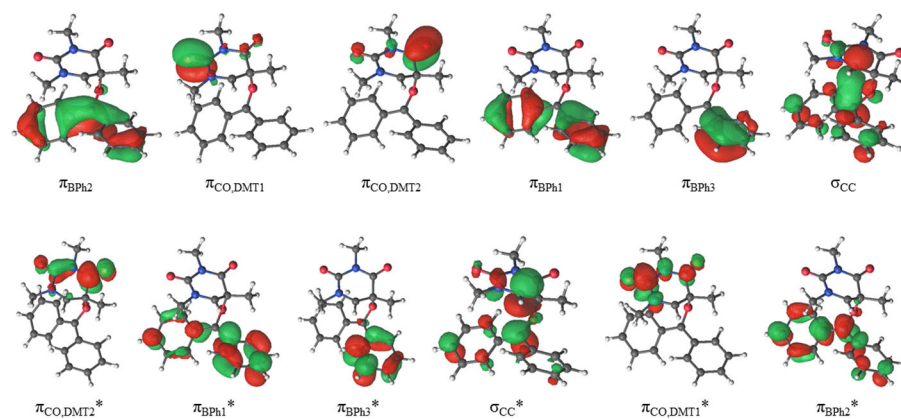


Figure S4.3. Natural orbitals of the CASSCF active space of the singlet states at the diradical structure ($^1\text{DIR}^*$) for HH-1.

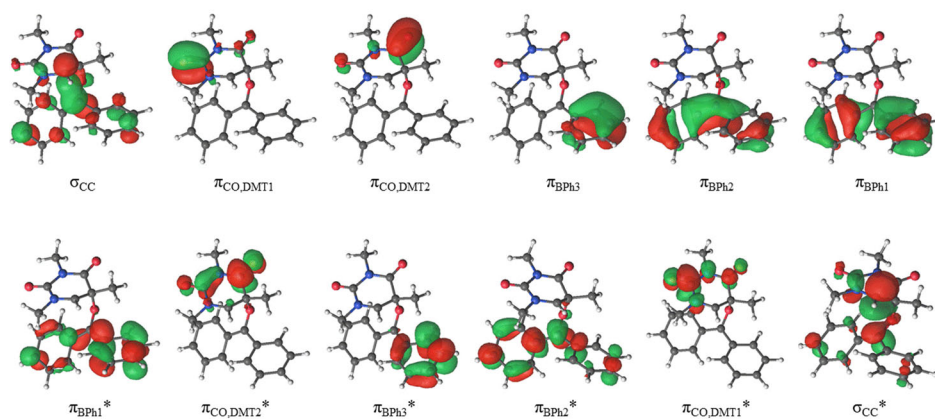


Figure S4.4. Natural orbitals of the CASSCF active space of the triplet states at the diradical structure ($^3\text{DIR}^*$) for HH-1.

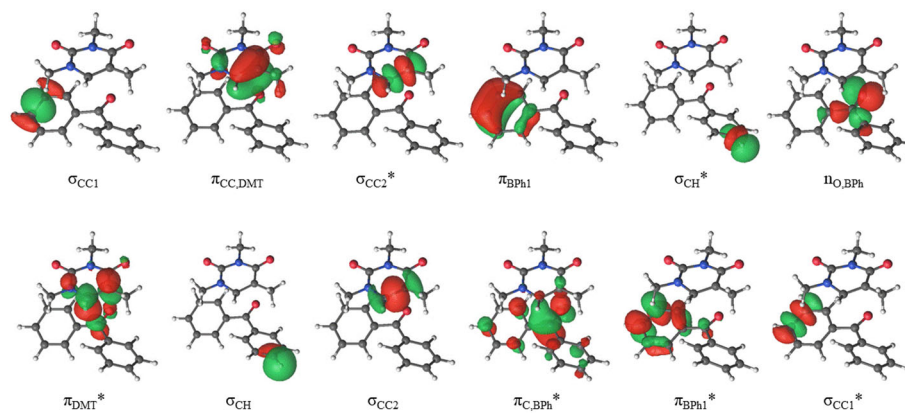


Figure S4.5. Natural orbitals of the CASSCF active space of the singlet states at the exciplex structure for HH-1. π_{DMT}^* and $\pi_{\text{C,BP}}^*$ can be considered the σ and σ^* orbitals of the C-C and C-O bonds that break throughout the process.

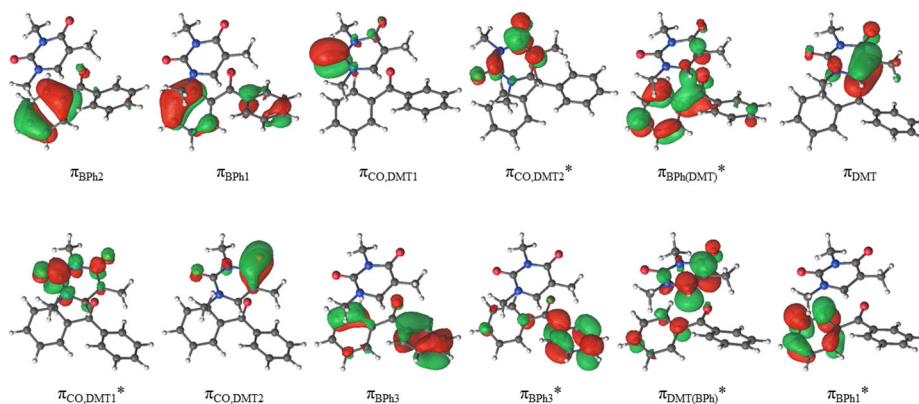


Figure S4.6. Natural orbitals of the CASSCF active space of the triplet states at the exciplex structure ($^3[\text{BP}\cdots\text{DMT}]^*$) for HH-1. $\pi_{\text{BP(DMT)}}^*$ and $\pi_{\text{DMT(BP)}}^*$ can be considered the σ and σ^* orbitals of the C-C and C-O bonds that break throughout the process.

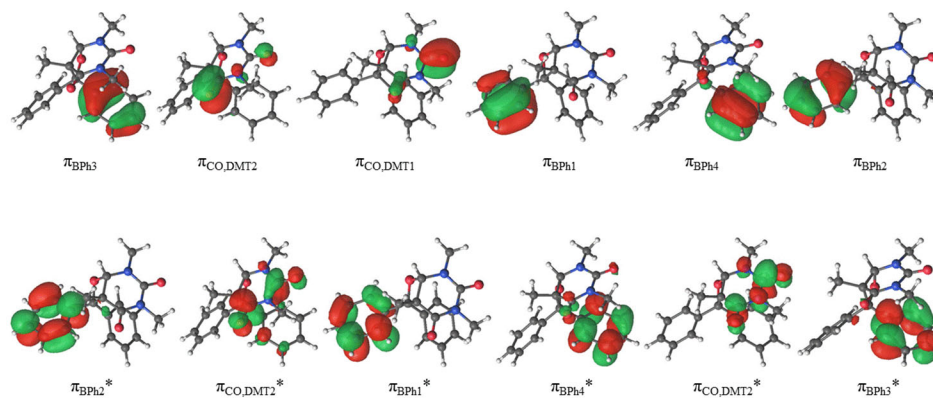


Figure S4.7. Natural orbitals of the CASSCF active space of the singlet states at the oxetane structure (OXE) for HT-1.

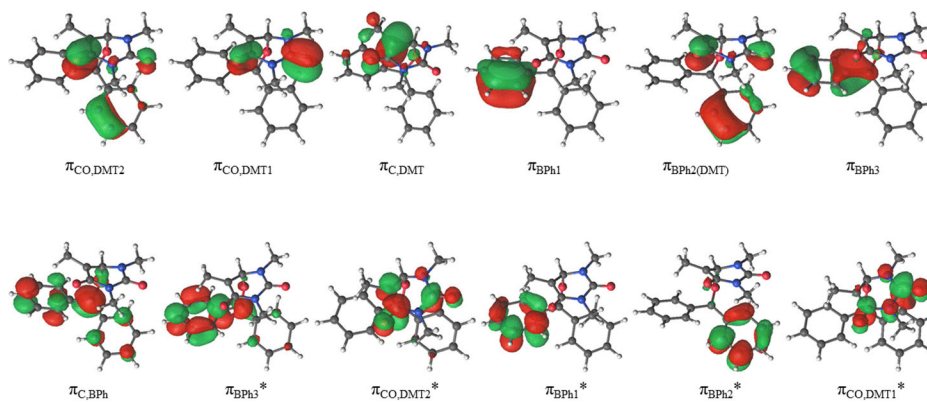


Figure S4.8. Natural orbitals of the CASSCF active space of the singlet states of at the diradical structure ($^1\text{DIR}^*$) for HT-1. $\pi_{\text{C,DMT}}$ and $\pi_{\text{C,BP}}$ can be considered the σ and σ^* orbitals of the C-C bond that breaks throughout the process.

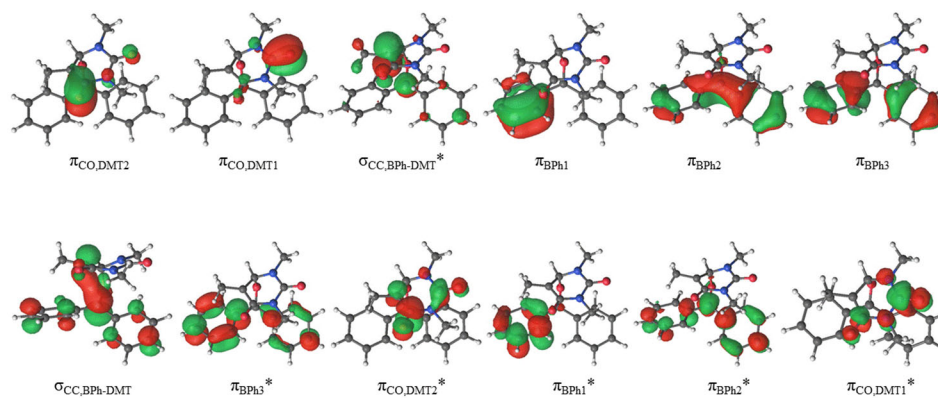


Figure S4.9. Natural orbitals of the CASSCF active space of the triplet states at the diradical structure ($^3\text{DIR}^*$) for HT-1.

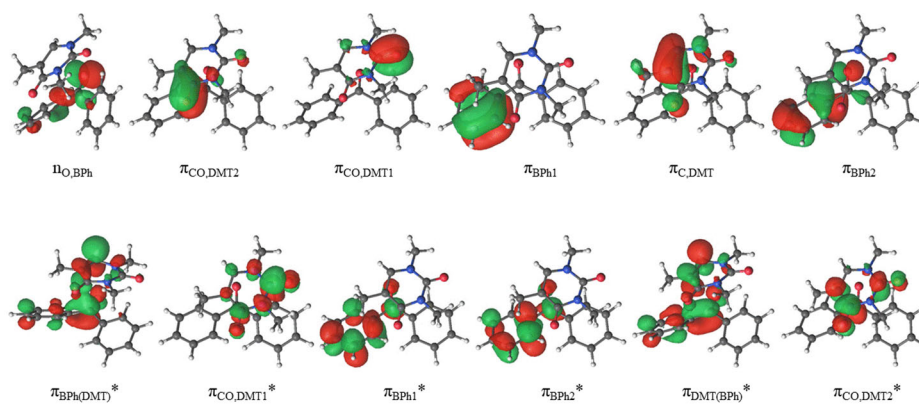


Figure S4.10. Natural orbitals of the CASSCF active space of the singlet states at the exciplex structure for HT-1. $\pi_{\text{BP(DMT)}}^*$ and $\pi_{\text{DMT(BP)}}^*$ can be considered the σ and σ^* orbitals of the C-C and C-O bonds that break throughout the process.

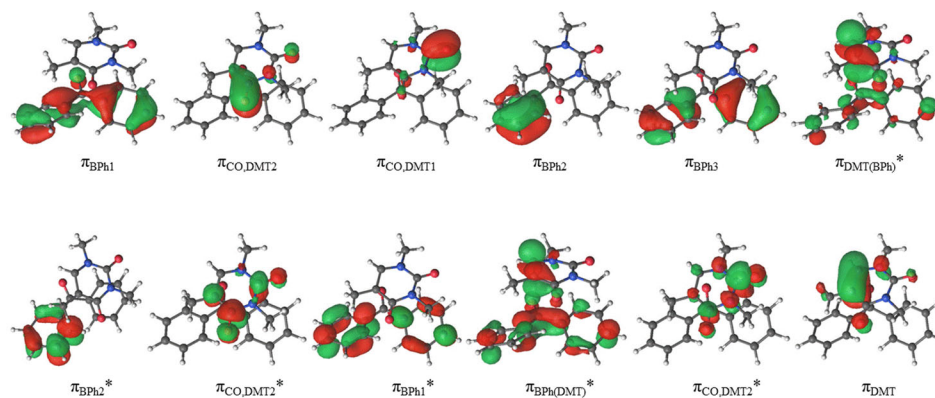


Figure S4.11. Natural orbitals of the CASSCF active space of the triplet states at the exciplex structure ($^3[\text{BP}\cdots\text{DMT}]^*$) for HT-1. $\pi_{\text{DMT}(\text{BP})}^*$ and $\pi_{\text{BP}(\text{DMT})}^*$ can be considered the σ and σ^* orbitals of the C-C and C-O bonds that break throughout the process.

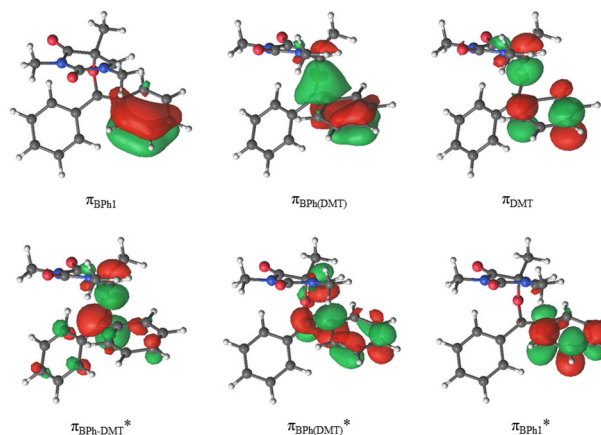


Figure S4.12. Natural orbitals of the CASSCF active space at the equilibrium structure of the S_1 state at the diradical region ($^1\text{DIR}^*$) for HH-1. $\pi_{\text{BP}(\text{DMT})}$ and $\pi_{\text{BP}(\text{DMT})}^*$ can be considered the σ and σ^* orbitals of the C-C bond that breaks throughout the process.

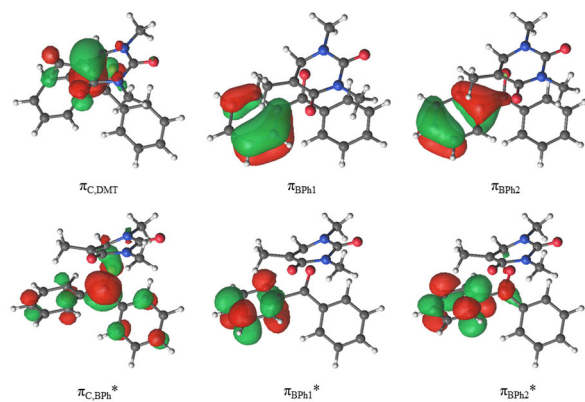


Figure S4.13. Natural orbitals of the CASSCF active space at the equilibrium structure of the S_1 state at the diradical region ($^1\text{DIR}^*$) for HT-1. $\pi_{\text{C,DMT}}$ and $\pi_{\text{C,BP}}^*$ can be considered the σ and σ^* orbitals of the C-C bond that breaks throughout the process.

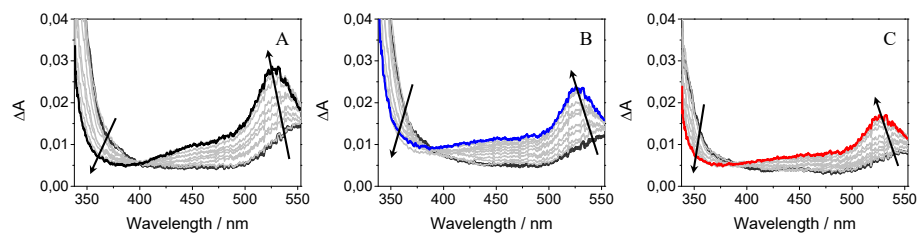


Figure S4.14. Femtosecond transient absorption spectra from 0.1 to 40 ps for (A) BP, (B), HH-1 and (C) HT-1 after excitation at 280 nm in MeCN.

6. References

1. Brash, D. E.; Haseltine, W. A., UV-induced mutation hotspots occur at DNA damage hotspots. *Nature* **1982**, *298*, 189-192.
2. Cadet, J.; Vigny, P., The photochemistry of nucleic acids. In *Bioorganic Photochemistry*, Morrison, H., Ed. John Wiley & Sons: New York, 1990, 1-272.
3. Pfeifer, G. P.; You, Y. H.; Besaratinia, A., Mutations induced by ultraviolet light. *Mutat. Res.* **2005**, *571*, 19-31.
4. Cadet, J.; Mouret, S.; Ravanat, J. L.; Douki, T., Photoinduced damage to cellular DNA: Direct and photosensitized reactions. *Photochem. Photobiol.* **2012**, *88*, 1048-1065.
5. Varghese, A. J.; Wang, S. Y., Thymine-thymine adduct as a photoproduct of thymine. *Science* **1968**, *160*, 186-187.
6. Fraga-Timiraos, A. B.; Lhiaubet-Vallet, V.; Miranda, M. A., Repair of a dimeric azetidione related to the thymine-cytosine (6-4) photoproduct by electron transfer photoreduction. *Angew. Chem. Int. Ed.* **2016**, *55*, 6037-6040.
7. Mitchell, D. L., The relative cytotoxicity of (6-4) photoproducts and cyclobutane dimers in mammalian cells. *Photochem. Photobiol.* **1988**, *48*, 51-57.
8. Taylor, J. S., Unraveling the molecular pathway from sunlight to skin cancer. *Acc. Chem. Res.* **1994**, *27*, 76-82.
9. Yu, S. L.; Lee, S. K., Ultraviolet radiation: DNA damage, repair, and human disorders. *Mol. Cell. Toxicol.* **2017**, *13*, 21-28.

10. Essen, L. O.; Klar, T., Light-driven DNA repair by photolyases. *Cell. Mol. Life Sci.* **2006**, *63*, 1266-1277.
11. Todo, T.; Ryo, H.; Yamamoto, K.; Toh, H.; Inui, T.; Ayaki, H.; Nomura, T.; Ikenaga, M., Similarity among the drosophila (6-4)photolyase, a human photolyase homolog, and the DNA photolyase-blue-light photoreceptor family. *Science* **1996**, *272*, 109-112.
12. Todo, T.; Takemori, H.; Ryo, H.; Ihara, M.; Matsunaga, T.; Nikaido, O.; Sato, K.; Nomura, T., A new photoreactivating enzyme that specifically repairs ultraviolet light-induced (6-4)photoproducts. *Nature* **1993**, *361*, 371-374.
13. Todo, T.; Tsuji, H.; Ootoshi, E.; Hitomi, K.; Kim, S. T.; Ikenaga, M., Characterization of a human homolog of 6-4 photolyase. *Mutat. Res.* **1997**, *384*, 195-204.
14. Asgatay, S.; Petermann, C.; Harakat, D.; Guillaume, D.; Taylor, J. S.; Clivio, P., Evidence that the (6-4) photolyase mechanism can proceed through an oxetane intermediate. *J. Am. Chem. Soc.* **2008**, *130*, 12618-12619.
15. Aubert, C.; Vos, M. H.; Mathis, P.; Eker, A. P. M.; Brettel, K., Intraprotein radical transfer during photoactivation of DNA photolyase. *Nature* **2000**, *405*, 586-590.
16. Kim, S. T.; Malhotra, K.; Smith, C. A.; Taylor, J. S.; Sancar, A., Characterization of (6-4) photoproduct DNA photolyase. *J. Biol. Chem.* **1994**, *269*, 8535-8540.
17. Li, J.; Liu, Z.; Tan, C.; Guo, X.; Wang, L.; Sancar, A.; Zhong, D., Dynamics and mechanism of repair of ultraviolet-induced (6-4) photoproduct by photolyase. *Nature* **2010**, *466*, 887-890.

18. Scannell, M. P.; Fenick, D. J.; Yeh, S. R.; Falvey, D. E., Model studies of DNA photorepair: Reduction potentials of thymine and cytosine cyclobutane dimers measured by fluorescence quenching. *J. Am. Chem. Soc.* **1997**, *119*, 1971-1977.
19. Sinha, R. P.; Hader, D. P., UV-induced DNA damage and repair: A review. *Photochem. Photobiol. Sci.* **2002**, *1*, 225-236.
20. Zhao, X.; Liu, J.; Hsu, D. D.; Zhao, S.; Taylor, J. S.; Sancar, A., Reaction mechanism of (6-4) photolyase. *J. Biol. Chem.* **1997**, *272*, 32580-32590.
21. Zhao, X.; Mu, D., (6-4) Photolyase: Light-dependent repair of DNA damage. *Histol. Histopathol.* **1998**, *13*, 1179-1182.
22. Prakash, G.; Falvey, D. E., Model studies of the (6-4) photoproduct DNA photolyase: Synthesis and photosensitized splitting of a thymine-5,6-oxetane. *J. Am. Chem. Soc.* **1995**, *117*, 11375-11376.
23. Joseph, A.; Prakash, G.; Falvey, D. E., Model studies of the (6-4) photoproduct photolyase enzyme: Laser flash photolysis experiments confirm radical ion intermediates in the sensitized repair of thymine oxetane adducts. *J. Am. Chem. Soc.* **2000**, *122*, 11219-11225.
24. Joseph, A.; Falvey, D. E., Photolysis of thymine oxetanes produces triplet excited carbonyl compounds with high efficiency. *J. Am. Chem. Soc.* **2001**, *123*, 3145-3146.
25. Joseph, A.; Falvey, D. E., Photoinduced electron transfer cleavage of oxetane adducts of uracil and cytosine. *Photochem. Photobiol. Sci.* **2002**, *1*, 632-635.

26. Encinas, S.; Belmadoui, N.; Climent, M. J.; Gil, S.; Miranda, M. A., Photosensitization of thymine nucleobase by benzophenone derivatives as models for photoinduced DNA damage: Paternò-Büchi vs energy and electron transfer processes. *Chem. Res. Toxicol.* **2004**, *17*, 857-862.
27. Trzcionka, J.; Lhiaubet-Vallet, V.; Paris, C.; Belmadoui, N.; Climent, M. J.; Miranda, M. A., Model studies on a carprofen derivative as dual photosensitizer for thymine dimerization and (6-4) photoproduct repair. *ChemBioChem* **2007**, *8*, 402-407.
28. Kwok, W. M.; Guan, X.; Chu, L. M.; Tang, W.; Phillips, D. L., Observation of singlet cycloreversion of thymine oxetanes by direct photolysis. *J. Phys. Chem. B* **2008**, *112*, 11794-11797.
29. Song, Q. H.; Wang, H. B.; Tang, W. J.; Guo, Q. X.; Yu, S. Q., Model studies of the (6-4) photoproduct photoreactivation: Efficient photosensitized splitting of thymine oxetane units by covalently linked tryptophan in high polarity solvents. *Org. Biomol. Chem.* **2006**, *4*, 291-298.
30. Belmadoui, N.; Encinas, S.; Climent, M. J.; Gil, S.; Miranda, M. A., Intramolecular interactions in the triplet excited states of benzophenone-thymine dyads. *Chem. Eur. J.* **2006**, *12*, 553-561.
31. Hei, X. M.; Song, Q. H.; Li, X. B.; Tang, W. J.; Wang, H. B.; Guo, Q. X., Origin of a large temperature dependence of regioselectivity observed for [2 + 2] photocycloaddition (Paternò-Büchi reaction) of 1,3-dimethylthymine with benzophenone and its derivatives: Conformational property of the intermediary triplet 1,4-diradicals. *J. Org. Chem.* **2005**, *70*, 2522-2527.
32. Nakatani, K.; Yoshida, T.; Saito, I., Photochemistry of benzophenone immobilized in a major groove of DNA: Formation of

thermally reversible interstrand cross-link. *J. Am. Chem. Soc.* **2002**, *124*, 2118-2119.

33. Bell, J. A.; Linschitz, H., Decay kinetics of the 1-naphthaldehyde and benzophenone triplet states in benzene. *J. Am. Chem. Soc.* **1963**, *85*, 528-532.

34. Murov, S. L.; Carmichael, I.; Hug, G. L., *Handbook of photochemistry*. 2nd ed.; Marcel Dekker: New York, 1993.

35. Gut, I. G.; Wood, P. D.; Redmond, R. W., Interaction of triplet photosensitizers with nucleotides and DNA in aqueous solution at room temperature. *J. Am. Chem. Soc.* **1996**, *118*, 2366-2373.

36. Zuo, Z. H.; Yao, S. D.; Luo, J.; Wang, W. F.; Zhang, J. S.; Lin, N. Y., Laser photolysis of cytosine, cytidine and dCMP in aqueous solution. *J. Photochem. Photobiol. B* **1992**, *15*, 215-222.

37. Miró, P.; Gómez-Mendoza, M.; Sastre, G.; Cuquerella, M. C.; Miranda, M. A.; Marín, M. L., Generation of the thymine triplet state by through-bond energy transfer. *Chem. Eur. J.* **2019**, *25*, 7004-7011.

38. Mattay, J., Charge transfer and radical ions in photochemistry. *Angew. Chem. Int. Ed.* **1987**, *26*, 825-845.

39. Serrano-Andres, L.; Merchan, M.; Lindh, R., Computation of conical intersections by using perturbation techniques. *J. Chem. Phys.* **2005**, *122*, 104107.

40. Giussani, A.; Serrano-Andres, L.; Merchan, M.; Roca-Sanjuan, D.; Garavelli, M., Photoinduced formation mechanism of the thymine-thymine (6-4) adduct. *J. Phys. Chem. B* **2013**, *117*, 1999-2004.

41. Tamai, N.; Asahi, T.; Masuhara, H., Intersystem crossing of benzophenone by femtosecond transient grating spectroscopy. *Chem. Phys. Lett.* **1992**, *198*, 413-418.
42. Marazzi, M.; Mai, S.; Roca-Sanjuan, D.; Delcey, M. G.; Lindh, R.; Gonzalez, L.; Monari, A., Benzophenone ultrafast triplet population: Revisiting the kinetic model by surface-hopping dynamics. *J. Phys. Chem. Lett.* **2016**, *7*, 622-626.
43. D'Auria, M.; Racioppi, R., Oxetane synthesis through the Paternò-Büchi reaction. *Molecules* **2013**, *18*, 11384-11428.
44. Freilich, S. C.; Peters, K. S., Observation of the 1,4-biradical in the Paternò-Büchi Reaction. *J. Am. Chem. Soc.* **1981**, *103*, 6255-6257.
45. Yang, Z. B.; Zhang, R. B.; Eriksson, L. A., A triplet mechanism for the formation of thymine–thymine (6-4) dimers in UV-irradiated DNA. *Phys. Chem. Chem. Phys.* **2011**, *13*, 8961-8966.
46. Frisch, M. J.; Trucks, G. W.; Schlegel, H. B.; Scuseria, G. E.; Robb, M. A.; Cheeseman, J. R.; Scalmani, G.; Barone, V.; Mennucci, B.; Petersson, G. A.; Nakatsuji, H.; Caricato, M.; Li, X.; Hratchian, H. P.; Izmaylov, A. F.; Bloino, J.; Zheng, G.; Sonnenberg, J. L.; Hada, M.; Ehara, M.; Toyota, K.; Fukuda, R.; Hasegawa, J.; Ishida, M.; Nakajima, T.; Honda, Y.; Kitao, O.; Nakai, H.; Vreven, T.; Montgomery, J. J. A.; Peralta, J. E.; Ogliaro, F.; Bearpark, M.; Heyd, J. J.; Brothers, E.; Kudin, K. N.; Staroverov, V. N.; Kobayashi, R.; Normand, J.; Raghavachari, K.; Rendell, A.; Burant, J. C.; Iyengar, S. S.; Tomasi, J.; Cossi, M.; Rega, N.; Millam, J. M.; Klene, M.; Knox, J. E.; Cross, J. B.; Bakken, V.; Adamo, C.; Jaramillo, J.; Gomperts, R.; Stratmann, R. E.; Yazyev, O.; Austin, A. J.; Cammi, R.; Pomelli, C.; Ochterski, J. W.; Martin, R. L.; Morokuma, K.; Zakrzewski, V. G.; Voth, G. A.; Salvador, P.; Dannenberg, J. J.; Dapprich,

S.; Daniels, A. D.; Farkas, Ö.; Foresman, J. B.; Ortiz, J. V.; Cioslowski, J.; Fox, D. J. *Gaussian 09, Revision D.01*, Wallingford, CT, 2013.

47. Aquilante, F.; Autschbach, J.; Carlson, R. K.; Chibotaru, L. F.; Delcey, M. G.; De Vico, L.; Fdez Galvan, I.; Ferre, N.; Frutos, L. M.; Gagliardi, L.; Garavelli, M.; Giussani, A.; Hoyer, C. E.; Li Manni, G.; Lischka, H.; Ma, D.; Malmqvist, P. A.; Muller, T.; Nenov, A.; Olivucci, M.; Pedersen, T. B.; Peng, D.; Plasser, F.; Pritchard, B.; Reiher, M.; Rivalta, I.; Schapiro, I.; Segarra-Marti, J.; Stenrup, M.; Truhlar, D. G.; Ungur, L.; Valentini, A.; Vancoillie, S.; Veryazov, V.; Vysotskiy, V. P.; Weingart, O.; Zapata, F.; Lindh, R., Molcas 8: New capabilities for multiconfigurational quantum chemical calculations across the periodic table. *J. Comput. Chem.* **2016**, *37*, 506-541.

48. Forsberg, N.; Malmqvist, P. Å., Multiconfiguration perturbation theory with imaginary level shift. *Chem. Phys. Lett.* **1997**, *274*, 196-204.

49. Grimme, S.; Antony, J.; Ehrlich, S.; Krieg, H., A consistent and accurate ab initio parametrization of density functional dispersion correction (DFT-D) for the 94 elements H-Pu. *J. Chem. Phys.* **2010**, *132*, 154104.

50. Parrish, R. M.; Thompson, K. C.; Martinez, T. J., Large-scale functional group symmetry-adapted perturbation theory on graphical processing units. *J. Chem. Theory Comput.* **2018**, *14*, 1737-1753.

51. Boys, S. F.; Bernardi, F., The calculation of small molecular interactions by the differences of separate total energies. Some procedures with reduced errors. *Mol. Phys.* **2002**, *100*, 65-73.

52. Roca-Sanjuan, D.; Olasso-Gonzalez, G.; Gonzalez-Ramirez, I.; Serrano-Andres, L.; Merchán, M., Molecular basis of DNA

photodimerization: Intrinsic production of cyclobutane cytosine dimers. *J. Am. Chem. Soc.* **2008**, *130*, 10768-10779.

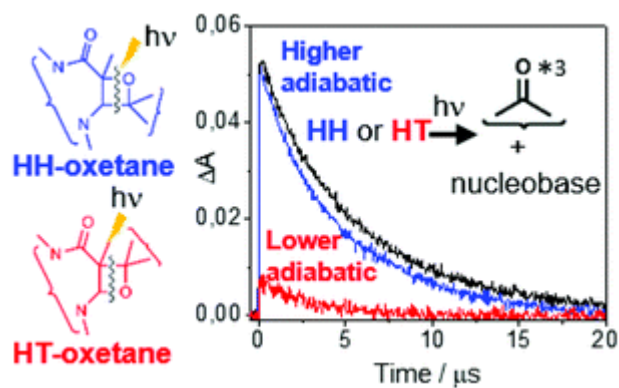
53. Sergentu, D. C.; Maurice, R.; Havenith, R. W.; Broer, R.; Roca-Sanjuan, D., Computational determination of the dominant triplet population mechanism in photoexcited benzophenone. *Phys. Chem. Chem. Phys.* **2014**, *16*, 25393-25403.

54. Serrano-Andrés, L.; Merchán, M., Are the five natural DNA/RNA base monomers a good choice from natural selection? *J. Photochem. Photobiol. C* **2009**, *10*, 21-32.

55. Serrano-Andres, L.; Merchan, M.; Lindh, R., Computation of conical intersections by using perturbation techniques. *J. Chem. Phys.* **2005**, *122*, 104107-104110.

CHAPTER 5:

Regioselectivity in the adiabatic photocleavage of DNA-based oxetanes



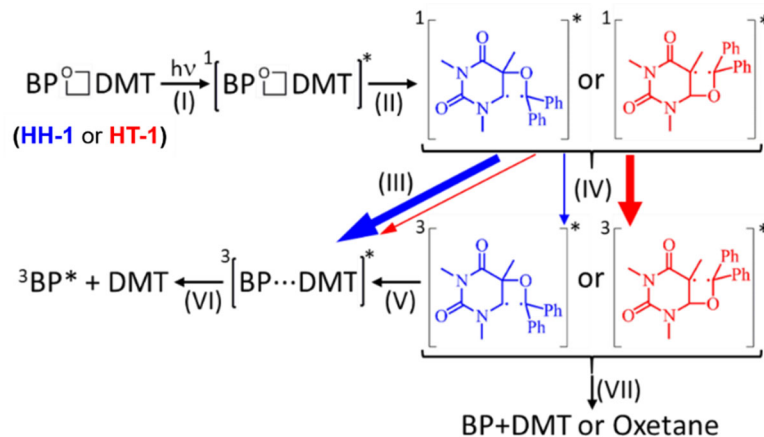
1. Introduction

The origin of human diseases such as skin cancer can be associated in many cases to photoinduced DNA damage.¹⁻³ Thus, when DNA absorbs UV light, a cascade of reactions may lead to the formation of cyclobutane pyrimidine dimers (CPDs) and to a lesser extent pyrimidine-pyrimidone (6-4) photoproducts ((6-4)PPs), which may result in the appearance of mutations and cell death.⁴⁻⁷ The CPD photolesions can also arise from photosensitization, where an endogenous or exogenous photosensitizer (PS) can absorb UVA light to generate long-lived reactive species such as excited triplet states that will be the initiators of the damaging reactions.⁸⁻⁹ Nature has developed efficient mechanisms to repair these lesions. In this context, the nucleotide excision repair operates in humans, while in other organisms such as bacteria or plants the involvement of a photolyase reverses the damage through a photoinduced electron transfer process.¹⁰⁻¹³

Benzophenone (BP) is a well-known photosensitizing moiety that is present in a variety of drugs.¹⁴ It can induce damage to DNA, and its main target is the thymine (Thy) nucleobase.¹⁵⁻¹⁷ In this regard, excitation of BP with UVA light generates its triplet excited state (³BP*), which can then induce formation of CPDs through a formal [2+2] cycloaddition between two adjacent thymine units, or alternatively it may lead to oxetane derivatives through a triplet exciplex ³[BP...Thy]*.¹⁸⁻²⁰

The photoreactivity of monomeric pyrimidine bases such as thymine or uracil (Ura) interacting with BP is highly influenced by the substituents at position C5 of the nucleobase, mainly due to steric hindrance. In this context, CPDs formation in solutions containing BP and Ura derivatives is completely blocked by the presence of a bulky group at the C5 position of

the nucleobase.²¹ In connection with oxetanes, the Paternò-Büchi photoreaction between Thy and BP derivatives has been reported in the course of model studies related to the photoenzymatic repair of DNA (6-4)PPs.²²⁻²⁷ Interestingly, direct photolysis of some of these oxetanes results in a rare adiabatic cleavage to form ³BP* and Thy in its ground state.^{23, 26} This process has recently been investigated in detail for two head-to-head (HH-1) and head-to-tail (HT-1) oxetane regioisomers obtained from 1,3-dimethylthymine (DMT) and BP (see Scheme 5.1).¹⁸ Irradiation of any of the two isomers induces instantaneous formation of its first excited singlet state, which rapidly evolves to a singlet biradical through C-C bond scission. For the HH-1 isomer, step (III) to reach the excited triplet exciplex ³[BP···DMT]* has been found to be much more efficient than for the HT-1 isomer, which may follow step (IV) to generate a triplet biradical that evolves to regenerate either the starting oxetane or the separated Thy and BP chromophores in the ground state. Alternatively, the triplet exciplexes are also formed from the HT-1 oxetane, albeit to a lesser extent; these species finally dissociate to give ³BP* and DMT in the ground state. Consequently, the adiabatic cycloreversion of the two investigated oxetanes seems to be markedly influenced by the HH- vs. the HT-regiochemistry.



Scheme 5.1. Schematic representation of the photoinduced cycloreversion process of the HH-1 and HT-1 oxetanes composed of BP and DMT.¹⁸ For clarification, the HH regioisomer follows the blue arrows, while the HT oxetane follows the red ones.

With this background, the aim of the present work is to establish the generality and scope of the adiabatic cycloreversion process and to gain further insight into its mechanistic features, using a variety of oxetanes with different regiochemistries and substitution patterns at positions 1 and 5 of the nucleobase. With this goal, different oxetanes have been obtained by the intermolecular photoreaction between BP and Ura or Thy derivatives. In addition, oxetanes arising from the analogous intramolecular process between Thy and BP units covalently connected by spacers of different nature have also been studied in order to evaluate the possible influence of the linker on the photolytic splitting. Thus, the photobehaviour of a variety of HH- and HT-oxetanes (see Figure 5.1) has been investigated by means of nanosecond laser flash photolysis (LFP) and, in some cases, femtosecond transient absorption spectroscopy. As a matter of fact, the obtained results confirm the generality of the adiabatic photocleavage in Thy/BP oxetanes, as well as its dependence on the HH-

vs. HT regiochemistry. Moreover, they indicate that the ring opening process is highly influenced by the nature of the substituents at positions 1 and 5 of the nucleobase.

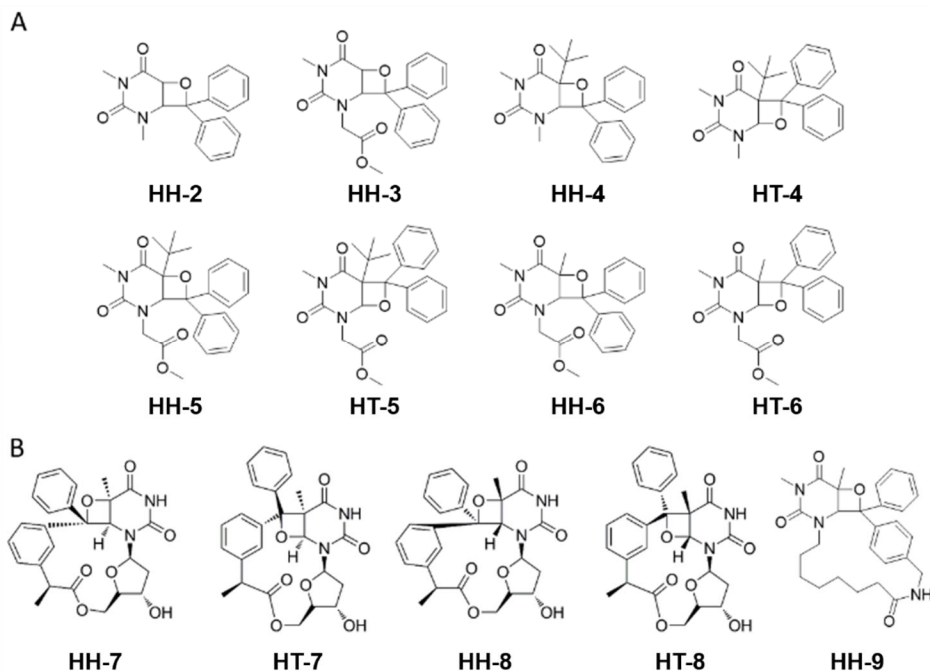
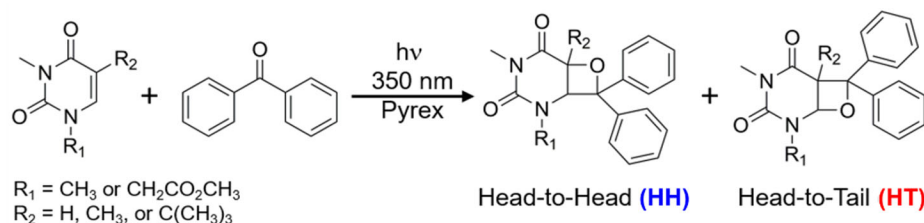


Figure 5.1. Chemical structure of the investigated systems. A) Oxetanes arising from the intermolecular photoreaction between BP and Ura (from HH-2 to HT-5) or Thy (HH-6 and HT-6) derivatives. B) Oxetanes arising from the intramolecular photoreaction between BP and Thy units covalently linked by spacers of different nature.

2. Results and discussion

The photobehaviour of oxetanes resulting from the intermolecular photoreaction between BP and Ura or Thy derivatives (see Figure 5.1A) was studied first. In general, for all investigated systems, direct steady-state photolysis with UVC light gave rise to the starting materials BP and the Ura or Thy derivatives as the only photoproducts. The synthesis of HH-2 has been described earlier;²⁸ however, we have slightly modified the synthetic procedure to get the different HH- and HT-regioisomers (see Scheme 5.2). Briefly, solutions containing BP (0.2 M) and the nucleobase derivative (0.1 M) in acetonitrile were placed into Pyrex tubes and irradiated *ca.* 6h under nitrogen in a Luzchem photoreactor emitting at $\lambda_{\text{max}} = 350 \text{ nm}$ (12 × 8 W lamps). The crudes were purified by column chromatography to get the final HH- and/or HT-oxetanes as white solids. The synthesis of the precursor nucleobase derivatives is explained in detail in the supplementary material.



Scheme 5.2. Schematic representation of the photoinduced cycloreversion process of oxetanes composed of BP and DMT.

Due to the chemical instability of the uracil-derived HT-1 and HT-2, which could not be isolated in pure form, only the photophysical properties of their HH-regioisomers were investigated. Thus, nanosecond laser flash photolysis (LFP) measurements were performed upon excitation at 266 nm in deaerated acetonitrile, using BP as a reference. Under these

conditions, photolysis of either HH-2 or HH-3 resulted in the instantaneous formation of a transient absorption peaking at 530 nm, where ${}^3\text{BP}^*$ displays its maximum.²⁹ This result agrees well with the previous observations for the HH BP-DMT oxetane.¹⁸ Thus, after the laser pulse, a nearly quantitative adiabatic population of ${}^3\text{BP}^*$ was achieved for both oxetanes (see Figure 5.2). The decay traces were properly fitted by a one-order exponential law with lifetimes of about 5 μs for BP and HH-2 and shorter for HH-3 (ca. 2 μs). The difference in the triplet lifetimes could be associated with a faster BP triplet quenching by HH-3 than by HH-2.

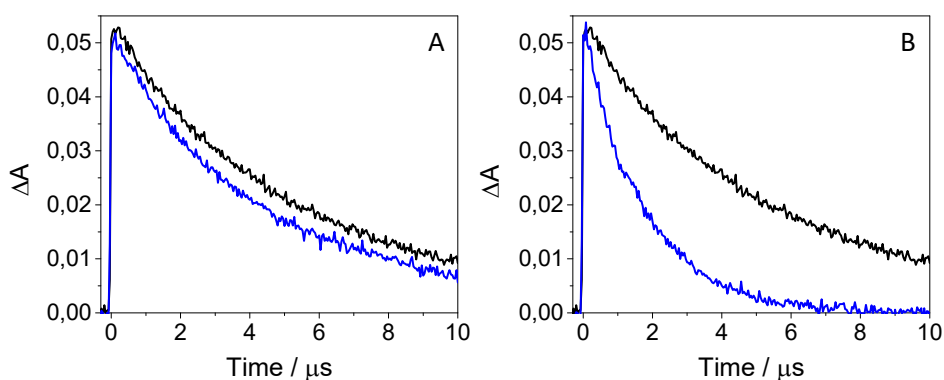


Figure 5.2. LFP decay traces at 530 nm for A) HH-2 (blue) and BP (black), and B) HH-3 (blue) and BP (black) after excitation at 266 nm in deaerated acetonitrile.

Since the influence of the regiochemistry on the photobehaviour of the HT-uracil derivatives could not be evaluated due to their chemical instability, two additional and more stable substituted uracil oxetanes, namely HH-4 and HT-4, were synthesized with a bulky *tert*-butyl group at position 5. In this context, LFP measurements evidenced clear differences between the two regioisomers (see Figure 5.3). Analysis of the kinetic traces at 530 nm showed again an almost quantitative end-of-pulse adiabatic population of ${}^3\text{BP}^*$ for HH-4, while this process was much less

efficient (ca. 35%) for HT-4. Therefore, a strong regioselectivity was observed in the photoinduced ring-opening reaction, which is in line with the results recently reported for the HH and HT BP-DMT oxetanes;¹⁸ noteworthy, in the case of regioisomers-3 the difference in the degree of adiabaticity found between the HH- and the HT-regioisomers was markedly enhanced. Thus, the presence of a *tert*-butyl substituent at position 5 had little if any effect on the photoreactivity of the HH derivative, but it clearly affected the photobehaviour of the HT-isomer.

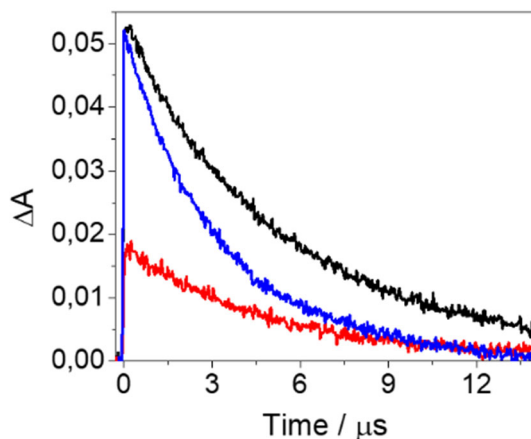


Figure 5.3. LFP decay traces at 530 nm for BP (black), HH-4 (blue) and HT-4 (red) after excitation at 266 nm in deaerated acetonitrile.

In order to complete the picture on the influence of the substituents at positions 1 or 5 on the adiabatic cycloreversion of nucleobase-derived oxetanes, two additional uracil-derived compounds were synthesized, namely HH-5 and HT-5 (with a bulky *tert*-butyl substituent at position 5 and a methyl acetate group at position 1) as well as the corresponding Thy analogues HH-6 and HT-6. As stated above for the related compounds HH-4 and HT-4, the ns LFP decay traces at 530 nm for HH-5 and HT-5 (Figure S5.11A in the supplementary material) evidenced a

remarkable regioselectivity (end-of-pulse $^3\text{BP}^*$ ratio ca. 4:1) in the adiabatic cycloreversion of the investigated oxetanes. Thus, replacement of the methyl group with a methyl acetate substituent at position 1 for the *tert*-butyl derivatives mainly affected the adiabaticity of the HT-isomer, which decreased from 35% in HT-3 to 20% in HT-5. This could be associated with a possible stabilization of the triplet biradical (see Scheme 5.1) by the influence of the methyl acetate moiety, which could hinder formation of the triplet exciplex (step III) thus favouring step VII to generate the starting oxetane HT-5 or the separated BP and Thy chromophores in the ground state. For the thymine derivatives HH-6 and HT-6 (Figure S5.11B in the supplementary material), a regiodifferentiation was again observed in the adiabatic ring-opening (end-of-pulse $^3\text{BP}^*$ ratio ca. 7:3), which was comparable to the results recently reported for BP-DMT oxetanes.¹⁸

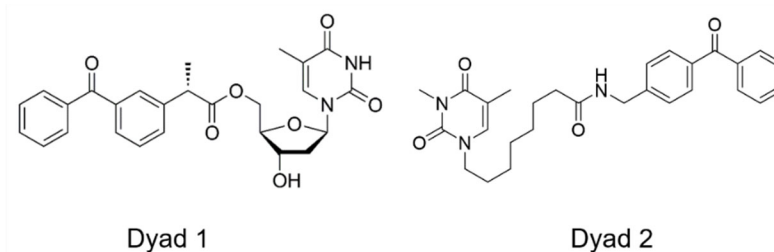


Figure 5.4. Chemical structures of dyad 1 and dyad 2.

In view of the photoreactivity observed for the nucleobase-derived oxetanes as a function of the substitution at positions 1 and 5, the photobehaviour of polycyclic oxetanes (see Figure 5.1B) whose splitting could lead to BP and Thy chromophores covalently linked through a spacer of different nature was also investigated. Their synthesis was achieved following the reported procedures,^{26, 30} by means of the Paternò-

Büchi photoreaction between the BP and Thy units of the precursor dyads 1 and 2 (see Figure 5.4). Thus, photolysis of the dyad 1 containing the BP and Thy chromophores linked through a sugar moiety resulted in the formation of HH-7, HT-7, HH-8 and HT-8,²⁶ whereas HH-9 was obtained from irradiation of dyad 2, where BP and Thy are connected through a linear chain of ten linking atoms.³⁰ Steady state photolysis of oxetanes HH-7, HT-7, HH-8 and HT-8 gave rise in all cases to dyad 1 as the only photoproduct, whereas, under the same conditions, oxetane HH-9 led cleanly to dyad 2.

Since the lifetime of ³BP* in dyad 1 was very short (~20 ns),²⁶ reliable transient absorption experiments could only be performed in the femtosecond time-scale. Under the employed experimental conditions, the degree of photodegradation was kept below 5%. As it is shown in Figure 5.5, excitation of the different regio- and stereoisomeric oxetanes HH-7, HT-7, HH-8 and HT-8 at 280 nm in acetonitrile led to the formation of the typical triplet-triplet absorption band of BP (see Figure S5.12 in the supplementary material);³¹⁻³² with maximum at ca. 530 nm with a time constant of about 9.5 ps. Accordingly, the photoinduced cycloreversion for the intramolecular oxetanes HH-7, HT-7, HH-8 and HT-8 also operates as an adiabatic process.

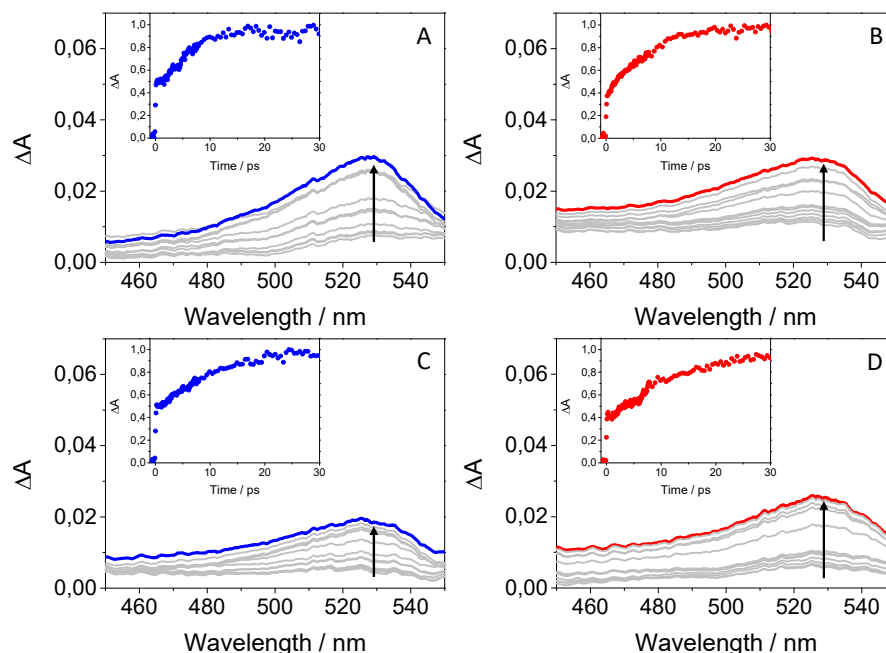


Figure 5.5. Femtosecond transient absorption spectra from 0.5 to 40 ps for A) HH-7, B) HT-7, C) HH-8 and D) HT-8. The insets show the kinetic traces at 530 nm. All measurements were performed at $\lambda_{\text{exc}} = 280$ nm in acetonitrile.

Finally, the photophysical properties of HH-9 were investigated and compared to those of dyad 2.³⁰ Kinetic analysis of the transient peaking at 530 nm in the ns- μ s time-scale upon LFP at 266 nm revealed that the decay traces in both systems could be fitted by a first order exponential law, with lifetimes of ca. 55 ns. More interestingly, HH-9 evidenced once more a complete adiabatic photoreversion process (see Figure S5.13 in the supplementary material). However, the spectra and the decay traces were noisy, due to the short triplet lifetime compared to the duration of the pulse. Hence, oxetane HH-9 was also submitted to femtosecond transient absorption measurements ($\lambda_{\text{exc}} = 280$ nm), which fully confirmed formation of the triplet excited state of the BP-derived chromophore with maximum

at ca. 530 nm³⁰ (see Figure 5.6A and B). As previously observed for the BP-DMT regioisomers,¹⁸ an absorption at about 400 nm with a flat profile, which is absent for the BP-derived chromophore, was formed in ca. 3.5 ps (see Figure 5.6C and D); this can be associated with the formation of an intermediate excited triplet exciplex between the BP and Thy chromophores (see Scheme 5.1).

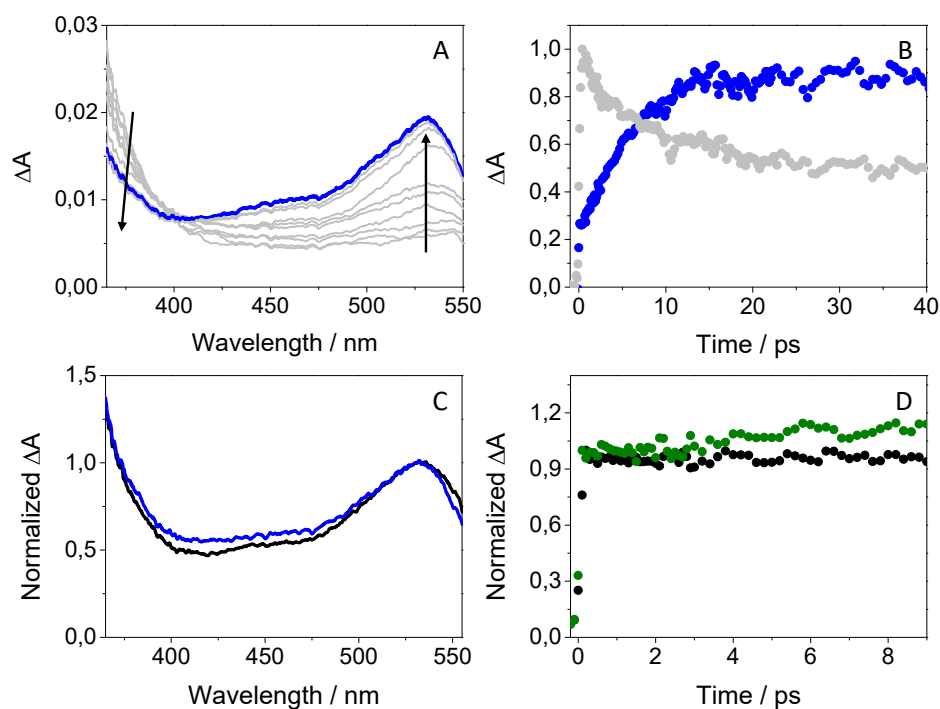


Figure 5.6. Femtosecond transient absorption measurements after excitation at 280 nm in acetonitrile: A) spectra from 0.5 to 40 ps and B) kinetic traces at 340 nm (gray) and 530 nm (blue) for HH-9; C) spectra recorded at 10 ps for the BP-derived chromophore (black) and HH-9 (blue); D) kinetic traces at 400 nm for the BP-derived chromophore (black) and HH-9 (green).

In summary, photolysis of the investigated oxetanes resulted in an adiabatic population of $^3\text{BP}^*$ after ring opening. In this context, a strong regioselectivity was detected for the oxetanes **1-5**, being the degree of adiabaticity much higher for the HH than for the HT isomers (see Table 5.1). In addition, the process was significantly affected by the substitution at position N1 and C5 of the nucleobase for the HT derivatives, whereas a less marked effect was noticed for the HH isomers.

Table 5.1. Relationship between the degree of adiabaticity and the substitution at positions N1 and C5 of the nucleobase for the photoreversion of the indicated oxetanes.

	Substituent at N1	Substituent at C5	Adiabaticity (%)
HH-2	CH ₃	H	100
HH-3	CH ₂ CO ₂ CH ₃	H	100
HH-4	CH ₃	<i>tert</i> -Bu	100
HT-4	CH ₃	<i>tert</i> -Bu	35
HH-5	CH ₂ CO ₂ CH ₃	<i>tert</i> -Bu	100
HT-5	CH ₂ CO ₂ CH ₃	<i>tert</i> -Bu	20
HH-6	CH ₂ CO ₂ CH ₃	CH ₃	75
HT-6	CH ₂ CO ₂ CH ₃	CH ₃	38

Likewise, the photoinduced cleavage of the polycyclic oxetanes was found to occur as an adiabatic process. Interestingly, for the tricyclic oxetane HH-9, a transient absorption at ~400 nm is detected, which is ascribed to formation of the purported triplet exciplex between the linked benzophenone and thymine chromophores.

3. Conclusions

The UV-induced photocleavage of a variety of oxetanes arising from the inter- or intramolecular Paternò-Büchi photoreaction between BP and Ura or Thy chromophores has been investigated by means of transient absorption spectroscopy from the femtosecond to the microsecond time-scales. In all cases, an adiabatic process is observed, which leads to the BP unit in its triplet excited state. The degree of adiabaticity depends on the oxetane regiochemistry and on the substitution pattern at positions 1 and 5 of the nucleobase. In general, a nearly quantitative adiabatic cycloreversion is observed for the HH-regioisomers; by contrast, for the HT-oxetanes the process is not fully adiabatic and becomes strongly influenced by the nature of the substituents at positions 1 and 5. The highest regiodifferentiation (4:1 ratio) is detected between HH-5 and HT-5. These results are consistent with the intermediacy of a triplet exciplex, whose formation is more favourable in the HH-regioisomers. In summary, the adiabatic cycloreversion of oxetanes derived from aromatic ketones and pyrimidine bases appears to be a rather general process, which occurs in all the investigated compounds. Regioselectivity (HH vs. HT) and substitution-dependence are interesting features of this process.

4. Experimental section

Chemicals and reagents. 1,3-dimethyluracil, benzophenone (BP), dimethyl sulphate, lithium diisopropylamide (LDA), ethyl formate 97%, thiourea, chloroacetic acid, thymine-1-acetic acid, ethyl bromoacetate, ethyl 4-bromobutyrate, were purchased from Sigma-Aldrich. Ethyl-8-bromooctanoate was purchased from Fluorochem. Methyl 3,3-dimethylbutanoate was purchased from Alfa-aesar. Sodium hydroxide (NaOH), potassium hydroxide (KOH), magnesium sulphate (MgSO₄), hydrochloric acid 37% (HCl) and acetonitrile spectroscopic grade were purchased from Scharlab.

Spectroscopic Techniques. The ¹H NMR and ¹³C NMR spectra were recorded at 400 and 100 MHz, respectively, using a Bruker AVANCE III instrument; chemical shifts are reported in ppm.

High-resolution mass spectrometry (HRMS) was performed in an Ultra Performance Liquid Chromatography (UPLC) ACQUITY system (Waters Corp.) with a conditioned autosampler at 4 °C. The separation was accomplished on an ACQUITY UPLC BEH C18 column (50 mm × 2.1 mm i.d., 1.7 μm), which was maintained at 40 °C. The analysis was performed using acetonitrile and water (60:40 v/v containing 0.01% formic acid) as the mobile phase with a flow rate of 0.5 mL/min, and injection volume was 5 μL. The Waters ACQUITY™ XevoQToF Spectrometer (Waters Corp.) was connected to the UPLC system via an electrospray ionization (ESI) interface. This source was operated in positive ionization mode with the capillary voltage at 1.5 kV at 100 °C and the temperature of the desolvation was 300 °C. The cone and desolvation gas flows were 40 L h⁻¹ and 800 L h⁻¹, respectively. The collision gas flow and collision energy applied were 0.2 mL/min and 12 V, respectively. All data collected in

Centroid mode were acquired using Masslynx™ software (Waters Corp.). Leucine-enkephalin was used at a concentration of 500 pg/μL as the lock mass generating an $[M+H]^+$ ion (m/z 556.2771) and fragment at m/z 120.0813 and flow rate of 50 μL/min to ensure accuracy during the MS analysis.

Steady-state absorption spectra were recorded in a JASCO V-760 spectrophotometer. Laser Flash Photolysis (LFP) measurements were performed using a pulsed Nd:YAG L52137 V LOTIS TII at the excitation wavelength of 266 nm. The single pulses were *ca.* 10 ns duration, and the energy was ~12 mJ/pulse. The laser flash photolysis system consisted of the pulsed laser, a 77250 Oriel monochromator and an oscilloscope DP04054 Tektronix. The output signal from the oscilloscope was transferred to a personal computer. Absorbances of all solutions were adjusted at ~0.20 at 266 nm in acetonitrile. All UV and LFP measurements were done using 10 × 10 mm² quartz cuvettes at room temperature in deaerated conditions (25 min N₂ bubbling), using 10 mL of fresh solution in order to avoid data acquisition from photodegraded products. Control experiments indicated that the degree of decomposition of all oxetanes after photolysis was lower than 5%.

Femtosecond transient absorption experiments were performed using a pump-probe system. The femtosecond pulses were generated with a mode-locked Ti-Sapphire laser of a compact Libra HE (4 W power at 4 kHz) regenerative amplifier delivering 100 fs pulses at 800 nm (1 mJ/pulse). The output of the laser was split into two parts to generate the pump and the probe beams. Thus, tuneable femtosecond pump pulses were obtained by directing the 800 nm light into an optical parametric amplifier. In the present case, the pump was set at 280 nm and passed through a chopper prior to focus onto a rotating cell (1 mm optical path)

containing the samples in organic solution. The white light used as probe was produced after part of the 800 nm light from the amplifier travelled through a computer controlled 8 ns variable optical delay line and impinge on a CaF₂ rotating crystal. This white light was in turn split in two identical portions to generate reference and probe beams that then were focused on the rotating cell containing the sample. The pump and the probe beams were made to coincide to interrogate the sample. The power of the pump beam was set to 180 μW. Under these conditions, the degree of photodegradation of all oxetanes was lower than 5%. A computer-controlled imaging spectrometer was placed after this path to measure the probe and the reference pulses to obtain the transient absorption decays/spectra. The experimental data were treated and compensated by the chirp using the ExciPro program.

Steady-state photolysis. Irradiations were performed in a Luzchem multilamp photoreactor emitting at $\lambda_{\text{max}} = 350$ nm (12 × 8 W lamps). Solutions containing the uracil or thymine derivative (0.1 M) and BP (0.2 M) were irradiated through Pyrex for *ca.* 6h; the crude products containing the HH- and HT-oxetanes were purified by silica gel chromatography (hexane:ethyl acetate 80:20 v/v).

Oxetane HH-2. ¹H NMR (400 MHz, CDCl₃) δ 7.44-7.29 (m, 10H), 5.20 (d, *J* = 8.8 Hz, 1H), 5.94 (d, *J* = 8.8 Hz, 1H), 3.04 (s, 3H), 3.01 (s, 3H); ¹³C NMR (100 MHz, CDCl₃) δ 167.0, 151.7, 143.3, 138.7, 128.7, 128.4, 128.3, 128.2, 125.9, 125.1, 96.0, 70.6, 60.7, 35.4, 27.3; HRMS (ESI): *m/z* calcd. for C₁₉H₁₉N₂O₃ [M+H]⁺: 323.1396, found: 323.1391

Oxetane HH-3. ^1H NMR (400 MHz, CDCl_3) δ 7.44-7.26 (m, 10H), 5.24 (d, $J = 8.8$ Hz, 1H), 5.02 (d, $J = 8.8$ Hz, 1H), 5.47 (d, $J = 17.6$ Hz, 1H), 3.77 (s, 3H), 3.37 (d, $J = 17.6$ Hz, 1H), 3.06 (s, 3H); ^{13}C NMR (100 MHz, CDCl_3) δ 168.9, 166.6, 151.9, 142.5, 138.4, 128.7, 128.5, 128.4, 126.1, 125.4, 95.3, 70.2, 59.4, 52.7, 48.0, 27.5; HRMS (ESI): m/z calcd. for $\text{C}_{21}\text{H}_{21}\text{N}_2\text{O}_5$ $[\text{M}+\text{H}]^+$: 381.1450; found: 381.1446.

Oxetane HH-5. ^1H NMR (400 MHz, CD_3CN) δ 7.41-7.23 (m, 10H), 5.94 (s, 1H), 3.21 (s, 3H), 2.70 (s, 3H), 0.98 (s, 9H); ^{13}C NMR (100 MHz, CDCl_3) δ 169.7, 152.0, 145.2, 139.0, 128.3, 127.8, 127.6, 125.2, 125.4, 91.1, 83.5, 61.5, 35.8, 29.7, 27.4, 25.6; HRMS (ESI): m/z calcd. for $\text{C}_{23}\text{H}_{27}\text{N}_2\text{O}_3$ $[\text{M}+\text{H}]^+$: 379.2022; found: 379.2027.

Oxetane HT-5. ^1H NMR (400 MHz, CD_3CN) δ 7.84-7.20 (m, 10H), 5.84 (s, 1H), 3.17 (s, 3H), 2.66 (s, 3H), 0.96 (s, 9H); ^{13}C NMR (100 MHz, CDCl_3) δ 169.1, 153.0, 145.5, 128.2, 127.7, 127.4, 127.2, 125.9, 89.5, 85.3, 66.0, 35.9, 35.2, 29.7, 27.5; HRMS (ESI): m/z calcd. for $\text{C}_{23}\text{H}_{27}\text{N}_2\text{O}_3$ $[\text{M}+\text{H}]^+$: 379.2022; found: 379.2026.

Oxetane HH-5. ^1H NMR (400 MHz, CDCl_3) δ 7.37-7.23 (m, 10H), 5.97 (s, 1H), 5.84 (d, $J = 17.6$ Hz, 1H), 3.82 (s, 3H), 3.73 (d, $J = 17.6$ Hz, 1H), 2.84 (s, 3H), 1.10 (s, 9H); ^{13}C NMR (100 MHz, CDCl_3) δ 169.8, 169.1, 152.1, 143.7, 139.1, 128.7, 128.4, 127.8, 125.4, 125.6, 90.6, 83.6, 59.7, 52.6, 48.3, 36.2, 27.5, 25.4; HRMS (ESI): m/z calcd. for $\text{C}_{25}\text{H}_{29}\text{N}_2\text{O}_5$ $[\text{M}+\text{H}]^+$: 437.2076; found: 437.2071.

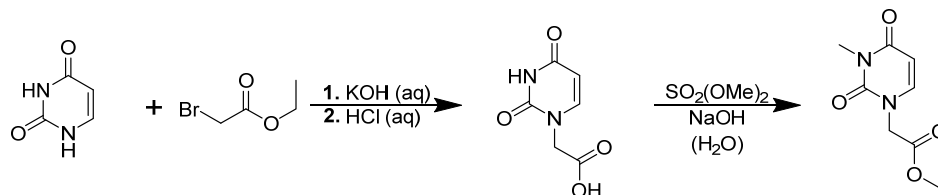
Oxetane HT-5. ^1H NMR (400 MHz, CDCl_3) δ 7.79-7.19 (m, 10H), 5.81 (s, 1H), 5.80 (d, $J = 17.6$ Hz, 1H), 5.07 (d, $J = 17.6$ Hz, 1H), 3.80 (s, 3H), 2.79 (s, 3H), 1.04 (s, 9H); ^{13}C NMR (100 MHz, CDCl_3) δ 169.2, 168.9, 152.0, 142.6, 141.4, 128.1, 127.8, 127.5, 127.3, 127.1, 126.0, 89.8, 83.3, 66.0, 52.5, 47.1, 36.1, 27.8, 27.3; HRMS (ESI): m/z calcd. for $\text{C}_{25}\text{H}_{29}\text{N}_2\text{O}_5$ $[\text{M}+\text{H}]^+$: 437.2076; found: 437.2073.

Oxetane HH-6. ^1H NMR (400 MHz, CDCl_3) δ 7.38-7.25 (m, 10H), 5.78 (d, $J = 17.6$ Hz, 1H), 5.64 (s, 1H), 3.79 (s, 3H), 3.58 (d, $J = 17.6$ Hz, 1H), 2.85 (s, 3H), 1.76 (s, 3H); ^{13}C NMR (100 MHz, CDCl_3) δ 169.0, 168.8, 151.9, 143.8, 138.6, 128.7, 128.4, 128.1, 125.6, 125.1, 91.3, 65.3, 52.7, 48.3, 27.5, 23.7; HRMS (ESI): m/z calcd. for $\text{C}_{22}\text{H}_{23}\text{N}_2\text{O}_5$ $[\text{M}+\text{H}]^+$: 395.1607; found: 395.1607.

Oxetane HT-6. ^1H NMR (400 MHz, CDCl_3) δ 7.55-7.18 (m, 10H), 5.29 (s, 1H), 5.64 (d, $J = 23.6$ Hz, 1H), 5.04 (d, $J = 23.6$ Hz, 1H), 3.78 (s, 3H), 2.78 (s, 3H), 1.52 (s, 3H); ^{13}C NMR (100 MHz, CDCl_3) δ 169.1, 151.7, 141.8, 141.1, 128.3, 128.0, 127.7, 127.6, 125.3, 125.1, 90.5, 87.1, 52.5, 46.1, 27.8, 20.1; HRMS (ESI): m/z calcd. for $\text{C}_{22}\text{H}_{23}\text{N}_2\text{O}_5$ $[\text{M}+\text{H}]^+$: 395.1607, found: 395.1606.

5. Supplementary material

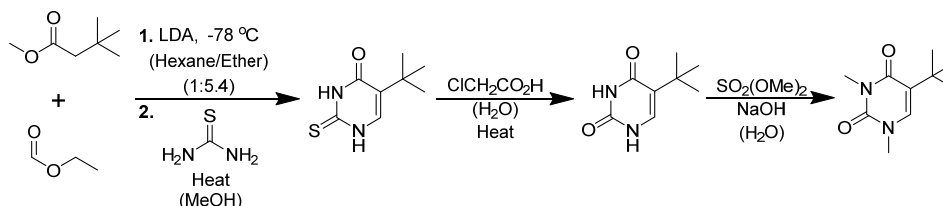
Synthesis of the uracil and thymine derivatives. Scheme and experimental protocol of the synthesis of the unknown uracil and thymine intermediates by ^1H and ^{13}C NMR, and HRMS.



Synthesis of methyl 3-methyluracil-1-acetate. The intermediate uracil-1-acetic acid was synthesized earlier.³³ Briefly, to a suspension of 5.4 g (45 mmol) of uracil in 110 mL of water, 110 mL of potassium hydroxide (1M) were added. The solution was stirred until clear and then 11 mL of ethyl bromoacetate (90 mmol) were added dropwise. The mixture was stirred overnight under reflux, then cooled down to 0 °C and acidified to pH 1 with concentrated hydrochloric acid. The resulting white precipitate was filtered under vacuum and washed with cold HCl (1M). The intermediate uracil-1-acetic acid (6.4 g) was obtained as a pure white solid (84% yield).

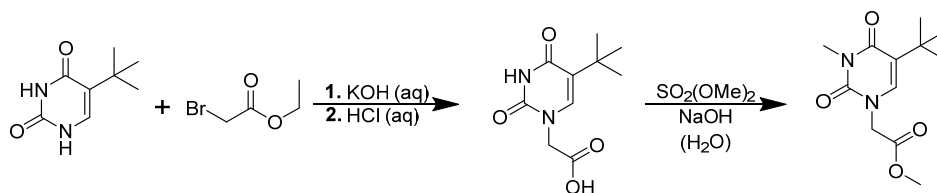
To a solution of 5.5 g of NaOH in water (42 mL), 6 g of uracil-1-acetic acid (35 mmol) were added upon stirring. After a few minutes, 8.4 mL of dimethyl sulphate (88 mmol) were added dropwise, and the solution was stirred overnight. The crude product was extracted with ethyl acetate. The final product was purified via silica gel chromatography using ethyl acetate as eluent. The final product methyl 3-methyluracil-1-acetate (2.77 g) was obtained as a white solid.

^1H NMR (400 MHz, CD_3OD) δ 7.54 (d, $J = 7.6$ Hz, 1H), 5.77 (d, $J = 7.6$ Hz, 1H), 5.58 (s, 2H), 3.77 (s, 3H), 3.29 (s, 3H); ^{13}C NMR (100 MHz, CD_3OD) δ 168.6, 165.1, 151.8, 143.9, 100.3, 51.7, 49.5, 26.6; Yield: 40%. HRMS (ESI): m/z calcd. for $\text{C}_8\text{H}_{11}\text{N}_2\text{O}_4$ $[\text{M}+\text{H}]^+$: 199.0719, found: 199.0717.



Synthesis of 1,3-dimethyl-5-*tert*-butyluracil. The synthesis of the different uracil intermediates and the final derivative has been described earlier.³⁴⁻³⁵ Briefly, 16 mL of lithium diisopropylamide (LDA) were dissolved in a mixture of 40 mL anhydrous diethyl ether and 25 mL dry hexane at -78°C in nitrogen atmosphere. A separate solution of 5.8 mL of methyl 3,3-dimethylbutanoate (0.04 mol) in 35 mL of anhydrous diethyl ether was prepared at -78°C and purged with N_2 for 15 minutes; then, it was added quickly via a purged glass syringe to the LDA solution. Another solution of 12.5 mL of ethyl formate (0.13 mol) in 60 mL of anhydrous diethyl ether was prepared at -78°C and purged with N_2 for 10 min, and then it was added via a purged glass syringe to the mother solution. The mixture was stirred under N_2 atmosphere at -78°C for 6 hours. The solvent was removed under reduced pressure. The crude was kept in the freezer overnight under N_2 . The crude product was subsequently transferred to a 25 mL round-bottom flask and 3.04 g of thiourea (0.04 mol) in 10 mL of anhydrous methanol was added. The solution was purged with N_2 for 15 mins and then refluxed for 6 hours; afterwards, it was cooled down to -10°C under vigorous stirring and acidified down to

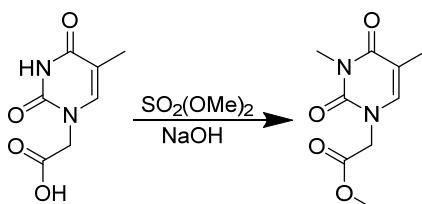
pH < 3 with HCl. The solution was stirred for 1 hour and the final intermediate uracil derivative was filtered under vacuum and washed with cold methanol. About 650 mg of this product (3 mmol) was dissolved in 26 mL of water and 3.9 g of chloroacetic acid (18 mmol) were added. The solution was stirred under reflux for 4 hours. The precipitated *tert*-butyl uracil was filtered under vacuum (615 mg, 95% yield). About 200 mg of the *tert*-butyl uracil (1.2 mmol) was dissolved in 2 mL of NaOH (2.5 M). Then, 0.4 mL of dimethyl sulphate (5.2 mmol) were added dropwise under stirring. The solution was stirred for 16 hours. The crude product was extracted with ethyl acetate and dried with MgSO₅. The solvent was removed under reduced pressure to get the final 1,3-dimethyl-5-*tert*-butyluracil (185 mg, 79% yield).



Synthesis of methyl 5-*tert*-butyl-3-methyluracil-1-acetate. The synthesis of the intermediate has been described earlier.²¹ Briefly, 2.5 g of *tert*-butyl uracil (15 mmol) was dissolved in 33 mL of water. Then, 33 mL of potassium hydroxide 2 M was added. Under vigorous stirring, 3.33 mL of ethyl bromoacetate (30 mmol) were added dropwise, and the solution was left under reflux for 13 hours. The solution was then acidified to pH 1 with 37% hydrochloric acid and cooled down in an ice-salt bath. The white precipitate was filtered off and washed with cold hydrochloric acid 1 M to give pure 5-*tert*-butyluracil-1-acetic acid. Then, 1.5 g of this compound (6.6 mmol) was dissolved in 8 mL of sodium hydroxide 2.5 M, and subsequently 1.57 mL of dimethyl sulphate (16.5 mmol) were added dropwise. The solution was stirred for 5 hours. The crude was extracted

with ethyl acetate, dried with MgSO_4 and the organic solvent was removed under reduced pressure to get the final product methyl 5-*tert*-butyl-3-methyluracil-1-acetate.

^1H NMR (400 MHz, CDCl_3) δ 6.87 (s, 1H), 5.46 (s, 2H), 3.80 (s, 3H), 3.33 (s, 3H), 1.28 (s, 9H); ^{13}C NMR (100 MHz, CDCl_3) δ 168.2, 162.3, 151.4, 136.8, 122.0, 52.8, 50.0, 33.2, 28.7, 27.9; Yield: 35%. HRMS (ESI): m/z calcd. for $\text{C}_{12}\text{H}_{19}\text{N}_2\text{O}_4$ $[\text{M}+\text{H}]^+$: 255.1345, found: 255.1346.



Synthesis of methyl 3-methyl-thymine-1-acetate. The synthesis has been previously reported.³⁶ Briefly, 2 g of thymine-1-methylacetate (12 mmol) was dissolved in 13 mL of NaOH (2.5 M). Then, 2.6 mL of dimethyl sulphate (27 mmol) were added dropwise under stirring. The mixture was stirred 24 hours. The crude product was extracted with ethyl acetate and dried with MgSO_4 to get the final product as a white solid.

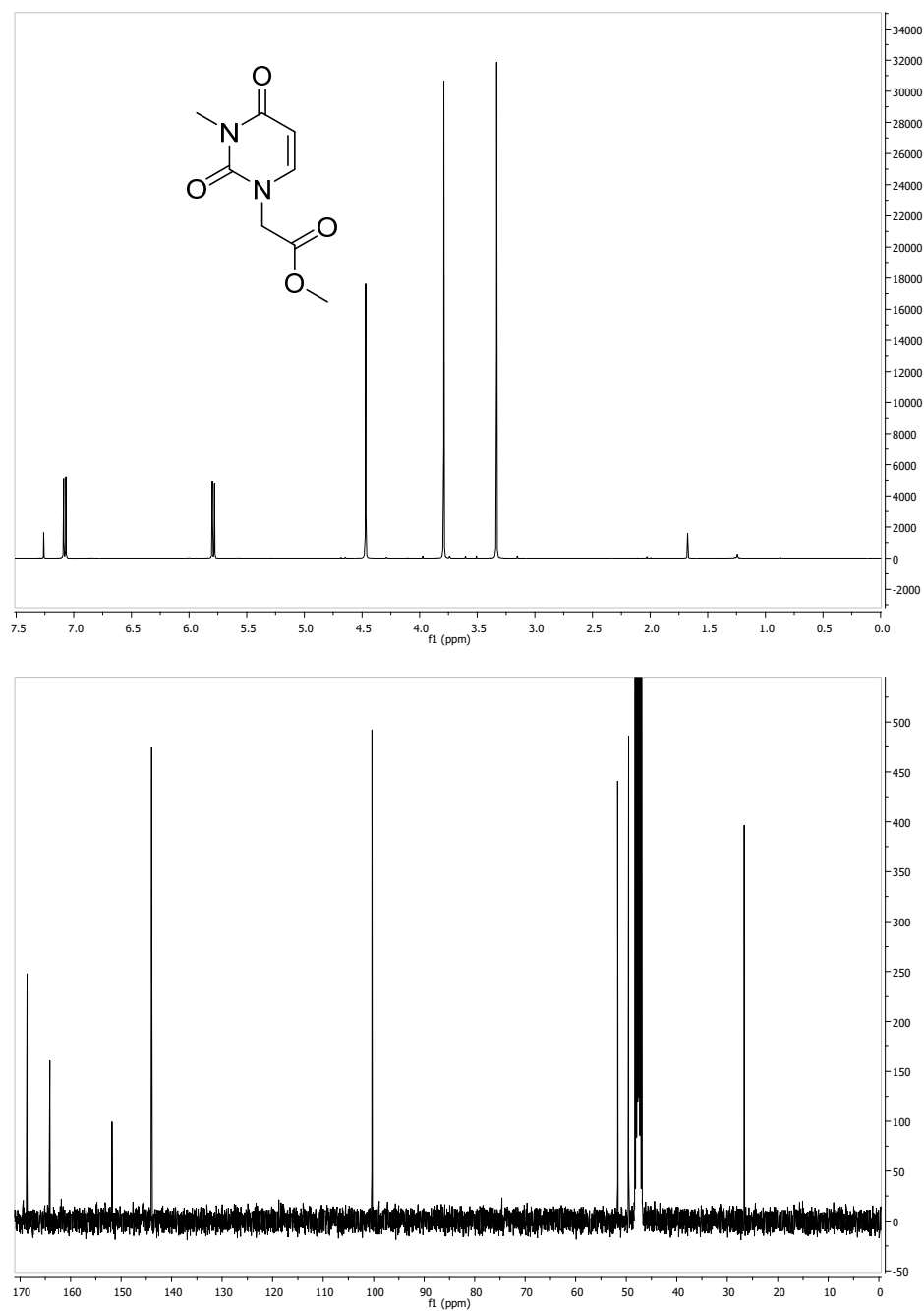


Figure S5.1. ¹H- and ¹³C-NMR for methyl 3-methyluracil-1-acetate in CD₃OD.

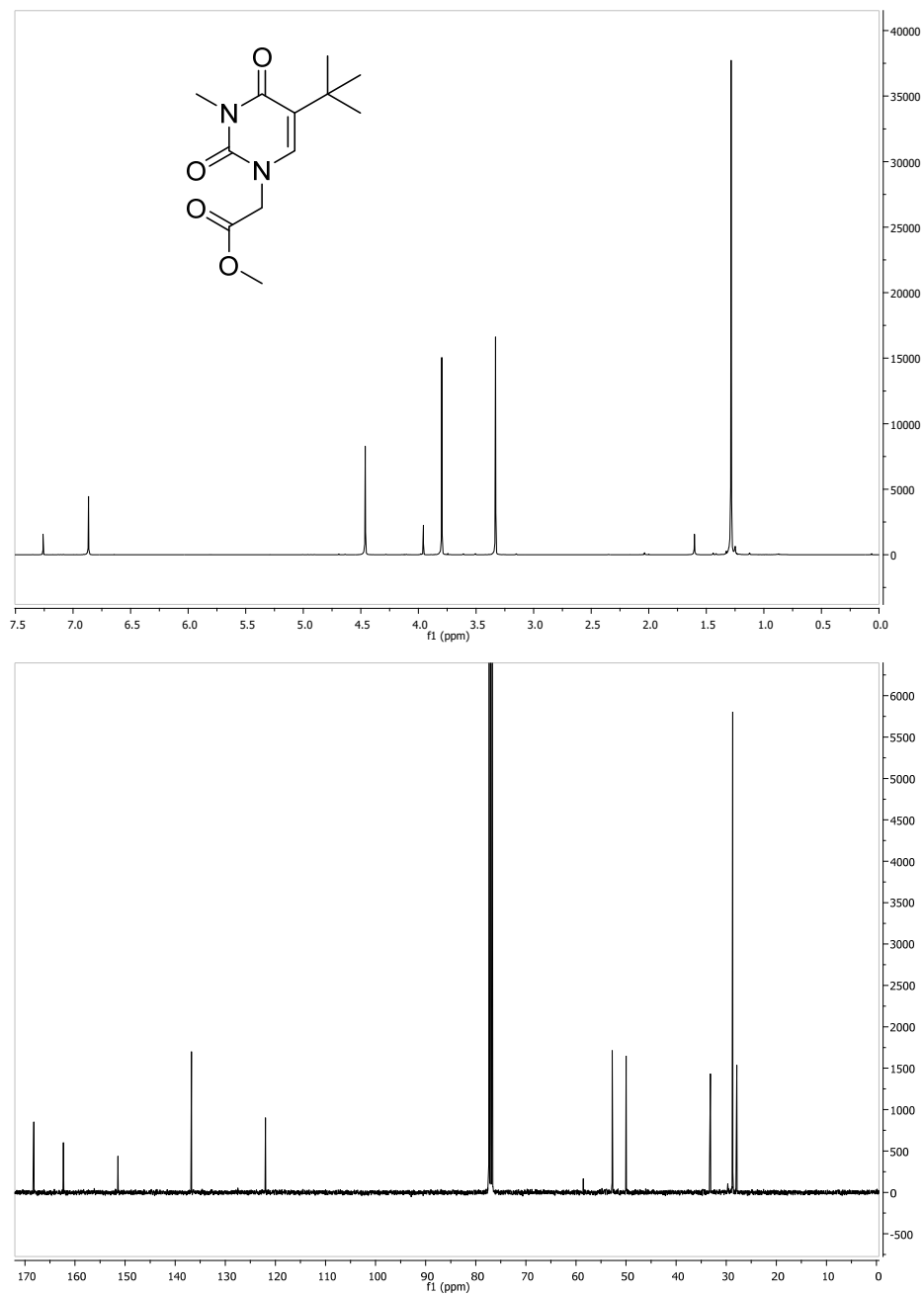


Figure S5.2. ¹H- and ¹³C-NMR for methyl 5-*tert*-butyl-3-methyluracil-1-acetate in CDCl₃.

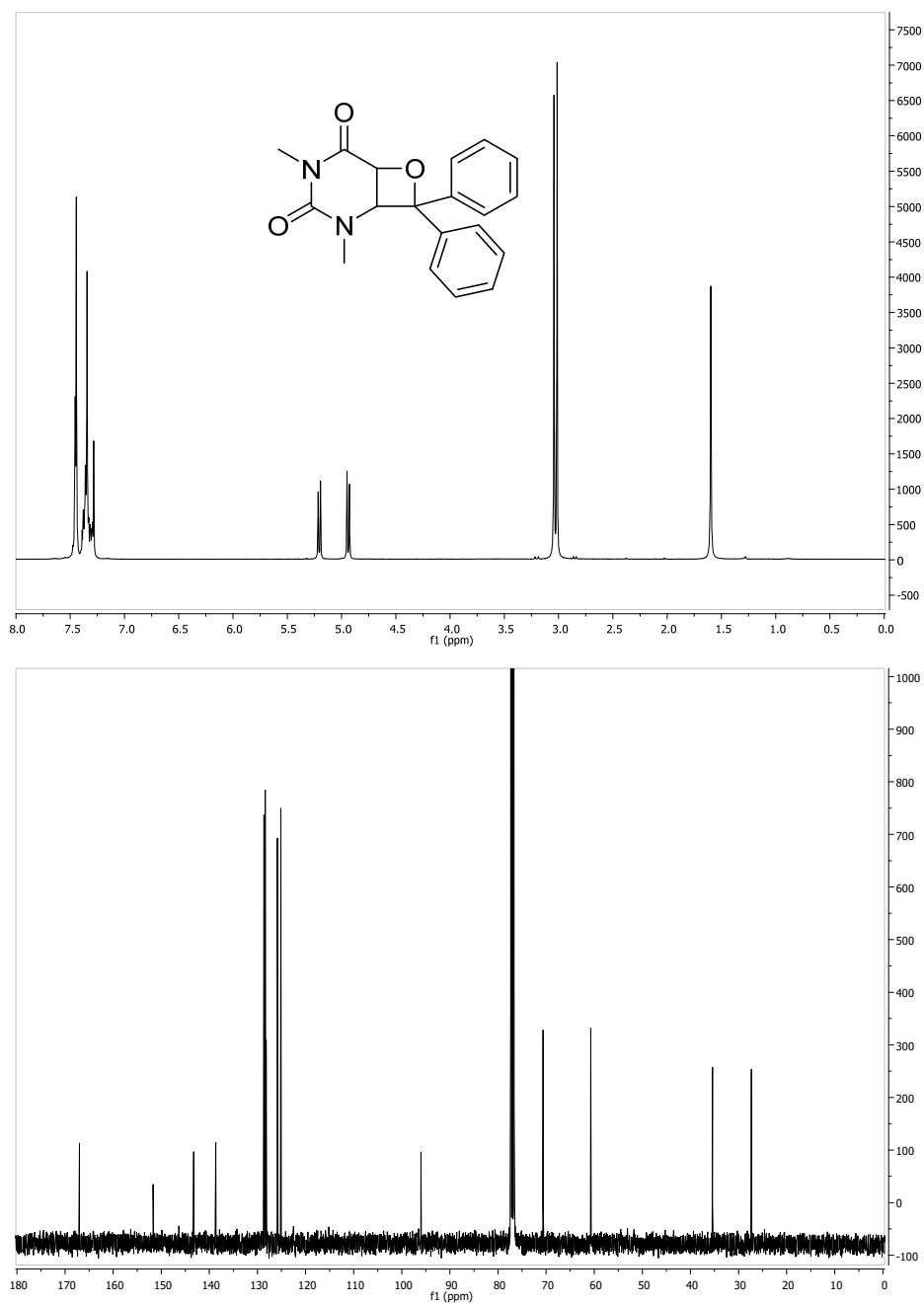


Figure S5.3. ¹H- and ¹³C-NMR for HH-2 in CDCl₃.

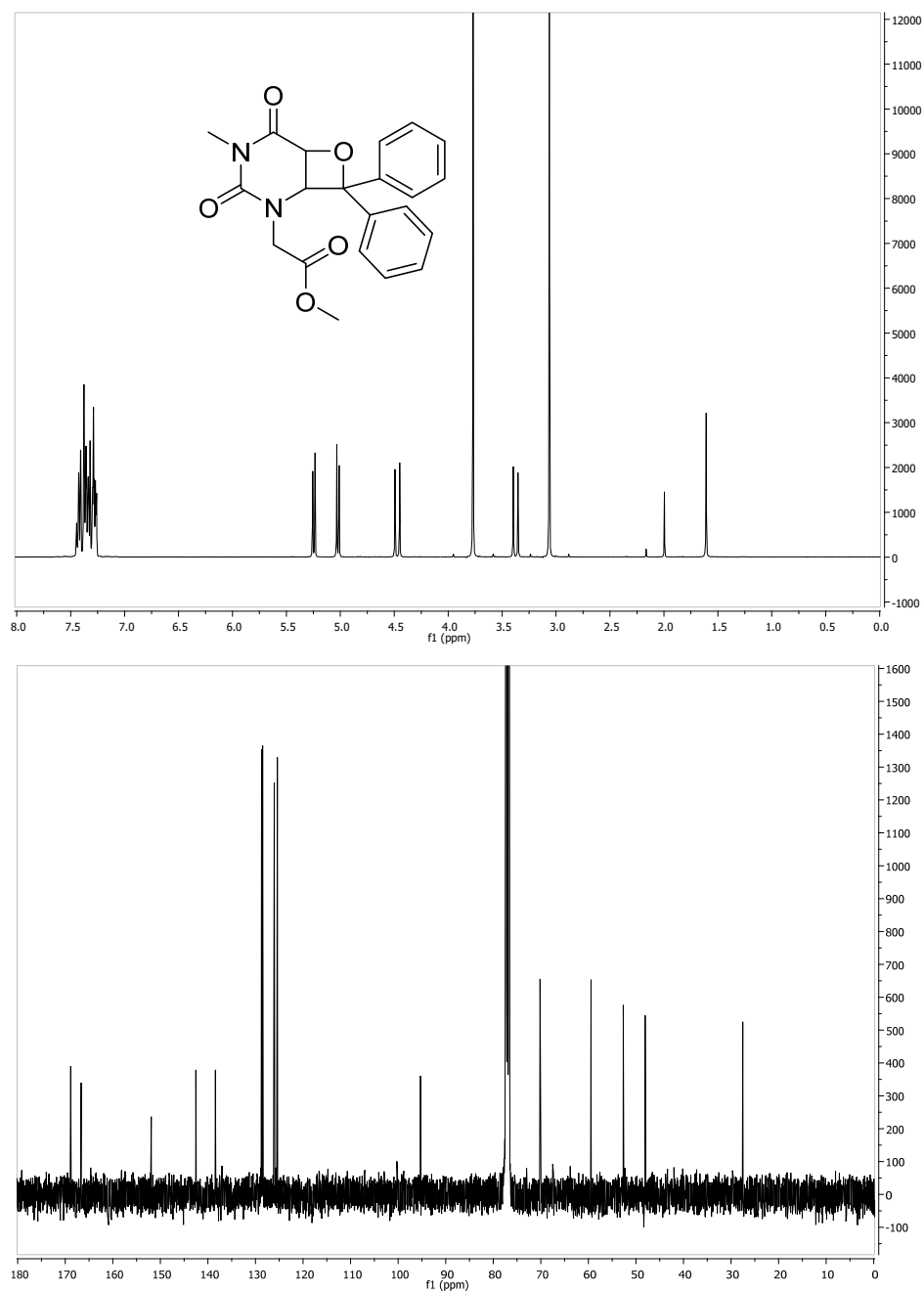


Figure S5.4. ¹H- and ¹³C-NMR for HH-3 in CDCl₃.

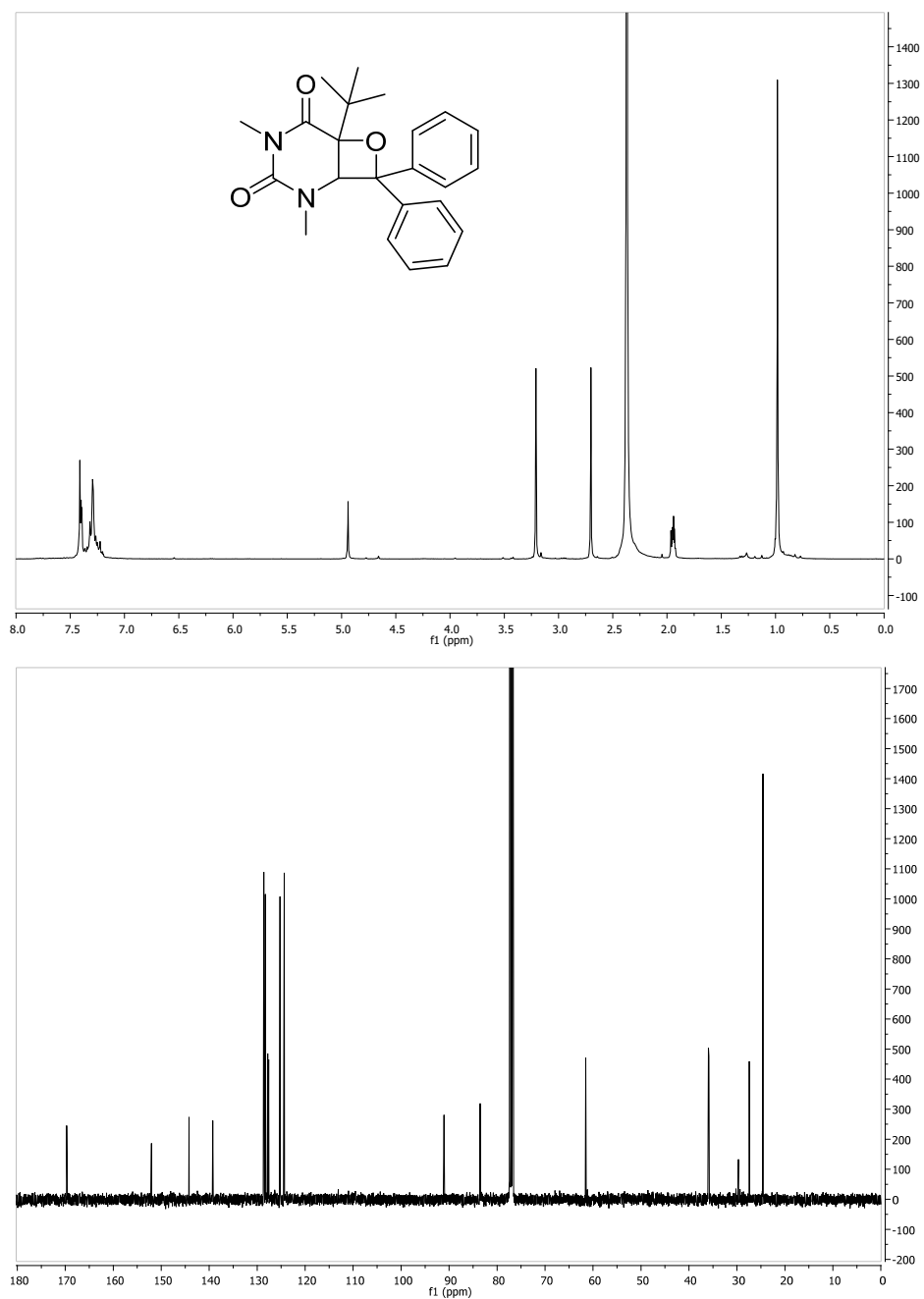


Figure S5.5. ¹H- and ¹³C-NMR for HH-4 in CDCl₃.

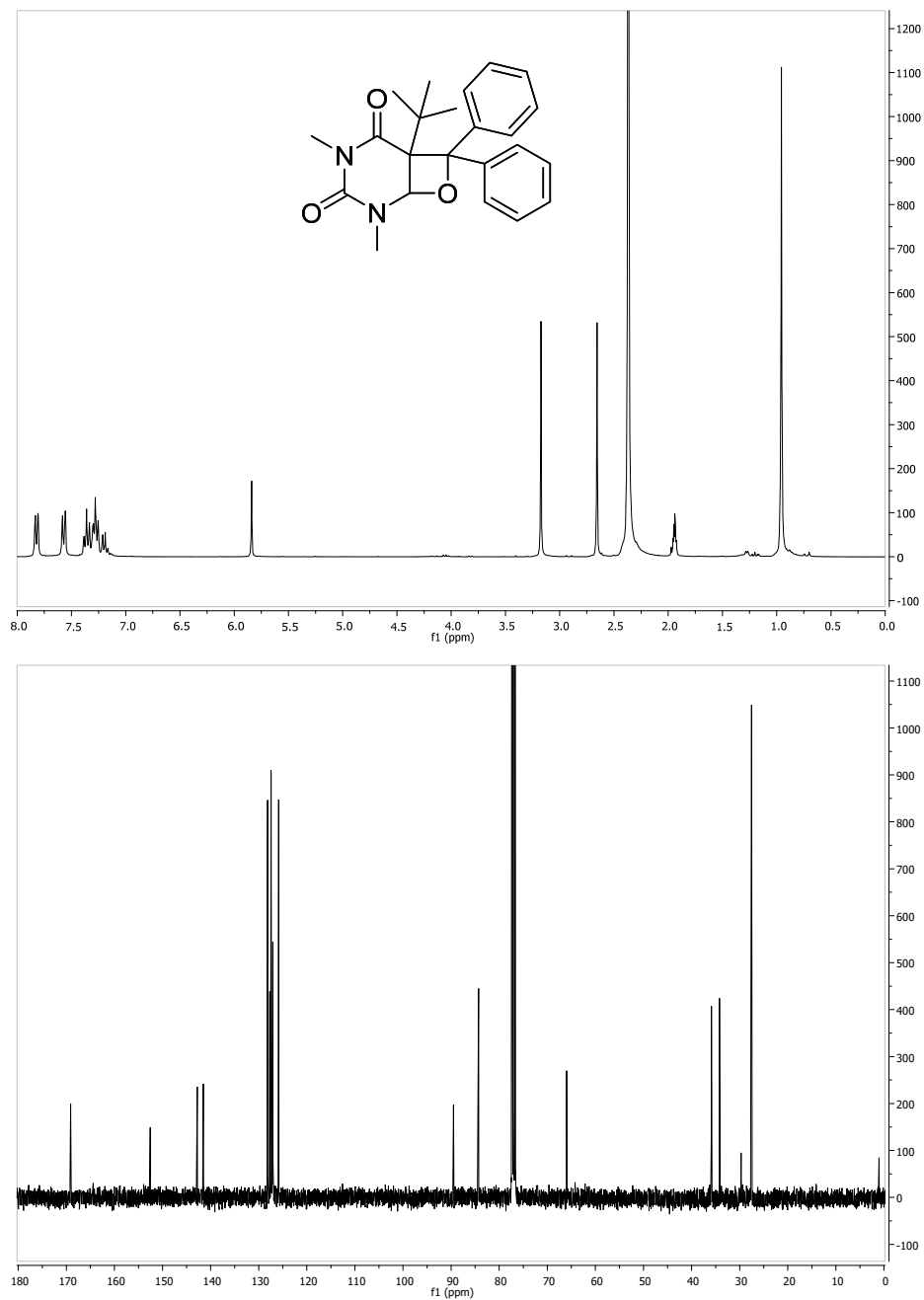


Figure S5.6. ¹H- and ¹³C-NMR for HT-4 in CDCl₃.

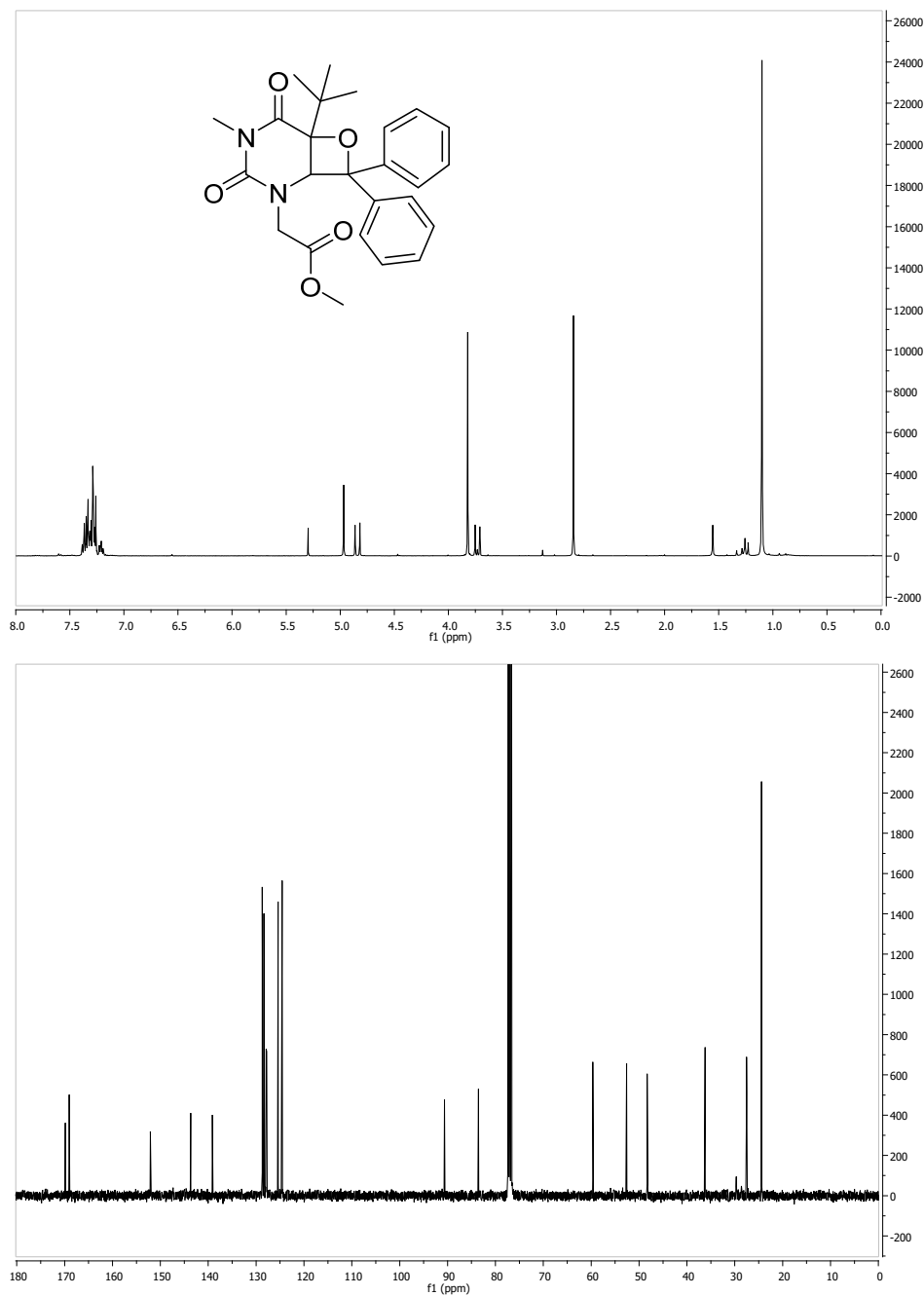


Figure S5.7. ^1H - and ^{13}C -NMR for HH-5 in CDCl_3 .

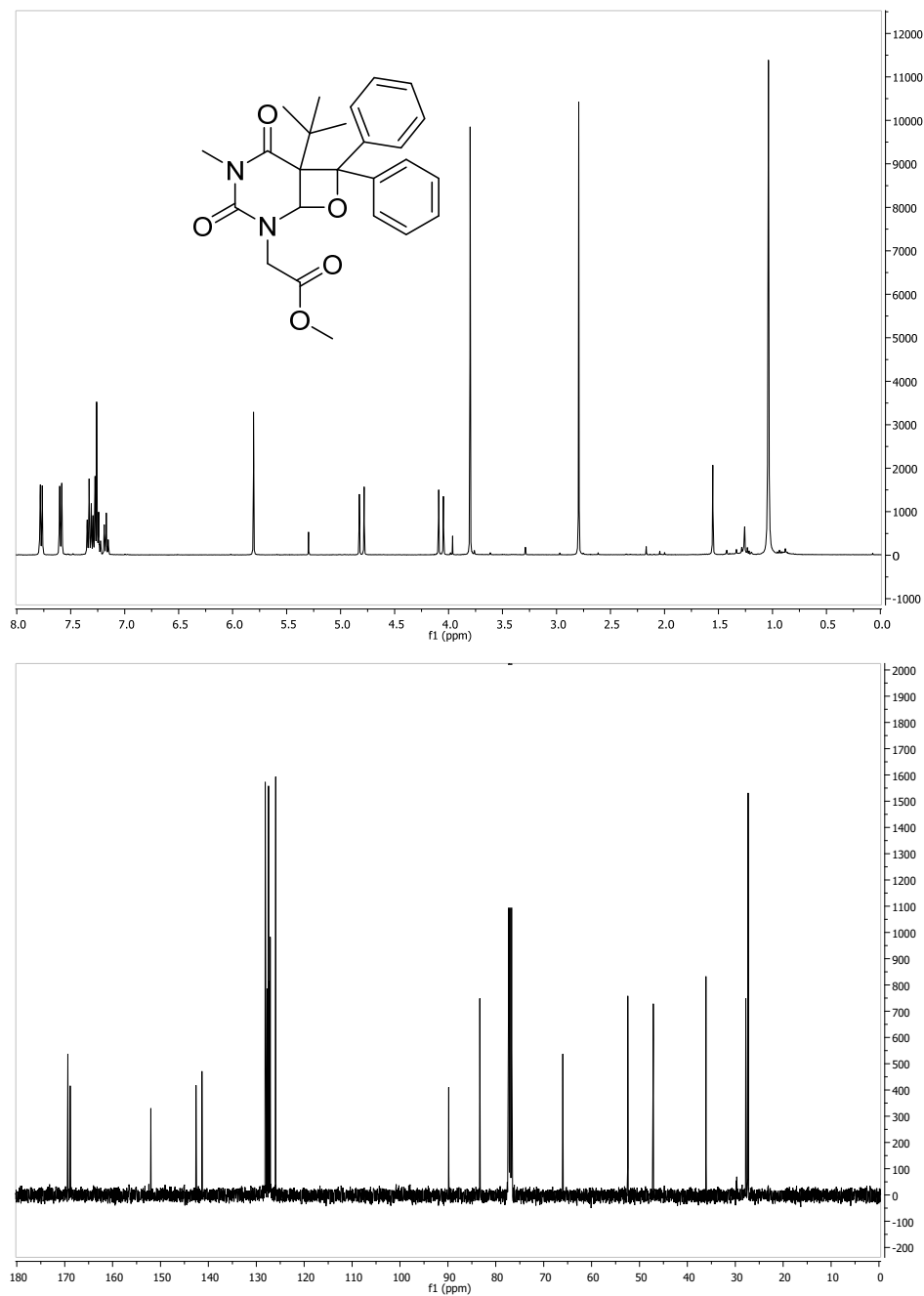


Figure S5.8. ^1H - and ^{13}C -NMR for HT-5 in CDCl_3 .

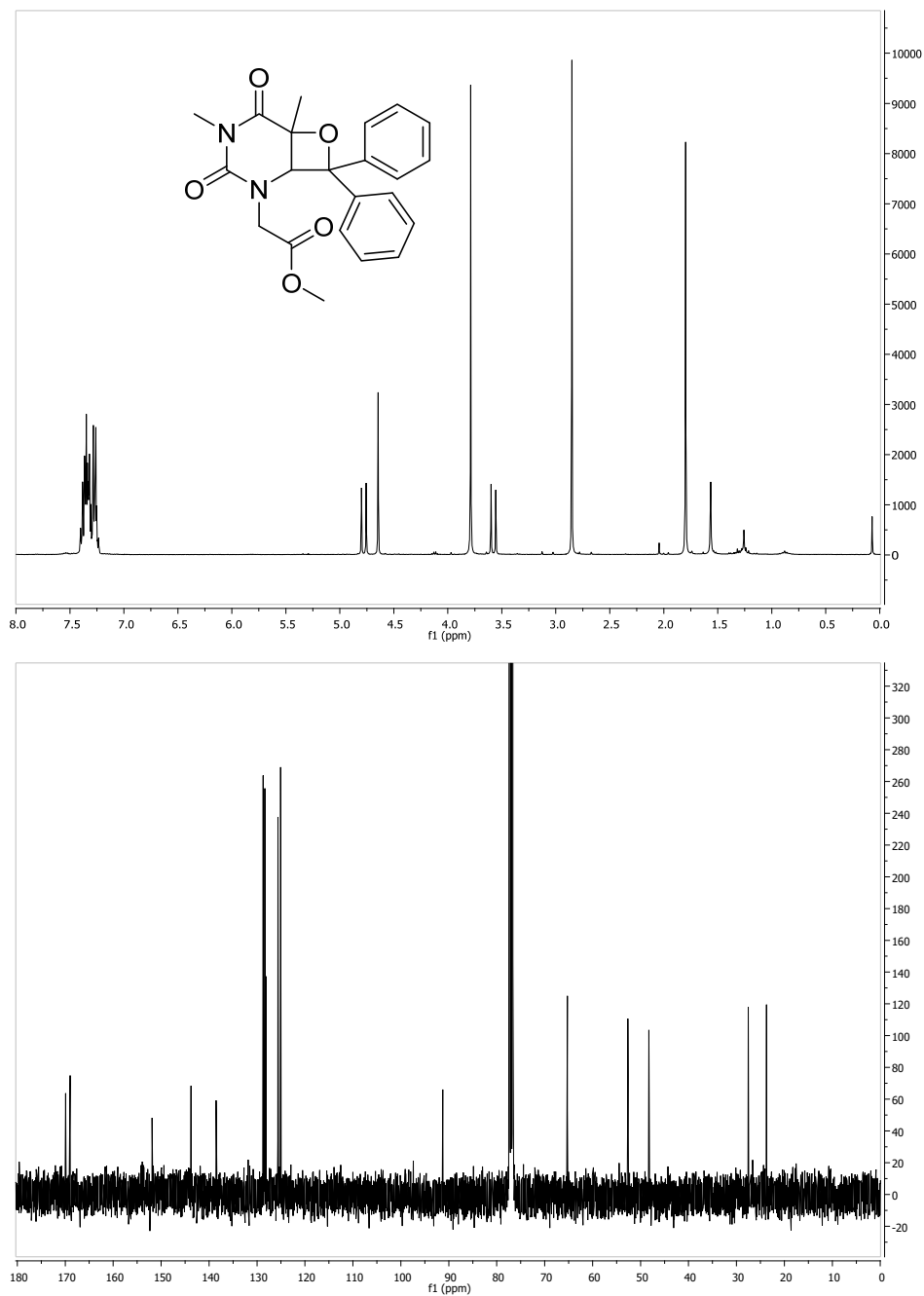


Figure S5.9. ^1H - and ^{13}C -NMR for HH-6 in CDCl_3 .

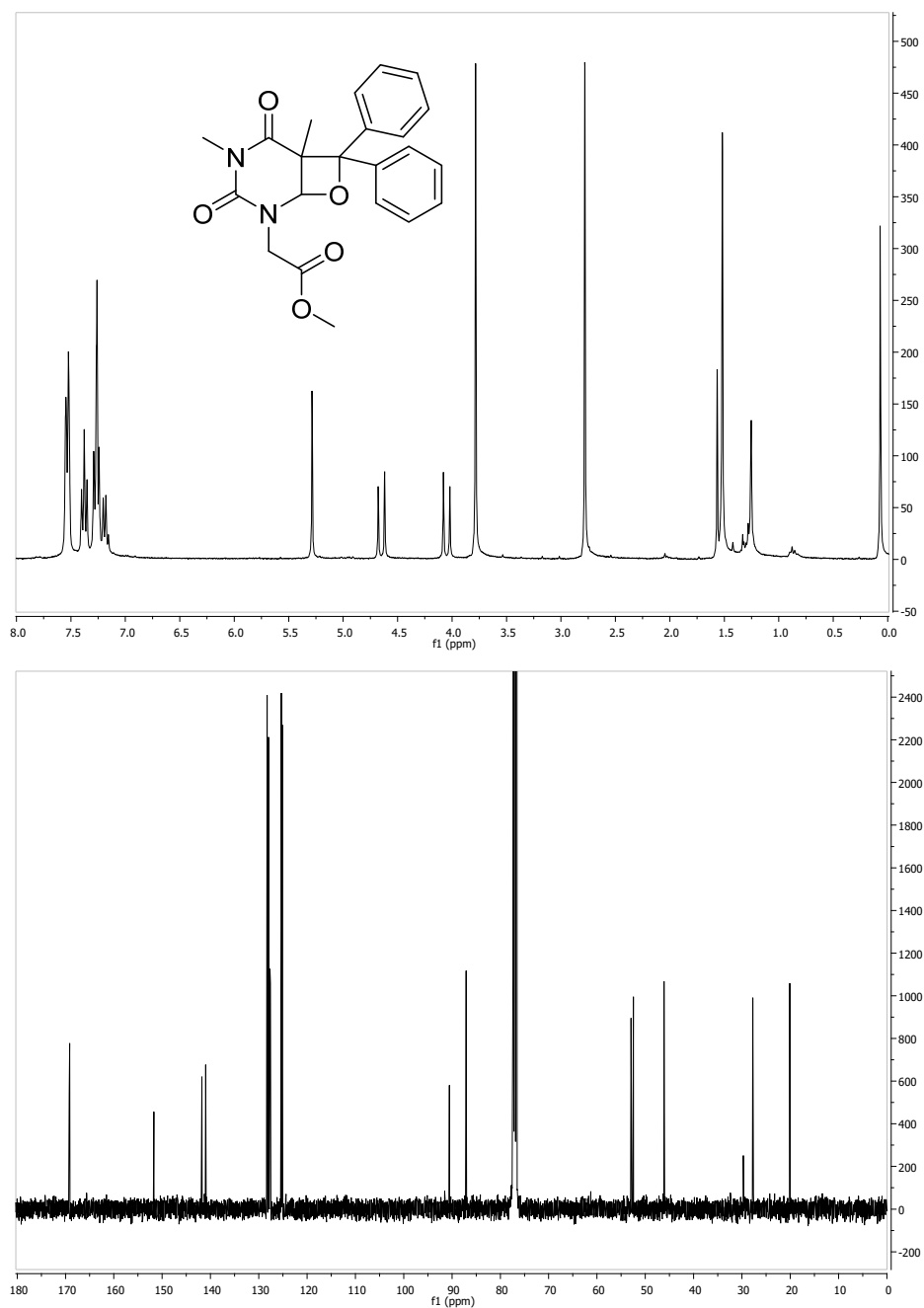


Figure S5.10. ^1H - and ^{13}C -NMR for HT-6 in CDCl_3 .

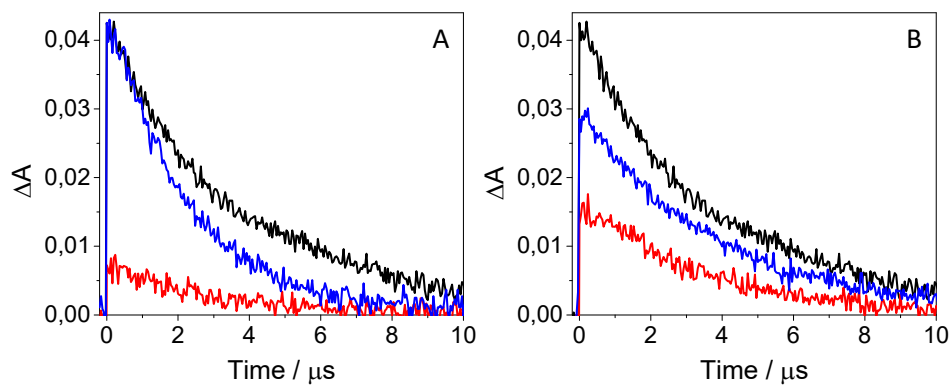


Figure S5.11. LFP decay traces at 530 nm for A) BP (black), HH-5 (blue) and HT-5 (red) and B) BP (black), HH-6 (blue) and HT-6 (red) after excitation at 266 nm in deaerated acetonitrile.

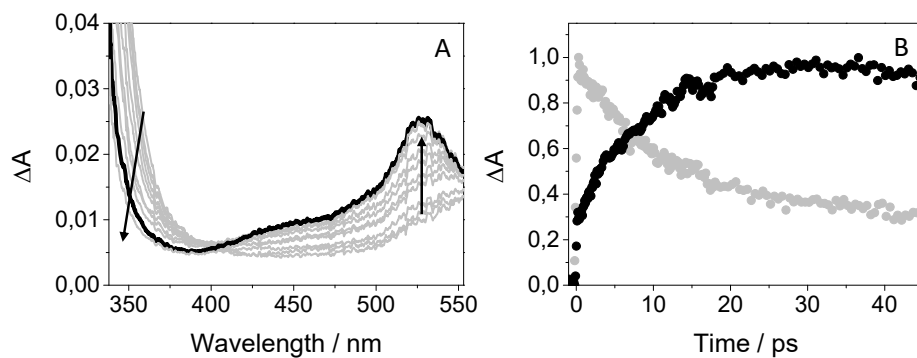


Figure S5.12. A) Femtosecond transient absorption spectra from 0.5 to 40 ps and B) kinetic traces at 340 nm (gray) and 530 nm (black) for BP after excitation at 280 nm in acetonitrile.

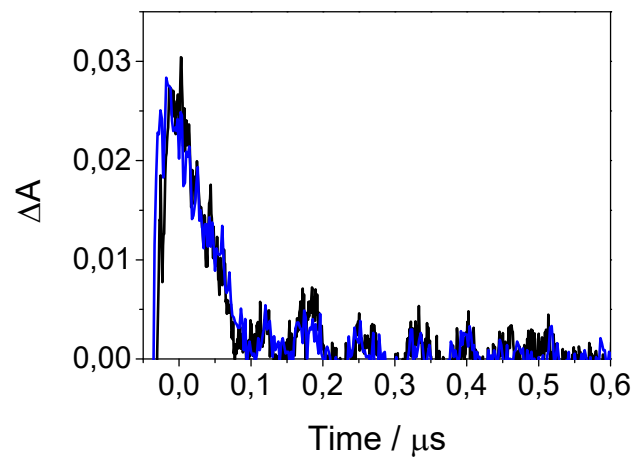


Figure S5.13. LFP decay traces at 530 nm for dyad 2 (black) and HH-9 (blue) after excitation at 266 nm in deaerated acetonitrile.

6. References

1. Kraemer, K. H., Sunlight and skin cancer: Another link revealed. *Proc. Natl. Acad. Sci. USA* **1997**, *94*, 11-15.
2. Taylor, J. S., Unraveling the molecular pathway from sunlight to skin cancer. *Acc. Chem. Res.* **1994**, *27*, 76-82.
3. Urbach, F., Ultraviolet radiation and skin cancer of humans. *J. Photochem. Photobiol. B* **1997**, *40*, 3-7.
5. Mukhtar, H.; Elmets, C. A., Photocarcinogenesis: Mechanisms, models and human health implications. *Photochem. Photobiol.* **1996**, *63*, 356-357.
5. Sutherland, B. M., Mutagenic lesions in carcinogenesis: Induction and repair of pyrimidine dimers. *Photochem. Photobiol.* **1996**, *63*, 375-377.
6. Tommasi, S.; Denissenko, M. F.; Pfeifer, G. P., Sunlight induces pyrimidine dimers preferentially at 5-methylcytosine bases. *Cancer Res.* **1997**, *57*, 4727-4730.
7. Cadet, J.; Grand, A.; Douki, T., Solar UV radiation-induced DNA bipyrimidine photoproducts: Formation and mechanistic insights. *Top. Curr. Chem.* **2015**, *356*, 249-275.
8. Cadet, J.; Mouret, S.; Ravanat, J. L.; Douki, T., Photoinduced damage to cellular DNA: Direct and photosensitized reactions. *Photochem. Photobiol.* **2012**, *88*, 1048-1065.

9. Epe, B.; Pflaum, M.; Boiteux, S., DNA damage induced by photosensitizers in cellular and cell-free systems. *Mutat. Res.* **1993**, *299*, 135-145.
10. Li, J.; Liu, Z.; Tan, C.; Guo, X.; Wang, L.; Sancar, A.; Zhong, D., Dynamics and mechanism of repair of ultraviolet-induced (6-4) photoproduct by photolyase. *Nature* **2010**, *466*, 887-890.
11. Todo, T.; Ryo, H.; Yamamoto, K.; Toh, H.; Inui, T.; Ayaki, H.; Nomura, T.; Ikenaga, M., Similarity among the drosophila (6-4)photolyase, a human photolyase homolog, and the DNA photolyase-blue-light photoreceptor family. *Science* **1996**, *272*, 109-112.
12. Todo, T.; Takemori, H.; Ryo, H.; Ihara, M.; Matsunaga, T.; Nikaido, O.; Sato, K.; Nomura, T., A new photoreactivating enzyme that specifically repairs ultraviolet light-induced (6-4)photoproducts. *Nature* **1993**, *361*, 371-375.
13. Todo, T.; Tsuji, H.; Otsoshi, E.; Hitomi, K.; Kim, S. T.; Ikenaga, M., Characterization of a human homolog of 6-4 photolyase. *Mutat. Res.* **1997**, *384*, 195-205.
15. Surana, K.; Chaudhary, B.; Diwaker, M.; Sharma, S., Benzophenone: A ubiquitous scaffold in medicinal chemistry. *Med. Chem. Commun.* **2018**, *9*, 1803-1817.
15. Bosca, F.; Miranda, M. A., Photosensitizing drugs containing the benzophenone chromophore. *J. Photochem. Photobiol. B* **1998**, *43*, 1-26.
16. Delatour, T.; Douki, T.; D'Ham, C.; Cadet, J., Photosensitization of thymine nucleobase by benzophenone through energy transfer, hydrogen abstraction and one-electron oxidation. *J. Photochem. Photobiol. B* **1998**, *44*, 191-198.

17. Rogers, J. E.; Kelly, L. A., Nucleic acid oxidation mediated by naphthalene and benzophenone imide and diimide derivatives: Consequences for DNA redox chemistry. *J. Am. Chem. Soc.* **1999**, *121*, 3854-3861.
18. Blasco-Brusola, A.; Navarrete-Miguel, M.; Giussani, A.; Roca-Sanjuán, D.; Vayá, I.; Miranda, M. A., Regiochemical memory in the adiabatic photolysis of thymine-derived oxetanes. A combined ultrafast spectroscopic and CASSCF/CASPT2 computational study. *Phys. Chem. Chem. Phys.* **2020**, *22*, 20037-20042.
19. Cuquerella, M. C.; Lhiaubet-Vallet, V.; Bosca, F.; Miranda, M. A., Photosensitized pyrimidine dimerisation in DNA. *Chem. Sci.* **2011**, *2*, 1219–1232.
20. Miró, P.; Gómez-Mendoza, M.; Sastre, G.; Cuquerella, M. C.; Miranda, M. A.; Marín, M. L., Generation of the thymine triplet state by through-bond energy transfer. *Chem. Eur. J.* **2019**, *25*, 7004-7011.
21. Vendrell-Criado, V.; Lhiaubet-Vallet, V.; Yamaji, M.; Cuquerella, M. C.; Miranda, M. A., Blocking cyclobutane pyrimidine dimer formation by steric hindrance. *Org. Biomol. Chem.* **2016**, *14*, 4110-4115.
22. Encinas, S.; Belmadoui, N.; Climent, M. J.; Gil, S.; Miranda, M. A., Photosensitization of thymine nucleobase by benzophenone derivatives as models for photoinduced dna damage: Paterno-Büchi vs energy and electron transfer processes. *Chem. Res. Toxicol.* **2004**, *17*, 857-862.
23. Joseph, A.; Falvey, D. E., Photolysis of thymine oxetanes produces triplet excited carbonyl compounds with high efficiency. *J. Am. Chem. Soc.* **2001**, *123*, 3145-3146.

25. Joseph, A.; Prakash, G.; Falvey, D. E., Model studies of the (6-4) photoproduct photolyase enzyme: Laser flash photolysis experiments confirm radical ion intermediates in the sensitized repair of thymine oxetane adducts. *J. Am. Chem. Soc.* **2000**, *122*, 11219-11225.
25. Prakash, G.; Falvey, D. E., Model studies of the (6-4) photoproduct DNA photolyase: Synthesis and photosensitized splitting of a thymine-5,6-oxetane. *J. Am. Chem. Soc.* **1995**, *117*, 11375-11376.
26. Belmadoui, N.; Encinas, S.; Climent, M. J.; Gil, S.; Miranda, M. A., Intramolecular interactions in the triplet excited states of benzophenone-thymine dyads. *Chem. Eur. J.* **2006**, *12*, 553-561.
27. Kim, S. T.; Malhotra, K.; Smith, C. A.; Taylor, J. S.; Sancar, A., Characterization of (6-4) photoproduct DNA photolyase. *J. Biol. Chem.* **1994**, *269*, 8535-8540.
28. Joseph, A.; Falvey, D. E., Photoinduced electron transfer cleavage of oxetane adducts of uracil and cytosine. *Photochem. Photobiol. Sci.* **2002**, *1*, 632-635.
29. Bell, J. A.; Linschitz, H., Decay kinetics of the 1-naphthaldehyde and benzophenone triplet states in benzene. *J. Am. Chem. Soc.* **1963**, *85*, 528-532.
30. Blasco-Brusola, A.; Vaya, I.; Miranda, M. A., Influence of the linking bridge on the photoreactivity of benzophenone-thymine conjugates. *J. Org. Chem.* **2020**, *85*, 14068-14076.
31. Tamai, N.; Asahi, T.; Masuhara, H., Intersystem crossing of benzophenone by femtosecond transient grating spectroscopy. *Chem. Phys. Lett.* **1992**, *198*, 413-418.

32. Kwok, W. M.; Guan, X.; Chu, L. M.; Tang, W.; Phillips, D. L., Observation of singlet cycloreversion of thymine oxetanes by direct photolysis. *J. Phys. Chem. B* **2008**, *112*, 11794-11797.
33. Mokhir, A. A.; Richert, C., Synthesis and monitored selection of 5'-nucleobase-capped oligodeoxyribonucleotides. *Nucleic Acids Res.* **2000**, *28*, 4254-4265.
35. Basnak, I.; Balkan, A.; Coe, P. L.; Walker, R. T., The synthesis of some 5-substituted and 5,6-disubstituted 2'-deoxyuridines. *Nucleosides and nucleotides* **1994**, *13*, 177-196.
35. Itahara, T.; Seto, Y., Reaction of 1,3-dimethyluracil, 1,3-dimethylthymine, and caffeine with carbon radicals. *Chem. Lett.* **1985**, 1441-1442.
36. Chaudhari, S. S.; Thomas, A.; Patil, N. P.; Joshi, N. K.; Mukhopadhyay, I., *Indian Pat. Appl.*, **2010**, IN 2008MU02512.

Conclusions

In this thesis, the role played by benzophenone (BP) in the photoreactivity of DNA model compounds, formed by thymine (Thy) or uracil (Ura) derivatives, has been investigated. A number of nucleobases with different substituents have been synthesized and irradiated with BP to investigate the Paternò-Büchi (PB) reaction to form the oxetane photoproducts. Besides, the photoinduced cycloreversion process of the isolated oxetanes has also been studied, in connection with the photorepair mechanism of DNA. In addition, the photoreactivity of several dyads containing BP and Thy covalently linked to spacers of different length and nature have also been investigated.

Concerning the oxetanes that arise from the intermolecular interaction between BP and Thy or Ura derivatives, different regiochemical memories are observed for head-to-head (HH) and head-to-tail (HT) oxetanes. For instance, femtosecond transient absorption spectroscopy shows a high degree of regioselectivity in the formation a triplet exciplex between BP and 1,3-dimethylthymine, strongly favoured in the HH regioisomer (HH-1). Theoretical computational analyses agree with the experimental data provided. For both HH-1 and HT-1, the photoinduced cycloreversion takes place via the formation of a transient diradical intermediate, but for HH-1 the process is significantly more adiabatic.

The adiabaticity of the photolysis process is highly influenced by the substituent pattern at positions 1 and 5 of the oxetane, especially for the HT regioisomers. While the cycloreversion process is nearly quantitative for the HH oxetanes, in the case of the HT the difference with respect to pure BP is sharp, the highest regiodifferentiation taking place for the *tert*-butyl and ester-substituted HH/HT, with a ratio of (4:1) respectively.

Additionally, the photobehavior of a series of dyads composed of BP and Thy separated by spacers of different length has been investigated. Femtosecond transient absorption spectroscopy reveals that, in all cases, the photochemical reactions occur once the triplet excited state of BP has been fully populated. In this context, LFP evidences that the dyads composed with longer spacers have shorter triplet lifetimes, due to a faster intramolecular quenching, in line with their higher photoreactivity. Interestingly, a transient absorption band with maximum centered at *ca.* 370 nm is detected upon laser flash photolysis, attributed to the formation of a triplet exciplex that finally evolves towards the formation of oxetanes. The obtained results suggest that both the interchromophoric BP-Thy distance and the conformational arrangement provided by the nature of the linker play a significant role in the photobehavior of the investigated dyads.

In summary, it has been proven that the photoreactivity of the oxetanes utilized for this thesis is heavily dependent on:

- Their regiochemistry (much more adiabatic for the HH isomers than for the HT ones).
- Substituents at positions 1 and 5 (the bulkier, the less adiabatic).
- Whether or not the nucleobase and chromophore are covalently fused together with a linear aliphatic spacer.
- The interchromophoric distance between BP and the nucleobase.
- The conformational arrangement of the spacer, as well as its degree of flexibility.

Although important steps have been taken to understand the reverse PB process, more research would still be needed to be able to fully reveal the reaction mechanism and how it applies to DNA photorepair.

As this thesis is being written, more work is being performed by this team for this purpose using 1,4-naphthoquinone as a model compound. Thus, an oxetane and a cyclobutane naphthoquinone-derived dimers have been obtained as simpler and more faithful models associated to the damage of DNA, which should hopefully shed more light on this mystery.

ABSTRACTS

Abstract

Earth is constantly exposed to light energy coming from the sun. Fortunately, the most dangerous radiation, UVC and UVB, is almost entirely blocked by the planet's ozone layer; however, that which *is* able to pass through the great filter can cause damage to certain biomolecules, including DNA. The generated harm can either be through direct absorption by DNA itself (UVB), or, more commonly, by induced photosensitization (UVA) via the excitation of an exogenous or endogenous drug, that acts as a photosensitizer. Benzophenone (BP) as a building-block is present in a wide variety of drugs, and have the potential to photosensitize damage to DNA, specially towards the thymine (Thy) nucleobase. The result of (photosensitized) DNA damage can give rise to bulky dimers, i.e. cyclobutane pyrimidine dimers (CPDs) and pyrimidine-pyrimidone (6-4) photoproducts ((6-4)PPs), which can cause severe mutations, melanomas, or even be fatal for the cell.

The (6-4)PP can be broken-down in humans via *nucleotide excision repair*; but the DNA repair is also very efficient in plants and bacteria because of photolyase enzymes, in what could be a reverse Paternò-Büchi (PB) reaction through an unstable oxetane intermediate.

With the aim of getting deeper insight into the photoreactivity of benzophenone-thymine derivatives and in the photoinduced cleavage of oxetanes, which is somehow related to the photorepair of the (6-4)PPs, a variety of dyads where Thy and BP are covalently linked by a linear spacer of different lengths were first synthesized. Additionally, another dyad with a BP-like structure, ketoprofen (KP), and thymidine was also synthesized. The photochemical reactivity and the photophysical properties of the different derivatives were investigated by means of laser flash photolysis

(LFP) and femtosecond transient absorption spectroscopy; besides, the main photoproducts (PPs) arising from steady-state irradiation of the different dyads were also isolated and characterized.

The results showed a high degree of chemoselectivity on the linking bridge length and conformation. Concerning the photochemical reactivity, photoproducts arising from the PB and from formal hydrogen abstraction were formed. In this context, the PB reaction took place for the dyads with the longest spacer with complete regio- and stereoselectivity, along with a hydrogen abstraction process that give rise to a larger overall ring structure. In relation to the thymidine-derived oxetane, its photolysis formed four oxetane regioisomers in addition to two structures arising from formal hydrogen abstraction. Finally, the oxetanes with shorter spacers gave rise to a formal hydrogen abstraction photoproduct and/or polymerization. Accordingly, the overall photoreactivity was proportional to the spacer length and was well correlated with the $^3\text{BP}^*$ lifetimes, the longer spacers giving rise to shorter lifetimes. In connection to the photocleavage of the oxetanes arising from irradiation of the thymidine derivative, photolysis of the different regio- and stereoisomeric oxetanes led to the formation of the typical triplet-triplet absorption band of BP. Accordingly, the photoinduced cycloreversion also operates as an adiabatic process. Finally, photolysis of the oxetane that results from irradiation of the dyad with the longest spacer evidenced once more a complete adiabatic photoreversion process, showing a transient absorption at ~400 nm, which is ascribed to formation of the purported triplet exciplex between the linked benzophenone and thymine chromophores.

Additionally, in connection with the cycloreversion process involved in the photorepair of (6-4)PPs, we have studied the photoinduced reactions to

Thy or uracil (Ura) using BP as a photosensitizer, investigating both the PB reaction and the cycloreversion process of the different oxetane derivatives. With this purpose in mind, a wide range of Thy-BP and Ura-BP oxetanes with varying substituents in the nucleobase region at positions 1 and 5 were synthesized, including both the head-to-head (HH) and head-to-tail (HT) regioisomers.

Spectroscopic studies were performed first with oxetanes composed of 1,3-dimethylthymine (DMT) and BP, namely HH-1 and HT-1. The main purpose was to investigate the reverse PB reaction in detail. Femtosecond transient absorption and LFP results, as well as theoretical multiconfigurational quantum chemistry analysis, agree that the photoinduced cycloreversion process for both HH-1 and HT-1 involved the formation of a triplet excited exciplex, $^3[\text{DMT}\cdots\text{BP}]^*$, before the cleavage takes place, just after the formation of an excited singlet diradical species. The photochemical reaction was fully adiabatic for HH-1, and the experimental procedures showed the formation of a transient absorption band at ca. 400 nm, corresponding to $^3[\text{DMT}\cdots\text{BP}]^*$. The exciplex formation was proven to be highly regioselective towards the HH regioisomer, being faster and more efficient. The experimental results are in line with the energy barrier predicted for HT-1, by computational analysis, to reach the triplet exciplex, showing a higher probability to reach intersystem crossing with the ground state, and hence inducing a radiationless deactivation towards the starting materials BP and DMT or the HT-1 oxetane in its ground state.

In connection to this, direct photolysis of substituted Ura or Thy oxetanes showed that the adiabaticity of the process was determined by both the regiochemistry of the oxetane and the nucleobase substitution. While the photoinduced cycloreversion process was quasi-quantitative for the HH

oxetanes, this was strongly influenced by the substituents present in the HT ones, with the lowest adiabaticity observed in the one with a *tert*-butyl group at position 5 and a methoxy ester at position 1.

In general, adiabaticity was observed in the photoreversion process for all investigated oxetanes, with a high degree of regioselectivity, which falls in line with the theory of the involvement of a triplet exciplex in the process. Therefore, the adiabatic cycloreversion of oxetanes derived from aromatic ketones and pyrimidine bases appears to be a rather general process, which occurs in all the investigated compounds. Regioselectivity (HH vs. HT) and substitution-dependence are interesting features of this process.

Resumen

La Tierra está constantemente expuesta a la energía lumínica proveniente del sol. Afortunadamente, la radiación más peligrosa asociada a la luz UVC y UVB se bloquea casi en su totalidad por la capa de ozono del planeta; sin embargo, aquella que es capaz de atravesarla puede causar daños a ciertas biomoléculas, incluyendo el ADN. Dicho daño se puede generar por absorción directa de luz UVB por el propio ADN o por un proceso de fotosensibilización tras absorción de luz UVA por parte de una sustancia exógena o endógena al organismo que actúa como fotosensibilizador (como, por ejemplo, un fármaco). La benzofenona (BP) está presente en una amplia variedad de fármacos; es capaz de generar daño fotosensibilizado al ADN, especialmente a la base de timina (Thy). Como resultado del daño directo o fotosensibilizado, se pueden generar diversos dímeros de pirimidina tales como ciclobutanos (CPDs) y fotoproductos (6-4) pirimidina-pirimidona ((6-4)PPs), cuya formación puede derivar en mutaciones graves, melanomas, o incluso en la muerte celular.

En humanos, los fotoproductos (6-4) pueden revertir a las bases pirimidínicas iniciales a través de un proceso denominado *reparación por escisión de nucleótidos*. En este contexto, ciertas plantas y bacterias también son capaces de reparar dicho daño a través de enzimas específicos (fotoliasas) por un proceso inducido por luz, en lo que podría ser una reacción inversa de la reacción Paternò-Büchi (PB) a través de un intermedio oxetano muy inestable.

Con el fin de conocer con mayor profundidad la fotorreactividad de los derivados de la interacción entre benzofenona y timina, así como el proceso de ruptura fotoinducida de los oxetanos generados, lo que de

alguna manera está relacionado con la fotorreparación de (6-4)PPs, se sintetizó por primera vez una serie de diadas donde Thy y BP están covalentemente unidos por un espaciador lineal de longitud variable. Además, también se sintetizó otra diada compuesta por ketoprofeno (KP), que contiene el cromóforo BP en su estructura, y timidina. Se investigó la reactividad fotoquímica y las propiedades fotofísicas de las diferentes diadas mediante el uso de la técnica de fotólisis de destello láser (LFP) y la espectroscopia de absorción transitoria a escala de femtosegundo; así mismo, se aislaron y caracterizaron los principales fotoproductos (PPs) derivados de la irradiación de las diferentes diadas.

Los resultados mostraron un alto grado de quimioselectividad en función de la longitud y de la conformación del puente de unión entre ambos cromóforos. En cuanto a la reactividad fotoquímica, se formaron PPs derivados de la reacción PB, así como de un proceso de abstracción formal de hidrógeno. En este contexto, la irradiación de las diadas con espaciadores largos dio lugar a la formación de oxetanos con una completa regio- y estereoselectividad, junto con otros PPs provenientes del proceso de abstracción de hidrógeno, dando lugar a estructuras macrocíclicas. En relación con el oxetano derivado de la diada KP-timidina, su fotólisis resultó en la formación de cuatro oxetanos de diferente regioquímica, además de dos estructuras derivadas de la abstracción formal de hidrógeno. Por último, la irradiación de los oxetanos con espaciadores más cortos dio lugar a la formación de un fotoproducto de abstracción de hidrógeno y/o polimerización. En consecuencia, la fotorreactividad fue proporcional a la longitud del espaciador y se correlacionó bien con los tiempos de vida de $^3\text{BP}^*$, los espaciadores más largos mostrando tiempos de vida más cortos. En relación con la fotoapertura de los oxetanos resultantes de la irradiación del derivado de

timidina, la fotólisis de los diferentes oxetanos regio- y estereoisoméricos dio lugar a la aparición de la típica banda de absorción triple-triplete de BP. En consecuencia, la ciclorreversión fotoinducida también ocurre por un proceso adiabático. Por último, la fotólisis del oxetano que resulta de la irradiación de la diada con el espaciador más largo evidenció una vez más un proceso completamente adiabático, mostrando una absorción transitoria a ~400 nm, que se atribuye a la formación del supuesto exciplexo triplete entre los cromóforos de benzofenona y timina unidos.

En relación con los procesos involucrados en la fotorreparación de (6-4)PPs, se han estudiado las reacciones fotoquímicas de Thy o uracilo (Ura) con BP, investigando tanto la reacción PB como el proceso de ciclorreversión de los diferentes derivados de oxetano. Con este propósito, se sintetizó una amplia gama de oxetanos Thy-BP y Ura-BP con diversos sustituyentes en las posiciones 1 y 5 de la nucleobase, incluyendo tanto los regioisómeros “head-to-head” (HH) como “head-to-tail” (HT).

Se realizaron estudios espectroscópicos en primer lugar con oxetanos compuestos por 1,3-dimetiltimina (DMT) y BP, nombrados como HH-1 y HT-1. El propósito principal fue el de investigar en detalle la reacción PB inversa. Los resultados de espectroscopía de absorción transitoria a escala de femtosegundos y de LFP, así como el análisis teórico de química cuántica multiconfiguracional, concuerdan con que el proceso de ciclorreversión fotoinducida para HH-1 y para HT-1 implica la formación de un exciplexo triplete en el estado excitado, $^3[\text{DMT}\cdots\text{BP}]^*$, antes de que se produzca la escisión, justo después de la formación de una especie dirradical singlete en el estado excitado. La reacción fotoquímica fue completamente adiabática para HH-1; los resultados experimentales mostraron la formación de una banda de absorción transitoria alrededor

de los 400 nm, correspondiente a $^3[\text{DMT}\cdots\text{BP}]^*$. Se demostró que la formación del exciplexo es altamente regioselectiva para el isómero HH, siendo más rápida y eficiente. Los resultados experimentales concuerdan con la barrera energética predicha por el análisis computacional para que HT-1 alcance el exciplexo triplete, mostrando este una mayor probabilidad de alcanzar el cruce intersistema con el estado fundamental, y por lo tanto induciendo una desactivación no radiante hacia los productos de partida BP y DMT o hacia el oxetano inicial HT-1 en su estado fundamental.

En relación con esto, la fotólisis directa de los oxetanos de Ura o Thy con distintos sustituyentes mostró que la adiabaticidad del proceso viene determinada tanto por la regioquímica del oxetano como por los sustituyentes de la nucleobase. Si bien el proceso de ciclorreversión fotoinducida fue cuasi-cuantitativo para los oxetanos HH, este se vio fuertemente influido por los sustituyentes en los derivados HT, observándose la menor adiabaticidad en el derivado que posee un grupo tert-butilo en la posición 5 y el sustituyente acetato de metilo en la posición 1.

En general, se observó adiabaticidad en el proceso de fotorreversión de todos los oxetanos investigados, con un alto grado de regioselectividad, lo que concuerda con la participación de un exciplexo triplete. Por consiguiente, la ciclorreversión adiabática de los oxetanos derivados de cetonas aromáticas y bases de pirimidina parece ser un proceso bastante general que se produce en todos los compuestos investigados. La regioselectividad (HH vs. HT) y la dependencia de la sustitución son características interesantes de este proceso.

Resum

La Terra està constantment exposada a l'energia lumínica provinent del sol. Afortunadament, la radiació més perillosa associada a la llum UVC i UVB es bloqueja quasi íntegrament per la capa d'ozó del planeta; no obstant això, aquella que és capaç de travessar-la pot causar danys a certes biomolècules, incloent l'ADN. Aquest dany es pot generar per l'absorció directa de llum UVB pel propi ADN o per un procés de fotosensibilització després d'absorció de llum UVA per part d'una substància exògena o endògena a l'organisme que actua com fotosensibilitzador (com, per exemple, un fàrmac). La benzofenona (BP) està present en una àmplia varietat de fàrmacs; és capaç de generar dany fotosensibilitzat a l'ADN, especialment a la base de timina (Thy). Com a resultat del dany directe o fotosensibilitzat, es poden generar diversos dímers de pirimidina com ara ciclobutans (CPDs) i fotoproductes (6-4) pirimidina-pirimidona ((6-4)PPs), la formació dels quals pot derivar en mutacions greus, melanomes, o fins i tot en la mort cel·lular.

En humans, els fotoproductes (6-4) poden revertir a les bases pirimidíniques inicials a través d'un procés denominat *reparació per escissió de nucleòtids*. En aquest context, certes plantes i bacteris també són capaços de reparar aquest dany a través de certs enzims específics (fotoliasas) per un procés induït per llum, en el que podria ser una reacció inversa de la reacció Paternò-Büchi (PB) a través d'un intermedi oxetà molt inestable.

Amb la finalitat de conèixer amb major profunditat la fotoreactivitat dels derivats de la interacció entre benzofenona i timina, així com el procés de ruptura fotoinduída dels oxetans generats, lo que d'alguna manera està relacionat amb la fotoreparació de (6-4)PPs, es va sintetitzar per primera

vegada una sèrie de diades on Thy i BP estan covalentment units per un espaiador lineal de longitud variable. A més, també es va sintetitzar una altra diada composta per ketoprofè (KP), que conté el cromòfor BP en la seua estructura, i timidina. Es va investigar la reactivitat fotoquímica i les propietats fotofísiques de les diferents diades mitjançant l'ús de la tècnica de fotòlisi de centelleig làser (LFP) i l'espectroscòpia d'absorció transitòria a escala de femtosegons; així mateix, es van aïllar i caracteritzar els principals fotoproductes (PPs) derivats de la irradiació de les diferents diades.

Els resultats van mostrar un alt grau de quimioselectivitat en funció de la longitud i de la conformació del pont d'unió entre tots dos cromòfors. Respecte a la reactivitat fotoquímica, es van formar PPs derivats de la reacció PB, així com d'un procés d'abstracció formal d'hidrogen. En aquest context, la irradiació de les diades amb espaiadors llargs va donar lloc a la formació d'oxetans amb una completa regi- i estereoselectivitat, juntament amb uns altres PPs provinents del procés d'abstracció d'hidrogen, donant lloc a estructures macrocícliques. En relació amb l'oxetà derivat de la diada KP-timidina, la seua fotòlisi va resultar en la formació de quatre oxetans de diferent regioquímica, a més de dues estructures derivades de l'abstracció formal d'hidrogen. Finalment, la irradiació dels oxetans amb espaiadors més curts va donar lloc a la formació d'un fotoproducte d'abstracció d'hidrogen i/o polimerització. En conseqüència, la fotoreactivitat va ser proporcional a la longitud de l'espaiador i es va correlacionar bé amb els temps de vida de ${}^3\text{BP}^*$, els espaiadors més llargs mostrant temps de vida més curts. En relació amb la foto-obertura dels oxetans resultants de la irradiació del derivat de timidina, la fotòlisi dels diferents oxetans regi- i estereoisomèrics va donar lloc a l'aparició de la típica banda d'absorció triplet-triplet de BP. En

conseqüència, la cicloversió fotoinduïda també ocorre per un procés adiabàtic. Finalment, la fotòlisi de l'oxetà que resulta de la irradiació de la diada amb l'espaiador més llarg va evidenciar una vegada més un procés completament adiabàtic, mostrant una absorció transitòria al voltant de 400 nm, que s'atribueix a la formació del supòsit exciplex triplet entre els cromòfors de benzofenona i timina units.

En relació amb els processos involucrats en la fotoreparació de (6-4)PPs, s'han estudiat les reaccions fotoquímiques de Thy o uracil (Ura) amb BP, investigant tant la reacció PB com el procés de cicloversió dels diferents derivats d'oxetà. Amb aquest propòsit, es varen sintetitzar una àmplia gamma d'oxetans Thy-BP i Ura-BP amb diversos substituents en les posicions 1 i 5 de la nucleobase, incloent tant els regioisòmers "head-to-head" (HH) com "head-to-tail" (HT).

Es van realitzar estudis espectroscòpics en primer lloc amb oxetans compostos per 1,3-dimetiltimina (DMT) i BP, nomenats com HH-1 i HT-1. El propòsit principal va ser el d'investigar detalladament la reacció PB inversa. Els resultats d'espectroscòpia d'absorció transitòria a escala de femtosegons i de LFP, així com l'anàlisi teòric de química quàntica multiconfiguracional, concorden amb el fet que el procés de cicloversió fotoinduït per a HH-1 i per a HT-1 implica la formació d'un exciplex triplet en l'estat excitat, $^3[\text{DMT}\cdots\text{BP}]^*$, abans que es produïska la ruptura, just després de la formació d'una espècie diradical singlet en l'estat excitat. La reacció fotoquímica va ser completament adiabàtica per a HH-1; els resultats experimentals van mostrar la formació d'una banda d'absorció transitòria al voltant dels 400 nm, corresponent a $^3[\text{DMT}\cdots\text{BP}]^*$. Es va demostrar que la formació de l'exciplex és altament regioselectiva per a l'isòmer HH, sent més ràpida i eficient. Els resultats experimentals concorden amb la barrera energètica predita per l'anàlisi computacional

perquè HT-1 arribe a l'exciplex triplet, mostrant aquest una major probabilitat d'aconseguir l'encreuament intersistema amb l'estat fonamental, i per tant induint una desactivació no radiant cap als productes de partida BP i DMT o cap a l'oxetà inicial HT-1 en el seu estat fonamental.

En relació amb això, la fotòlisi directa dels oxetans de Ura o Thy amb diferents substituents va mostrar que l'adiabaticitat del procés ve determinada tant per la regioquímica de l'oxetà com pels substituents de la nucleobase. Si bé el procés de cicloversió fotoinduída va ser quasi-quantitatiu per als oxetans HH, aquest es va veure fortament influït pels substituents en els derivats HT, observant-se la menor adiabaticitat en el derivat que posseeix un grup tert-butil en la posició 5 i el substituent acetat de metil en la posició 1.

En general, es va observar adiabaticitat en el procés de fotoreversió de tots els oxetans investigats, amb un alt grau de regioselectivitat, la qual cosa concorda amb la participació d'un exciplex triplet. Per consegüent, la cicloversió adiabàtica dels oxetans derivats de cetones aromàtiques i bases de pirimidina sembla ser un procés prou general que es produeix en tots els compostos investigats. La regioselectivitat (HH vs. HT) i la dependència de la substitució són característiques interessants d'aquest procés.

Annex:

Publications and conferences

Publications related to this thesis

1. Blasco-Brusola, A.; Navarrete-Miguel, M.; Giussani, A.; Roca-Sanjuán, D.; Vayá, I.; Miranda, M. A., Regiochemical memory in the adiabatic photolysis of thymine-derived oxetanes. A combined ultrafast spectroscopic and CASSCF/CASPT2 computational study. *Phys. Chem. Chem. Phys.* **2020**, *22*, 20037-20042.
2. Blasco-Brusola, A.; Vaya, I.; Miranda, M. A., Influence of the linking bridge on the photoreactivity of benzophenone-thymine conjugates. *J. Org. Chem.* **2020**, *85*, 14068-14076.
3. Blasco-Brusola, A.; Vaya, I.; Miranda, M. A., Regioselectivity in the adiabatic photocleavage of DNA-based oxetanes. *Org. Biomol. Chem.* **2020**, *18*, 9117-9123.

Other publications

4. Pavanello, A; Blasco, A; Johnston, P. F.; Miranda, M. A.; Marin, M. L., Enhanced photodegradation of synthetic dyes mediated by Ag₃PO₄-based semiconductors under visible light irradiation. *Catalysts* **2020**, *10*, 774.

Congresses

"DNA base oxetane photolysis". 3rd Workshop on DNA Damage and Repair (DNADNR): Chemistry, Biology, and Medicine, València (Spain), September, **2019**. *Award to the best Flash Communication*.

"Light-induced cycloreversion of DNA-benzophenone oxetanes". XVI symposium of young researchers of the real spanish society of chemistry, RSEQ - Sigma Aldrich (Merck), Universitat Politècnica de València, València (Spain), November **2019**. Poster presentation.

5th ESP Photobiology School, CNR Istituto Nanoscienze, Brixen/Bressanone (Italy), June **2018**. Examined but not participated.

"Mechanistic Studies on the Photochemical Formation and Cleavage of Oxetanes Derived from Pyrimidine Bases". 3rd ITQ Winter Meeting Universitat Politècnica de València, València (Spain), December **2020**. *Award to one of the best Oral Communications*.